

CENTRAL LIBRARY

TEZPUR

Accession No. T 309

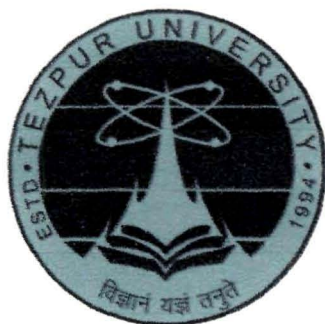
Date _____

BIODEGRADABLE HYPERBRANCHED POLYURETHANE NANOCOMPOSITES FOR BIOMEDICAL APPLICATION

**A thesis
submitted in partial fulfillment of the requirements
for the degree of
Doctor of Philosophy**

Beauty Das

Registration Number TZ121482 of 2012



**School of Sciences
Department of Chemical Sciences
Tezpur University**

August, 2014

Dedicated
to my
Maa & Baba

ABSTRACT

Material science has revolutionized the biomedical research in a range of applications from development of catheter to drug delivery vehicle. The emergence of biomedical domain like tissue engineering and regenerative medicines necessitate the development of biodegradable biomaterial to repair or regenerate the damaged or lost organs. Thus, polyurethane with its two phasic structure, biocompatibility, tunable properties and biodegradability evolved as one of the strongest contenders as a synthetic biomaterial. Moreover, the recent researches also showed that architecture of a material played a pivotal role in guiding its bio-interfacial attributes. In this avenue, hyperbranched polymers have shown to control the biological performance, mainly due to the presence of proliferated surface functionalities and branched geometry. They are reported to escort the cellular behavior and protein interactions in a beneficial way. Similarly, in presence of nanostructural material in polymer matrix, the cells can respond in an efficient and organized manner. Thus, hyperbranched polyurethane nanocomposite using suitable nanomaterials can boost the performance of a biomaterial. However, investigation on vegetable oil based hyperbranched polyurethanes and their nanocomposites as biomaterials is still in infancy. Thus, it prompted a wider scope to exploit such materials in the biomedical realm.

In this avenue, hyperbranched polyurethane was synthesized using *Helianthus annuus* oil. The incorporation of vegetable oil derived moiety ameliorated the biodegradability, cell adherence capability and reduced the toxicity of the degraded products compared to polyurethane without oil. Moreover, content of the branch generating unit and branched architecture tuned the physico-mechanical, chemical and biological properties of polyurethane. Among the studied polyurethanes, the best performing one was used as the matrix for the preparation of nanocomposite using biologically important nanomaterials like multiwalled carbon nanotubes and Fe_3O_4 nanoparticles. These nanomaterials were functionalized by employing different facile approaches and their subsequent effects on the performance of nanocomposites, especially at the bio-interface were examined.

It was observed that Fe_3O_4 based nanocomposites showed dose dependent improvement in mechanical, thermal and shape memory properties. Fe_3O_4 also conferred antibacterial activity and magnetic behavior to the polymer. Whereas, the inclusion of carboxyl functionalized carbon nanotubes improved the osteoconductivity of the polymer and facilitated better adherence and proliferation of MG63 mammalian osteoblast cell lines. The mechanical strength of the polymer improved drastically on inclusion of MWCNT compared

to Fe₃O₄, due to higher aspect ratio of the former than the later. Moreover, Fe₃O₄ decorated pristine MWCNT nanohybrid based nanocomposites showed the best physico-mechanical performance, drug loading efficiency, antibacterial activity and fluid retention ability among all the studied nanocomposites. The nanohybrid based nanocomposites showed accelerated wound healing potency with wound closure rate comparable to a commercially available dressing, with controlled drug release profile. This studies thus depicted that variation of nanomaterials can modulate the properties of nanocomposites even based on the same polymeric matrix.

Interestingly, it was observed that functionalization of nanotubes with biomolecule (rapeseed protein that was extracted from an industrial waste), improved the osteoconductivity and cell differentiation ability of nanocomposite. Therefore, this nanocomposite witnessed rapid *in vivo* healing of a critical sized tibial fracture of a tested animal within a short span of time. The bridging of fracture was completed (90-93%) within 5-6 weeks as well as the normal locomotion of the rats was regained. The toxicological studies also ascertained that the anchorage of appropriate modifying agent (rapeseed protein) on MWCNT surmounted the toxic nature of the latter. Moreover, the protein functionalized MWCNT based nanocomposite showed better mechanical performance, cell adherence, proliferation and biocompatibility compared to the carboxyl functionalized MWCNT based one.

Furthermore, each of these aforementioned nanocomposites and hyperbranched polyurethane showed biodegradable behavior and the degraded as well as leached/released products were found to be non-toxic to the tested cell lines. The non-immunogenic nature of these studied material were confirmed by analysis of the hematological parameters and cytokines expression on the peripheral blood of the rats post-implantation. The absence of cardinal symptoms and biopsy of vital organs of the implanted rats confirmed the biocompatibility.

Thus, this investigation sparks a beam on the importance of until unexplored prospective of *Helianthus annuus* oil based hyperbranched polyurethane and its nanocomposites in the domain of biomedical science. These nanocomposites could effectively address a wide range of health related issues like organ failure, wound treatment, fractured or degenerated bone, etc. However, more comprehensive studies like clinical investigation must be undertaken before attesting any concrete conclusion, as laboratory performance and clinical performance has to be synchronized.

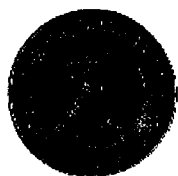
DECLARATION

I do hereby declare that the thesis entitled “*Biodegradable hyperbranched polyurethane nanocomposites for biomedical application*”, submitted to the Tezpur university in the Department of Chemical Sciences under School of Sciences, is a record of original research work carried out by me. All sources of assistance have been assigned due acknowledgment. I also declare that neither this work as a whole nor a part of it has been submitted to any other University or Institute for any other degree, diploma or award.

Place: Tezpur University, Tezpur

Beauty Das
(Beauty Das)

Date: 12/12/2014



TEZPUR UNIVERSITY

Ph: 03712-267004

(A Central University established by an Act of Parliament) 03712-267005

NAPAAM, TEZPUR-784028

Fax: 03712-267006

DISTRICT: SONITPUR:: ASSAM:: INDIA

03712-267005

E-mail: nkarak@tezu.ernet.in

CERTIFICATE

This is to certify that the thesis entitled “*Biodegradable hyperbranched polyurethane nanocomposites for biomedical application*” submitted to the Tezpur University in the Department of Chemical Sciences under the School of Sciences, in partial fulfillment for the award of the Degree of Doctor of Philosophy in Science, is a record of research work carried out by Ms Beauty Das under my personal supervision and guidance.

All helps received by her from various sources have been duly acknowledged. No part of this thesis has been reproduced elsewhere for award of any other degree.

Place: Tezpur University

Date: 12/12/2019


(Dr. Niranjana Karak)

Professor

Department of Chemical Sciences

School of Sciences



TEZPUR UNIVERSITY

Ph 03712-267004

(A Central University established by an Act of Parliament) 03712-267005

NAPAAM, TEZPUR-784028

Fax 03712-267006

DISTRICT SONITPUR ASSAM INDIA

03712-267005

CERTIFICATE

This is to certify that the thesis entitled "*Biodegradable hyperbranched polyurethane nanocomposites for biomedical application*" submitted to the Tezpur University in the Department of Chemical Sciences under the School of Sciences, in partial fulfillment for the award of the Degree of Doctor of Philosophy in Science, has been examined by us on 13/01/15 and found to be satisfactory

The committee recommends for the award of the degree of Doctor of Philosophy

Niranjana Karak
Principal Supervisor

Ansuman Chattopadhyay
External Examiner

Date: 13/01/15

Date: 13.1.2015

PREFACE

This work endeavors to confer comprehensive understanding on the role of polymer nanocomposite in the niche of biomedical science. By exploiting the domains of polymer science, biology and nanotechnology, this work designed advanced functional biomaterials for various bio-applications. Herein, hyperbranched polyurethane and its nanocomposites with nanomaterials like carboxyl or protein functionalized MWCNT, Fe₃O₄ nanoparticles and Fe₃O₄-MWCNT nano hybrid have been investigated. The performance of these nanocomposites was examined by varying the dose of the nanomaterials in the matrix. Moreover, the bio-interfacial attributes of these nanocomposites were probed into to ensure their safety issues and non-immunogenic behavior on post-implantation

This investigation also explored the essence of *Helianthus annuus* oil at the bio-interface. The *Helianthus annuus* oil served two vital purposes. Firstly, its inclusion in polyurethane is a greener approach, and secondly polyurethane with vegetable oil moiety showed improved biodegradation and cells adherence aptitude. Furthermore, the role of architectural features was also proved in this study. Hyperbranched polyurethane with high concentration of surface end groups embraced excellent physico-mechanical and biological attributes. Moreover, this hyperbranched architecture led to finer interfacial interaction with the above mentioned nanomaterials. Furthermore, the nanocomposites exhibited excellent mechanical performance along with biodegradability in physiological environment with cyto/hemo-compatible degraded and leached out products. Notably, it was also confirmed that on proper functionalization, the toxicity issues related to a nanomaterial can be suppressed. The studies proposed that the nature of nanomaterials and the extent of interfacial interactions alter the bulk as well as surface chemistry of the nanocomposites, which get reflected from their improved bio-physico-mechanical attributes.

Precisely, this work is a multidisciplinary attempt to address a few vital health related issues like damage/loss organ, orthopaedic problems, wound treatment or major invasive surgical procedures. The conjoining benefits of hyperbranched topology, vegetable oil and nanomaterials were investigated to address such problems. The results encouraged the potentiality of such nanocomposites in the biomedical realm and thus provided a wider scope to explore them as multifunctional biomaterials.

Date:
Place: Napaam, Tezpur

Beauty Das
(Beauty Das)

ACKNOWLEDGMENT

This thesis has been completed with the support, encouragement and blessings of numerous people including my supervisor, family and well wishers. It is my utmost pleasure to convey my gratitude to all those who contributed indirectly or directly to make my journey beautiful and fruitful.

Foremost, I would like to take this opportunity to express of heartiest gratitude to my supervisor Prof. Niranjana Karak, Tezpur University, for his motivation, continuous support, guidance and priceless suggestions. His commitment towards research, honesty and truthfulness would always inspire me throughout my life. I could not imagine having a better mentor with his excellence. I will always treasure his belief and hard work to make me flourish in a new direction.

I sincerely acknowledge the co-operation extended to me by the authority of Tezpur University and Department of Chemical Sciences, for providing the privilege to use technical and administrative facilities for successful accomplishment of my research work.

My sincere thanks goes to the Head of the Department Prof. R.C. Deka and Dean, Research and Development, Prof. C.L. Mohanta for allowing me to work on my topic and co-operation.

I would also like to express my sincere gratitude and humble respect to Dr. M. Mandal and Dr. A. Thakur, members of my doctoral research committee for their timely help, co-operation and advises.

I am immensely grateful to all the faculty members and staffs of Department of Chemical Sciences, Tezpur University for valuable suggestions and providing a working as well as friendly environment to precede my work, without any difficulty.

It is my great pleasure to acknowledge Dr. P. Chattopadhyay, DRL, Tezpur for his co-operation, personal attention and providing me the facility to perform the biology related work in his laboratory. I also want to thank the research scholars under his supervision, to well equip me with the experimental rodent and to handle them with care.

Also I take this opportunity to give my special thanks to Dr P. Barman, Radiologist, Assam X-ray, Tezpur, for allowing me to use the X-ray facility, to successfully complete one of my research objectives. I am also thankful to T.K. Maity, IIT Kharagpur and his research scholars, for their support to accomplish important in vitro studies related to my Ph.D work.

I am also grateful to UGC-RGNF, New Delhi for allotting the financial support as JRF and SRF. IIT Guwahati, NEHU Shillong and DRL, Tezpur are also highly acknowledged for their help in analyzing and experimental works.

My heartfelt thanks goes to my senior lab-mates Dr. Gautam Das, Dr. Buddhadeb Roy, Dr. Uday Konwar, Dr. Rocktotpal Konwarh and Dr. Hemjyoti Kalita for their suggestion and to make me trained to the basic instrumentation of a polymeric laboratory. I thanks my fellow labmates Shaswat Borua, Satyabrat Gogoi, Suman Thakur, Bibekananda De, Shivani Paul and Purnima Boruah for stimulating discussion about our work. Moreover, they are the sole reason to have fun in between my lab work or spoilt mood. I wish to thanks all my friends, especially P. Bhattacharya and A. Chatterjee for their blessing and support during the course of my work and life.

I am grateful to Mrs. Sushmita Karak for her encouragement, co-operation and for providing a homely environment during each festival.

To end with, I whole heartedly give my gratitude and high regards to my Maa (Pratibha Das) and Baba (Badal Chandra Das) for their immense love, prayer and belief. I am also thankful to my elder sister Papiya Bhattacharya, brothers Biplob Das and Neelkanta Bhattacharyya for their care and blessings. Their support and motivation encouraged me to carry out my research work to completion and to overcome every hurdles with ease. I owe everything to them. Finally, my bouquet of thank to God to be with me always and guide me.

Place : Tezpur University, Tezpur

Date : 12/12/2014

Beauty Das
(Beauty Das)

CONTENTS

<i>Content</i>	<i>Page No.</i>
Abstract	i
Declaration	iii
Certificate of Supervisor	iv
Certificate of Examiners	v
Preface	vi
Acknowledgement	vii
Contents	ix
List of Abbreviations and Symbols	xvii
List of Tables	xxii
List of Figures	xxiii
List of Schemes	xxvii
Chapter 1	
General introduction	
<i>Highlights</i>	1
1.1. Introduction	2
1.2 Historical background	4
1.3 Classification of biomaterial	6
1.3.1 Metal	6
1.3.2 Ceramic	6
1.3.3 Polymer	8
1.3.4 Composite	10
1.4 Classification of polymeric nanocomposite	11
1.5 Materials and methods	12
1.5.1 Polyurethane	12
1.5.1.1 Diisocyanate	12
1.5.1.2 Macroglycol	14
1.5.1.3 Chain extender	16
1.5.1.4 Vegetable oil	17
1.5.1.5 Catalyst	18

1.5.1.6 Synthetic method	20
1.5.2 Nanomaterial	21
1.5.2.1 Zero dimensional	22
1.5.2.2 One dimensional	24
1.5.2.3 Two dimensional	26
1.5.3 Preparative technique for polymer nanocomposite	26
1.5.3.1 Solution	27
1.5.3.2 <i>In situ</i> polymerization	27
1.5.3.3 Melt mixing	28
1.5.4 Fabrication of polymeric biomaterials	28
1.6 Characterization	31
1.6.1 Chemical structure	31
1.6.2 Physical structure	33
1.6.3 Thermal	34
1.6.4 Biological	35
1.6.4.1 Biodegradation study	35
1.6.4.2 <i>In vitro</i> cytotoxicity assay	35
1.6.4.3 Cell adhesion/spreading assay	36
1.6.4.4 <i>In vitro</i> immunocompatibility assay	36
1.6.4.5 <i>In vitro</i> hemocompatibility assay	37
1.6.4.6 <i>In vivo</i> assessment of biocompatibility and inflammatory response	37
1.7 Properties	38
1.7.1 Mechanical	38
1.7.2 Thermal	38
1.7.3 Surface	39
1.7.4 Biological	40
1.7.4.1 Biocompatibility	40
1.7.4.2 Biodegradation	41
1.8 Applications	42
1.8.1 Tissue engineering	42
1.8.2 Wound dressing	43
1.8.3 Catheter and stent	44
1.8.4 Drug delivery	45

1.8.5 Shape memory biomaterial	45
1.9 Scopes and objectives of the present investigation	46
1.10 Plans of present work	46
Reference	47
Chapter 2	
<i>Helianthus annuus</i> oil based hyperbranched polyurethane	
<i>Highlights</i>	56
2A. Synthesis, characterization and properties evaluation	57
2A.1 Introduction	57
2A.2 Experimental	58
2A.2.1 Materials	58
2A.2.2 Instrumentation	59
2A.2.3 Methods	60
2A.2.3.1 Preparation of monoglyceride	60
2A.2.3.2 Synthesis of hyperbranched and linear polyurethanes	61
2A.2.3.3 Sample preparation for performance studies	62
2A.2.3.4 Broth culture technique for biodegradation	62
2A.2.3.5 Statistical analysis	63
2A.3 Results and discussions	63
2A.3.1 Synthesis of hyperbranched polyurethanes	63
2A.3.2 FTIR study	64
2A.3.3 XRD study	67
2A.3.4 NMR study	67
2A.3.5 SEM study	68
2A.3.6 Mechanical properties	68
2A.3.7 Thermal study	69
2A.3.8 Chemical resistance test	70
2A.3.9 Biodegradation study	71
2A.4 Conclusion	73
2B Effect of vegetable oil and multifunctional content	74
2B.1 Introduction	74
2B.2 Experimental	75
2B.2.1 Materials	75

2B.2.2 Instrumentation	75
2B.2.3 Methods	76
2B.2.3.1 Synthesis of hyperbranched polyurethanes	76
2B.2.3.2 Preparation of porous samples	76
2B.2.3.3 <i>In vitro</i> degradation study	77
2B.2.3.4 <i>In vitro</i> cytocompatibility assay	77
2B.2.3.5 <i>In vitro</i> hemolytic activity assay	78
2B.2.3.6 Histopathological and cell adherence study post-implantation	78
2B.2.3.7 Cytokines detection and alkaline phosphatase assay	79
2B.2.3.7 Statistical analysis	79
2B.3 Results and discussions	79
2B.3.1 Synthesis of hyperbranched polyurethane	79
2B.3.2 FTIR study	79
2B.3.2 XRD study	80
2B.3.4 NMR study	80
2B.3.5 SEM study	81
2B.3.6 Mechanical properties	83
2B.3.7 Thermal study	84
2B.3.8 Chemical resistance test	85
2B.3.9 <i>In vitro</i> cytocompatibility	86
2B.3.10 <i>In vitro</i> hemocompatibility	86
2B.3.11 <i>In vitro</i> biodegradation	87
2B.3.12 <i>In vivo</i> immunocompatibility	88
2B.3.13 Alkaline phosphatase activity	89
2B.3.14 Histopathological study	89
2B.3.15 <i>In vivo</i> cell adherence and proliferation	90
2B.4 Conclusion	91
Reference	91

Chapter 3

***Helianthus annuus* oil based hyperbranched polyurethane/Fe₃O₄ nanocomposite as an implantable material**

<i>Highlights</i>	93
3.1 Introduction	94

3.2 Experimental	95
3.2.1 Materials	95
3.2.2 Instrumentation	96
3.2.3 Methods	96
3.2.3.1 Preparation of Fe ₃ O ₄	96
3.2.3.2 Preparation of nanocomposites	97
3.2.3.3 <i>In vitro</i> degradation study	97
3.2.3.4 <i>In vitro</i> cytocompatibility assay	97
3.2.3.5 <i>In vitro</i> hemolytic activity assay	97
3.2.3.6 Shape memory behavior study	98
3.2.3.7 Antibacterial activity assay	98
3.2.3.8 Histopathological study	98
3.2.3.9 Cytokine analysis	99
3.2.3.10 statistical analysis	99
3.3 Results and discussions	99
3.3.1 Preparation of nanocomposites	99
3.3.2 FTIR and UV-visible studies	100
3.3.3 XRD study	101
3.3.4 SEM and TEM studies	102
3.3.5 Mechanical properties	103
3.3.6 Thermal study	103
3.3.7 Magnetic behavior of Fe ₃ O ₄ and nanocomposites	104
3.3.8 Study of shape memory behavior	105
3.3.9 <i>In vitro</i> biodegradation study	106
3.3.10 Antibacterial activity	107
3.3.11 <i>In vitro</i> cytocompatibility and hemocompatibility	108
3.3.12 Histopathological study	109
3.3.13 <i>In vivo</i> immunocompatibility	109
3.4 Conclusion	110
Reference	111

Chapter 4

***Helianthus annuus* oil based hyperbranched polyurethane/MWCNT nanocomposite as a scaffold for bone tissue engineering**

<i>Highlights</i>	113
4.1 Introduction	114
4.2 Experimental	115
4.2.1 Materials	115
4.2.2 Instrumentation	116
4.2.3 Methods	116
4.2.3.1 Functionalization of MWCNT	116
4.2.3.2 Preparation of nanocomposites	117
4.2.3.3 <i>In vitro</i> degradation study	117
4.2.3.4 <i>In vitro</i> cytocompatibility assay	118
4.2.3.5 <i>In vitro</i> hemolytic activity assay	118
4.2.3.6 Osteoblast adhesion assay	118
4.2.3.7 Osteoblast proliferation assay	118
4.2.3.8 Hematological parameters of rats post-implantation	119
4.2.3.9 Histopathological study	119
4.2.3.10 Cytokine detection	119
4.2.3.11 Statistical analysis	120
4.3 Results and discussions	120
4.3.1 Preparation of nanocomposites	120
4.3.2 FTIR study	120
4.3.3 XRD study	122
4.3.4 SEM and TEM studies	122
4.3.5 Mechanical properties	123
4.3.6 <i>In vitro</i> cytocompatibility	125
4.3.7 Analysis of hematological parameters	126
4.3.8 <i>In vitro</i> hemocompatibility	127
4.3.9 <i>In vivo</i> immunocompatibility	128
4.3.10 Adhesion and proliferation of MG63 cells	128
4.3.11 Histopathological study	130
4.3.12 <i>In vitro</i> biodegradation study	131
4.4 Conclusion	133
References	133

Chapter 5

***Helianthus annuus* oil based hyperbranched polyurethane/Fe₃O₄ decorated MWCNT nanocomposite as a wound healing material**

<i>Highlights</i>	135
5.1 Introduction	136
5.2 Experimental	137
5.2.1 Materials	137
5.2.2 Instrumentation	138
5.2.3 Methods	138
5.2.3.1 Preparation of Fe ₃ O ₄ -MWCNT nanohybrid	138
5.2.3.2 Preparation of nanocomposites	139
5.2.3.3 Preparation of porous samples	139
5.2.3.4 Fluid handling capacity	139
5.2.3.5 Moisture vapor permeability	141
5.2.3.6 Loading of gentamicin sulfate and <i>in vitro</i> drug release profile study	141
5.2.3.7 Antibacterial activity assay	141
5.2.3.8 <i>In vitro</i> cytocompatibility study	141
5.2.3.9 <i>In vitro</i> hemolytic activity assay	141
5.2.3.10 Hematological parameters of rats post-implantation	141
5.2.3.11 Circular excision experimental model and wound contraction rate analysis	142
5.2.3.12 Statistical analysis	142
5.3 Results and discussions	142
5.3.1 Preparation of nanohybrid and nanocomposites	142
5.3.2 FTIR study	144
5.3.3 XRD study	145
5.3.4 SEM and TEM studies	145
5.3.5 Mechanical properties	147
5.3.6 Fluid handling capacity and moisture vapor permeability	147
5.3.7 Drug loading efficacy of NC and <i>in vitro</i> controlled release profile	149
5.3.8 <i>In vitro</i> cytocompatibility and hemocompatibility	151
5.3.9 Antibacterial activity	151
5.3.10 Analysis of hematological parameters	153

5.3.11 Histopathological study and wound contraction rate	155
5.4 Conclusion	157
References	157

Chapter 6

***Helianthus annuus* oil based hyperbranched polyurethane/rapeseed protein functionalized MWCNT NC as a rapid bone healing material**

<i>Highlights</i>	159
6.1 Introduction	160
6.2 Experimental	162
6.2.1 Materials	162
6.2.2 Instrumentation	162
6.2.3 Methods	163
6.2.3.1 Functionalization of MWCNT by rapeseed protein	163
6.2.3.2 Oxidative modification of MWCNT by carboxyl group	162
6.2.3.3 Preparation of nanocomposites	163
6.2.3.4 <i>In vitro</i> and <i>in vivo</i> biodegradation studies	164
6.2.3.5 <i>In vitro</i> cytocompatibility and hemolytic activity assay	164
6.2.3.6 Osteoblast proliferation assay and cell adhesion	164
6.2.3.7 <i>In vitro</i> osteoblast differentiation study	165
6.2.3.8 Tibial shaft critical sized defect model	165
6.2.3.9 Implantation procedure of the sticky nanocomposite	165
6.2.3.10 Radiographic analysis	166
6.2.3.11 Hematological parameters of rats post-implantation	166
6.2.3.12 Serum biochemistry and cytokine detection post implantation	166
6.2.3.13 <i>In vivo</i> toxicity analysis of protein, MWCNT and protein functionalized MWCNT	166
6.2.3.14 Histopathological study of fractured tibia	167
6.2.3.15 Statistical analysis	167
6.3 Results and discussions	167
6.3.1 Functionalization of MWCNT	167
6.3.2 Preparation of nanocomposites	168
6.3.3 FTIR and UV-visible studies	169
6.3.4 XRD study	170

6.3.5 TEM study	170
6.3.6 Mechanical properties	171
6.3.7 <i>In vitro</i> hemocompatibility and cytocompatibility	172
6.3.8 <i>In vitro</i> proliferation and differentiation study of MG63 cells	174
6.3.9 <i>In vitro</i> biodegradation study	176
6.3.10 <i>In vivo</i> bone healing potency of PNC	176
6.3.11 Radiographic analysis	176
6.3.12 Analysis of biochemical and hematological parameters	178
6.3.13 Bio-toxicity study of protein, MWCNT and protein functionalized MWCNT	180
6.3.14 <i>In vivo</i> fate of the implanted PNC in the tibial defect rat model	183
6.3.15 Histopathological study at the fracture site	184
6.4 Conclusion	186
Reference	186
Chapter 7	
Conclusions and future scopes	
<i>Highlights</i>	188
7.1 Summary and concluding remarks	189
7.2 Future scopes	193
List of Publications	194

LIST OF ABBREVIATIONS AND SYMBOLS

AC	alternative current
ALP	alkaline phosphatase
BD	butandiol
bp	boiling point
cc	cubic centimeter
cm	centimeter(s)
CNT	carbon nanotubes(s)
CTAB	cetyl trimethylammonium bromide
°C	degree centigrade
dL	deciliter(s)
DNA	deoxyribonucleic acid
dia.	diameter
DCM	dichloromethane
DSC	differential scanning calorimetry
DMSO	dimethyl sulfoxide
DBTDL	dibutyl tin dilaurate
DMAc	N,N-dimethylacetamide
DB	degree of branching
DMEM	Dulbecco's Modified Eagle's Medium
DMTA	dynamic mechanical thermal analysis
EBBS	Eagle's balanced salts
emu	electromagnetic unit
EB	elongation at break
ELISA	enzyme-linked immunosorbent assay
EDTA	ethylenediaminetetraacetic acid
ECM	extracellular matrix
FCS	fetal calf serum
fl	femtoliters
FTIR	Fourier transform infrared
F _w	formula weight
g	gram(s)

GO	graphene oxide
h	hour(s)
HA	hydroxyapatite
HB	hyperbranched
HBPU	hyperbranched polyurethane(s)
IL	interleukine(s)
IR	infrared
IPDI	isophorone diisocyanate
K	kelvin
kN	kilo-Newton
kV	kilo-volt
L	liter(s)
lb	pound(s)
LDI	lysine diisocyanate
m	meter(s)
mA	mili ampere
min	minute(s)
mL	mili liter(s)
mm	mili meter(s)
mol	mole
mp	melting point
M_n	number average molecular weight
M_w	weight average molecular weight
MPa	mega pascal
MDI	4,4-diphenylmethane diisocyanate
MTT	(3-(4,5-dimethylthiazol-2-yl)-2,5-diphenyltetrazolium bromide
MRI	magnetic resonance imaging
MG	monoglyceride
MMT	montmorillonite
MWCNT	multiwalled carbon nanotubes(s)
N	Newton
NC	nanocomposite(s)
NMR	nuclear magnetic resonance
nm	nano meter(s)

Oe	oersted
OD	optical density
pg	Pico gram
ppm	parts per million
PBS	phosphate buffer saline
PCL	poly(ϵ -caprolactone) diol
PDMS	Poly(dimethyl siloxane)
PE	pentaerythritol
PEG	poly(ethylene glycol)
PLGA	poly(lactic-glycolic) acid
PMMA	poly(methyl methacrylate)
POSS	polyhedral oligomeric silsesquioxane
PP	polypropylene
PU	polyurethane(s)
RBC	red blood cell
RNA	ribonucleic acid
ROS	free radical species
rpm	rotation per minute
s	second(s)
SEM	scanning electron microscope
SWCNT	single walled carbon nanotubes(s)
TDI	toluene diisocyanate
TE	tissue engineering
TEM	transmission electron microscopy
T_g	glass transition temperature
TGA	thermogravimetric analysis
T_m	melting temperature
TMS	tetramethyl silane
TNF	tumor necrosis factor
UTM	universal testing machine
UV	ultraviolet
v	volume
wt.	weight

XRD	X-ray diffraction
μm	micro meter(s)
μM	micro molar(s)
μL	micro liter(s)
%	percentage
λ_{max}	wavelength maximum
θ	scattering angle

LIST OF TABLES

Table 1.1: Commonly used metals and alloys in biomedical applications with their pros and cons

Table 1.2: Commonly used ceramics in biomedical applications with their pros and cons

Table 1.3: Commonly used polymers in biomedical applications with pros and cons

Table 1.4: Important diisocyanates with their structures

Table 1.5: Important macroglycols and their structures

Table 1.6: Important chain extenders with their structures

Table 1.7: Important catalysts with their structures

Table 1.8: Commonly used techniques to fabricate porous biomaterials

Table 2A.1: Composition of reactants (mmol) with 33% of hard segment

Table 2A.2: Mechanical properties of HBPU and LPU

Table 2A.3: Thermal degradation parameters for HBPU and LPU

Table 2A.4: The weight loss (%) of LPU and HBPU in different chemical media

Table 2B.1: Composition of reactants (mmol) for synthesis of HBPU

Table 2B.2: Mechanical properties and thermal degradation parameters of HBPU and SHBPU

Table 3.1: Mechanical properties of HBPU and FNC

Table 4.1: Mechanical properties of HBPU and MNC

Table 4.2: Hematological parameters of Wistar rats before and after implantation

Table 5.1: Mechanical properties of HBPU and NC

Table 5.2: Hematological parameters of Wistar rats upon exposure to NNC

Table 5.3: Wound contraction rate in albino mice

Table 6.1: Mechanical properties of PNC, MNC and HBPU

Table 6.2: Biochemical profiles of Wistar rats upon exposure to studied materials

Table 6.3: Hematological parameters of Wistar rat upon exposure to the studied materials

LIST OF FIGURES

Figure 1.1: Prospective applications of biodegradable HBPU NC

Figure 2A.1: ^1H (a) and ^{13}C (b) NMR spectra of MG of *Helianthus annuus* oil

Figure 2A.2: Representing the FTIR spectra (a), XRD patterns (b), ^1H NMR spectra (c and d) as well as ^{13}C NMR (e and f) of HBPU and LPU, respectively

Figure 2A.3: Representing the SEM images of LPU and HBPU

Figure 2A.4: TGA thermograms (a) and DCS curves (b) of HBPU and LPU

Figure 2A.5: Bacterial growth curves of *Pseudomonas aeruginosa* SD2 (a), *Pseudomonas aeruginosa* SD6 (b) and *Bacillus subtilis* MTCC73 (c) on HBPU and LPU as well as the standard deviation for bacterial growth for LPU (d) and HBPU (e)

Figure 2A.6: Representative SEM images of the biodegraded HBPU (a) and LPU (b) by *Bacillus subtilis* MTCC73 after 4 weeks of incubation

Figure 2B.1: FTIR spectra (a) of HBPU, SHBPU and degraded HBPU (DHBPU) and XRD patterns (b) of HBPU and SHBPU

Figure 2B.2: ^1H NMR (a and b) and ^{13}C NMR (c and d) spectra of HBPU and SHBPU

Figure 2B.3: Representative SEM images of HBPU (a and b), degraded HBPU matrix (c-f) at 15, 30, 45 and 60 days and degraded SHBPU (g-i) at 7, 15 and 20 days of degradation study

Figure 2B.4: Representative SEM images of porous HBPU (a) and SHBPU (b)

Figure 2B.5: TGA thermograms and DSC curves of HBPU (a and c) and SHBPU (b and d)

Figure 2B.6: Cell viability (%) of heart and liver cells on HBPU and SHBPU scaffold

Figure 2B.7: RBC hemolytic activity (%) of HBPU and the degraded products (DP) after 15, 30, 45 and 60 days (a) as well as of SHBPU and the degraded products (DP) after 7, 15 and 20 days (b), weight retention (%) of HBPU (c) and SHBPU (d) during degradation study (* $p > 0.05$, ** $p < 0.05$ and *** $p < 0.001$)

Figure 2B.8: Microscopic view of representative histological sections of heart (a₁, a₂ and a₃), kidney (b₁, b₂ and b₃), liver (c₁, c₂ and c₃) and skin (d₁, d₂ and d₃) sections [subscript 1, 2 and 3 indicates control, HBPU and SHBPU treated rats, respectively]

Figure 2B.9: SEM images of skin cells adherence and proliferation on HBPU matrix after 15 (a) and 30 (b) days as well as on SHBPU matrix after 15 days (c) of post-implantation

Figure 3.1: FTIR spectra (a) of HBPU, NC and Fe_3O_4 , UV spectrum of Fe_3O_4 (b) and XRD patterns (c) of Fe_3O_4 , HBPU and FNC15

Figure 3.2: Representative SEM images of HBPU (a) and FNC (b), TEM images of Fe₃O₄ (c) and FNC (d) as well as histogram (d) for particle size distribution of Fe₃O₄

Figure 3.3: TGA thermograms (a) of HBPU and FNC and DSC curves (b) of FNC

Figure 3.4: Hysteresis loop of Fe₃O₄ (a) and FNC15 (b)

Figure 3.5: Representing the thermo-responsive shape memory behaviors (a) of HBPU and FNC, SEM images of degraded FNC after 15 (b) and 60 (c) days as well as *in vitro* degradation (d) of HBPU and FNC in terms of weight loss (%) against their incubation period (*p>0.05, **p<0.05 and ***p<0.001)

Figure 3.6: Representing the antibacterial activity of Fe₃O₄, HBPU and FNC15 against *Staphylococcus aureus* (a) and *Klebsiella pneumonia* (b)

Figure 3.7: The cell viability percentage (a) of the liver and cardiac cells and hemolytic activity (b) of HBPU, non-degraded FNC (coded as ND) and the degraded by-product after 15 (DP15), 30 (DP30), 45 (DP45) and 60 (DP60) days of *in vitro* biodegradation study

Figure 3.8: Microscopic view of representative histological sections of kidney (a), skin (b), liver (c) and heart (d) of FNC implanted rat

Figure 4.1: FTIR spectra (a) and XRD diffractograms (b) of MWCNT, HBPU and MNC

Figure 4.2: Representative SEM images of MNC (a) and porous MNC (b)

Figure 4.3: Representative TEM images of MNC (a and b).

Figure 4.4: Stress-strain profiles (a) of HBPU and MNC as well as cell viability % (b) of heart cells on HBPU and MNC scaffolds

Figure 4.5: Cell adherence on representative MNC (a) and HBPU (b) scaffolds

Figure 4.6: Representing the anti-hemolytic activity % (a) of control, HBPU and MNC as well as cytokine expression (b) in HBPU and MNC treated animals as well as in the control group

Figure 4.7: MG63 cells adhered (a) against time (min) on control, HBPU and MNC3.0 as well as MG63 cells proliferation % (b) against day of incubation with HBPU and MNC3.0

Figure 4.8: Microscopic view of representative histological sections of brain (a and a₁), liver (b and b₁), kidney (c and c₁), heart (d and d₁) and skin (e and e₁) of Wistar rat implanted with MNC3.0 (a-e) and HBPU(a₁- e₁)

Figure 4.9: SEM images (a-c) showing the morphological changes during progressive degradation of representative MNC film, the weight retention % (d) of NC against their incubation period in PBS at regular interval (*p>0.05, **p<0.05 and ***p<0.001) and XRD diffractograms (e) of degraded MNC3.0

Figure 5.1: FTIR spectra (a) and XRD diffractograms (b) of nanomaterials, NC and HBPU

Figure 5.2: FESEM images of Fe₃O₄-MWCNT nanohybrid (a), NNC (b), FNC (c) and MNC (d) as well as TEM images of MWCNT (e), Fe₃O₄-MWCNT nanohybrid (f and g), NNC (h-j at different magnifications), FNC (k) and MNC (l)

Figure 5.3: Representative SEM images of porous NNC3 (a) and drug loaded porous NNC3 (b), NNC2 (c) and NNC1 (d)

Figure 5.4: Representing the fluid handling capacity (a) (light brown indicated the moisture vapor permeability when materials are in direct contact with the fluid) and (b) moisture vapor permeability of HBPU, porous HBPU (PHBPU), FNC, porous FNC (PFNC) MNC, porous MNC (PMNC), NNC and porous NNC (PNNC1, PNNC2 and PNNC3)

Figure 5.5: Representing the cumulative drug release profile (a) of HBPU and NNC and anti-hemolytic activity % (b) of HBPU, NC and the control system

Figure 5.6: Representative antibacterial activities of (a): HBPU (A₁), NNC (B₁), MNC (C₁) and FNC (D₁), (b): drug loaded HBPU, NNC, MNC and FNC as well as (c): drug eluted from NNC at different time interval of 12, 24, 48 and 72 h against *Klebsiella pneumonia* and *Staphylococcus aureus*

Figure 5.7: Microscopic view of the representative skin sections of non-treated (A), standard treated (B), NNC3 treated (C) animal groups showing the hematoxylin and eosin stained epidermis-dermis in A₁, B₁ and C₁ (magnification 100×) and the dermis stained with Masson's trichrome in A₂, B₂ and C₂ (magnification 400×)

Figure 6.1: Representing the FTIR spectra (a), UV-visible spectra (b) and XRD pattern (c) of r-protein, nanomaterials and PNC

Figure 6.2: Representing the TEM images of pristine MWCNT (a), MWCNT (b), PNC0.1 (c) and PNC2.0 (d)

Figure 6.3: Hemolytic activity % (a) of HBPU, PNC and their degradation products as well as of r-protein, MWCNT and mMWCNT (b), MG63 cell proliferation (c) on PNC scaffold and the control as well as MG63 cells differentiation (d) on PNC, MNC, HBPU scaffolds and the control

Figure 6.4: Representing the proliferation and differentiation of MG63 cells on the control (a and b), PNC (c-e), MNC (f and g) and HBPU (h and i)

Figure 6.5: The pictorial representation of the operative procedure: creation of tibial shaft defect (a-c), implantation of the sticky PNC at the fractured site (d and e) and stitching of inner and outer layers (f-h); scale bare=5 mm

Figure 6.6: Representing the radiography of the fractured site of ST (a-f), BT (g-l) and UT (m-r) groups before fracture and at 1st, 15th, 22nd, 60th and 90th days of experiment

Figure 6.7: Cytokine expression (a) on M, P and MM groups of rats after the administration of MWCNT, r-protein and mMWCNT, respectively as well as SEM images showing cross section view of tibia shaft of normal (b) and BT- group (c) after 90 days of post implantation

Figure 6.8: Microscopic view of the respective tibial sections of UT (a and a₁), ST (b and b₁) and BT (c and c₁) groups stained with hematoxylin and eosin stain (a, b and c) as well as Masson's trichrome stain (a₁, b₁ and c₁) after 90th day of experiment

LIST OF SCHEMES

Scheme 1.1: General synthetic scheme for the synthesis of linear and HBPU

Scheme 2A.1: Synthesis of HBPU

Scheme 2A.2: Synthesis of LPU

Scheme 3.1: Probable interactions between HBPU and Fe_3O_4 nanoparticles

Scheme 4.1: Diagram representing the preparation of MNC

Scheme 5.1: Diagram for the preparation of Fe_3O_4 -MWCNT nanohybrid and NNC

Scheme 6.1: Representing the probable interactions between MWCNT and r-protein as well as functionalized MWCNT with HBPU matrix

Chapter 1

General Introduction

Highlights

This chapter provides the general introduction of the present investigation. It includes brief discussion on biomaterials with special emphasis on hyperbranched polyurethane and its nanocomposites. The chapter also describes the importance of biodegradable polymeric biomaterials and the contribution of nanomaterials on their performance. The materials and methods for the preparation of polyurethane and nanocomposite are discussed here. The techniques like FTIR, XRD, TGA, DSC, SEM and TEM including biological testing methods are elaborated for the characterization of such biomaterials. Various physico-mechanical, thermal and biological properties like surface roughness, hydrophilicity/hydrophobicity, strength, ductility, thermostability, biodegradability, cytocompatibility, hemocompatibility including immunocompatibility are also mentioned, briefly. This chapter also provides an insight to the various applications of biodegradable polyurethane and its nanocomposite as biomaterials. The scopes, objectives and plans of the present investigation are also included in this chapter.

Parts of this chapter are ready for communication

Das B., & Karak, N. Biodegradable polyurethane and its nanocomposite in health care research.

1.1 Introduction

The ultimate rationale of any scientific advancement is the improvement of human health and society. Many advances in biomedical research have been made through the multidisciplinary interactions of different branches of science. One of the outstanding spheres that contributed significantly to the scientific improvement is biomaterial science. The encompassment of medical science, chemistry, biology, material science and engineering leads to the evolution of biomaterials.¹ A biomaterial is defined as a “material of synthetic or natural origin in contact with cells or biological fluids, and projected to use for diagnostic, therapeutic, prosthetic or storage applications without adversely affecting the living organism”.¹⁻³ Precisely, the study of biomaterials associated with the living system is known as biomaterial science.^{3, 4} The biomaterials address numerous health related issues like artificial prostheses, regenerative medicine, tissue engineering (TE), drug delivery, cancer therapy and so on.^{1, 2} Thus, the contribution of biomaterials in biomedical realm is sensed considerably. Further, the innovations in material chemistry, nanotechnology and biological sciences with deeper understanding of ‘bio-nano’ interfacial interactions at the molecular level aid to design advanced biomaterials.^{2, 4}

In this context, polymeric biomaterials are significantly more competent than metallic and ceramic based ones due to the tunable and versatile properties of the former.⁵ The flexibility in synthetic route, easy modification, composite formation capability, controllable physico-chemical attributes and easy processing are the few advantages of polymer. In contrast, poor ductility and slow degradation rate of ceramics, and non-biodegradability, toxic issues, corrosion sensitivity, lack of efficient osteointegration, etc. of metallic biomaterials cause great challenges for their practical applicability.⁶ Moreover, in many bio-applications like TE, drug delivery and other medical devices, the non-biodegradable biomaterials are being replaced by the biodegradable one. Thus, biodegradable polymers are gaining a lot of impetus. They avoid the risk of long term biocompatibility and ethical as well as technical issues linked with repetitive surgeries.⁷ Further, they facilitate the host tissues to replace/regenerate the lost or damaged organs. Hence, many innovative strategies are being made to fabricate biodegradable biomaterials with biocompatibility. In this avenue, the use of vegetable oil moiety as a component of the polymeric backbone may address these issues by enhancing such properties.⁸ Moreover, the vegetable oils are renewable, eco-friendly, available in variety of compositions

and structures and are easily modifiable. Hence, the inclusion of vegetable oil based moiety in polymers is a promising approach.

Despite these positive attributes, polymeric biomaterials also suffer from some major disadvantages in the biomedical realm. These embrace insufficient mechanical strength for high load bearing applications, susceptibility to microbial infection, poor bioactivity, low cell adherence ability and uncontrolled degradation.^{9, 10} Therefore these problems can be addressed by fabrication of polymer nanocomposite(s) (NC) using suitable nanomaterials. The excellence of polymer NC lies in the fact that properties of the polymers are improved as well as new features are endowed to them due to the incorporation of nanomaterials.¹¹ NC often shows an exceptional balance between mechanical strength and toughness due to the inherent high surface area to volume ratio of nanomaterials.¹⁰ Thus, the vital properties of biomaterials can be tailored to meet the service requirement by appropriate selection of nanomaterial, correct dose and fabrication technique.

Again, polyurethane (PU) is the most versatile polymer and has emerged as an excellent biomaterial for myriads of biomedical applications. It encompasses some influential properties like superior mechanical, elastomeric, fatigue, compliance, *in vivo* acceptance/tolerance, hemocompatibility, rough surface and biodegradability.¹² These properties are mainly related to its two phasic structures comprising of dispersed hard segment in the continuous soft segment matrix as well as compatible urethane linkages.^{12, 13} PU played a pivotal role in the advancement of many medical devices from catheters to total artificial heart.¹²⁻¹⁴ Moreover, PU structure supports the bulk and surface modification¹³ via hydrophilic/hydrophobic balance by maintaining hard and soft segment content or by immobilizing biologically active agents such as anticoagulants, peptide and so on.¹⁵ These modifications enhance its biological acceptance in many applications including healing device or implant.

Furthermore, the branched polymers have received considerable attention in recent times due to their unique architectural features and useful properties. However, the synthesis of dendrimers (perfectly regular three dimensional macromolecules) requires a controlled synthetic protocol of multistep design and purification step, which restricts their vast utility.¹⁶ On the other hand, single step synthetic protocol based hyperbranched (HB) polymers in spite of having an imperfect skeletal geometry exhibit equivalent properties like dendrimers, especially compact structure with proliferation of surface functionalities.¹⁷ They show high solubility, low melt and

solution viscosity, high reactivity and freely exposed surface groups compared to their linear analogs. Moreover, especially designed HB polymers with long segments show better mechanical strength than the conventional linear polymers.¹⁸ Presence of large number of surface end group has also reported to modulate the bio-interfacial interactions with the cells and the biomolecules, thereby finding applications in the biomedical niche.¹⁹ Again, these surface functionalities help in the homogenous distribution of nanomaterials in HB polymer matrix through strong interaction. Thus, the efficacy of HB PU (HBPU) in the biomedical niche could be appraised by exploiting the advantages of vegetable oil based PU NC together with HB geometry.

The inclusion of nanomaterials in HBPU has the potential to alter the surface chemistry and modify the nanoscale architecture of NC. The tailoring of the physico-chemical intricacies is directly related to the biological performance of biomaterials. Moreover, the creation of nanoscale architecture in polymer NC helps to match the mechanical properties of desired tissues.²⁰⁻²² As reported, the cellular behavior is guided by the surrounding micro/nano-scale environment.^{20, 22} Thus polymer NC based on nanomaterials such as metal oxide nanoparticle, carbon nanotube (CNT), clay, etc. are very interesting topics of research in recent times. Fe₃O₄ nanoparticles have been investigated for a range of applications including drug delivery vehicle, magnetic resonance imaging (MRI) contrast enhancement to cellular therapy.²¹ CNT due to its excellent mechanical toughness, electrical properties and biological properties has also established itself as a prospective nanomaterial to be used in PU matrix for different biomedical uses.²³

Thus, vegetable oil based biodegradable HBPU NC with suitable nanomaterials are appeared to be promising biomaterials for different biomedical applications.

1.2 Historical background

The concept of biomaterials was prevalent from prehistoric period like using of sutures and sea shell as dental implant.^{4, 6, 24} In earlier days crude biomaterials were used without any prior knowledge on biological mechanism of action or biocompatibility.²⁵ Thus, the development of biomaterials progresses with the human civilization. Metals based biomaterials were in used much earlier than polymer based biomaterials.^{4, 26} After the end of Worldwar II, different types of materials (metals, ceramics and polymers)⁴ have been developed, and hence many materials

were used to treat patient in innovative ways for temporary replacement, conduit and even to create artificial organ systems like artificial heart, kidney, hip and knee prosthesis and so on.⁴ Thereafter, some well known materials like silicone, PU, poly(ethylene glycol) (PEG), teflon, hydrogel, hydroxyapatite (HA), bioglass, titanium, poly(lactic-glycolic) acid (PLGA), among many others were designed, especially for biomedical applications.^{4, 27-29}

The journey of polymer in the biomedical domain has started after the discovery of poly(methyl methacrylate) (PMMA) based ocular lens⁴ and polyethylene³⁰ based synthetic implantable material. The first polymer based synthetic suture made up of nylon/dacron was reported probably in 1940s.^{4, 31} The period from 1928 to 1960s, showed the controlled synthesis of many polymers including polyethylene, PU, polyamide and Kevlar (which is stronger than steel) and so on.^{32, 33} After the pioneering works of Staudinger (1920) and Carother on the covalent nature of polymers,^{33, 34} the development of polymer chemistry is still continuing with vast knowledge on role of surface properties, self assembly, etc. along with basic biological concept like cell surface receptor, protein interactions and so on.^{32, 35, 36} Moreover, literature showed the biodegradability and biocompatibility of such materials by studies in animal models.³⁷ The development of biodegradable polymeric disposals, medical devices and scaffold materials made up of poly(glycolic acid), PLGA, PU, polyester, polyester amide, polycaprolactum, etc. have slowed the leap towards degradable biomaterials.^{5, 37-39} However, the first biomedical PU was reported by Boretos and Pierce, where it was used as cannulas and vascular tubing in dogs.⁴⁰ This tubing exhibited no change in mechanical performance, no thrombosis and emboli formation, or induction of tumor. Their work subsequently established PU as a potential biomaterial for cardio-vascular application, artificial organ, ligament construction and so on.^{5, 12, 14, 41}

Again, vegetable oil based PU was also reported as a biomaterial. The first and widely explored vegetable oil for synthesis of PU is castor oil and in 2002, Dongyan et al. reported on vegetable oil based PU NC.^{42, 43} In 2008, Petrovic and co-workers reviewed the transformation of vegetable oil into polyol (chain extender) by hydroformylation, epoxidation, and transesterification⁴⁴⁻⁴⁷ and these polyols were used in preparation of PU. Further, the HB polymers stretched their wings in biomedical zone after the first establishment of HB polypropylene with superior properties (in 1988) over its linear analog.¹⁸ Again, by exploring the concept of the polymer NC (introduced in 1970s)⁴⁸ as an advanced material, plethora of investigations were

carried out on varieties of polymers and nanomaterials to develop different NC.^{11, 49-51} These creative ideas soon translated by the material scientists to develop polymer NC as biomaterials. Fabrication techniques like salt leaching, electrospinning, lyophilization, etc. have been projected eventually to develop NC for TE, drug delivery and so on.^{51, 52} In 2011, Jungebluth et al. transplanted the first engineered airway based on a NC of poly([carbonate-urea] urethane) and polyhedral oligomeric silsesquioxane (POSS).⁵³ The success of such transplantation thus helped to eradicate the need of donor organ. In addition, a large number of reports on PU NC as biomaterials are also found in literature.⁴⁹

1.3 Classification of biomaterial

Biomaterial is intended to repair or replace the damaged or lost tissue, organ or function at interface with the biological systems. Depending upon the types of materials used, biomaterials are categorized as metallic, polymeric, ceramic or composite. Therefore, different types of biomaterials, their properties and applications are briefly presented in this section.

1.3.1 Metal

Metal includes inorganic material comprising non-directional metallic bonds with large numbers of mobile electrons. Metal and metal alloy are used as biomaterials since ancient times. They are strong and can be fabricated into delicate shapes. The attractive attributes like high mechanical strength, high fatigue and wear resistance, easy sterilization and so on, have made them suitable for myriad of applications.⁵⁴ The pros and cons of metallic biomaterials are presented in **Table 1.1**. However, a few vital characteristics of biomaterials like bioactivity, osteointegration, degradation and bioresorbability are difficult to achieve by metals. They are also sensitive to corrosion and leached metal ions are reported to be toxic.^{54, 55} Hence, metallic biomaterials are not preferred in many biomedical applications.

1.3.2 Ceramic

Ceramic is an inorganic material formed by ionic bonds through electron-donating and accepting elements. It is very hard and resistant to degradation. It possesses high compressive strength, high wear and corrosion resistance unlike metals and it can be highly polished. The key advantages of ceramic as a biomaterial are biocompatibility and bioactivity. The chemical

composition of ceramic (especially HA) is similar to the native bone which encourages its use in orthopaedic, dental materials and TE.^{6, 56} However, the brittle nature of ceramic due to the presence of ionic bonds limits their applicability in many domains.^{6, 55} Bioceramic is very difficult to fabricate as well as possesses low fracture toughness, low strength in tension and heavy weight. Thus, the use of pristine ceramic is difficult. The biomedical aspect of ceramic is presented in **Table 1.2**.

Table 1.1: Commonly used metals and alloys in biomedical applications with their pros and cons

Metal and alloy	Application	Advantage	Disadvantage
Stainless steel (SS) ^{6, 54, 57}	Dental prosthesis Orthopaedic fixative plates Vascular stent	Low cost and excellent fabrication Cr oxides leads to passive adhesion Self-healing tendency	Prone to crevices, pitting and corrosion Low wear resistance Allergic reaction
Cobalt-chromium alloys ^{6, 54, 57}	Heart valve Dental prosthesis Artificial joint, etc.	Highly resistant to corrosion, fatigue and cracking Good wear resistant	Release of toxic ions of Cr and Co Harmful to patients
Ti and Ti alloy ^{6, 57}	Artificial heart valve Dental implant Pacemaker cases Joint component	Resistance to corrosion Biocompatible Osteointegration Avoid loosening and failure	Releases toxic ions of Al and Va causes Alzheimer disease and neuropathy
Gold and Platinum ^{6, 57}	Dental filling Electrode for cochlear implants	Biocompatible Inert implant	Expensive Lack of osteo-integration
Shape memory alloy ^{6, 57} (NiTi)	Artificial organ Dental instruments Catheter	High strength and Young modulus closure to bone High fatigue resistance and ductile	Allergic reaction Pneumonia, nostril, lung cancer due to release of Ni

Table 1.2: Commonly used ceramics in biomedical applications with their pros and cons

Ceramic	Application	Advantage	Disadvantage
Aluminium oxides ^{6, 55, 58}	Orthopaedic and dental Joint replacement Implant coating	Biocompatible Intact material structure/strength	Catastrophic failures Femoral fracture Loosening of alumina acetabular cap
Calcium phosphates ^{6, 55, 56}	Dental and orthopaedic implant coating Bone graft substitute Bone cement	Biocompatible Similar composition like bone Osteoconductive Biodegradable	Inability to control pore size Inefficiency for high load bearing applications
Bioactive glasses ^{6, 59}	Dental and orthopaedic implant coating Facial component for reconstruction Bone graft/dental implant	Biocompatible Bioactive Neovascularization ability	Mechanically weak Low fracture toughness
Zirconia ^{6, 55, 58, 59}	Total hip replacement Ball heads Total knee arthroplasty	High mechanical and fracture toughness No mutagenic effect	Low temperature degradation Toxicity

1.3.3 Polymer

Polymer is a giant molecule with repeating units formed by covalent bonds. It is the youngest among all the other categories of materials, but its versatile and favorable properties projected it as the most demanding biomaterial. The polymer is dominating the health care industry with 45-60% of worldwide market.⁶⁰ The unique properties of polymer includes versatility in terms of choosing raw materials, structural manipulation with tailorable properties, light weight characteristic, ease of processing and fabrication, low overall cost and so on.^{33, 34} The flexibility in choosing the starting material is very much facile and hence the finish product can be modulated according to the service requirements. Moreover, the structure and surface properties can also be tuned during its synthesis. This may help to interact favorably with the cells and

tissues upon implantation^{7, 37, 61} and thereby aiding in regeneration of new cells and cellular matrix. The easy strategy for modification of polymer with biomolecules, chemical reagents, micro/nano materials, blending with other polymers, etc. are few other advantages of the polymeric biomaterial over other categories of material.^{7, 34, 61} Thus, it can meet the biomechanical and biochemical requirements of the tissues/organs. The range of biomedically important polymers include both synthetic and natural like poly(α -hydroxy acids), poly(ϵ -caprolactone) (PCL), poly(glycolic acid), PLGA, PMMA, PU, sucrose, cellulose, silk, etc.^{37, 62-65} The list of commonly used synthetic polymers and their different applications are presented in **Table 1.3**. The biodegradable polymer with biocompatibility flourishes as an efficient next generation biomaterial. However, insufficient mechanical strength and bioactivity, poor control over degradation rate and lack of biomimetic structural/compositional features derail its wide utility.⁶⁶

Table 1.3: Commonly used polymers in biomedical applications with pros and cons

Polymer	Application	Advantage	Disadvantage
PMMA ^{55, 67}	Contact lenses Bone cement Denture	Comparable elastic modulus to bone Biostable or bio-inert	Brittle Low tolerance to organic solvent Inability to modify with biomolecules
PU ^{7, 12, 66}	Wound dressing Artificial organ Tissue scaffold Cardio-vascular devices	Tunable property Blood-compatible Biodegradable with no significant pH change	Toxic degraded products Lack of biostability for permanent implants
Poly(dimethyl siloxane), PDMS ⁶⁸	Contact lens Breast implants	Skin protectant Biodurable	Immunogenic activation of anti-silicon antigens

Continue

Polyethylene ^{55, 62}	Orthopaedic joint implant, Component of catheter	Good toughness Resistance to fat and oil	Cannot withstand sterilization temperature
PEG ⁵⁵	Wound dressing Fillers	Hydrophilic Biocompatible Low immunogenic	Insufficient strength High degradation rate
PCL ⁷	Drug delivery Suture and scaffold	Good ductility Biocompatible	Low tensile strength Slow degradation rate
PLGA ^{7, 66}	Resorbable suture Scaffold, bone graft Stents/drug delivery	Biodegradable Easily processable	Degradation products are acidic

1.3.4 Composite

Composite is made up of two or more different materials or phases of micro/macro scale. The nature based composite material includes wood, bone, cartilage, skin, etc. The excellence of these natural composites motivated the scientists to apply this concept in biomaterial sciences. The significance of composite material arises from the fact that the benefit of individual system can be exploited in the combined system, while the poor properties of each are augmented. Generally, the composite of metal-ceramic, ceramic-polymer, polymer-metal and polymer-polymer are investigated as biomaterials. However, the polymer based composites are most frequently used. The biocompatibility and mechanical load bearing ability and vascularization are found to be improved in case of polymer composites.⁶⁹⁻⁷¹ For example, two-component injectable PU composite with tricalcium powder showed improved mechanical and biological properties, as reported by Bonzani et al.⁷² However, in polymer composites the amount of reinforcing material required is high, which causes processing difficulty, inhomogeneous distribution and inefficient interfacial interaction. These hamper the performance of composites, particularly mechanical integrity.^{34, 73}

Under such circumstances, the advent of nanotechnology in biomaterial science is gaining tremendous momentum.^{73, 74} Polymer NC using a suitable nanomaterial is thus in the forefront

of many research strategies. This is due its superior properties compared to the conventional microscale composite.^{2, 9, 10} NC preparation techniques are simple and need inexpensive tools. The polymer NC with nano-HA, CNT, Fe₃O₄, clay, etc. have been reported by researchers to improve biological and mechanical performance of the pristine polymer for biomedical applications.^{73, 75-78} The inclusion of nanomaterial augmented the physico-chemical and bio-interfacial attributes of NC with positive cellular responses.⁷³⁻⁷⁸ However, the positive feedbacks are dependent on good intermixing between the phases. Polymer NC thus sculpted a unique niche of its own in the domain of biomaterial science and hence discussed further.

1.4 Classification of polymeric nanocomposite

Polymer NC is formed by the combination of two phases. The nanomaterials with at least one dimension in nano-regime (generally within 1-100 nm) is dispersed in the continuous polymeric phase.^{2, 34} The nanomaterial due to high aspect ratio and high surface energy confers adequate interaction with the polymer matrix. The presence of different types of interfacial interactions as well as compatibility between these two phases ultimately decides the structure and performance of the polymer NC.

Based on the types of interactions between the polymers and the nanomaterials, these can be classified as intercalated and exfoliated NC.^{11, 34} In intercalated NC, the polymer chains are penetrated within the nanomaterials in a regular crystallographic fashion. Whereas in exfoliated NC, the nanomaterials are delaminated completely into their primary nano-scale sizes and dispersed into continuous polymeric phase. However, based on the mode of mixing, nature of functional groups and extent of interfacial interactions, the nanomaterial may be intercalated, exfoliated or aggregated.³⁴

Again depending upon the dimension of the used nanomaterials, polymer NC can be further classified into three categories. The first category of NC is based on zero dimensional nanomaterial like quantum dots, fullerene, metal oxide nanoparticle, etc. The second category contains one dimensional nanomaterial like nanotube, nanofibre and nanowire. Whereas, NC prepared with two dimensional nanomaterial like nanolayer or nanofilm is included in the third category.

1.5 Materials and methods

There are plenty of polymers and the nanomaterials that are utilized for the preparation of polymer NC. However, as PU based biomaterials have occupied a unique niche, thus the discussion is focused mainly on NC of PU, especially HBPU.

1.5.1 Polyurethane

Thermoplastic elastomeric PU, an important biomaterial comprises blocks of soft and hard segments in an alternative fashion. It is due to good mechanical properties and biocompatibility of such PU.^{12, 13} The raw materials used for the synthesis of PU are macroglycol, diisocyanate and chain extender. The presence of urethane linkages (-COONH) and phase separation are alleged to be responsible for its outstanding biocompatibility. The other linkages present in PU are ester, ether, urea, allophanate, etc. depending on the chain extender and macroglycol used. The physico-mechanical and biological properties of PU can be tailored by choosing the appropriate raw materials at correct proportion.^{12, 13} In this context, renewable resource derived component can also be incorporated as a raw material for the synthesis of PU by considering the seventh tenet of green chemistry.^{44, 79} The most extensively utilized renewable resource based eco-friendly feed stock is vegetable oil. Vegetable oil and its derivatives (di/polyol) are promising components for the synthesis of PU, due to the ready availability, inherent biodegradability and low toxicity.^{44, 80}

1.5.1.1 Diisocyanate


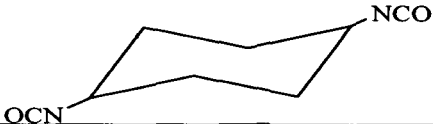
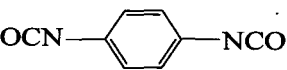
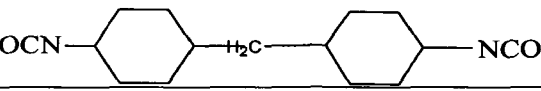
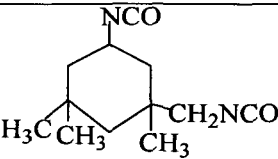
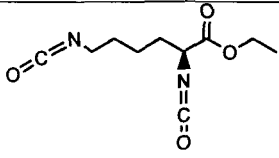
It is the elemental starting material for synthesis of PU. Both aliphatic and aromatic isocyanates can be utilized for this purpose. The aromatic isocyanate is more reactive compared to the aliphatic one.¹² The use of aromatic isocyanate confers better mechanical strength and stiffer PU chains with higher melting point (mp) than aliphatic isocyanate based PU. But aromatic isocyanate based PU is light sensitive and also reported to be toxic to the host after degradation.^{12, 13, 81} Whereas, aliphatic isocyanate based PU is assumed to be low toxic, more resistance to hydrolytic degradation and light stable. Toluene diisocyanate (TDI) and 4,4-diphenylmethane diisocyanate (MDI) are the most common aromatic isocyanates used for synthesis of PU for biomedical applications.^{12, 13} However, literature reported the detection of toluene diamine, a carcinogenic compound in the urine of polyester PU based breast implanted

recipient.⁸² Although, under physiological environment, a minute toluene diamine leached out on the surface of PU implant is ignored by the researchers⁸³ as no correlation between it released and occurrence of cancer was established.¹² The aliphatic isocyanate like dicyclohexyl methane diisocyanate, hexamethylene diisocyanate and lysine diisocyanate (LDI) are also commonly used for preparing PU to be employed as biomaterials.^{12, 13, 66} But, reports suggested that such PU are prone to undergo severe cracks and hence unstable, when implanted to rabbits. Stokes showed that Pellethane™ 2363-55D (MDI based PU) is more stable to surface cracking in comparison to Tecoflex® EG-60D (Methylene bis (p-cyclohexyl isocyanate) based PU).⁸⁴ Greater stability and mechanical strength of aromatic isocyanate based PU is due to the formation of more rigid hard segment, owing to stronger π - π interaction and molecular symmetry.⁸⁵ Different isocyanates used for PU synthesis are presented in **Table 1.4**.

Table 1.4: Important diisocyanates with their structures

Isocyanate	Structure
Toluene diisocyanate (TDI) ⁸⁶	
4,4-Diphenylmethane diisocyanate (MDI) ^{12, 87}	
1,5-Naphthalene diisocyanate ^{12, 88}	
Polymeric methylene diphenyl diisocyanate ⁸⁹	
3,3- Dimethyl diphenyl methane diisocyanate ⁸⁸	
Methylene bis (p-cyclohexyl isocyanate) ^{12, 84}	

Continue

Norbornane diisocyanate ⁸⁸	
Cyclohexyl diisocyanate ^{12, 90}	
p-Phenylene diisocyanate ⁹¹	
Dicyclohexyl methane diisocyanate ^{88, 90}	
Hexamethylene diisocyanate ⁸⁸	$\text{OCN}-(\text{CH}_2)_6-\text{NCO}$
Isophorone diisocyanate (IPDI) ^{12, 90}	
Lysine diisocyanate (LDI) ¹⁴	

1.5.1.2 Macroglycol

The macroglycol is the integral part for the synthesis of PU and it represents the soft segment. The molecular weight (M_w) of it generally lies between 400-5000 g/mol. Macroglycol includes the diols of polyester, polyether, polycarbonate, hydrocarbon and PDMS.¹² Different macroglycols that are mostly utilized for synthesis of PU are listed in **Table 1.5**. However, the polyester and polyether based macroglycols are mostly preferred. It provides flexibility to the entire PU chain, wherein the hard segments remain dispersed. The polyester based PU is susceptible to hydrolytic cleavages in physiological environment and also exhibits good physico-mechanical performance.^{12, 85} Poly(ϵ -caprolactone) diol (PCL) is used extensively as the component for soft segment for biomedical PU.^{38, 92, 93} A biodegradable PCL based PU NC was reported using POSS for TE.⁹⁴ This is due to the fact that PCL is biocompatible and it possesses

long alkyl chain that aids in the good performance of PU as biomaterials, especially for TE and drug delivery applications. Cardiothane 51 (based on PDMS as polyol) is used in catheter, artificial heart, blood tubing and so on.⁹⁵ Polyether based PU is more resistant to degradation and hence used to fabricate heart valve, artificial organs, etc., where the long term bio-stability is required.^{12, 85}

Table 1.5: Important macroglycols and their structures

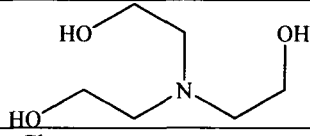
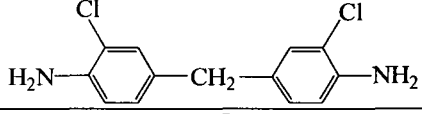
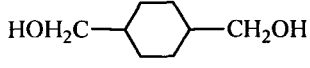
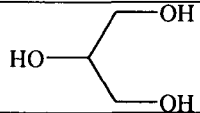
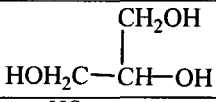
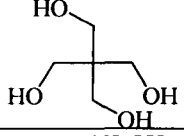
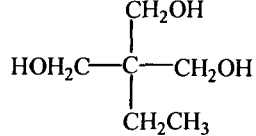
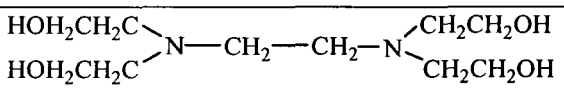
Macroglycol	Structure
Poly(ϵ -caprolactone)diol (PCL) ^{92, 93}	
Poly(ethylene glycol) (PEG) ⁹⁶	
Poly(propylene oxide) ¹²	
Poly(tetramethylene adipate) ¹²	
Polyhydroxyl ⁹⁰	$\begin{array}{c} \text{CH}_2\text{-OROH} \\ \\ (\text{CH-OROH})_x \\ \\ \text{CH}_2\text{-OROH} \end{array}$ <p>Where x=1 for triol, and x=6 for hexol</p>
Hydroxy terminated poly(1,4-butadiene) ¹²	
Hydroxybutyl terminated poly(dimethylsiloxane) (PDMS) ¹²	
Poly(ethylene adipate) ¹²	
Poly(hexamethylene carbonate glycol) ¹²	
HB polyol ^{81, 97}	<p>X = </p> <p>Y = </p>

For example, poly(tetramethylene oxide) is used in PU like Pellethane® 2363 80A and Elasthane™ 80A⁹⁸ However, when environmental stability is the criteria then poly(alkyl glycol)s are the preferred polyol. Thus, the choice of macroglycol is an essential criterion to tune the ultimate properties of PU. HBPU have also been reported to be synthesized using dendritic polyol moieties like commercialized Boltorn™ (HB polyester polyol). Petrovic et al. reported the synthesis of soybean oil based HB polyol pre-polymer by reacting hydrogenated epoxidized soybean oil and hydroformylated polyol with dicyclohexyl methane diisocyanate or adipoyl dichloride.⁴⁴

1.5.1.3 Chain extender

Chain extender together with diisocyanate accomplishes the hard segment of PU structure. Chain extender is the low M_w component (below 400 g/mol, generally) that provides rigidity to PU. Both aromatic and aliphatic diols as well as diamines are used as chain extenders.^{12, 93} It generally extends the hard segment and increases the overall M_w of PU along with increased hydrogen bond density. The incorporation of multifunctional chain extender results in the formation of highly branched PU network. Chain extenders such as ethylenediamine and 1,4-butandiol (BD) are generally used in PU formulations.^{12, 93} Diamine reacts rapidly with diisocyanate and form PU-urea and the latter further produces crosslinked polymer with biuret linkages.¹² Biomolecules based chain extenders like amino acids, have also been used during synthesis of PU as they have functionalities like amine, hydroxyl and carboxylic groups.⁹³ These types of chain extenders are utilized to synthesize biodegradable and biocompatible PU. In 2010, Parrag and Woodhouse reported a biodegradable PU, where dipeptide (Glu-leu linkages) was used as a chain extender.⁹⁹ However, for biomedical purpose, a combination of BD and MDI is generally used as a hard segment.^{85, 100} Recently an X-ray opaque non-cytotoxic PU based on iodinated hydroquinone bis(2-hydroxyethyl) ether as the chain extender was reported.¹⁰¹ Zhang et al.¹⁰² depicted the effect of chain extenders like BD and 2,2'-(methylimino)diethanol on the hydrophilicity, mechanical properties and cytophilicity of biodegradable PU (based on PCL and MDI). The 2,2'-(methylimino)diethanol based PU showed better hydrophilic nature, elongation and fibroblast adhesion compared to BD based PU. Thus depending on the application, type of chain extender plays an important role for PU formulation. The chain extenders commonly used for synthesis of PU are listed in **Table 1.6**.

Table 1.6: Important chain extenders with their structures

Chain extender	Structure
1,4-Butanediol (BD) ^{86, 87}	$\text{HO}-\text{CH}_2-\text{CH}_2-\text{CH}_2-\text{CH}_2-\text{OH}$
Ethylene glycol ¹²	$\text{HO}-\text{CH}_2-\text{CH}_2-\text{OH}$
1,6-Hexanediol ¹²	$\text{HO}-\left(\text{CH}_2\right)_6-\text{OH}$
Diethylene triamine ¹⁰³	$\text{H}_2\text{N}-\text{CH}_2-\text{CH}_2-\text{NH}-\text{CH}_2-\text{CH}_2-\text{NH}_2$
Ethylenediamine ⁹⁸	$\text{H}_2\text{N}-\text{CH}_2-\text{CH}_2-\text{NH}_2$
Amino ethanol ⁸⁸	$\text{H}_2\text{N}-\text{CH}_2-\text{CH}_2-\text{OH}$
Triethanol amine (TEA) ⁸⁶	
4,4'-Methylene bis(2-chloroaniline) ¹²	
1,4-Cyclohexane dimethanol ⁹⁰	
Glycerol ⁸⁷	
1,2,3-Propanetriol ⁸⁸	
Pentaerythritol (PE) ¹⁰⁴	
Trimethylol propane ⁸⁸	
N,N,N,N-Tetrakis (2-hydroxyethyl) ethyl diamine ⁸⁹	

1.5.1.4 Vegetable oil

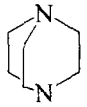
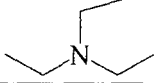
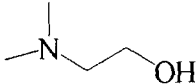

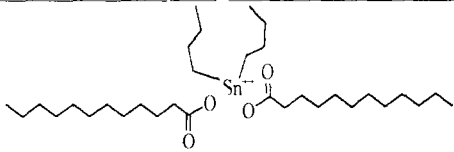
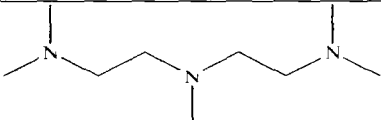
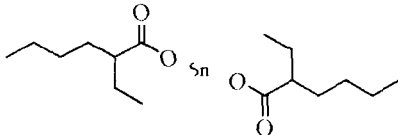
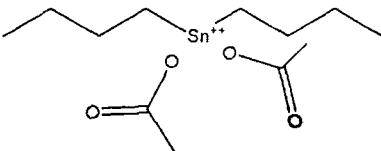
The global focus on sustainable environment and depletion of petroleum based resources entail the use of renewable resources. Thus vegetable oil, an eminent green resource is extensively utilized to synthesize PU. It is the triglyceride of long chain fatty acids. The amalgamation of

varied types of fatty acids results in different triglycerides, but for a particular oil the fatty acid composition is generally fixed. Vegetable oils employed for synthesis of PU have been derived from soybean, linseed, palm, kernel oil, sunflower, nahar and so on.^{86, 96, 105-108} The oil is converted into monoglyceride (MG)/polyol and then utilized as a component for synthesis of PU.^{44, 86, 96, 107} This is commonly achieved by using the chemical routes like transesterification, epoxidation, alkoxylation and hydroxyformylation. Among these methods, transesterification is mostly used, where vegetable oil is reacted with polyfunctional ols like glycerol and is catalyzed by base, acid or enzyme.^{44, 87, 106} Further, vegetable oil of *Ricinus communis* can also be used directly as a feedstock for synthesis of PU. In one of the reports, *Ricinus communis* oil derived MG based PU was found to exhibit better performance than the unmodified same oil based PU.¹⁰⁹ Recently a *Vernicia fordii* oil based biodegradable PU composite was also investigated.¹¹⁰ Similarly, *Mesua ferrea*, *Ricinus communis* and *Helianthus annuus* oils based MG are used as the bio-based chain extenders to synthesize HBPU.^{86, 87, 96, 107} The incorporation of vegetable oil based moiety showed to improve the biodegradability of HBPU. Other properties like the flexibility of HBPU is also reported to be improved.⁴⁴ Though plenty of literature cited the significance of vegetable oil for preparation of HBPU and liner PU , but vegetable oil based HBPU is not explored extensively as a biomaterial.

1.5.1.5 Catalyst

Isocyanate, especially the aromatic one is highly reactive, but low temperature synthesis requires the use of catalyst. It is noteworthy that the reaction rate decreases rapidly when the steric hindrance of the substitute on higher polyols increases, thus in such cases catalyst is required for the synthesis of PU.¹² Moreover, catalyst is required for the synthesis of low reactive aliphatic isocyanate based PU. The commonly used catalysts for assisting urethane bond formation are mild and strong bases or organometallic compounds. The pioneering investigation on such catalysts was studied by Baker and co-workers.^{111, 112} They used tertiary amine based catalyst.^{12, 97} Different catalysts used for synthesis of PU are provided in **Table 1.7**. Lenz reported that tertiary amines aid in the complexation of amine with isocyanate followed by reaction with hydroxyl groups to form urethane bond.¹¹³

Table 1.7: Important catalysts with their structures

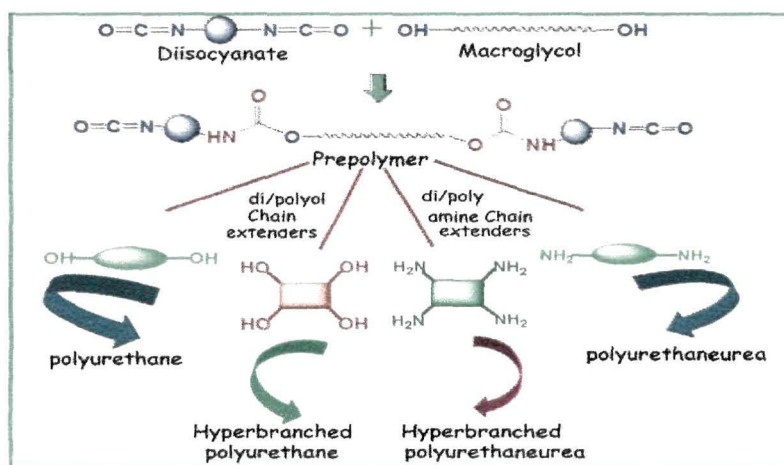
Catalyst	Structure
Cyclo-triethyldiamine ⁸¹⁻⁹⁷	
Triethylamine ⁸¹⁻⁹⁷	
Dimethylethanol amine ⁸¹⁻⁹⁷	
Dimethylcyclohexyl amine ⁸¹⁻⁹⁷	
Dibutyltin dilaurate (DBTDL) ⁸¹⁻⁹⁷	
N,N,N',N',N''-Pentamethyldiethylene triamine ⁹⁰⁻⁸⁷	
Tetravalent tin compound ^{90, 87}	$R_nSnX_{(4-n)}$ <p>where R=alkyl, aryl etc and X= halogen/ carboxylate group</p>
Stannous octoate ⁸¹⁻⁹⁷	
Dibutyltin diacetate ⁸¹⁻⁹⁷	

Organometallics based on mercury, lead, tin and zinc are reported to be effective catalysts for urethane reaction¹¹³⁻¹¹⁴ However, the best catalysts are considered to be organotin compounds like dibutyltin dilaurate (DBTDL), dioctyltin mercaptide, dibutyltin oxide and stannous octoate¹²⁻⁹⁷ DBTDL is used most often for the synthesis of PU However, concern for using catalysts for biomedical applications is their alleged toxicity¹²⁻¹¹⁴ Spurred by this, Tanzi et al¹¹⁴ investigated the cytotoxicity aspect of four catalysts namely DBTDL, stannous octoate, tetramethylbutanediamine and triethylenediamine All of them were found to be cytotoxic,

though the level of toxicity decreased from DBTDL to triethylenediamine. Therefore for biomedical purposes, if the use of catalyst is unavoidable then it should be eliminated from PU before processing. Thus, two step synthesis of PU is appreciated as use of catalyst can be circumvented and thus the conventional fabrication technique can be used.

1.5.1.6 Synthetic method

PU reaction is referred as a rearrangement reaction and it is propagated through step growth mechanism.^{12, 34} However, during this polymerization process, generally no small molecule is eliminated. PU can be synthesized by means of single and multistep processes, but the two-step process is preferred for the synthesis of biomedical PU. This process is also known as pre-polymerization technique. In synthesis of HBPU, during polymerization process generally a branch generating moiety with more than two functionalities is incorporated as a chain extender. A general scheme for synthesis of PU (both linear and HB) is shown in **Scheme 1.1**.



Scheme 1.1: General synthetic scheme for the synthesis of linear and HBPU

The HB polymers are synthesized by two different methodologies.^{17, 18, 34} In single monomer methodology, AB_n or latent AB_n monomers (where, 'A' and 'B' are two mutually reactive functionalities and 'n' denotes number of functionalities) are polymerized. While in double monomer methodology, HB polymers are synthesized by using two different monomers. Again, this methodology can be subdivided into two groups. The first subclass includes direct polymerization of A_x and B_y (x and $y \geq 2$), whereas in second one, monomer pairs are formed *in*

nanomaterials are of different types and according to their dimensions they are classified as zero, one and two dimensional nanomaterials. The entry of nanomaterial into the biomedical world has bestowed new, fascinating and desired properties to the existing biomaterials. A brief discussion on different categories of nanomaterials and their role in biomedical domain is presented here. The emphasis is given on the pivotal contributions of Fe_3O_4 and CNT in biomedical domain.

1.5.2.1 Zero dimensional

Zero dimensional nanomaterial is represented by nanoparticle, nanoclusture and nanocrystal.¹²⁰ It is the simplest among other types of nanomaterials and all the dimensions of it ranges within the nano-regime. The term nanoparticle is usually used to include all the zero dimensional nanosized materials. Generally, amorphous/semicrystalline nanoparticles with size distribution less than 1-10 nm are referred to as nanocluster, whereas crystalline zero dimensional nanomaterials with a crystalline region are termed as nanocrystal. In general, the nanoparticles are obtained by different routes such as chemical precipitation, sol-gel process, hydro/solvo-thermal synthesis, micro-emulsion, pyrolysis, vapor deposition and so on.^{34, 120, 121}

Quantum dot is a special case of nanocrystal, which is made of semiconductor material. Extensive researches attested its utilization in cell trafficking and imaging, tumor targeting and diagnosis.¹²² This dot could replace the radioactive markers and dyes conventionally used for labeling and visualizing technique of biomolecules because of its photo-bleaching stability and high luminescent nature. Yaghini et al. also reported the conjugation of quantum dot with photosensitizers and targeting agents for both diagnostic imaging and photodynamic therapy in treating a range of malignant tumors and certain non-malignant pathologies.¹²³ However, the alleged toxicity of quantum dot is a prime issue.¹²²

Fullerene, an allotrope of carbon is the first discovered zero dimensional nanoparticle. It is used in biological realm as MRI agent, chemotherapy, photothermal therapy, etc. due to its immunostimulatory, anti-angiogenesis and oxidative stress modulation capability.¹²⁴ The amino acids functionalized fullerene can be made to be absorbed by cancer cells (HeLa cell line)¹²⁵ and can selectively kill the malignated cells by triggered light radiation. But *in vivo* toxicity and non aqueous solubility of fullerene is a concern.

Similarly, metal and metal oxide nanoparticles like iron oxide, Ag, Au and Co are the other important zero-dimensional nanomaterials for biomedical uses. Their simple synthetic

situ from their monomers intermediates. Kumar and Ramakrishnan reported synthesis of HBPU through *in situ* formation of AB₂ monomer, 3,5-dihydroxyphenyl isocyanate using carbonyl azide as a precursor.^{115, 116} Hong et al. also reported the synthesis of HBPU by using the same approach from 3,5-dihydroxybenzoic acid through *in situ* generation of the dihydroxy isocyanate monomer by thermally decomposing the azide precursor.¹¹⁷ Due to the high reactivity of isocyanate groups towards nucleophile, HBPU cannot be directly synthesized from AB₂ monomer and such approaches are generally followed by using carbonyl azide precursor as a protective functional group. But this approach offers some complexity in the synthesis as well as purification steps. Therefore, A₂+BC_n approaches (where, 'C' is an another reactive functionality) are generally preferred over the aforementioned approach by using commercially available diisocyanates and poly/diol or hydroxyl amines.¹⁸ Rannard et al. reported the synthesis of water soluble HBPU through the selective activation of A of the unprotected AB₂ amino-diol monomer by incorporating 1,1'-carbonyl diimidazole.¹¹⁸ The active monomer further undergoes self condensation to form HBPU. Totally aromatic HBPU has also been reported to form by self condensational of AB₂ and A₂B monomers. Jena et al. synthesized HBPU by a different approach as they first synthesized HB polyesters using 2,2-bis(methylol propionic acid) as an AB₂ monomer using different core moieties (PE, trimethylol propane and glycerol) and reacted them further with excess IPDI followed by exposure to atmospheric moisture to get HBPU.¹¹⁹

Similarly, vegetable oil based HBPU were synthesized by using A₂+B₃ approach. Using this approach, Kalita and Karak recently synthesized bio-based HBPU via two step one pot reaction using TEA as the branch generating units.⁸⁶ The same group also reported the synthesis of HBPU using glycerol as the B₃ monomers.⁸⁷ Karak et al. again synthesized *Helianthus annuus* oil based HBPU using *s*-triazine containing HB polyether polyol for the formation of HB architecture.¹⁰⁷ HBPU was also synthesized utilizing the triglyceride of ricinoleic acid (*Ricinus communis* oil) as a B₃ monomer and isocyanate terminated pre-polymer as the A₂ monomer.⁹⁶ Besides these cited examples, ample of literature reported the synthesis of vegetable oil based HBPU using different approaches.

1.5.2 Nanomaterial

The nanomaterial is the most important component of polymer NC. The ultimate properties of polymer NC depend on the nature and surface chemistry of the incorporated nanomaterial. The

protocols add to the charm. Ag nanoparticles, due to their microbicidal activity have made their own niche as important biomaterials as wound healing bandage, coating on biomedical devices, arthroplasty, stent, etc.^{126, 127} Ag nanoparticles based HB polymer NC have been reported to confer antibacterial activity.^{127, 128} Ag ions can bind to bacterial proteins, causing structural alteration in bacterial cell membranes and denatures bacterial DNA and RNA by generation of free radical species (ROS).¹²⁹ However, reports also expressed concern on its associated side effects like delaying of re-epithelialization, staining of skin, toxicity and hindrance of some cellular mechanisms.¹³⁰

Therefore, researchers shift their interest on other nanoparticles like iron oxide. They are of two forms namely magnetite (Fe_3O_4) and maghemite (Fe_2O_3). However, the profound biocompatibility, superparamagnetic nature and antibacterial activity of Fe_3O_4 make it a strong candidate in MRI, drug targeting, biomedical devices like catheter, hyperthermia, TE, etc. applications.^{20, 131} Fe_3O_4 has inverse spinel structure where oxygen forms the face centric cubic crystal structure and the octahedral sites are occupied by Fe^{3+} and Fe^{2+} , whereas the tetrahedral site is solely occupied by Fe^{3+} . There are various routes to prepare iron oxide nanoparticles like arc discharge, microemulsion, mechanical grinding, co-precipitation, laser ablation, microwave, etc.²⁰ Weissleder et al. depicted the utility of Fe_3O_4 as a non-invasive MRI agent to visualize transgenic expression. Human holo transferrin was coupled to Fe_3O_4 and changes in MRI signal observed, when receptor level increased on cell surface.¹³² In a similar approach, conjugated Fe_3O_4 with second component of human complement protein (C_2) that binds to the plasma membrane of apoptotic cells, was investigated.¹³³ Thus, C_2 - Fe_3O_4 conjugate can detect tumor containing apoptotic cells region by increasing the MRI image contrast significantly. Recently, Anghel et al. demonstrated the potential of eugenol and limonene modified Fe_3O_4 as an effective component of wound dressing.¹³⁴ The dressing showed both anti-biofilm adherent (due to Fe_3O_4) as well as microbicidal activity owing to the presence of oil. The bactericidal activity of Fe_3O_4 against *Staphylococcus aureus* has also been demonstrated.¹³⁵ They postulated that the generation of ROS and nano-structural form to be responsible for this bactericidal effect. Silva et al. reviewed the potentiality of Fe_3O_4 induced hyperthermia for treatment of cancer like malignant glioma.¹³⁶ Jordhan et al. showed that aminosilica magnetite uptake was 10 times higher by glioblastoma cells than by normal glial cells.¹³⁷ Dextran-magnetite potential for oral cancer hyperthermia was demonstrated by employing temperature between 43-45 °C using AC

current.¹³⁸ Moreover, plenty of literature showed enhanced performance of Fe₃O₄ based polymer NC in multitude of applications including shape memory biomaterials.¹³⁹

1.5.2.2 One dimensional

Two dimensions of one dimensional nanomaterial fall within the nano-regime, whereas the third dimension is in micrometer range. As a consequence, it includes needle shaped materials like nanorod, nanowire, nanofibre and nanotube.¹²⁰ The techniques used for synthesis of such nanomaterials include wet chemical, vapor-liquid-solid approach, mechanical alloying, cation exchange, arc discharge, laser ablation, suspension, vapor/electro-chemical deposition and catalytic decomposition.¹²⁰ Typical examples are ZnO, Au and Ag nanorods. In biomedical domain, they are extensively investigated as cancer therapeutics. Nanorod, mainly the Au nanorod can be conjugated with tumor targeting motifs to reach inside the tumor site.^{140, 141} It absorbs IR light to generate local heat and thereby destroying only the cancerous cells. It is also useful to deliver drug and detect targeting sequences of infectious agents. However, it is expensive.

Unlike nanorods with rigid side wall, nanowire, nanofibre and nanotube possess interwoven array.¹²⁰ Other than electrical and optical applications, nanowire is used as biosensor, drug delivery, detector for cancer marker and so on.^{142, 143} Among others, silicon nanowire as well as carbon and polyaniline nanofibres find lots of applications in TE, drug delivery, orthopaedic, etc.^{142, 143}

The nanotubes with hollow core are different from other types of one dimensional nanomaterial. Among others, CNT is the most studied and important nanotube. This is due to its excellent mechanical, chemical, electrical and biological attributes.^{23, 120} It is the allotropes of carbon having sp² hybridized carbon atoms, arranged in rolled up graphite sheet. These sheets are rolled up into specific and discrete angles. Depending up on number of graphene layers, CNT is classified as single-walled CNT (SWCNT) and multi-walled CNT (MWCNT). It has very high aspect ratio and high surface energy that contribute to their extra-ordinary performance. It is mainly prepared by arc evaporation, pyrolysis, laser ablation, electrochemical and chemical vapor decomposition methods.^{120, 144} CNT is getting myriads of applications in drug and gene delivery, TE, cancer therapy, bone grafts, biosensors and so on.^{23, 145} In drug delivery system, CNT hosts the drug molecules by adsorption or immobilization, improves the stability of the

biomolecules and protect them from chemical/enzymatic degradation.¹⁴⁵ Moreover, CNT has contributed significantly in TE, especially for bone and nerve tissue regeneration. It is similar in size to the triple helical fibrils of collagen, an important component of extracellular matrix (ECM).¹⁴⁶ This similarity is believed to aid in the mineralization and crystallization of HA on CNT. Further, the degree of porosity including high contact surface area of CNT is similar to ECM. Thus, it is regarded as the most potent nano-biomaterial for bone TE.¹⁴⁶ Reports suggested its potency to support the adherence as well as proliferation of osteoblasts by increasing the level of alkaline phosphatase (ALP). CNT also reported to stimulate the activity of brain circuit and increase the synaptic activity of hippocampal neurons. Hu et al. demonstrated the controlling of outgrowth and branching pattern of neurons by tuning the surface charge of CNT.¹⁴⁷ It is also utilized as a non-viral molecular transporter for release of short interfering RNA.¹⁴⁸

However, inert surface, lack of solubility/dispersability, surface toxicity, presence of metal contaminants, agglomeration and immunogenic nature vouched for the surface functionalization of CNT. Thus, it is functionalized by various non-covalent and covalent routes.¹⁴⁹ Most commonly, carboxyl and amine groups are introduced on the surface of CNT through covalent approach and these groups are reported to attract calcium ions. Further, the addition of phosphate and hydroxide ions on calcium ion deposited functionalized CNT, a chemical composition similar to calcium phosphate can form.¹⁵⁰ Moreover, surface modification with biomolecules (peptides, proteins and carbohydrates) has found to bestow biocompatibility and biological activity to the pristine CNT.¹⁵¹ This modification is also carried out by covalent, non-covalent and hybrid approaches. The covalent modification by biomolecules is generally done on carboxyl or amine functionalized CNT. The non-covalent modification depends on the electrostatic or hydrophobic interactions between the biomolecules and aromatic (π -electrons) hydrophobic surface of CNT. It was also reported that the integration of CNT with polymers notably decrease its toxic effect. Moreover, Kagan et al. in 2010 postulated the degradation of CNT by human neutrophil enzymes myeloperoxidase.¹⁵² The degraded nanotubes did not elicit any inflammatory response in the tested mice. Therefore, these studies encourage to explore CNT in the biomedical domain.

1.5.2.3 Two dimensional

Two dimensional nanomaterial with only one dimension in nano-regime appears to be a plate like nanostructure. It can be either amorphous or crystalline and includes nanolayer, nanocoating and nanofilm.¹²⁰ The most commonly investigated two dimensional nanomaterial are graphene based nanomaterial and nanoclay. Graphene is a one atom thick sp^2 hybridized carbon atoms packed in a honeycomb crystal structure. It has high surface area, strong mechanical strength, notable biocompatibility and easy functionalization ability. Literature shows the potent applications of graphene in biomedical fields such as biosensor (for glucose, dopamine, etc.), drug delivery, bio imaging, protein and DNA detection and so on.¹⁵³ Moreover, graphene oxide (GO) possesses lots of oxygen containing functionalities and therefore it can be efficiently attached to drugs and ligands, photothermal agent, antibacterial material and so on.^{153, 154} However, the safety issue of graphene related to environment and human health is necessary to investigate.

Again, nanoclay is the most widely investigated nanomaterial considered for the formation of polymer NC including biomaterial.^{155, 156} It is nanolayered aluminosilicate inorganic nanomaterials and has high aspect ratio. Montmorillonite (MMT), saponite and hectorite are the most commonly used nanoclays. They are the natural cationic exchanger and can undergo ion exchange with basic drugs, as a consequence MMT and saponite are generally used as drug carrier.¹⁵⁵ Layered double hydroxides can also be used in drug carrier systems as it has positive charged layer and thus can host negatively charged biomolecules. Nanoclay based polymeric NC has been reported to be used as a scaffold for TE.¹⁵⁶

Besides the above, other nanomaterials employed for preparation of NC includes cellulose nanofibres, nano-HA, whiskey, Cu nanoparticles, Ag nanorods, etc.

1.5.3 Preparative technique for polymer nanocomposite

The fundamental goal in the preparation of polymer NC is homogeneous dispersion of nanomaterials into the polymer matrix with good interfacial interactions to achieve thermodynamically stable high performing material. The level of intermixing influences the extent of interfacial interaction between them which is co-linked to the performance of the biomaterials. Thus, the applied technique indeed plays a significant role in designing of biomaterial. Techniques used for the preparation of polymer NC are thus discussed underneath.

1.5.3.1 Solution

This method uses suitable solvent to swell and disperse the nanomaterial. The nanomaterial is then mixed into the polymer solution by vigorous mechanical shear and ultrasound energy. This technique generally provides intercalated NC.^{11, 34} The mobility of soluble polymer chains eventually replaces the solvent molecules, thereby decreasing the entropy of the mixture owing to the confinement of polymer chains within the nanomaterials. However, this is compensated by desorption of solvent molecules which increases the entropy, the driving force for the intercalation of nanomaterials. The work on solution based NC was illustrated by Chen et al.¹⁵⁷ SWCNT/PU NC was prepared using tetrahydrofuran as the solvent and authors observed good orientation of the nanotubes in the matrix. Recently, Kalita and Karak¹⁵⁸ also reported MWCNT/bio-based HBPU by solution polymerization technique with good interfacial interaction between the polymer and the nanotubes. In another report, epoxy modified clay/HBPU NC was prepared using solution technique as a prospective biomaterial.¹⁵⁹ Well distributed partially exfoliated nanoclay was observed in the HBPU matrix. Magnetic nanoparticles based PU NC was also prepared by employing this technique.¹⁶⁰ However, the limitation of this technique in commercial scale is the utilization of large amount of organic solvent which is environmentally hazardous and non-economical.³⁴ Moreover, the appropriate choice of solvent, high VOC and toxicity issue are the major concerns for biomedical uses. However, for water soluble polymers, it is an efficient and attractive route.

1.5.3.2 *In situ* polymerization

It is the most preferred technique for the formation of polymer NC. The polymer precursor/pre-polymer is polymerized in presence of the nanomaterials. This allows the expansion/dispersion of the nanomaterials by insertion of the polymer chains into the nanomaterials.³⁴ Due to the low viscosity of the monomer/pre-polymer, the mixing and breaking up of the agglomerates are easy and thus it results in homogenous dispersion of nanomaterials within the matrix. *In situ* technique is well accepted for the formation of CNT based NC as it allows uniform dispersion of nanotubes into the monomers/pre-polymer and polymer chain can be grafted into their side walls. MDI based PU NC foam was prepared by reacting the monomers in the presence of MWCNT.¹⁶¹ Porous nano-HA/alcoholized castor oil based PU NC and electroactive shape memory PU/CNT NC with good interfacial interactions were also prepared by *in situ* technique.^{162, 163}

Again, Chen et al. prepared polyester based nano-SiO₂/PU NC by this technique.¹⁶⁴ The polyester polyol with nano-SiO₂ was reacted with IPDI by *in situ* polymerization to form strong chemical linkages between polymer and nanoparticles. Graphene/PU was also prepared by *in situ* polycondensation of MDI and poly(tetramethylene glycol) in presence of the graphene sheets using ethylene glycol as the chain extender.¹⁶⁵ Further, GO and Ag nanoparticles/HBPU NC were prepared with efficient dispersion of the respective nanomaterial in HBPU due to the combined effect of branched morphology and the use of *in situ* polymerization technique.^{128, 166}

1.5.3.3 Melt mixing

Mechanical mixing of molten polymer and nanomaterials either under static or shear condition usually by implying extrusion or kneading or injection molding is carried out in this technique.³⁴ In molten state of polymer, the nanomaterial gets efficiently dispersed into the matrix to form intercalated or exfoliated NC. However, this technique is considered less efficient than the above two techniques. But for industrial application, this technique is preferred as it does not require solvent and is thus, safe to health and environment. It is widely used for clay based polymer NC. Barick and Tripathy reported the formation of organoclay/PU NC by employing melt mixing technique.¹⁶⁷ They demonstrated that melt mixing is an efficient technique to disperse organoclay in the polymer matrix. Chun et al. also reported MMT/PU NC together with a compatibilizer to augment the dispersion of MMT in a twin screw extruder by using this technique.¹⁶⁸ Generally, the temperature is kept below the decomposition temperature of the involved components of NC as higher temperature can degrade the polymer. Thus, for biomolecules immobilized or drug loaded polymeric system, this technique is not preferred.

Besides the above methods, the other techniques used for NC formation are template synthesis, sol-gel process, thermal spraying, plasma induced polymerization, milling, etc.

1.5.4 Fabrication of polymeric biomaterials

Biomaterials (like medical devices/permanent implant/scaffold) are necessary to process and fabricate for a specific application. The fabrication is generally sub divided into three processes which is discussed briefly in this section.

The first one is one dimensional process used in coating and adhesives applications.¹² PU coating by solvent casting technique requires relatively polar solvent with low boiling point (bp)

like tetrahydrofuran.¹² For implant coating the solvent should be removed carefully before use. The wettability of the substrate is also an important factor as it affects the coating quality. Therefore, the surface is etched by employing liquid or plasma etching or by electrical discharge. This is followed by coating process via static dipping or inflow of coating solution.

On the other hand, two dimensional fabrication is carried out by extrusion, fiber spinning and lamination.^{6, 12, 34} In extrusion, a screw is rotated to force the polymer fluid through a die that shapes the final products (tubing, rods, flat film, etc.). In fiber spinning, molten polymers are pumped through a spinneret and thus single polymeric fiber come out from each hole and solidify in air. Now-a-days electrospinning technique is commonly used to prepare PU nanofibers for biomedical uses. In this technique, a polymer jet is ejected and stretched due to the applied electric field.¹⁶⁹ Eventually, the diameter of polymer jet is decreased with the increase in its length followed by solvent evaporation and the fibers get deposited in a collector. Electrospun PU and their NC are extensively researched for TE, implantable glucose sensor and wound dressing materials.^{170, 171} Rockwood et al. in 2008, reported PCL based PU scaffold by electrospinning technique by dissolving PU in dichloromethane.¹⁷² Hashizume et al. designed a biodegradable PU scaffold by wet electrospinning technique for abdominal wall replacement, where the fibres were deposited at the same time with electrosprayed serum culture medium.¹⁷³

Again, the three dimensional fabrication of polymeric biomaterials is also one of the most important techniques for biomedical applications for making tubing, foam, balloons, bladder or porous scaffolds.¹² Among three dimensional processes like molding, sheet forming, weaving, knitting, etc., the fabrication of the three dimensional porous architecture is the pre-requisite for TE applications and hence discussed here.^{6, 12} **Table 1.8** listed the pros and cons related to each technique used for the fabrication of porous biomaterials. There are various techniques to form interconnected porous architecture for polymers and their NC. The commonly used fabrication techniques¹⁷⁴⁻¹⁷⁶ are described beneath.

Solvent-casting and particulate-leaching: A uniform suspension of polymer and sieved particulates (like sodium chloride crystal, sodium tartrate and sodium citrate) of required diameters is prepared. After proper mixing, the medium is allowed to evaporate, followed by removal of particulates by immersing in another appropriate medium (generally water). Using this technique, geometry like tube, nose and other specific organs can be designed.

Gas foaming: The polymeric matrix is saturated with CO₂ gas and then allowed to a sudden expansion of the gas by decreasing the solubility. This results the formation of a spongy structure due to the nucleation and simultaneous growth of gas bubbles in the polymeric matrix.

Phase separation: Here, homogenous multicomponent polymeric system becomes unstable thermodynamically and forms phase separation (polymer rich and polymer poor phases) that may be liquid-liquid phase separation or liquid solid phase separation. The subsequent removal of solvent leads to the formation of porous architecture.

Fiber mesh: The polymer solution is deposited over nonwoven mesh of other polymer. The subsequent removal of solvent forms woven/inter woven fibers with variable pore size.

Solution casting: The evaporation of solvent from the polymeric solution fabricates porous structures, either by dipping the mold in polymer solution or adding the solution into the mold.

Freeze drying: This method is based on the principle of sublimation where polymer solution is frozen and then solvent is removed using lyophilization technique to fabricate the scaffold.

Emulsion freeze drying: Two immiscible layers (polymer solution and water) are homogenized to form water-in-oil emulsion and quenched in liquid nitrogen followed by freeze drying.

Rapid prototyping: It is a computer assisted fabrication technique. In brief, a powdered or liquid is layered at a time defined by computer generated program. Upon the completion of one layer, the process is repeated to form other layers as required. It is thus an additive process.

Table 1.8: List of commonly used fabrication techniques with pros and cons

Fabrication technique	Merit	Demerit
Solvent-casting and particulate leaching ¹⁷⁴⁻¹⁷⁶	Good control on porosity and pore size Tailorable crystallinity Highly porous structure	Poor mechanical performance Restricted membrane thickness and interconnectivity Residual porogens or solvent
Fiber mesh ¹⁷⁴⁻¹⁷⁶	High surface area for cell adherence.	Structural stability is low

Continue

Gas foaming ¹⁷⁴⁻¹⁷⁶	No loss of bioactive molecules Avoid organic solvent/leaching process	Presence of skimming layers Poor interconnectivity Poor mechanical performance
Phase separation ¹⁷⁴⁻¹⁷⁶	Highly porous structures Molecules activity remains intact Allow incorporation of biomolecule	Limited control on internal architecture and pore sizes Interconnectivity
Fiber blending ¹⁷⁴⁻¹⁷⁶	High porosity and aspect ratio	Limited to few polymers
Freeze drying ¹⁷⁴⁻¹⁷⁶	Highly interconnected porous matrix Avoid high temperature Avoid leaching process Allow immobilized of biomolecules	Long processing time Small pore size
Membrane lamination ¹⁷⁴⁻¹⁷⁶	Control over pore size and porosity	Low mechanical strength Poor interconnectivity
Melt moulding ¹⁷⁴⁻¹⁷⁶	Control on pore size and porosity	Require higher temperature for non-amorphous polymers
Rapid prototyping ¹⁷⁴⁻¹⁷⁶	Excellent control over pore size, porosity and geometry	Expensive Limited to some polymers

1.6 Characterization

Different spectroscopic and analytical techniques as well as biological tests are performed to examine the structure, chemical composition and bio-interfacial attributes of polymers and their NC. These are briefly elaborated in this section.

1.6.1 Chemical structure

The chemical structures of polymers and their NC are very vital as it is directly related to their properties. Therefore, they are generally analyzed by FTIR, NMR, UV-visible, Raman and mass spectroscopic studies.¹⁷⁷ FTIR spectroscopy is very effective to prove the presence of characteristic linkages in the polymer, identify the polymer and different types of interactions in polymer NC. The shifting of band position and its broadening as well as increasing intensity of the band indicate the status of hydrogen bonding within the polymer NC. FTIR spectra of Fe₃O₄-

MWCNT/*Mesua ferrea* oil based HBPU NC (reported by Kalita and Karak) revealed broadening of the band corresponding to -NH stretching vibration ($3406\text{-}3430\text{ cm}^{-1}$) and blue shifting of carbonyl band after the formation of NC from the pristine one.¹⁷⁸ The same group also observed the shifting of carbonyl from 1698 to 1667 cm^{-1} with the increase of MWCNT content that suggested the presence of more secondary interactions in the NC.¹⁵⁸ A *Ricinus communis* oil based PU NC exhibited increase in intensity of characteristic bands of urethane (for carbonyl and -C-N vibration) compared to pristine one owing to the formation of more number of urethane linkages.¹⁷⁹ IR spectra also distinguish between branched polymer and co-polymer as well as degradation pattern of a biodegradable biomaterial. Guelcher et al. characterized the degraded products (after 2 and 8 months of test) of LDI based PU by IR spectroscopy.¹⁴ They postulated that the polymer degraded by the hydrolysis of ester linkages by the detection of strong bands at $1070\text{-}1050$ (-C-O stretching vibration of carboxylic acid and alcohol) and $1675\text{-}1650\text{ cm}^{-1}$ (O=C-O asymmetric vibration due to the carboxylic acid salt formed in phosphate saline buffer). The IR spectroscopy also helps to monitor a reaction by observing the appearance or disappearance of particular bands. For the synthesis of PU, it is a very important tool as disappearance of the band at around 2200 cm^{-1} corresponding to -NCO group depicts the completion of the reaction. However, it is not easy to interpret the subtle features in IR spectra. In such cases, other techniques like NMR spectroscopy are very useful.

^1H and ^{13}C NMR are generally used to study both the linear and HB polymers. NMR is also used for polymer identification, confirmation of molecular structure and determination of degree of branching (DB) in case of branched polymers.¹⁷⁷ The NMR peaks due to branch point aid to reveal the chemical characteristic of those branching points and thus provide the mechanism of branch formation. NMR spectroscopy, mainly ^{13}C NMR demonstrated its importance by providing quantitative information of molecular microstructural features not accessible by any other technique. The DB of HBPU was efficiently calculated by using ^1H NMR by taking the integration ratio of -CH of substituted -OH to the total -OH (both unsubstituted and substituted -OH) as reported by Karak and co-workers.^{86, 87, 96} The same group also determined the DB of HBPU based on *Ricinus communis* oil or its MG by this method using ^1H NMR.

UV-visible spectroscopy is not sufficient to suggest detailed chemical structural attributes. It helps to establish the presence of particular types of chromophore and metal

nanoparticles in the polymer and NC. However in case of nanomaterials, it is one of the very important tools. The peak position, its nature as well as peak shifting provide a preliminary idea on the types of nanoparticles as well as their size distribution. In polymer NC with different doses of nanomaterials, the position, intensity and nature of the peaks seem to differ. Chen et al. observed that with increase in the content of nano-SiO₂ (prepared via chemical route), intensity of the absorbance band (around 290-400 nm) also increased in polyester based PU NC.¹⁶⁴ However, the same group reported no alteration in the absorbance peak at the same band when the nano-SiO₂ was obtained by the fume method.

Besides these, Raman spectroscopy is also used for the characterization of polymers and their NC to identify the linkages and functionalities. Now-a-days, Raman spectroscopy is widely used for studying the morphological features and micromechanic of deformation in polymer, composite, fiber and blend.¹⁷⁷ Again, mass spectroscopy is also a powerful tool to determine subtle detail of polymer structure. The mass spectra of polymer can be used to evaluate the molar mass of repeating unit, chemical structure of end groups as well as to determine the existence of other groups or modified side chain, even if present in minute quantity.

1.6.2 Physical structure

The morphological study of the polymeric NC based biomaterials is one of the important requirements for their characterization. This study is mainly done with the help of scanning electron microscopy (SEM) and transmission electron microscopy (TEM). SEM images provide the surface morphology of the samples. The phase difference within the samples can be distinguished as well as the cells morphology on contact with the biomaterials can be detected.¹² Moreover, the surface roughness and types of porous network created on a sample can be studied. The atomic force microscopy or SEM is also used for imaging, measuring and determining the nanoscale materials or polymer NC. However, the size and distribution of nanostructure in a NC is difficult to be determined by these tools. But, TEM provides a direct observation of the size, shape and distribution of the nanomaterials in the polymer NC. It can also predict the intercalation or exfoliation of the nanomaterials upon NC formation. Moreover, the number of layers or tubes can be visually detected through the TEM analysis. However, TEM analysis is only the localized qualitative information of the sample. Therefore to be statistically significant, large number of images from different parts of the samples must be analyzed. HBPU

NC with nanomaterials like CNT, metal nanoparticles, clay, nano-SiO₂ or their hybrids were analyzed by TEM to understand the dispersion and distribution of nanomaterials in PU matrix.^{7, 128, 159, 164, 166, 180} Karak and coworkers reported excellent orientation and dispersion of MWCNT in the bio-based HBPU NC matrix owing to HB morphology with high surface end groups.^{158, 180} A TEM image of nano-SiO₂/PU NC showed even dispersion of nanomaterial in the matrix.¹⁶⁴ However, the presence of few aggregates was observed in the matrix due to strong hydrogen bonding of nano-SiO₂ particles.

The crystallinity of polymers, nanomaterials and polymer NC are generally analyzed by XRD studies¹⁷⁷ using wide angle diffraction and small angle diffraction. Wide angle diffraction is used frequently due to easy availability and simple analysis. From XRD diffractogram, the degree of crystallinity, size and distribution of crystallites in samples can be detected.^{34, 177} Moreover in polymer NC, the presence of characteristic peaks of a particular nanomaterial proves the presence of nanomaterial with the matrix. The d-spacing and approximate size of nanomaterials can also be determined by Bragg's equation and Scherrer's equation (in case of homogenous strain systems), respectively.³⁴ Rana et al. reported sharpening of diffraction intensity of diffraction peaks at $2\theta = 21.2^\circ$ and 23.4° upon incorporation of MWCNT in vegetable oil based HBPU NC, however the crystal structure of PCL remained intact.¹⁸¹ Deka et al. also observed increase in intensity of the peaks corresponding to PCL crystal in *Messua ferrea* oil based MWCNT/HBPU NC.¹⁸⁰ They observed increase in crystallinity (24.5%, 26.4% and 28.5%) with the increase of wt.% of MWCNT (1, 2.5 and 5 wt.%, respectively) in NC.

1.6.3 Thermal

There are two modes for thermal analysis i.e. static and dynamic modes. The most common techniques applied for thermal characterization are thermogravimetric analysis (TGA), dynamic mechanical analysis (DMTA) and differential scanning calorimetry (DSC).^{34, 177} TGA is an important analytical tool to determine the thermostability of a polymeric material (under air or inert atmosphere).³⁴ It also helps to understand the thermal degradation pattern and effect of nanomaterials on thermostability of NC. DSC is used to characterize glass transition (T_g) and melting (T_m) temperature along with the degree of crystallinity, phase separation and reaction exotherm of polymer and its NC.^{34, 177} The thermal analysis of segmented PU indicates the presence of multi-thermal transitions. In case of PU and its NC, the difference in T_g of soft and

hard segments is a measure of phase separation.¹² Greater the difference, higher is the phase separation.

DMTA technique is capable of providing significant information on position of transition and mechanical properties of polymer. It measures the storage and loss modulus as a function of dynamic temperature. Herein, information on the first and second order transition, degree of crystallinity, phase separation, crosslinking reaction of polymer and NC as well as mechanical properties under dynamic condition can be obtained.^{12, 34, 177}

1.6.4 Biological

1.6.4.1 Biodegradation study

Biodegradation study of biomaterials is generally carried out through either *in vivo* or *in vitro* assessment.^{6, 12} *In vitro* test is conducted by incubating the samples in a stimulated body fluid (such as phosphate buffer saline, PBS) under physiological conditions of pH 7.4 and temperature 37 °C. If the *in vitro* degradation rate is found to be acceptable, then only *in vivo* test is conducted. In *in vivo* experiment, weighed sample is implanted in an experimental model using laboratory animals. Care is taken to implant the samples in an intended location based on final application. For both methods, the samples are taken out at a regular interval of time and analyzed further to determine the weight loss, change in physical, chemical and mechanical properties as well as morphological changes.

1.6.4.2 *In vitro* cytotoxicity assay

In vitro cytotoxicity study is the preliminary step to determine the biocompatibility of a biomaterial. ASTM and ISO methods have developed a number of accepted cytotoxicity assays such as direct contact assay, agar diffusion assay and elution or extract assay.^{6, 182} Conceptually, the direct contact assay is the most simplest one. Fabricated polymeric biomaterial is placed in direct contact with the cultured cells in a cell culture plate and incubated for a required time period. The percentage of dead or survived cells can be detected by microscopic observation (extent of cell swelling and lysis) or qualitative assessment by using dye (like trypan blue test) or by quantitative measurement of enzymes released from the lysed cells (lactase dehydrogenase assay).⁶ Alternatively, cell viability can also be checked by using dye that can change color only

in response to the viable cells, like 3-(4,5-dimethylthiazol-2-yl)-2,5-diphenyltetrazolium bromide (MTT) assay.

In agar diffusion method, the extent of cell survivability was checked by using agar (in combination with cell culture media) as a barrier between the adhered cells and the tested samples. In this method, soluble products from the sample may diffuse into the agar, come in contact with the cells and the viability of the cells is examined after a predefined period by observing the affected zone or using cellular dyes. Whereas, the elution assay is done to evaluate the cytotoxicity of leachable components or degraded products from the biomaterials.^{6, 13} Here, the samples are dipped in a vial containing stimulated body fluid, incubated for a definite time period and the extracts are exposed to the cultured cells to check the cell viability. The inclusion of positive and negative controls is must for each type of cytotoxicity assay.

1.6.4.3 Cell adhesion/spreading assay

Cell adhesion is generally quantified by indirect adhesion assay by allowing a known number of cells to attach on a biomaterial and then the number of non-adhered cells is calculated after rinsing.⁶ Number of cells adhered on the sample is thus calculated by subtracting the non-adhered cells from the total number of seeded cells. Cell adherence can also be calculated directly by staining them with dyes such as MTT or by radioactive labeling. Whereas, spreading of cells is analyzed directly by microscopic observation or images analyzing software.⁶

1.6.4.4 *In vitro* immunocompatibility assay

In vitro inflammatory response is an important test to ascertain the biomaterial immunocompatibility. It can be analyzed through the detection of pro-cytokines (interleukins, IL and tumor necrosis factor, TNF) that are released into the media (upon exposure to sample) using enzyme-linked immunosorbent assay (ELISA) test.^{6, 183} Determinations of leukocytes adhesion, migration and death are other useful techniques.^{6, 183} The upregulated cell surface markers on endothelial cells upon exposure to biomaterials are used to determine the inflammatory responses, as they promote migration of macrophages and neutrophils.⁶ Cell counting, fluorescence-activated cell sorter and flow cytometer techniques are generally employed for this purpose.

1.6.4.5 *In vitro* hemocompatibility assay

The interfacial interaction between blood and biomaterial is crucial, as the biomaterial in due course of action comes in direct or indirect contact with the vascular system. The assessment of blood compatibility is generally conducted by exposing the biomaterial (polymer or NC) to freshly drawn blood sample in static or dynamic mode.⁶ Hemocompatibility and anti-thrombogenic effect are also determined by the platelet adhesion test, coagulation time and thrombosis formation assay.¹⁸³ *In vitro* anti-hemolytic activity of biomaterial by exposing them directly to erythrocytes is an another important method to scrutinize the hemocompatibility.

1.6.4.6 *In vivo* assessment of biocompatibility and inflammatory response

In vivo assessment of biocompatibility and inflammatory response upon exposure to biomaterial is important, as *in vitro* test cannot replace the complex interplay of cell types and signal molecules that accomplish the *in vivo* environment. The choice of appropriate animal model, implantation site and length of study are very important criteria for such *in vivo* test.

The methods of assessment as approved by regulatory agencies (ASTM F1983-99, ASTM F1904-98e1, ASTM F981-04, ISO, U.S FDA) include histology/immuno-histochemistry to visualize tissue organization, detection of lymphocytes at implantation site and microscopic observation using electron microscopy.⁶ The other techniques involve biochemical assay, determination of hematological parameters and cytokines detection on the experimental animals.⁶ Moreover, the observation of cardinal signs at the implanted site is an indicator of hypersensitivity due to the interaction with the biomaterials.¹⁸³

In vivo cell/tissue regeneration or healing potentiality of the biomaterial is the most important assessment to establish it in a alleged application. This is generally done by implanting the biomaterial at the desired defect/wound site and healing process is monitored by direct observation of progressive changes, histopathology and other biochemical techniques.

Besides above mentioned characterizations, the optical, electrical, magnetic, shape memory behavior, antimicrobial test, etc. are also performed for polymers and their NC depending upon the requirements.

1.7 Properties

NC must cover a gamut of properties to meet the need of their practical utilities. Some of the desired properties of NC related to the confined scope of biomaterials are discussed in this section.

1.7.1 Mechanical

Desired mechanical integrity of a biomaterial after the formation of NC is a fundamental requirement to match the biomechanical properties of the native tissues. The mechanical strength is found to increase dramatically upon incorporation of suitable nanomaterials.^{158, 180} Greater the interfacial interaction between them, better is the load transfer ability and hence better is the performance.^{11, 34} However, above an optimal amount of nanomaterial in NC, decrement in the performance is also observed. Generally, tensile strength and modulus increases with the increased doses of nanomaterial. But, the ductility may decrease, remain constant or even increase depending on the nature of nanomaterial and modifying agent used. Thus, formation of a suitable NC with homogeneously dispersed and perfectly groomed nanomaterial enhances the overall toughness including impact resistance and flexibility.

Further, improvement in tensile strength is also observed in vegetable oil based HBPU NC. It was reported that on addition of 5 wt.% of MWCNT, the tensile strength of vegetable oil based HBPU NC increased to 46 MPa from 6 MPa.¹⁸⁰ Rana et al. also reported improvements in modulus (30 MPa) and breaking strength (47.2 MPa) of *Ricinus communis* oil modified MWCNT/HBPU NC compared to pristine HBPU (modulus 14.1 MPa and breaking strength 37.8 MPa).¹⁸¹ The incorporation of nanoclay, Ag and Fe₃O₄ nanoparticles were also reported to improve the mechanical performance of the bio-based HBPU NC.^{128, 139, 184} In NC, the storage modulus is also improved upon inclusion of nanomaterials into a polymer matrix. The storage modulus and loss modulus were also found to be higher for PU NC (384 kPa and 156 kPa) upon incorporation of 3% of Fe₃O₄-SiO₂ nanoparticles compared to pristine PU (348.9 kPa and 126 kPa).¹⁸⁵

1.7.2 Thermal

In most of the cases, it is found that upon NC formation the thermal stability increases from the pristine polymer. Nanomaterial (in general nanotube, nanofibre or nanolayer) acts as an insulator

and mass transport barrier to the volatile components formed during decomposition.¹⁷⁸ Fe₃O₄-MWCNT nanohybrid (0.2, 1 and 2 wt.%) increased the thermal stability of bio-based HBPU by 9, 13 and 18.3% upon formation of NC.¹⁷⁸ Fe₃O₄/HBPU NC showed enhancement in thermal stability from the pristine HBPU by 30 °C (using 10 wt.% of Fe₃O₄).¹³⁹ In case of vegetable oil based PU, a two or three step degradation is observed. However in NC, the degradation pattern may change to a single step degradation but the thermostability is often improved.¹⁵⁹ Deka et al. reported one step degradation pattern of a bio-based MWCNT/HBPU NC with thermostability up to 275 °C, whereas the pristine polymer showed two step degradation with stability up to 215 °C.¹⁸⁰

Further, in PU two values of T_g corresponding to the soft and hard segments are observed. The vegetable oil based HBPU and their NC also follow the same characteristic feature. Moreover, the effect of composition on microphase separation can be evaluated by determining the variation in T_g. The increase of T_g with the increase of TEA, as multifunctional moiety resulted more phase separation of HBPU.¹⁸⁶ In HBPU NC, variations in T_g and T_m values with varying wt.% of nanomaterials were also observed. T_m of NC based on bio-based HBPU was reported to increase with increase in the content of MWCNT and Fe₃O₄, as nanomaterials.^{139, 180} Moreover, the degree of crystallinity also reported to improve after the formation of NC with MWCNT due to nucleating effect in HBPU.¹⁸⁰ T_g of the same oil based clay/HBPU NC was increased from -41 to -35 °C and T_m was enhanced to 55 from 50 °C with the inclusion of 5 wt.% of clay.¹⁸⁴

1.7.3 Surface

Surface properties of polymeric biomaterials are very important to control the bio-interfacial interactions between tissue and biomaterial. Physico-chemical properties that influence these interactions include hydrophilic/hydrophobic ratio, surface charge, presence of surface functionalities and receptor sites including surface roughness. The surface free energy of biomaterials is an indicator of hemocompatibility. The extent of wettability required for the biomaterial differs depending upon the application.¹² It was reported that the modification of PU with dihydroxybutyl-terminated PDMS altered the surface properties of unmodified PU. The surface tension decreased, whereas the contact angle increased and hence the wettability improved with increasing PDMS content (0-9 wt.%).¹⁸⁷ Kessler et al. reported that UV treated

PU film (in presence of oxygen) improved the wettability, cell adherence and spreading ability compared to the untreated PU.¹⁸⁸ Electrospun MWCNT/PU NC was also reported to be more hydrophilic than pristine PU, owing to the increase in surface roughness.¹⁸⁹ Surface roughness acts as a boon for cell adherence in TE scaffold. Mirabedini et al.¹⁹⁰ reported enhancement of surface roughness of PU NC from pristine PU (as studied by atomic force microscopy) with the addition of untreated TiO₂ and amino-propyltrimethoxy silane treated TiO₂ nanoparticles. Further, HBPU texture is rougher compared to linear PU, although quantitative investigation on the degree of roughness for HBPU NC is tough to find.

1.7.4 Biological

1.7.4.1 Biocompatibility

Implantation of biomaterial is accompanied by local inflammatory response, an initial indicator of biocompatibility in host.^{6, 183} Depending on the physico-chemical attributes of biomaterial and bio-interfacial interactions, the extent of immune response varies.^{6, 12} There is an interplay of cytokines and anti-cytokines, which works in a cascade to deal with the injury and the implanted biomaterial. In this process, interferon gamma, TNF, IL-1, IL-2 and IL-6 are involved in acute inflammatory responses.^{6, 183} Generally, these cytokines are observed post implantation in the tissue culture medium or in blood of the recipient of the biomaterial. However, the exact scenario can only be understood through the histology/immunohistochemistry at the tissue-material interface. In case of blood-material interaction, the adsorption of important proteins namely albumin, fibrinogen and gamma-globulin on biomaterials was studied.^{6, 12, 183} The adsorption of albumin on biomaterial is believed to improve the hemocompatibility, whereas the adsorption of other two is considered unfavorable.¹² Moreover, number of lymphocytes in peripheral blood also approves the hemo/immuno-compatibility of biomaterial.

Again, recent researches have shown significant leap towards development of bioactive polymeric materials, especially for TE application. In this regard, the immobilization of bioactive agent in PU and formation of PU NC with suitable nanomaterials sought to improve the bioactivity. Presence of nanostructures emulates the natural niche of ECM comprising of micro/nano sized elements.²² Thus, the positive cellular activity improves on exposure to PU/MWCNT NC compared to the pristine one.¹⁸⁹ The biocompatibility of PEG-PU hydrogel coatings on PDMS neural electrode as evaluated by *in vitro* and *in vivo* studies illustrated that the

absorption of protein was reduced to 93% on electrodes with better glial scarring and reduced the neuronal cell loss around the implants.¹⁹¹ Ho et al. reported the *in vitro* and *in vivo* responses of epithelial cells on Au/PU NC.¹⁹² The epithelial cells showed lamellipodia formation and good cell proliferation while seeded on the above NC. This NC activated valosin-containing protein, which has immunomodulating effect. Moreover, *in vivo* test with this NC showed less inflammatory response and more extensive endothelial cells growth. Similarly, better biocompatibility of implanted Ag/PU NC was observed in rat jugular vein compared to the pristine PU.¹²⁷ The *in vitro* results suggested less platelet adherence, but good adherence as well as proliferation of endothelial cells and fibroblast along with good antibacterial activity. Hemocompatibility of nanoclay/PU NC using different chain extenders was also investigated in terms of RBC lysis and platelet adhesion.¹⁵⁶ At lower doses (5 mg/mL), NC exhibited nominal hemolytic activity as well as platelet aggregation with normal shapes and spreading. Ag nanoparticles and MWCNT based vegetable oil based HBPU NC also exhibited good anti-hemolytic and antibacterial activities.^{128, 180} Thus, these results are opening up a new avenue for possible application of such vegetable oil based HBPU NC in biomedical niche.

1.7.4.2 Biodegradation

Biodegradable polymers are the vivid material of choice for different biomedical applications like TE, drug delivery and temporary implant. However, the polymer and its NC should be degraded in such a way that the native cells and tissues can regenerate to repair/replace the damaged region. Meanwhile, the degraded products should be non-toxic to the host. Biodegradation occurs through different routes (hydrolytic or oxidative) by the body fluids including water, salts, enzymes and peroxides.^{6, 12} Depending on hydrophilic/hydrophobic ratio, the degradation may be limited to surface or happen to bulk of the material. In body, the immune cells (macrophage and neutrophils) and enzymes (esterase, papain and trypsin) are directly responsible for degradation of polymers including PU.^{6, 12}

Moreover, in PU based biomaterial, degradation mechanism varies depending on the chemical linkages present in the structure.^{12, 13, 85} In polyester based PU, hydrolysis of bond predominates, where in polyether based PU, oxidation is responsible for the degradation. It is speculated that vegetable oil based HBPU are more prone to degradation compared to the petroleum based one as well as linear PU.^{87, 180} This may be due to the presence of ester linkages

in vegetable oil moiety, architectural geometry, less chain entanglement and void space in HB structure. Interestingly, the urethane linkages are not susceptible to hydrolysis under normal physiological environment. Zhang et al. reported degradation of LDI-glycerol based PU network into non-toxic by-products like lysine, ethanol and glycerol.¹⁹³ It was observed that porosity of PU based biomaterial is directly proportional to its degradation rate. Immune cells are actively involved in calcification, surface cracking and stress cracking leading to the degradation of PU. Literature reported either the enhancement or decrement in biodegradation rate after the formation of NC.^{156, 194} Recently, Mishra et al. demonstrated the slow degradation rate after the incorporation of nanoclay in PU, due to increase in crystallinity.¹⁵⁶ However, Okamoto et al. reported that degradation improved after formation of NC based on poly(lactic acid) and trimethyl octadecylammonium modified MMT.¹⁹⁴ They postulated that hydroxyl group heterogeneously catalyzed the hydrolysis of the matrix upon water adsorption due to intercalated silicate layers.

1.7 Applications

Biomedical domain demands to design biodegradable polymers as they possess considerable advantages over non-degradable ones. The important applications of biodegradable PU and its NC are briefed in this section.

1.8.1 Tissue engineering

TE has demonstrated its significance to develop biological substituent to repair, replace or augment the lost or damaged organs. TE surmounts the shortage of donor's organ, use of immuno-suppressor drugs, compatibility and alarming risk of organ rejection related to transplantation process. TE is sometimes used synonymous with regenerative medicines but the latter is a broader concept including TE itself, stem cell technology, progenitor cell, bio-artificial cell construct, etc.^{195, 196} One of the most important components in TE is a biodegradable and biocompatible scaffold to support the formation of tissue by mimicking the ECM and hence restored the original function.^{195, 196} The excellence of PU and its NC forwards them as the preferred scaffold materials.¹⁵⁶ Zawadzak et al. demonstrated CNT coated PU foam as a bioactive scaffold for bone TE.¹⁹⁷ The presence of CNT has shown to accelerate the deposition of calcium phosphates by providing more nucleation centers. A porous biodegradable

(Cloisite®30B)/PU NC was reported as a potential scaffold for TE.⁹ *In vitro* and *in vivo* experiments demonstrated the feasibility of this NC to be employed as an artificial ECM onto which cells can nicely adhered and formed new tissues. CNT/PU NC was also reported to promote the formation of skeletal myotube.¹⁸⁹

Moreover, PU including vegetable oil based one and their NC have shown remarkable performance in bone TE. A reactive CNT/PU foam exhibited immense potential to serve as a bone scaffold for promoting the growth, proliferation and differentiation of bone cells.¹⁶¹ *Ricinus communis* oil based PU (BioOsteo®) is approved in 1999 for clinical use.¹⁹⁸ Pereira-junior et al. carried out a comparative study between this *Ricinus communis* oil based PU and cancellous bone autograft to heal the radial segment bone defect in rats.¹⁹⁸ They demonstrated that vegetable oil based PU can be used as a potential scaffold material for bone healing. In another investigation the potency of the same oil based PU was compared with human demineralized bone matrix to repair the bone defects. PU showed better performance than the demineralized bone matrix.¹⁹⁹ Whereas, Miao et al. reported soybean oil based PU as a potential material to support the adherence and growth of mouse fibroblast cells by using *in vitro* studies.²⁰⁰ Further, PU of alcoholized *Ricinus communis* oil and nano-HA based NC was used as a potent candidate for TE.¹⁶² Asefnezad et al. depicted nano-HA and polyester based aliphatic PU NC with homogenously interconnected porous structure of pore sizes 50-250 µm as a scaffold material for bone TE.⁷⁵ However, they did not investigate the biological properties of this NC. The above reports thus illustrated the immense role of bio-based PU and PU NC in TE.

1.8.2 Wound dressing

Wound is referred to any kind of disruption to the integrity of anatomical tissues due to trauma, burn, ulcer or accidental injuries. The maintenance of chronic wound is very difficult and requires long period to heal. It is susceptible to microbial infection due to the secretion of wound exudates and is accompanied with huge pain, bad odor and peripheral vascular diseases. PU and its NC are widely utilized as wound dressings and some of them are also commercialized.¹² PU based dressings like Opsonite®, Blisterfilm®, Omnidem®, Epiguard® and Xeroform® are used for treatment of severe ulcer, donor site, peritoneal wound and burn.¹² Kim et al. prepared a gelatin nanofibrous/PU mat as a wound dressing. Blending with gelatin resulted in enhancement of mechanical strength, water uptake and cell uptake ability of the dressing.²⁰¹ Ruff et al.

demonstrated that a PU adhesive dressing assisted epidermal suturing and minimized the post operative wound care.²⁰² Patient with this epidermal scaffold showed well approximated wound edges. Linseed oil based PU was also postulated as a prospective antibacterial wound dressing.²⁰³ Moreover, Unnithan et al. reported emu oil blended PU as an antimicrobial wound dressing with good cell adherence and growth.²⁰⁴

PU NC based on metal nanoparticles are extensively investigated as potent dressings as they provide protection against microbial attack. A NC of electrospun PU and *in situ* prepared Ag nanoparticles was reported as an antibacterial wound dressing.²⁰⁵ The dressing showed 100% reduction in bacterial growth with good water vapor transmission rate and fluid drainage ability. Collagen was grafted to this fiber surface to attain better hydrophilicity. CuraVAC Ag (Daewoong Pharm Co, LTD, South Korea), a PU foam and Ag nanoparticles based product was evaluated by Park et al. as an efficient antimicrobial dressing.²⁰⁶ It functions as a negative pressure wound therapy and releases silver nanoparticles to the wound site once moistened by the exudates and efficiently killed both Gram positive and negative bacteria. Similarly, Karak and co-workers reported Ag nanoparticles/HBPU NC as an antimicrobial and cytocompatible material that may be used as a potent wound dressing.¹²⁸ However, Ag containing dressing is related to toxic issues and researches are focusing on biocompatible and antibacterial nanoparticles, like Fe₃O₄ nanoparticles.

1.8.3 Catheter and stent

Catheter and stent are employed for both therapeutic and diagnostic purposes. These are used for the delivery of fluids/drug or removal of fluid/blood clot and monitoring the central venous pressure. They are fabricated by utilizing various types of polymeric biomaterials including PU.¹² The parameters for controlling the performance of catheter include stiffness, surface roughness as well as susceptibility towards bacterial colonization and inflammatory responses. Thus, many PU NC with above attributes are extensively researched for such catheter applications. Ho et al. investigated Au/PU NC as a prospective catheter material. They observed better biocompatibility with better growth of epithelia cells on NC compared to the pristine PU based catheter.¹⁹² Hsu et al. in 2010 also reported Ag/PU NC as a prospective antibacterial coating or catheter for biocompatible cardiovascular application.¹²⁷ Chlorohexidine diacetate modified MMT based PU NC demonstrated an excellent 2-log reduction in adherent bacteria and

decreased adhesion of platelet and fibroblast compared to the control PU²⁰⁷ Thus, PU NC are potential materials to be used for such applications

1.8.4 Drug delivery

Conventional drug delivery system often adversely affects the unspecific organ/function and thereby leading to various side effects Thus, targeted drug delivery system using biodegradable polymer (including PU) and its NC have many advantages^{208 209} Polymeric matrix aids in providing stability to the drug and protects it from enzymatic degradation along with the controlled release of the drug molecule in blood plasma over a specified period Barcon et al reported PU based hollow microstructure prepared by combination of interfacial polyaddition and emulsion techniques²¹⁰ It exhibited good transdermal drug delivery as analyzed in murine skin test with no cytotoxic effect on mesenchyme stem cells A biodegradable LDI based PU showed controlled release of 7-tert-butyldimethylsilyl-10-hydroxy-camptothecin, an anticancer drug²¹¹ PU system successfully delivered therapeutic concentration of the drug and thus projected to be used for post operative intracranial chemotherapy Biodegradable self assembled aliphatic nanoclay/PU NC was also demonstrated by Mishra et al as a controlled drug delivery vehicle¹⁵⁶ Tuning of crystalline size of PU by alteration of the aliphatic chain length or incorporation of disc like nanoclay delayed the diffusing rate of drug by creating a torturous path A dexamethasone loaded clay/PU NC was also investigated to release drug via ocular route²¹²

1.8.5 Shape memory biomaterial

Biomedical devices like suture, stent, clot removal or cardiac assist device with shape memory effect bestow a new direction to the conventional surgical technique Baer et al reported the suitability of shape memory PU as a stent or clot extractor²¹³ Vegetable oil based HBPU and NC were also reported by Karak and co-workers^{28 158 178 180} with excellent shape memory behavior, cytocompatibility, biodegradability and good toughness along with flexibility These NC, thus unwrap new opportunities for their potential applications as stimuli responsive shape memory biomaterials

Further, the prospective applications of biodegradable HBPU NC are shown in **Figure 1.1**

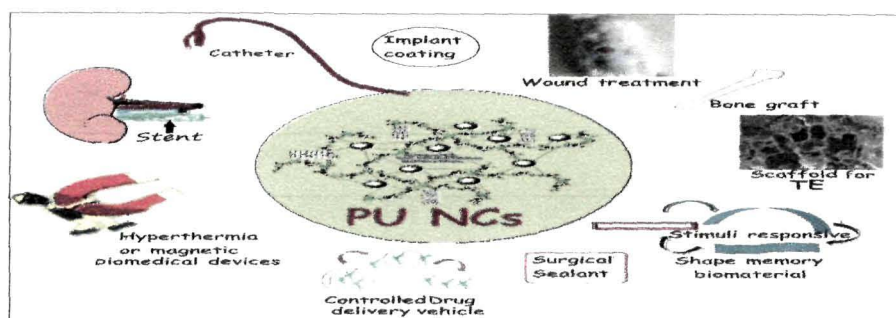


Figure 1.1: Prospective applications of biodegradable HBPU NC

1.9 Scopes and objectives of the present investigation

From the above discussions and literature survey, the utility of nanomaterials and renewable or non-renewable resources based PU as well as their NC is evident in plethora of biomedical applications. Moreover, lots of literatures on bio-based HBPU NC are reported. However, these types of NC are not explored sufficiently in the biological realm like TE, drug delivery, biomedical devices and wound dressing amongst many other related bio-applications. Thus, there is ample scope to investigate vegetable oil based HBPU NC with suitable nanomaterials in various biomedical applications, especially TE. The excellence of hyperbranched architecture together with vegetable oil based biodegradable PU NC is yet to be explored comprehensively in the biomedical domain.

Under the above background, the main objectives of the present investigation are as follows.

- 1) To synthesize vegetable oil based HBPU by varying the compositions of the reactants.
- 2) To characterize the synthesized HBPU by using different spectroscopic and analytical tools.
- 3) To evaluate the properties of HBPU and to find out the most suitable PU for further study.
- 4) To prepare NC of the best HBPU using different types of nanomaterials like MWCNT, Fe_3O_4 , Fe_3O_4 decorated MWCNT and protein functionalized MWCNT.
- 5) To characterize the prepared NC using different analytical and spectroscopic techniques.
- 6) To evaluate the properties of the prepared NC as biomaterials.
- 7) To optimize the performance of the biomaterials to obtain the best biodegradable HBPU NC as a prospective biomaterial for a possible biomedical application.

1.10 Plans of present work

To fulfill the above objectives, the following plans are adopted.

- 1) Vegetable oil based HBPU by varying the compositions and weight percentages of the reactants will be synthesized by pre-polymerization technique using slow addition and high dilution approach.
- 2) The synthesized HBPU will be characterized by using different tools like FTIR, UV, NMR, XRD, SEM, etc. for structural analysis as well as TGA and DSC for thermal behavior, etc.
- 3) The properties of HBPU will be evaluated to find out the most suitable PU for further study by comparing their mechanical strength, thermal stability, chemical and biological properties.
- 4) NC of HBPU will be prepared by *in situ* technique as reported in literature using different types of nanomaterials like MWCNT, Fe₃O₄, Fe₃O₄ decorated MWCNT and protein functionalized MWCNT
- 5) The prepared NC will be again characterized using different techniques such as XRD, TEM, SEM, etc. to determine their structural morphologies.
- 6) The properties of the prepared NC will be evaluated as biomaterials by testing the biocompatibility and biodegradability of HBPU and its NC through both *in vitro* and *in vivo* studies.
- 7) Optimization the performance of the biomaterials will be done to obtain the best biodegradable HBPU NC as a prospective biomaterial for a possible biomedical application.

References

1. Whitesides, G.M. & Wong, A.P. *The Intersection of Biology and Materials science*, MRS Bulletin, Cambridge, 2006.
2. Kalita, S.J. *Nanostructured Biomaterials*, Springer, New York, 2008.
3. Bronzino, J.D. *The Biomedical Engineering Handbook*, 2nd ed., CRC press LLC, U.S.A, 2000.
4. Ratner, B.D. Hoffman, A.S. Schoen, F.J. & Lemons, J.E. *Biomaterial Sciences: A Multidisciplinary Endeavor*, 2nd ed., Elsevier Academic press, San Diego, 2004.
5. Gisselalt, K., et al. *Biomacromolecules* 3 (5), 951--958, 2002.
6. Temenoff J.S. & Mikos, A.G. *Biomaterials: The Interaction of Biology and Material Science*, Prentice Hall, USA, 2008.
7. Nair, L.S. & Laurencin, C.T. Polymers as Biomaterials for Tissue Engineering and Controlled Drug Delivery, in *Tissue engineering I. Advances in biochemical*

- engineering/biotechnology*, K. Lee & D. Kaplan, eds., Springer Verlag Review Series, Berlin, 2006, 47—90.
8. Lligadas, G. *Biomacromolecules* **11** (11), 2825--2835, 2010.
 9. Dias, R.C.M., et al. *Mater. Res.* **13** (2), 211--218, 2010.
 10. Armentano, I. et al. *Polym. Degrad. Stab.* **95** (11), 2126--2146, 2010.
 11. Anandhan, S. & Bandyopadhyay S. Polymer Nanocomposites: From Synthesis to Applications, in *Nanocomposites and Polymers with Analytical Methods*, J. Cuppoletti, ed., InTech, Europe, 2011, 3—28.
 12. Lamba, N.M.K. Woodhouse, K.A. & Cooper, S.L. *Polyurethane in Biomedical Application*, CRC Press, Boca Raton, 1997.
 13. Marois, Y. & Guidoin, R. Biocompatibility of Polyurethanes, in *Biomedical applications of polyurethanes*, P. Vermette et. al, eds., Landes Bioscience, Georgetown, Austin, 2011, 77—96.
 14. Guelcher, S.A., et al. *Biomaterials* **29** (12), 1762--1775, 2008.
 15. Takahara, A., et al. *Polymer* **26** (7), 987--996, 1985.
 16. Inoue, K. *Prog. Polym. Sci.* **25** (4), 453--571, 2000.
 17. Jikei, M., & Kakimoto, M. *Prog. Polym. Sci.* **26** (8), 1233--1285, 2011.
 18. Gao, C., & Yan, Y. *Prog. Polym. Sci.* **29** (3), 183--275, 2004.
 19. Zhou, Y., et al. *Adv. Mater.* **22** (41), 4567--4590, 2010.
 20. Gupta, A.K., & Gupta, M. *Biomaterials* **26** (18), 3995--4021, 2005.
 21. Berry, C.C. *J. Mater. Chem.* **15** (1), 543--547, 2005.
 22. Khademhosseini, A., & Peppas, N.A. *Adv. Healthcare Mater.* **2** (1), 10--12, 2013.
 23. Yang, W., et al. *Nanotechnology* **18** (41), 412001--412013, 2007.
 24. Williams, D.F. & Cunningham, J. *Materials in Clinical Dentistry*, Oxford University Press, Oxford, UK, 1979.
 25. Langer, R. *Nature Mater.* **8** (6), 444--445, 2009.
 26. Black, M., et al. *Phys. Technol.* **13** (2), 50--65, 1982.
 27. LeVeen, H.H., & Barberio, J.R. *Ann. Surg.* **129** (1), 74--84, 1949.
 28. Katz, J. *Development of Medical polymers for Biomaterials Applications*, Medical Device and Diagnostic Magazine, MDDI Article index, 2001.
 29. Apple, D.J., & Sims, J. *Surv. Ophthalmol.* **40** (4), 279--292, 1996.

30. Ingraham, F.D., et al. *J. Am. Med. Assoc.* **135** (2), 82--87, 1947.
31. Modjarrad, K. & Ebnesajjad (ed.), S. *Handbook of Polymer Applications in Medicine and Medical Devices*, Applied Science publisher, London, 2013.
32. Merrill, E.W. Poly(ethylene oxide) and Blood Contact, in *Poly(ethylene glycol) Chemistry: Biotechnical and Biomedical Applications*, J.M. Harris, ed., Plenum Press, New York, 1992, 199—220.
33. Ebewele, R.O. *Polymer Science and Technology*, CRC Press, Boca Raton, 2000.
34. Karak, N. *Fundamentals of Polymers: Raw Materials to Finish Products*, PHI Learning Private Limited, New Delhi, 2009.
35. Chen, H., et al. *Prog. Polym. Sci.* **33** (11), 1059--1087, 2008.
36. Ratner, B.D. Properties of Materials, in *Biomaterials Science: An Introduction to Materials in Medicine*, B.D. Ratner et. al, eds., Academic Press Inc, San Diego, 2004.
37. Ulery, B.D., et al. *J. Polym. Sci. Part B: Polym. Phys.* **49** (12), 832--864, 2011.
38. Gomes, M.E., & Reis, R.L. *Int. Mater. Review*, **49** (5), 261--273, 2004.
39. Gogolewski, S., & Gorna, K. *Polym. Degrad. Stab.* **75** (1), 113--122, 2002.
40. Boretos, J.W., & Pierce, W.S. *J. Biomed. Mater. Res.* **2** (1), 121--130, 1968.
41. Yang, T.F., et al. *Biomacromolecules* **5** (5), 1926--1932, 2004.
42. Palaskar, D.V., et al. *Biomacromolecules* **11** (5), 1202--1211, 2010.
43. Dongyan, T., et al. *J. Apply. Polym. Sci.* **84** (4), 709--715, 2002.
44. Petrovic, Z.S. *Polym. Rev.* **48** (1), 109--155, 2008.
45. Petrovic, Z.S., et al. *Biomacromolecules* **6** (2), 713--719, 2005.
46. Javni, I., et al. *J. Appl. Sci.* **77** (8), 1723--1734, 2000.
47. Guo, A., et al. *J. Polym. Environ.* **10** (1/2), 49--52, 2002.
48. Theng, B.K.G. *Formation and Properties of Clay-Polymer Complexes*, Oxford, UK, 1970.
49. Bajaj, P., et al. *Int. J. Nanomed.* **1** (3), 361--365, 2006.
50. Khudyakov, I.V., et al. *Des. Monomers Polym.* **12** (4), 279--290, 2009.
51. Sahoo, N.G., et al. *Nanomedicine* **8** (4), 639--653, 2013.
52. Fisher, M.B., & Mauck, R.L. *Tissue Eng. Part B Rev.* **19** (1), 1--13, 2013.
53. Jungebluth, P., et al. *The Lancet*, **378** (9808), 1997--2004, 2011.
54. Roach, P., et al. *J. Mater. Sci: Mater. Med.* **18** (7), 1263--1277, 2007.
55. Mantripragada, V.P., et al. *J. Biomed. Mater. Res. A* **101** (11), 3349--3364, 2013.

56. Oh, S., et al. *Am. J. Biochem. Biotechnol.* **2** (2), 49--56, 2006.
57. Nasab, M.B., et al. *Trends Biomater. Artif. Organs* **24** (2), 69--82, 2010.
58. Sarkar, R., & Banerjee, G. *Interceram.* **59** (2), 98--102, 2010.
59. Thamaraiselvi, T.V., & Rajeswari, S. *Trends Biomater. Artif. Organs* **18** (1), 9--17, 2004.
60. Saenz, A., et al. *J. Mater. Educ.* **21** (5-6), 297--306, 1999.
61. Pruitt, L., & Furmanski, J. *Biomed. Mater. Devices; Overview* **41** (6), 14--20, 2009.
62. Yannas, I.V. Classes of Materials Used in Medicine: Natural Materials, in *Biomaterials Science- An Introduction to Materials in Medicine*, B.D. Ratner et. al, eds., Elsevier Academic Press, San Diego, USA, 2004, 127--136.
63. Dhandayuthapani, B., et al. *Int. J. Polym. Sci.* **2011** (2011), 290602--290621, 2011.
64. Ma, P.X. *Mater Today*, **7** (5), 30--40, 2004.
65. Chen, L.J., & Wang, M. *Biomaterials*, **23** (13), 2631--2639, 2002.
66. Chen, Q., et al. *Prog. Biomater.* **1**, 2--24, 2012.
67. Frazer, R.Q., et al. *J. Long Term Eff. Med. Implants* **15** (6), 629--639, 2005.
68. Wolf, L.E., et al. *Faseb J.* **7** (13), 1265--1268, 1993.
69. Boccaccini, A.R., et al. *Compos. Sci. Technol.* **70** (13), 1764--1776, 2010.
70. Davis, H.E. & Leach J.K. Hybrid and Composite Biomaterials in Tissue Engineering, in *Topics in Multifunctional Biomaterials and Devices*, N. Ashammakhi et. al, eds., e-book, 2008. pp. 1--26.
71. Park, H.C., et al. *J. Biomech. Eng.* **108** (2), 141--148, 1986.
72. Bonzani, I.C., et al. *Biomaterials* **28** (3), 423--433, 2007.
73. Gaharwar, A.K. Schexnaider, P.J. & Schmidt, G. *Nanocomposite Polymer Biomaterials for Tissue Repair of Bone and Cartilage: A Material Science Perspective*, Taylor and Francis, LLC, 2011.
74. Spear, R.L., & Camero, R.E. *Int. J. Mater. Form.* **1** (2), 127--133, 2008.
75. Asefnezad, A., et al. *Int. J. Nanomed.* **6**, 93--100, 2011.
76. Jell, G., et al. *J. Mater. Chem.* **18** (16), 1865--1872, 2008.
77. Zhang, X., et al. *J. Biomater. Sci., Polym. Ed.* **24** (9), 1057--1070, 2013.
78. Shah, K., et al. *J. Appl. Polym. Sci.* **131** (10), 40230--40239, 2014.
79. Xia, Y., & Larock, R.C. *Green Chem.* **12** (11), 1893--1909, 2010.
80. Galia, M., et al. *Eur. J. Lipid. Sci. Technol.* **111** (1), 87--96, 2010.

81. Chattopadhyay, D.K., & Raju, K.V.S.N. *Prog. Polym. Sci.* **47** (3), 352--418, 2007.
82. Chan, S.C., et al. *Clin. Chem.* **37** (12), 2143--2145, 1991.
83. Guidoin, R., et al. *Ann. Plast. Surg.* **28** (4), 342--353, 1992.
84. Stokes, K. *J. Biomater. Appl.* **3** (2), 228--259, 1988.
85. Gunatillake, P.A. Meijs, G.F. & McCarthy, S.J. Developments in Design and Synthesis of Biostable Polyurethanes, in *Biomedical Applications of Polyurethanes*, P. Vermette et. al, eds., Landes Bioscience, Georgetown, Texas, 2001, 161—174.
86. Kalita, H., & Karak, N. *Iran. Polym. J.* **21** (4), 263--271, 2012.
87. Deka, H., & Karak, N. *Prog. Org. Coat.* **66** (3), 192--198, 2009.
88. Ulrich, H. *Chemistry and Technology of Isocyanates*, Wiley and Sons, New York, 1996.
89. Salamore, J.C. *Concise Polymeric Materials Encyclopedia*, 5th ed., CRC press, Boca Raton, 1999.
90. Hepburn, C. *Polyurethane Elastomers*, 2nd ed., Elsevier Applied Science, London, 1992.
91. Xiao, H.X., et al. *J. Elastomers Plast.* **26** (3), 237--251, 1994.
92. Asefnejad, A., et al. *Int. J. Nanomed.* **6**, 2375--2384, 2011.
93. Rodriguez, J.V.C. Chan, L.H.C. Sánchez, F.H & Cervantes-Uc, J.M. Degradation of Polyurethanes for Cardiovascular Applications, in *Advances in Biomaterials Science and Biomedical Applications*. R. Pignatello, ed., Intech, Rijeka, Croatia, 2013, 51—82.
94. Raghunath, J., et al. *J. Biomed. Mater. Res. A* **91** (3), 834--844, 2009.
95. Iwamoto, R., et al. *J. Biomed. Mater. Res.* **20** (4), 507--520, 1986.
96. Karak, N., et al. *J. Appl. Polym. Sci.* **112** (2), 736--743, 2009.
97. Deka, H. *Development of Polyurethane Nanocomposites*, Ph. D. Thesis, Tezpur University at Assam, India, 2011.
98. Silvestri, A., et al. *J. Appl. Polym. Sci.* **122** (6), 3661--3671, 2011.
99. Parrag, I.C., & Woodhouse, K.A. *J. Biomater. Sci. Polym. Ed.* **21** (6), 843--862, 2010.
100. Thomson, T. *Polyurethanes as Specialty Chemicals: Principle and Applications*, Boca Raton, Fl, CRC, 2005.
101. Kiran, S., & Joseph, R. *J. Biomed. Mater. Res: A* **102** (9), 3207--3215, 2014.
102. Zhang, C., et al. *J. Biomed. Mater. Res. B Appl. Biomater.* **79** (2), 335--344, 2006.
103. Su, J.F., et al. *J. Appl. Polym. Sci.* **102** (5), 4996--5006, 2006.
104. Valero, M.F., & Díaz, L.E. *Quím. Nova* **37** (9), 1441--1445, 2014.

105. Bahr, M., & Mulhaupt, R. *Green Chem.* **14** (2), 483--489, 2012.
106. Yeganeh, H., & Mehdizadeh, M.R. *Eur. Polym. J.* **40** (6), 1233--1238, 2004.
107. Karak, N., et al. *Macromol. Mater. Eng.* **295** (2), 159--169, 2010.
108. Zlatanovic, A., et al. *J. Polym. Sci., Part B: Polym. Phys.* **42** (5), 809--816, 2004.
109. Thakur, S., & Karak, N. *Prog. Polym. Coat.* **76** (1), 157--164, 2013.
110. Aranguren, M.I., et al. *Polym. Test.* **31** (1), 7--15, 2012.
111. Baker, J.W., & Gaunt, J. *J. Chem. Soc.* **7**, 9--18, 1949.
112. Baker, J.W., & Bailey, D.N. *J. Chem. Soc.* **17**, 4649--4651, 1957.
113. Lenz, R.W. *Organic Chemistry of Synthetic High Polymers*, Wiley Interscience, New York, 1967.
114. Tanzi, M.C., et al. *J. Mater. Sci. Mater. Med.* **5** (6-7), 393--396, 1994.
115. Kumar, A., & Ramakrishnan, S.J. *Chem. Soc. Chem. Commun.* **18**, 1453--1454, 1993.
116. Kumar, A., & Ramakrishnan, S.J. *Polym. Sci. Part A Polym. Chem.* **34** (5), 839--848, 1996.
117. Hong, L., et al. *J. Polym. Sci. Part A. Polym. Chem.* **40** (3), 344--350, 2002.
118. Rannard, S.P., et al. *Macromolecules* **37** (25), 9418--9430, 2004.
119. Jena, K.K., et al. *Eur. Polym. J.* **43** (5), 1825--1837, 2007.
120. Fahlman, B.D. *Material chemistry*, 2nd ed., Kindle edition, Springer, New York, 2011.
121. Alagarasi, A. *Introduction to Nanomaterials*, NCCR internal bulletin. Retrieved on 10/5/2011 from Catalysis database.
122. Yu, W.W., et al. *Biochem. Biophys. Res. Commun.* **348** (3), 781--786, 2006.
123. Yaghini, E., et al. *Nanomedicine* **4** (3), 353--363, 2009.
124. Chen, Z., et al. *Theranostics* **2** (3), 238--250, 2012.
125. Hu, Z., et al. *Chemico-biological interactions* **195** (1), 86--94, 2012.
126. Huang J., et al. *J. Nanosci. Nanotechnol.* **11** (11), 9395--9408, 2011.
127. Hsu, S.H., et al. *Biomaterials* **31** (26), 6796--6808, 2010.
128. Deka, H., et al. *Polym. Degrad. Stab.* **95** (9), 1509--1517, 2010.
129. Park, H.G., et al. *Water. Res.* **43** (4), 1027--1032, 2009.
130. Fredriksson C., et al. *Wounds* **21** (5), 116--123, 2009.
131. Pankhurst, Q.A., et al. *J. Phys. D: Appl. Phys.* **36**, R167--R181, 2003.
132. Weissleder, R., et al. *Nat Med.* **6** (3), 351--355, 2000.
133. Zhao, M., et al. *Nat. Med.* **7** (11), 1241--1244, 2001.

134. Anghel, I., et al. *Nanoscale Res. Lett.* **7** (1), 690--697, 2012.
135. Tran, N., et al. *Int. J. Nanomed.* **5**, 277--283, 2010.
136. Silva, A.C., et al. *Int. J. Nanomed.* **6**, 591--603, 2011.
137. Jordan, A., et al. *J. Magn. Magn. Mater.* **194** (1-3), 185--196, 1999.
138. Wada, S., et al. *Oral Dis.* **9** (4), 218--223, 2003.
139. Kalita, H., & Karak, N. *Polym. Adv. Technol.* **24** (9), 819--823, 2013.
140. Liao, H., & Hafner, J.H. *Chem. Mater.* **17** (18), 4636--4641, 2005.
141. Huang, X., et al. *Adv. Mater.* **21** (48), 4880--4910, 2009.
142. Coffey, J. (ed.), *Semiconducting Silicon Nanowires for Biomedical Applications*, Woodhead Publishing Limited, Cambridge, 2013.
143. Vasita, R., & Katti, D.S. *Int. J. Nanomed.* **1** (1), 15--30, 2006.
144. Sinha, N., & Yeow, J.T.W. *IEEE Trans. Nanobiosci.* **4** (2), 180--195, 2005.
145. Zhang, W., et al. *Nanoscale Res. Lett.* **6**, 555--577, 2011.
146. Tonelli, F.M.P., et al. *Int. J. Nanomed.* **7**, 4511--4529, 2012.
147. Hu, H., et al. *Nano Lett.* **4** (3), 507--511, 2004.
148. Liu, Z., et al. *Angew. Chem. Int. Edn.* **46** (12), 2023--2027, 2007.
149. Firme III, C.P., & Bandaru, P.R. *Nanomed. Nanotechnol. Biol. Med.* **6** (2), 245--256, 2010.
150. Aryal, S., et al. *Mater. Sci. Eng. A* **426** (1-2), 202--207, 2006.
151. Hwang, J.Y., et al. *Nanoscale*, **5** (2), 487--497, 2013.
152. Kagan, V.E., et al. *Nat. Nanotechnol.* **5** (5), 354--359, 2010.
153. Yang, Y., et al. *Mater. Today* **16** (10), 365--373, 2013.
154. Zhu, Y., et al. *Adv. Mater.* **22** (35), 3906--3924, 2010.
155. Suresh, R., et al. *Int. J. Pharm. Sci Nanotechnol.* **3** (2), 901--905, 2012.
156. Mishra, A., et al. *Acta. Biomater.* **10** (5), 2133--2146, 2014.
157. Chen, W., & Tao, X. *Appl. Surf. Sci.* **252** (10), 3547--3552, 2006.
158. Kalita, H., & Karak, N. *Polym. Compos.* **35** (4), 636--643, 2013.
159. Dutta, S., et al. *Bioresour. Technol.* **100** (24), 6391--6397, 2009.
160. Ashjari, M., et al. *J. Inorg. Organomet. Polym. Mater.* **20** (2), 213--219, 2010.
161. Verdejo, R., et al. *J. Biomed. Mater. Res. A.* **88** (1), 65--73, 2009.
162. Mei, L.L., et al. *J. Inorg. Mater.* **28** (8), 811--817, 2013.

163. Yoo, H.J., et al. *J. Macromol. Sci. Part B: Phys.* **45** (4), 441--451, 2006.
164. Chen, X., et al. *Polym. Int.* **52** (6), 993--998, 2003.
165. Wang, X., et al. *J. Mater. Chem.* **21** (12), 4222--4227, 2011.
166. Thakur, S., & Karak, N. *RSC Adv.* **3** (24), 9476--9482, 2013.
167. Barick, A.K., & Tripathy, D.K. *J. Appl. Polym. Sci.* **117** (2), 639--654, 2010.
168. Chun, B.C., et al. *J. Appl. Polym. Sci.* **106** (1), 712--721, 2007.
169. Konwarh, R., et al. *Biotechnol. Adv.* **31** (4), 421--437, 2013.
170. Wang, N., et al. *Biomaterials* **34** (4), 888--901, 2013.
171. Kundu, S.J. & Kundu, S.C. Biomaterial Scaffold Fabrication Techniques for Potential Tissue Engineering Applications, in *Tissue engineering*, D. Eberli, ed., Intech, Eupore, 2010, 140—157.
172. Rockwood, D.N., et al. *Biomaterials* **29** (36), 4783--4791, 2008.
173. Hashizume, R., et al. *Biomaterials* **31** (12), 3253--3265, 2010.
174. Sachlos, E., & Czernuszka, J.T. *Eur. Cells Mater.* **5**, 29--40, 2003.
175. Buckley, C.T. & O'Kelly, K.U. Regular Scaffold Fabrication Techniques for Investigations in Tissue Engineering, in *Topics in Bio-Mechanical Engineering* P.J. Prendergast & P.E. McHugh, eds., TCBE & NCBES, Ireland, 2004, 147—166.
176. Hutmacher, D.W. *Biomaterials* **21** (24), 2529--2543, 2000.
177. Young, R.J. & Lovell, P.A. *Introduction to Polymer*, 3rd ed., CRC press, Boca Raton, 2011.
178. Kalita, H., & Karak, N. *J. Nanoeng. Nanomanuf.* **3** (3), 194--201, 2013.
179. Pradhan, K.C., & Nayak, P.L. *Adv. Appl. Sci. Res.* **3** (5), 3045--3052, 2012.
180. Deka, H., et al. *Carbon*, **48** (7), 2013--2022, 2010.
181. Rana, S., et al. *Nanotechnology* **19** (49), 495707--495715, 2008.
182. Shalaby, S.W. & Burg K.J.L. *Absorbable and Biodegradable polymers*, CRC Press, Boca Raton, 2004.
183. Rihovi, B. *Adv. Drug Delivery Rev.* **21** (2), 157--176, 1996.
184. Deka, H., et al. *Nanoscale Res. Lett.* **4** (7), 758--765, 2009.
185. Nikje, M.M.A., et al. *Colloid Polym. Sci.* **291** (4), 903--909, 2013.
186. Kalita, H., & Karak, N. *Polym. Eng. Sci.* **52** (11), 2454--2461, 2012.
187. Feng, L., et al. *Front. Chem. China* **3** (1), 1--5, 2008.

188. Kessler, F., et al. *Tissue Eng. Regen. Med.* **11** (1), 23--31, 2014.
189. Sirivisoot, S., & Harrison, B.S. *Int. J. Nanomed.* **6**, 2483--2497, 2011.
190. Mirabedini, S.M., et al. *Appl. Surf. Sci.* **257** (9), 4196--4203, 2011.
191. Rao, L., et al. *Acta Biomater.* **8** (6), 2233--2242, 2012.
192. Ho, T.T., et al. *Gold Bull.* **45** (3), 161--170, 2012.
193. Zhang, J.Y., et al. *Biomaterials* **21** (12), 1247--1258, 2000.
194. Okamoto, M. *Mater. Sci. Technol.* **22** (7), 756--779, 2006.
195. Pharaon, M.R. Scholz, T. & Evans, G.R.D. Tissue Engineering, in *Plastic and Reconstructive Surgery* M.Z. Siemionow & M. Eisenmann-Klein, eds., Springer-Verlag, London , 2010.
196. Gunatillake, P.A., & Adhikari, R. *Eur. Cells Mater.* **5**, 1--16, 2003.
197. Zawadzak, E., et al. *Biomed. Mater.* **4** (1), 015008--015017, 2009.
198. Pereira-Junior, O.C.M., et al. *J. Biomater. Appl.* **21** (3), 283--297, 2007.
199. Filho, J.R.L., et al. *J. Oral Sci.* **51** (3), 451--456, 2009.
200. Miao, S., et al. *Eur. J. Lipid Sci. Technol.* **114** (10), 1165--1174, 2012.
201. Kim, S.E., et al. *Biomed. Mater.* **4** (4), 044106--044117, 2009.
202. Ruff, C.A., et al. *J. Drugs Dermatol.* **7** (7), 675--677, 2008.
203. Yucedag, F., et al. *J. Appl. Polym. Sci.* **115** (3), 1347--1357, 2010.
204. Unnithan, A.R., et al. *Colloids Surf. A: Physicochem. Eng. Aspects* **415**, 454-- 460, 2012.
205. Chen, J.P., & Chiang, Y. *J. Nanosci. Nanotechnol.* **10** (11), 7560--7564, 2010
206. Park, J.K., et al. *Wounds* **25** (6), 153--159, 2013.
207. Fong, N., et al. *J. Biomed. Mater. Res. B Appl. Biomater.* **101** (2), 310--319, 2013.
208. Shaik, M.R., et al. *Int. J. Pharma Sci.* **2** (4), 112--116, 2012.
209. Chung, J.H.Y. *Polyurethane Nanocomposites as Potential Drug Delivery Systems*, Ph. D. Thesis. The University of New South Wales Sydney, Australia, 2011.
210. Borcan, F., et al. *Chemis. Central J.* **6** (1), 87--97, 2012.
211. Sivak, W.N., et al. *Acta Biomaterialia* **4** (4), 852--862, 2008.
212. Da-Silva, G.R., et al. *Mater. Sci. Eng. C* **31** (2), 414--422, 2011.
213. Baer, G., et al. *J. Appl. Polym. Sci.* **103** (6), 3882--3892, 2007.

Chapter 2

***Helianthus annuus* oil based hyperbranched polyurethane**

Highlights

This chapter comprises of two subchapters. The first subchapter deals with the synthesis, characterization and properties evaluation of *Helianthus annuus* oil based HBPU. The properties of HBPU were compared with a linear analog. HBPU was synthesized from PCL as a macroglycol, BD as a chain extender, MG of *Helianthus annuus* oil as a renewable resource based chain extender, PE as a branch generating unit and TDI by using an A₂+B₂+B₄ approach. Linear PU was also synthesized using the aforementioned starting materials, excluding the branch generating unit (PE) to examine the role of hyperbranched architecture on ultimate performance of polymers. The results demonstrated the superiority of HB architecture over the linear one in terms of mechanical, thermal, chemical and biological properties. In this venture, the second subchapter describes the effect of multifunctional component (PE) content in tailoring the mechanical, thermal, chemical and bio-interfacial attributes of HBPU. The performance of HBPU was also compared with a similar architectural PU without using *Helianthus annuus* oil. Bio-based HBPU with 5 wt.% of PE exhibited the best performance among the studied PU. The chapter, thus provides an insight into the concomitant benefits of multidimensional HB architectural and vegetable oil based PU in biomedical domain like TE. Therefore, the best performing *Helianthus annuus* oil based HBPU with 5 wt.% of PE was carried forwarded as the matrix for preparation of various NC based biomaterials.

Parts of the chapter are published in

- 1) Das B., Konwar, U., Mandal. M., & Karak, N. *Ind. Crops Prod.* **44**, 396--404, 2013.
- 2) Das B., Chattopadhyay, Mandal, M., P., Voit, B., & Karak, N. et al. *Macromol. Biosci.* **13**, 126--139, 2013.

2A Synthesis, characterization and properties evaluation

2A.1 Introduction

There is an escalating environmental concern on use of polymers due to the depletion of petroleum based resources, global warming and heaping up of non-degradable wastes. Thus, utilization of renewable resources for material fabrication and shifting towards biodegradability have attained significant impetus.^{1, 2} Exploration of vegetable oil, among other renewable resources is one of the prime routes for the synthesis of polymer. This is due to ready availability, low toxicity, suitable structural composition and inherent biodegradability of vegetable oil.² Moreover, the history of PU chemistry depicts its strong association with renewable resources like utilization of glycerol derived from hydrolysis of natural oil, naturally hydroxylated castor oil (castor beans), epoxidized soybean oil and so on.^{1, 3, 4} Moreover, *Helianthus annuus* L. seed oil with suitable fatty acids' composition (palmatic acid-5.2%, stearic acid-2.7%, oleic acid-37.2%, linoleic acid-53.8%, linolenic acid-1% and others 0.1%) is also exploited to synthesize bio-based PU.^{2, 5} This is regarded as dual purpose oil as it can be used both in industry and is edible as well. Thus, its inclusion in PU backbone could confer biocompatibility for biomedical applications. In this outlook, the prospective of *Helianthus annuus* oil in PU synthetic route will be endeavored in this chapter to obtain the biodegradable polymeric material.

Furthermore, ample of investigation suggested better efficacy of HB polymer over its linear analog, in terms of solubility, viscosity, reactivity and compatibility with other systems. Reports also suggested better physico-mechanical performance, thermo-chemical stability and degradability of HBPU compared to its linear analog.⁴⁻⁷ Different approaches like polycondensation of AB₂ monomers (with and without multifunctional core unit) and A₂+B₃ method are generally used to synthesize HB polymers.^{8, 9} However in A₂+B₃ approach, different structural intermediate units as well as crosslinked products may be formed. Thus, to direct the formation of AB₂ intermediates, approaches like A₂+B₂B* and AA*+B₂B* are investigated.^{8, 9} In these approaches, the selectivity and reactivity of functionalities are enhanced, thus eliminating the formation of undesired intermediates. Abdelherim et al. reported the synthesis of HBPU-urea by AA*+B₂B* approach where three different diisocyanate (AA* monomers) reacted with two bishydroxyamines (B₂B* monomer).⁸ Furthermore, the advantages of vegetable oil based HBPU

(utilizing A₂+B₃ approach) over its linear HBPU were also illustrated by Karak and co-workers.^{4, 5, 7} However, the aforementioned approaches encase some pros and cons and therefore appropriate strategy should be opted delicately to obtain a high quality product. In this regard, an approach like A₂+B₂+B₄ using commercially available and bio-based starting materials may be an alternative option. Moreover, HBPU exhibits more complex surface properties than its linear analog due to its proliferated end groups.¹⁰ These end groups are easily available for chemical modification and interactions with biomolecules, water, volatile organic component, etc. and thereby making HBPU as interesting biomaterials for biosensors, devices, catheters, etc. applications.¹⁰

Therefore, driven by the excellence of HB topology, benefits of vegetable oil and biodegradability of PU, this chapter demonstrated the synthesis, characterization and properties evaluation of *Helianthus annuus* oil based HBPU. Linear PU was also studied for comparison purpose.

2A.2 Experimental

2A.2.1 Materials

Helianthus annuus oil was procured from Sigma-Aldrich, Germany. It has density of 0.92 g/mL at 25 °C. It contains mainly saturated fatty acids (stearic and palmitic acids), monounsaturated fatty acid (oleic acid) and polyunsaturated acid (mostly linoleic acid). It was used to prepare MG, a chain extender.

Glycerol was obtained from Merck, India. It density is 1.26 g/mL with minimum assay 99%, M_w is 90.09 g/mol and maximum sulphated ash (0.005%). Glycerol was used as a triol (alcoholizing reagent) for converting the triglyceride of *Helianthus annuus* oil into its MG.

TDI was purchased from Sigma-Aldrich, Germany. It has formula weight (F_w) of 174.16 g/mol, and is a mixture of 2,4-isomer (80%) and 2,6-isomer (20%). It density is 1.214 g/mL, mp is 21.8 °C and bp is 251 °C. Herein, TDI was used as a diisocyanate in the synthesis of HBPU. It was used as received.

PCL was obtained from Solvay Co., UK. It has density of 1.071 g/mL, the hydroxyl number is 37 mg KOH/g and M_w is 3000 g/mol. It was used after drying in vacuum oven at 45 °C for overnight. Properly dried PCL was used as a macroglycol for the synthesis of HBPU.

BD was obtained from Merck, Germany. Its M_w is 90.12 g/mol, density is 1.02 g/mL and minimum assay is 99%. It was subjected to vacuum drying and used as one of the chain extenders.

PE was procured from Sigma–Aldrich, Germany. It bp is 276 °C and mp is 253-258 °C with minimum assay $\geq 99\%$. It was recrystallized from ethanol and was vacuum dried before use. It was used as the branch generating unit for the synthesis of HBPU.

Xylene was bought from Merck, India. It has M_w 106.17 g/mol, density is 0.86 g/mL (at 20 °C) and bp is 137-143 °C. It was distilled before use and preserved in 4A molecular sieve. It was used as a solvent for the synthesis of PU.

N, N'-Dimethyl acetamide (DMAc) was bought from Merck, India. It has density 0.94 g/mL (at 25 °C) and bp is 165-167 °C. DMAc was soaked overnight in CaO followed by vacuum distillation and then preserved in a 4A type molecular sieve before use. It was used as an auxiliary solvent.

Methanol was obtained from Merck, India. It has F_w 58.0 g/mol, purity $\geq 99.5\%$, density 0.97 g/mL and bp 56-57 °C. It was used as a solvent to check the solubility of prepared MG.

Calcium oxide was purchased from S.D. fine chemical Ltd., Mumbai. The minimum assay is 95% and it was used as received. It was used to serve twin purpose i.e for drying solvent and as catalyst for the preparation of MG.

Sodium bicarbonate was purchased from Sigma-Aldrich, Germany with minimum assay $\geq 99.5\%$ and M_w 84.01 g/mol. It was used for the purification of MG.

Molecular sieve of 4A type was procured from Merck, India. Its equilibrium capacity for water is $\geq 20\%$ at 30 °C and 75% relative air humidity. It was used to entrap trace amount of moisture from solvents.

All other reagents used for biological tests are reagent grade and used directly without any further purification.

2A.2.2 Instrumentation

FTIR spectra of PU were recorded by a Nicolet (Madison, USA) FTIR Impact 410 spectrophotometer using KBr pellets. Finely powdered polymeric samples were dispersed and grounded in KBr to form the transparent KBr pellets, to characterize the samples. ^1H NMR and ^{13}C NMR spectra of the synthesized polymers were also recorded by a 400 MHz FTNMR

(JEOL, Japan) spectrometer using d_6 -DMSO as the solvent and TMS as the internal standard. UV spectra were studied at room temperature ($\sim 27^\circ\text{C}$) in a Hitachi (U2001, Tokyo, Japan) UV spectrophotometer. TGA was done by a Shimadzu, USA thermal analyzer, TG 50 with nitrogen flow rate of 30 mL/min at a heating rate of $10^\circ\text{C}/\text{min}$. X-ray diffraction (XRD) studies were done at room temperature ($\sim 27^\circ\text{C}$) using a Rigaku X-ray diffractometer (Miniflex, UK) under 40 kV and 30 mA source with $\text{CuK}\alpha$ ($\lambda = 0.154\text{ nm}$) radiation in a sealed tube at a scan rate of $5^\circ/\text{min}$ over the range of 10 - 70° . The surface morphology of PU was studied by a JEOL scanning electron microscope, Model JSM-6390LV (Japan) after platinum coating on the surface.

Tensile strength and elongation at break (EB) were measured with the help of a universal testing machine (UTM), Zwick Z010, Germany with a 10 kN load cell. The test was performed at a crosshead speed of 50 mm/min by using samples of dimensions $10\text{ cm}\times 1\text{ cm}\times 0.02\text{ cm}$. Scratch hardness of the sample was measured by a scratch hardness tester, Model No.705 (Sheen instrument limited, UK) with stylus accessory and a travel speed of 3-4 cm/s. Impact resistance was determined by a falling weight tester (SC Dey & Co., India) as per the standard ASTM D 1037.⁷ In this method, a weight of 0.85 kg was allowed to fall on the film coated on a mild steel plate from minimum to maximum falling heights. The maximum height up to which the film was not damaged was taken as impact resistance. Bending test was used for assessing the resistance of the film coated on a galvanized tin plate to damage/crack when subjected to bending around a cylindrical mandrel. The film was bent over a 1-3 mm diameter mandrel through 180° as per the standard procedure.⁷ The film is said to be flexible if it does not show any damage or crack.

Chemical resistance test was performed in a number of different chemical media as per the ASTM D 543-67 standard procedure by taking weighted amount of samples in 100 mL beakers containing 75 mL of individual chemical medium for the period of 21 days.⁷ The chemical resistance was determined by weight loss percentage and visual observation.

2A.2.3 Methods

2A.2.3.1 Preparation of monoglyceride

MG was prepared by the standard procedure as reported elsewhere.¹¹ A three-necked round bottom flask was flushed with nitrogen and charged with 1:2 mole ratio of oil to glycerol (and extra 10 wt.% glycerol of the total glycerol to accommodate the loss during heating process) and 0.05 wt.% of CaO (with respect to the oil) under continuous mechanical stirring. The mixture

was then heated up to (220±5) °C for at least 1 h until it was converted to MG, confirmed by its solubility in 1:3 volume of methanol at room temperature. The prepared MG was purified from uncombined glycerol by dissolving the fatty acid product in ether and then washing with 20% solution of sodium sulfate in water.¹² Free fatty acids were removed from the ether solution by several washings with small portions of sodium bicarbonate solution and again washed with sodium sulfate solution to remove soaps. Ether solution was finally dried over anhydrous sodium sulfate and the ether was evaporated under vacuum.

MG was further characterized by ¹H and ¹³C NMR analyses for the assessment of its purity. In ¹H NMR spectrum, general pattern of peaks is produced by protons attached to the mono-, di-, and tri-glycerides. There may be an alteration in the chemical shift of protons attached to glycerol carbon due to the chemical structure of the different fatty acids, but these shiftings are small and the patterns are generally the same.¹³ ¹H and ¹³C NMR spectra of the prepared MG, represented in **Figure 2A.1(a and b)** clearly indicated the structure and purity of MG.¹³ The other peaks corresponding to the protons and carbon atoms present in different fatty acids (represented by R of MG) are also assigned in the **Figure 2A.1**.

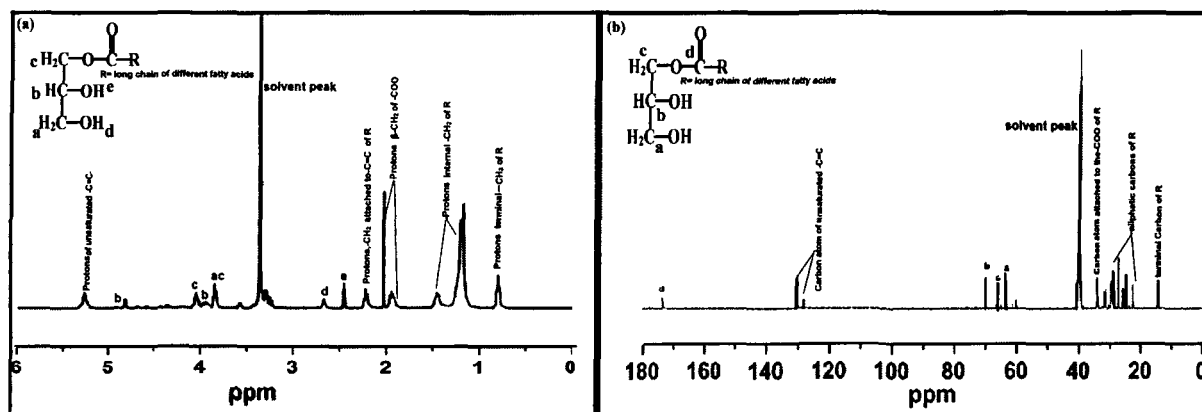


Figure 2A.1: ¹H (a) and ¹³C (b) NMR spectra of MG of *Helianthus annuus* oil

2A.2.3.2 Synthesis of hyperbranched and linear polyurethanes

A three-neck round bottom flask was equipped with a nitrogen gas inlet, a mechanical stirrer and a dropping funnel for this polymerization reaction. Required amounts of MG and PCL were taken in the flask with 10-15 mL xylene. Measured solution of BD in DMAc was then added to the reactor and the overall solid content of the reaction mixture was kept at 45%. Required

amount of TDI was added dropwise into the reactor at room temperature (ca 25°C) by maintaining NCO/OH ratio <1. The mixture was heated at (75±2) °C for 3-4 h under constant stirring to obtain a viscous mass and it was treated as –OH terminated pre-polymer (a B₂ reactant).

The pre-polymer was cooled down to room temperature and the rest amount of TDI was added into the reactor. The reaction mixture was diluted with xylene, then the desired amount of PE solution was added dropwise to synthesize HBPU by maintaining the NCO/OH ratio equal to 1. In the second step, the solid content was brought down to 20% to avoid gelation. The reaction was then heated for 3-4 h at (75±2) °C until the sufficient viscosity was reached without gel formation. Linear PU (coded as LPU) was synthesized by the same procedure except in the second step instead of PE, BD was added. A part of the viscous product was precipitated in water and then dried in a vacuum oven at 50 °C for 48 h for structural analysis and the rest amount was solution cast on different substrates for further studies. The exact mole compositions of the synthesized PU are given in **Table 2A.1**.

Table 2A.1: Composition of reactants (mmol) with 33% of hard segment

Polymer code	MG	PCL	BD	PE	TDI	NCO/OH ratio
HBPU	2	1.5	2.5	1	8	1:1
LPU	2	1.5	4.5	-	8	1:1

2A.2.3.3 Sample preparation for performance study

Mild steel strips (15 cm×10 cm×0.144 cm) were coated with the polymer solutions for gloss and impact resistance studies. Similarly, tin (15 cm× 5cm × 0.019cm) and glass (7.5cm ×2.5 cm×0.139 cm) strips were coated for the bending and chemical resistance tests, respectively. The dried films from the glass plates were peeled off by immersing the plates in hot water, followed by drying under vacuum and stored for 7 days before testing. The thickness of the films was measured by a Pentest coating thickness gauge (Model 1117, Sheen Instrument Ltd., UK).

2A.2.3.4 Broth culture technique for biodegradation

Broth culture technique was used for the biodegradation study as reported earlier.¹⁴ In brief, the nutrient broth medium was prepared to culture the bacteria by dissolving 3.61 g KH₂PO₄, 1.75 g

MgSO₄·7H₂O, 2 g (NH₄)₂SO₄, 2 g Na₂HPO₄, 0.2 g CaCl₂·2H₂O, 50 mg FeSO₄·7H₂O, 1 mg CuSO₄·7H₂O, 50 µg MnSO₄·5H₂O, 70 µg ZnSO₄·7H₂O, 10 µg H₃BO₃·5H₂O and 10 µg MoO₃ in 1.0 L of Milli-Q water. The culture media was sterilized by autoclaving at 121 °C and 15 lb pressure for 15 min. Two *Pseudomonas aeruginosa* strains SD2 and SD6 and one *Bacillus subtilis* strain MTCC73 were used in this test. The bacteria was cultured at 37 °C in the prepared media for two days, separately. In brief, the test tubes containing the culture medium (100 µL) were inoculated with 10⁸/mL of bacterial culture of each strain (as calculated from McFarland turbidity method). The test tubes were incubated under sterile condition at 37 °C for the degradation study. Further, the polymer films (in triplicates) were immersed in 10 mL of bacterial culture, in test tubes under sterile condition inside a laminar air hood and incubated at 37 °C for the required time period. The bacterial growth was evaluated by spectrophotometer at 600 nm against the blank culture media at every 7 days of interval. The growth was inferred from the optical density (OD) using McFarland turbidity as the standard. A negative control was considered where no polymer was used.

McFarland standard preparation

The McFarland turbidity was taken as standard to keep the bacterial count in a given range by adjusting the turbidity of the suspension.¹⁴ Five McFarland standards were prepared by mixing solution of 1% BaSO₄ and 1% H₂O₂ in different proportion. The absorbance plot at 600 nm against known number of bacterial population provided a straight line. Thus from the plot, unknown population was calculated by measuring the absorbance.

2A.2.3.5 Statistical analysis

Experiments were repeated three times or more with triplicate samples and data were represented as means±standard derivations. Statistical significant difference ($p < 0.05$) was performed by one-way ANOVA using appropriate software.

2A.3 Results and discussions

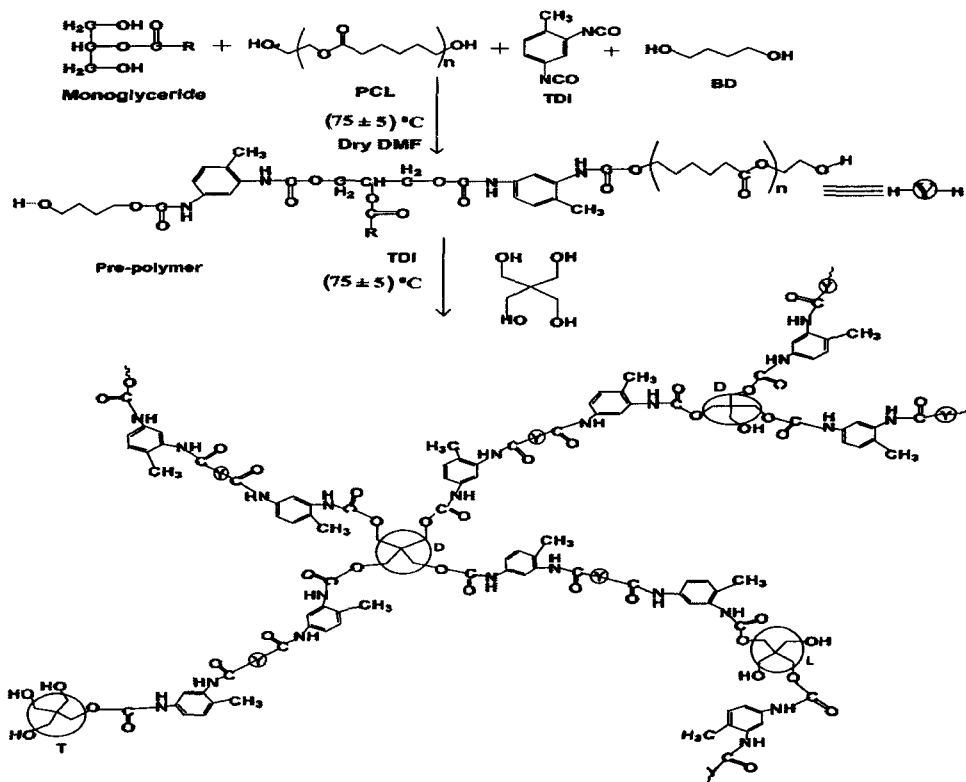
2A.3.1 Synthesis of polyurethanes

HBPU with PE as branched generating polyol moiety was synthesized by one pot polymerization technique using A₂+B₂+B₄ approach (Scheme 2A.1). In the first step, mole ratio of diisocyanate

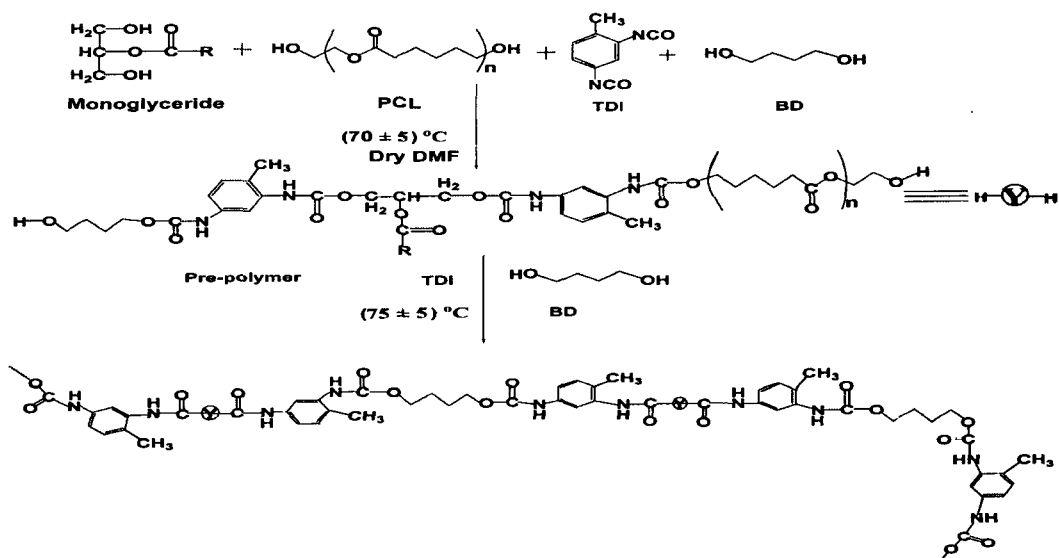
to diols (PCL, MG and BD) was maintained at <1 such that -OH terminated pre-polymer was formed. This pre-polymer acts as a diol based B_2 monomer and tetra-functional PE, as the B_4 monomer reacted with TDI as diisocyanate based A_2 monomer in the second step to form HBPU. The reaction mixture was diluted to 20% solid content and the tetra-functional PE was added dropwise in the second step to prevent gelation which may form in this synthetic process. The polymerization reaction was carried out below $80\text{ }^\circ\text{C}$, as gel formation for the reaction was observed at above $80\text{ }^\circ\text{C}$. LPU was synthesized by the same procedure but PE was replaced by BD in the second step (**Scheme 2A.2**). For the synthesis of LPU, the solid content was maintained 40-45% throughout the reaction. The time required for the completion of the reaction was more for linear analog as compared to HBPU. The synthesis of PU requires complete monitoring of temperature, solid content, nitrogen flow, maintaining of composition of the reactants, rate of addition, concentration of the branch generating unit and speed of stirring to obtain the good quality of polymer. The second step of this synthetic procedure is very crucial as the multifunctional moiety reacts very fast with the diisocyanate and can lead to crosslinking of the product. The tendency of gelation is much less for LPU because of the absence of highly reactive multifunctional PE.

2A.3.2 FTIR study

FTIR is used to confirm the chemical groups or linkages within a polymeric structure along with the extent of hydrogen bonding, conformation, accessibility as well as interaction between hard and soft segments in PU. FTIR analysis confirmed the formation of urethane linkages by observing the desired bands at their respective positions.⁷ The absence of band for free $-\text{NCO}$ at 2270 cm^{-1} indicated the completion of the reaction (**Figure 2A.2**). The band at $3200\text{-}3500\text{ cm}^{-1}$ represented the overlapping of $-\text{OH}$ and $-\text{NH}$ stretching vibrations in both the PU. Higher intensity of the $-\text{OH}$ and $-\text{NH}$ overlapping band for HBPU may be due to the presence of larger number of such surface functionalities and hydrogen bonding compared to LPU. In addition to this, the use of more amount of sample while taking the spectra as indicated by higher intensity of all the observed bands of HBPU compared to LPU is also another reason for such observation. Two bands were appeared at $2945\text{-}2900$ and $2830\text{-}2800\text{ cm}^{-1}$ for symmetric and asymmetric vibration of $-\text{CH}_2$, respectively. **Figure 2A.2a** showed the FTIR spectra of the oil, HBPU and LPU. Thus, these spectra confirmed the presence of urethane linkage in both the polymer owing



Scheme 2A.1: Synthesis of HBPU



Scheme 2A.2: Synthesis of LPU

to the presence of characteristic bands at $1710-1729\text{ cm}^{-1}$ for $-\text{C}=\text{O}$ stretching vibration, at $1530-1536\text{ cm}^{-1}$ for $-\text{CN}$ stretching/ $-\text{NH}$ bending vibration and at $1040-1060\text{ cm}^{-1}$ for $-\text{O}-\text{C}=\text{O}$ stretching vibration of urethane.⁷ The extent of interaction between $-\text{NH}$ and $-\text{OH}$ group hints the phase separation between soft and hard segments in PU. Therefore, the phase separation in PU can be determined by evaluating the intensity and position of $-\text{NH}$ stretching vibration. A significant amount of $-\text{N}-\text{H}\cdots\text{O}=\text{C}$ (urethane) hydrogen bonding also indicates an extensive phase separation in PU.¹⁵ In this investigation, lowering in the absorption frequency of HBPU (1734 cm^{-1}) was observed as compared to LPU (1745 cm^{-1}) indicated an increase in hydrogen bonded $-\text{C}=\text{O}$ in the former than the later. Similarly, comparatively little increase in intensity of hydrogen bonded $-\text{OH}$ in HBPU than LPU spectra suggested difference in the phase separation behavior between PU.

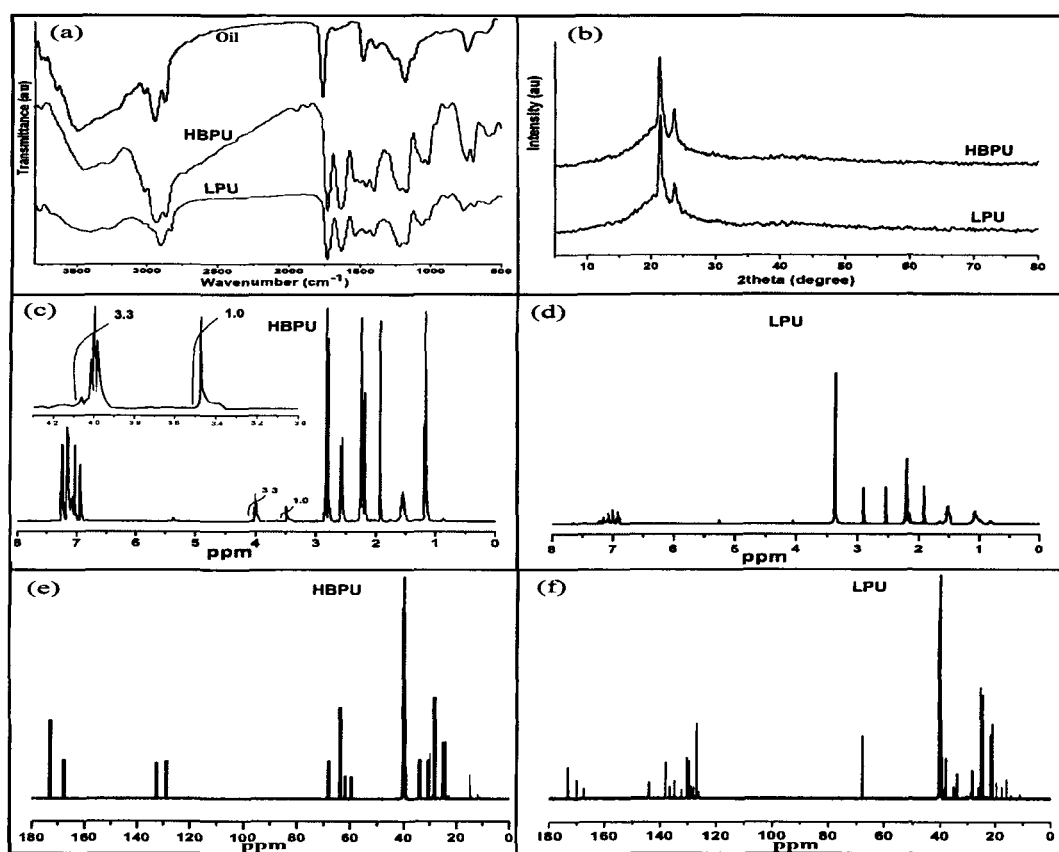


Figure 2A.2: Representing the FTIR spectra (a), XRD patterns (b), ^1H NMR spectra (c and d) as well as ^{13}C NMR (e and f) of HBPU and LPU, respectively

2A.3.3 XRD study

In this present investigation, XRD study reveals two diffraction peaks at $2\theta = 21.2^\circ$ and 23.4° due to the lattice plane corresponding to (110) and (200) of the PCL crystal.^{7, 14} LPU and HBPU both showed these diffraction peaks as shown in the **Figure 2A.2b**. The mole and wt.% of PCL used in the both HBPU and LPU are almost same. However, little difference in crystallinity between the polymers was observed in the XRD as well as supported by DSC study. Less crystallinity of HBPU compared to LPU is due to confined geometry of the former.

2A.3.4 NMR study

¹H NMR and ¹³C NMR spectra as shown in **Figure 2a.2(c-f)** confirmed the formation of HBPU and LPU. Peaks at δ (ppm) = 0.84, 1.18 and 1.53 are due to the protons of terminal methyl group, all internal $-\text{CH}_2$ and the protons for $-\text{CH}_2$ attached next to the terminal methyl group of the fatty acid chains of the vegetable oil, respectively.⁴ The peaks for protons of allylic $-\text{CH}_2$ of long chain fatty acids of MG of the oil, $-\text{CH}_2$ attached to $-\text{NH}$ of urethane bond/ $-\text{CH}_2$ attached to the ester group and $-\text{CH}_3$ of TDI were observed at δ (ppm) = 1.92, 2.2 and 2.5 respectively. The $-\text{CH}_2$ protons attached to the unsubstituted $-\text{OH}$ and double bond of fatty acid appeared at δ (ppm) = 3.47 and 5.3, respectively. The peaks ranging from δ (ppm) = 7.46-6.9 indicated the presence of aromatic protons of TDI present in PU. The peaks distinguishing the structure of HBPU from LPU are δ (ppm) = 4.04, 4.01, 4.00 and 3.98 which are due to the presence of tetra-, tri-, di-, and mono-substituted PE respectively in HBPU structure.¹⁶ In this case, the integration ratio of substituted $-\text{OH}$ and unsubstituted $-\text{OH}$ was found to be 3.07, which clearly indicates that the synthesized PU has HB structure as branching is generated when this ratio is >2 . DB was calculated by taking the integration ratio of the substituted $-\text{OH}$ with the integration ratio of both the substituted and unsubstituted $-\text{OH}$ and it was found to be 0.76 (**Figure 2A.2c**). Thus, the ¹H NMR data confirmed the formation of vegetable oil based HBPU and its linear analog.

In ¹³C NMR spectra (**Figure 2A.2(e and f)**), the aliphatic carbon atoms of long chain fatty acid in MG were represented by the peaks at δ (ppm) = 11.3-33.8 and 24.6-28. The peak corresponding to values δ (ppm) = 167.5 represented the carbon atom of urethane linkage. The peak at δ (ppm) = 59.8, 62.1 and 67.9 in the ¹³C NMR spectrum of HBPU represented the carbon atom of tetra-, tri-, mono- substituted PE moiety, respectively. However, these peaks were not observed for LPU. The peak value at δ (ppm) = 63.9 ppm represented the di-substituted PE or $-\text{C}(\text{O})-\text{O}-$

CH₂ attached to urethane was observed for the both PU. Carbon atom of benzene ring was denoted by the peaks corresponding to values δ (ppm) =128.2-132.2 and 140. The peak value at δ (ppm) = 173.5 denoted the carbon atom of ester carbonyl of MG.

2A.3.5 SEM study

The morphological study of the synthesized PU was done by the analysis of SEM images. The SEM images of PU revealed that surfaces were not smooth and there was a degree of inhomogeneity, which may be due to the presence of soft and hard segments that leads to the phase separation. Moreover, HBPU exhibited rougher surface than LPU. Difference in the surface roughness (**Figure 2A.3**) of HBPU and LPU may be attributed to the differences in the hydrogen bonding in their structure and the composition of the hard segments. The presence of tetra-functional branching moiety in the hard segment of HBPU may enhance the hydrogen bonding between hard segment-hard segment as well as hard segment-soft segment.¹⁷ Both of these factors are thus responsible for such morphological differences.

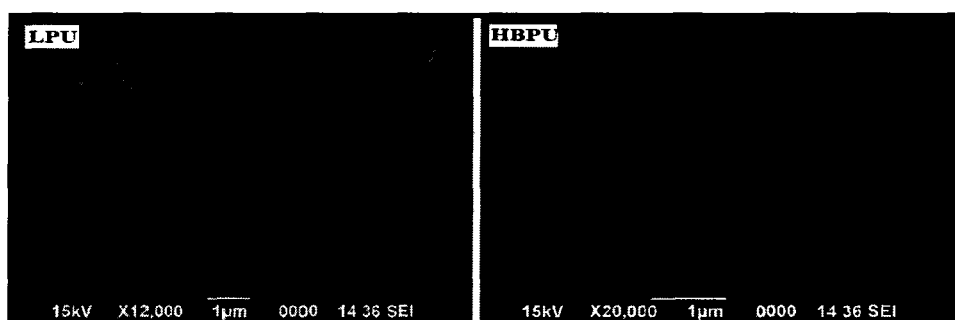


Figure 2A.3: Representing the SEM images of LPU and HBPU

2A.3.6 Mechanical properties

Mechanical properties of PU depend upon the presence of hydrogen bonding, polar groups, entanglement of chains, crystallinity, the reactivity of the multifunctional groups and interactions of the hard segments present in the structure.⁷ HBPU showed higher tensile strength and EB as compared to the linear analog (**Table 2A.2**) due to the predominance of above factors in HBPU than the linear analog. The impact resistance of HBPU was found to be 100 cm which was the limit of the instrument used whereas for LPU, it was 90 cm. The scratch hardness of both HBPU

and linear analog was found to be almost equal, (4.7±0.01) kg and (4.3±0.04) kg respectively. The flexibility of the synthesized PU was very good, though HBPU showed higher flexibility than the linear one (Table 2A.2). The enhanced flexibility of HBPU is due to the presence of long PCL segment and long chain fatty acid moiety in the highly branched compact structure and the presence of larger void spaces and non-entangled structure in comparison to the linear one. HBPU could be bent over a mandrel of diameter of <1 mm compared to <2 mm diameter for LPU. Better mechanical properties of HBPU compared to LPU may be attributed to combined effect of stronger intra/inter-molecular secondary interactions (due to high number of surface end groups), hydrogen bonding and compact confined geometry of the former than the later. Furthermore, the overall good performance of both PU is due to the presence of long alkyl chain of MG, crystallinity of PCL moiety with ether and ester linkages along with polar urethane linkages.

Table 2A.2: Mechanical properties of HBPU and LPU

Polymer code	Tensile strength (MPa)	EB (%)	Impact resistance (cm)	Scratch hardness (kg)	Bending (mm)
HBPU	23.18±0.5	750±6.0	100	4.7±0.01	<1
LPU	18.9±0.72	700±4.3	90	4.3±0.04	<2

2A.3.7 Thermal study

The thermal stability of PU is related to the different factors such as chemical structure, composition, linkages, M_w and intra/intermolecular forces. TGA thermograms and DSC curves for the synthesized PU are presented in Figure 2A.4. HBPU showed two-step degradation and it is supported by the literature.¹⁸ The initial degradation temperature is dependent on the thermal stability of the weakest point in the macromolecular structure.¹⁹ The most thermolabile portion within the structure is assigned to the aliphatic long chain of MG and other aliphatic chain present in the structure. The next degradation temperature could be assigned due to the degradation of the urethane bond and the most thermostable aromatic moieties in the macromolecular structure. The temperature corresponding to the onset decomposition temperature ($T_{1st\ ON\ and\ END}$, $T_{2nd\ ON\ and\ END}$), 50% and 90% weight loss as well as the weight residue at 500 °C for HBPU and LPU are given in the Table 2A.3. The significant difference in

percentage residue obtained for both the sample is due to the structural differences between the polymers. The HB structure with globular confined geometry, reactive tetra-functional moiety and high surface functionalities leads to stronger intra/inter-molecular structure that might be responsible for enhancing the thermostability of HBPU compared to LPU. Further, DSC analyses showed that the mp of HBPU was 41 °C, whereas for LPU it was found to be 54 °C. This may also be attributed to the differences in secondary interactions and structural compactness in PU which might have hindered the crystallinity of HBPU.

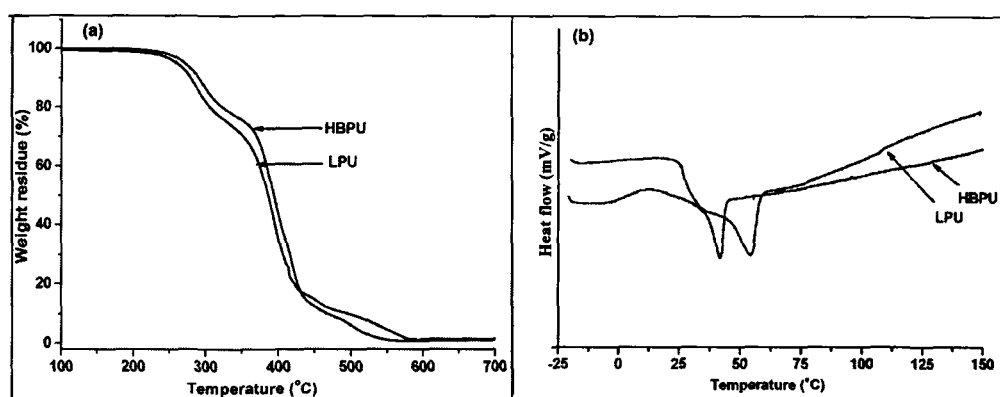


Figure 2A.4: TGA thermograms (a) and DCS curves (b) of HBPU and LPU

Table 2A.3: Thermal degradation parameters for HBPU and LPU

Polyme r code	T _{1st ON} (°C)	T _{1st END} (°C)	T _{2nd ON} (°C)	T _{2nd END} (°C)	T _{50%} (°C)	T _{90%} (°C)	Wt. residue (500 °C)
HBPU	250	317	363	453	393	495	9.8
LPU	239	305	342	442	384	467	5.4

2A.3.8 Chemical resistance test

Both HBPU and LPU (weighing 0.7-1.0 g) showed very good chemical resistance in all the chemical environments viz. 10% aqueous sodium chloride, 20% aqueous ethanol, 5% aqueous HCl and distilled H₂O except in the alkaline environment of 3% aqueous NaOH (Table 2A.4). This is attributed to the presence of different types of strong interactions in the structures of the synthesized PU. However, the poor alkali resistance is due to the presence of hydrolysable ester bonds in the structure of MG and PCL moieties of the polymers. There is no such significant

difference ($p > 0.05$) observed between both the polymers in terms of weight loss percentages in different chemical environments. However, the little improved resistance of HBPU against the chemicals may be due to their compact structure and more secondary interactions.

Table 2A.4 The weight loss (%) of LPU and HBPU in different chemical media

Polymer code	5% HCl	20% Ethanol	Distilled water	10% NaCl	3% NaOH
HBPU	0.12±0.003	0.25±0.002	0.0	0.01±0.001	5.3±0.003
LPU	0.33±0.005	0.14±0.001	0.0	0.02±0.003	6.5±0.006

2A.3.9 Biodegradation study

Biodegradation of the synthesized polymers was done by broth culture technique using both the Gram positive (*Bacillus subtilis*, MTCC73) and Gram negative (*Pseudomonas aeruginosa* SD2 and SD6) bacterial strains. In broth culture technique, the samples were exposed to selected strains of bacteria directly and remained immersed in the bacterial culture. Therefore, the biodegradable behavior of the synthesized polymer can be evaluated within a short time period compared to soil burial or other field methods.²⁰ Moreover, a comparative study was performed by monitoring the bacterial growth time to time. Depending upon the polymer, duration of 20-40 days is sufficient to get a preliminary idea on the biodegradation properties. In this present investigation, after one month of incubation of HBPU and LPU with the bacteria, it was found that both the synthesized PU were biodegradable as tested by bacterial growth. Further, it was observed that the degradation rate upto 2 weeks was almost same for HBPU and LPU (**Figure 2A.5**). After that induction period, the degradation was rapid for HBPU in comparison to that of LPU. Thus, HBPU was more susceptible to bacterial degradation. The standard deviation is also represented in **Figure 2A.5(d and e)**. It was observed that the *Pseudomonas aeruginosa* strain SD6 has the maximum growth on PU films compared to the other strains of bacteria ($p < 0.01$) used in the present study. This is due to the fact that this strain is well known for possessing the metabolic versatility and it can consume more than seventy five organic compounds. Moreover, the well exposed and expanded HB structure of HBPU together with their rough surface compared to its linear analog favored better attachment of the bacteria to form a bio-film which can easily metabolized HBPU to extract the nutrients. SEM images (**Figure 2A.6**) also witnessed

that HBPU had undergone better biodegradation as compared to the linear analog in the same time period by *Bacillus subtilis* MTCC73. This is due to the globular, confined structural geometry of HBPU that favored easy penetration of the bacterial strains within the macromolecular structure and better interaction with HBPU matrix. Thus, HBPU has enhanced biodegradation compared to LPU. The extent of biodegradation is apparently more in HBPU compared to LPU, when analyzed through SEM images, whereas the difference in bacterial growth count was not that large. This may be due to the fact that a small amount of bacterial culture was taken from the tested media where polymeric film was present. However, numbers of bacteria that remain adhered to the polymeric sample and metabolizing it may vary depending upon the adherence nature and susceptibility of polymer.

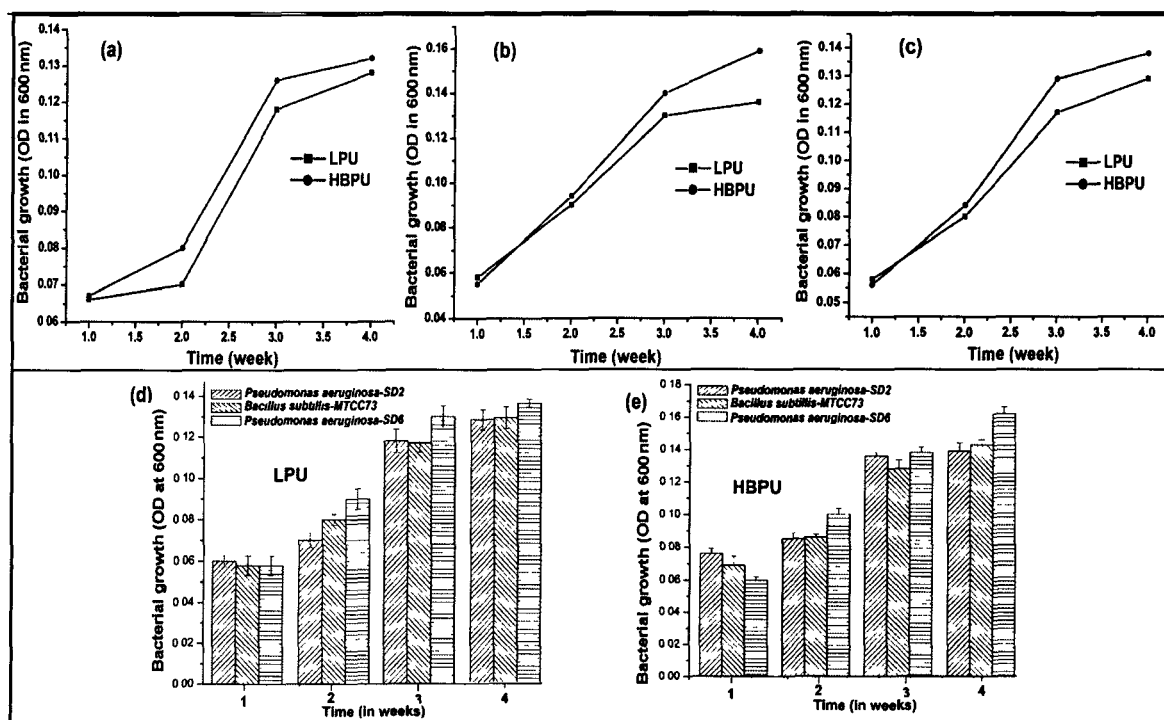


Figure 2A.5: Bacterial growth curves of *Pseudomonas aeruginosa* SD2 (a), *Pseudomonas aeruginosa* SD6 (b) and *Bacillus subtilis* MTCC73 (c) on HBPU and LPU as well as the standard deviation for bacterial growth for LPU (d) and HBPU (e)

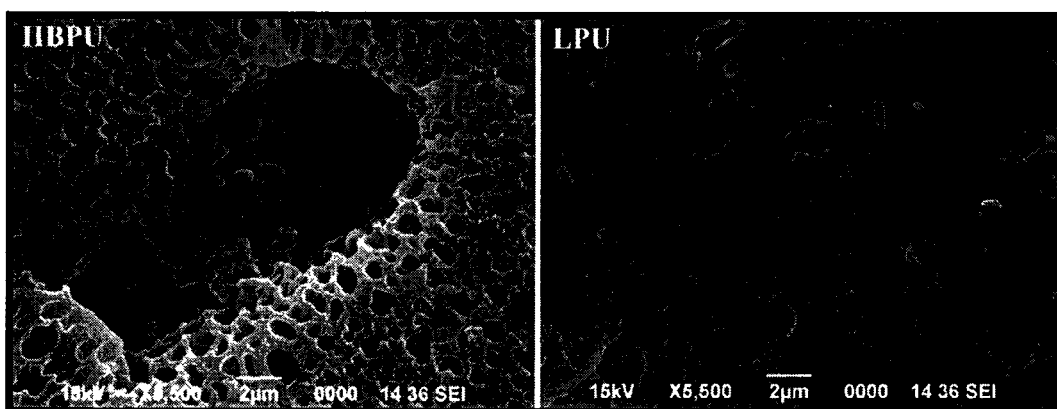


Figure 2A.6: Representative SEM images of the biodegraded HBPU (a) and LPU (b) by *Bacillus subtilis* MTCC73 after 4 weeks of incubation

2A. 4 Conclusion

The environmentally benign *Helianthus annuus* oil based HBPU and its linear analog were synthesized successfully by using the pre-polymerization method and characterized by using various analytical and instrumental techniques. It was established that HB architecture conferred better performance to PU compared to linear analog in terms of mechanical, thermal, chemical and biodegradation attributes. It could also be inferred that the biodegradable HBPU with the branching points, large number of peripheral end groups and globular confined structure has the structural and compositional benefits. Thus, this HBPU has the potential to replace or minimize the use of non-biodegradable and petroleum based products.

2B Effect of vegetable oil and multifunctional content

2B.1 Introduction

The tailored made properties of PU along with the desirable biological attributes forwarded it as the most explored synthetic biomaterial, especially in TE. Literatures are available on tuning of properties of PU by a subtle variation in chemical composition, NCO/OH ratio, changing the hard and soft segment ratio, etc.^{4, 7, 21} Further, a minute quantitative change (wt.%) of a particular component can influence the performance of such PU.²² Kalita and Karak have tailored the toughness, thermostability and the shape memory behavior of HBPU by variation of TEA content, a branch generating unit.²² They have also varied the vegetable oils (*Mesua ferrea*, *Helianthus annuus* and *Ricinus communis* oils) and tuned the performance of the same HBPU. The rate of biodegradation of PU could also be tailored by varying the chemical nature of a macroglycol.^{23, 24} Thus appropriate choice of feed stocks and their relative amount as well as architectural features are indeed important to achieve tunable properties of PU. Moreover, the previous subchapter also illustrated the advantageous effect of HB architecture on the performance of bio-based PU.

The presence of large number of freely exposed surface groups in HB polymers may alter the absorption profile of biomolecule/protein in a positive way. These polymers due to their special topological structures have found applications in the biomedical domains like drug delivery, gene transfection, protein purification/delivery/detection, etc.^{6, 10} Reichelt et al. reported enhancement in protein absorption with the increase in DB, –OH group, flexibility, etc.¹⁰ DB, multidimensional compact structure and end functionalities are important factors to tune the performance of HB polymers. The extent of branching influences the chain entanglement, thus the physico-mechanical attributes of the final product.^{25, 26} Generally, long chain branched structure confers better strength and toughness than short branched architecture. Moreover, Elherim et al. also reported that the properties of PU-urea are governed by the strong intra/inter-molecular secondary interactions.²⁷ The cited literature thus revealed the influence of multitude of parameters on controlling the properties of HB polymers. However, the effect of such chemical nature and composition on bio-interfacial performance of biomaterials is not explored substantially, particularly for bio-based HBPU. It is also pertinent to mention that vegetable oil based HBPU has not been utilized as a promising scaffold material for TE to the best of our

knowledge. Thus, bio-based HBPU with its unique structural features and tailor-made properties can provide a platform to design advanced tissue scaffold.

Thus, this subchapter was focused to examine the effect of content of branching unit (PE) on the physico-mechanical and bio-interfacial performance of HBPU in a comprehensive manner. Further, the role of vegetable oil moiety in HBPU for biomedical applications (like TE), PU with and without the MG of *Helianthus annuus* oil was also investigated.

2B.2 Experimental

2B.2.1 Materials

Chemicals for the synthesis of HBPU such as TDI, PCL BD, PE, *Helianthus annuus* oil and solvents like xylene, methanol and DMAc were the same as elaborated in section 2A.2.1. Dulbecco's Modified Eagle's Medium (DMEM) and fetal calf serum (FCS) were procured from Life Technologies, USA. Multi-well tissue culture plates were purchased from Nunc, Denmark and Peerless, India, respectively. K3 ethylenediaminetetraacetic acid (EDTA) tubes and vacuum blood collection tubes were obtained from Peerless Biotech, India. All the other items used for the biological studies were of reagent grade.

Animals

Male Wistar rats weighting 200 to 250 g were obtained from the Laboratory Animal Resources, Division of Pharmaceutical Technology, Defense Research Laboratory, Tezpur, India. The animals were housed in a specific pathogen-free facility with temperature range of 22-26 °C, relative humidity range of 70-75% with 12 h alternating light and dark cycles and given adequate standard rodent chow (Pranav Agrotech Ltd, Delhi, India) and filtered water *ad libitum*. All animals received care in accordance with the guide of Care and Use of Laboratory Animals (National Institute of Health, with publication no. 85-23, revised 1985). All experimental protocols were reviewed and accepted by the Institutional Animal Ethics Committee (IAEC).

2B.2.2 Instrumentation

The physico-chemical structural and thermal analyses were recorded using the same instruments like XRD, FTIR, NMR, TGA, DSC and UV-visible spectroscopic technique as described in section 2A.2.2. The morphological studies of PU, porous PU and degraded products were carried

out by the same SEM instrument as described in section 2A.2.2. The mechanical performance of the materials was done by using UTM, scratch hardness and falling weight tester as mentioned in section 2A.2.2.

2B.2.3 Methods

2B.2.3.1 Synthesis of hyperbranched polyurethanes

MG of *Helianthus annuus* oil was prepared and purified by the same protocol as elaborated in section 2A.2.3.1. For the synthesis of oil based HBPU, same A₂+B₂+B₄ approach was adopted as mentioned in section 2A.2.3.2. However, in the second step of the reaction, PE solution in different wt.% (1-5) was added dropwise (NCO/OH ratio equal to 1), separately. Thus, HBPU with 1, 2, 3 and 5 wt.% of PE were synthesized and coded as HBPU1, HBPU2, HBPU3 and HBPU5, respectively. HBPU without MG (SHBPU) were also synthesized following the same procedure with 2 and 6 wt.% of PE and coded as SHBPU2 and SHBPU6, respectively. The exact mole compositions of the reactants for synthesizing PU are shown in **Table 2B.1**.

Table 2B.1: Composition of reactants (mmol) for synthesis of HBPU with varying wt.% of PE

Sample code	MG	PCL	BD	PE	TDI (1st/2 nd steps)
HBPU1	2	1.5	2	0.5	5/1.5
HBPU2	2	1.5	2.5	1	5.5/2.5
HBPU3	2	1.5	1.5	1.5	4.5/3.5
HBPU5	2	1.9	1.1	3.4	4.5/7.3
SHBPU2	-	1.5	2.5	1	3.5/2.5
SHBPU5	-	1.9	1.1	3.4	2.5/7.3

2B.2.3.2 Preparation of porous samples

Porous HBPU and SHBPU were prepared from the above synthesized PU by gas forming salt, ammonium bicarbonate as a porogen additive and these HBPU were used for *in vitro* biocompatibility study.²⁸ In DMAc, highly viscous solution of PU was prepared. Ammonium bicarbonate salt particulates (weight ratio of NH₄HCO₃ to PU was 10:1 and size in the range of

120–300 μm) were added to the polymer solution and mixed thoroughly. The paste mixture was cast into Teflon mold (2 cm diameter and 1.1 mm thickness). The semi-solidified samples were immersed into an excess amount of hot water (90 °C) until no gas bubble was generated (5 min). Further, the samples were kept into cold water for 20 min and then freeze-dried.

2B.2.3.3 *In vitro* degradation study

The *in vitro* degradation study was carried out according to ASTM standard method F 1635-04.²⁹ The degradation medium was 0.1 M PBS with pH of 7.4 ± 0.2 and PBS replenished when pH approached to 7.2. The polymer films were incubated at 37 °C and the results were reported as an average of six replicates. Each specimen was immersed in PBS that was placed in an individual vial and stored in oven at 37 °C under a static mode. The polymer film to PBS wt. ratio was maintained at 1:3. Films were taken out from the media after 7, 15, 30, 45 and 60 days of incubation, rinsed with deionized water to remove embedded salts within the film and surface was wiped. The films were then further dried under vacuum for 4 days at 40 °C to determine the retention of wt.% and FTIR analysis. The toxicity of degraded or eluted products was estimated by MTT assay and hemolytic assay.

2B.2.3.4 *In vitro* cytocompatibility assay

Liver and heart was collected from Wistar rat and single cells were isolated by collagenase reperfusion method from rats and harvested in Eagle's balanced salts medium containing EDTA.³⁰ The remaining EDTA was washed out by soaking them by Eagle's balanced salts for 7 min and liver and heart cells were cultured in William medium and DMEM, respectively. The cell counting was done by trypan blue exclusion test. Cells were further cultured for 24 h in humid incubator at 5% CO₂ flow at 37 °C. Porous polymer films (0.1 cm \times 0.1 cm \times ~0.002 cm) were kept in the wells of the culture plate and 2 mL of the established culture was poured. The experiment is performed in triplicate, both for the cardiac and liver primary cell lines, separately. Then, it was again cultured for 24 h under the same conditions. After 24 h, 50 μL of MTT was added to each well for the treated as well as the control culture and incubated for 24 h. Finally, the blue crystals of formazan formed in the wells were dissolved in 40 μL of DMSO in each well. UV spectra were taken finally at 540 nm and the absorbance was compared with the control system.

2B.2.3.5 *In vitro* hemolytic activity assay

The hemolytic test was done to examine hemocompatibility of the synthesized PU and the degradation by-products with erythrocytes based on the modified protocol as reported by Nair et al.³¹ Briefly, goat blood was collected in a K3 EDTA tubes and was centrifuged at 3000 rpm for 10 min. Supernatant was discarded and the erythrocytes were collected, carefully. The erythrocytes were further washed thrice by PBS (pH 7.4). A 10% (v/v) suspension of erythrocytes in PBS was prepared in a 50 mL centrifuge tube. 1.9 mL of this erythrocyte solution was taken in a 2 mL centrifuge tube and 100 μ L of each polymer solution and degraded/eluted products in PBS after 1, 15, 30, 45 and 60 days of incubation were added into it, separately. The tubes were then incubated for 2 h at 37 °C. The experiment was done in triplicate. Triton X-100 and PBS were taken as the positive and the negative control, respectively. After incubation the tubes with 2 mL medium each, were centrifuged at 3000 rpm for 10 min. Then, 200 μ L of the supernatant was taken and 2.8 mL of PBS was added to it and finally absorbance was taken at 540 nm in a UV-visible spectrophotometer. The results were compared to the positive and the negative controls and

2B.2.3.6 Histopathological and cell adherence study post-implantation

A major survey was done on rats after anesthetized using sodium pentobarbital (50 mg per kg body weight of the rats). HBPU and SHBPU implant were placed inside the subcutaneous layer in vertebral region of Wistar rat divided in two groups (three replicates). After 15 days of implantation, the Wistar rats implanted with polymer film and the control Wistar rats (three replicates) without any implantation were sacrificed by cervical dislocation. Organs (heart, kidney, liver and skin) were collected in normal saline solution and tissues were fixed in 10% neutral formaldehyde for 16-24 h. These tissues were dehydrated in ascending grades of alcohol, treated in xylene and finally embedded in paraffin to prepare blocks. These tissue blocks were cut into thin series of sections (5-7 μ m thickness) using a microtome. The sections were stained with hematoxylin and eosin stains, followed by microscopic observation to examine cellular arrangements and their changes compared to the control rats to ascertain the compatibility of the synthesized PU. PU films were taken out from treated animals after 15 days and 30 days of post-implantation and sample were prepared for SEM study to witness cell adherence.

2B.2.3.7 Cytokines detection and alkaline phosphatase assay

Blood was collected in vacuum blood collection tubes from the orbital sinus nerve of the PU implanted rats and the control rats (without polymer film). Blood samples were kept for 2 h at room temperature followed by centrifugation at 4500 rpm for 10 min. Serum was collected and subjected for cytokine detection (IL-6 and TNF- α) by using test kit according to the manufacturer's protocol (USCN Life Sciences Inc. Wuhan 108, Zhuayang Ayence, China). This detection was to check the effect of HBPU on the immune system of the treated animals after post implantation compared to that in terms of cytokine expression in control rats. Further, ALP activity was measured by using kits (Coral, India) on semi-automatic analyzer (Discovery, Tulip Diagnostic, India) as per the manufacturer's instructions.

2B.2.3.8 Statistical analysis

Statistical analysis was done similarly as mentioned in section 2A.2.3.5 of Chapter 2.

2B.3 Results and discussions

2B.3.1 Synthesis of hyperbranched polyurethane

HBPU with four different wt.% (1-5) of tetra-functional polyol moiety, PE were synthesized successfully by pre-polymerization technique using an $A_2+B_2+B_4$ approach. The reaction mechanism was same as described in section 2A.3.1. The amount of MG (2 mmol) was kept constant in all the cases. HBPU without MG were also synthesized to examine the role of vegetable oil moiety on their performance for a comparative study. The reaction mixture was diluted to 20% solid content and the temperature was kept at 80 °C in the second step. Further, the tetra-functional moiety, PE was added dropwise to prevent gelation. This step is very critical as discussed in section 2A.3.1. Most importantly, the amount of PE has a direct effect on it, as the reaction became more vigorous and difficult to control with the increasing amount of PE.

2B.3.2 FTIR study

FTIR spectral analysis confirmed the formation of urethane linkages due to the appearance of desired bands at their respective positions.⁷ The absence of stretching vibration band for free –NCO at 2270 cm^{-1} indicated the completion of the reaction (**Figure 2B.1a**). The band at 3400-3404 cm^{-1} represented the overlapping of –OH and –NH stretching vibrations. Two distinct

bands appeared at 3019 and 2932-2938 cm^{-1} for aromatic $-\text{CH}$ and $-\text{CH}_2$ stretching vibrations, respectively. Presence of urethane linkage was confirmed by the presence of characteristic bands at 1710-1729 cm^{-1} for $-\text{C}=\text{O}$ stretching vibration, at 1520-1536 cm^{-1} for $-\text{CN}$ stretching/ $-\text{NH}$ bending vibration and at 1040-1100 cm^{-1} for $-\text{O}-\text{C}=\text{O}$ stretching vibration of urethane/ester linkages.⁷

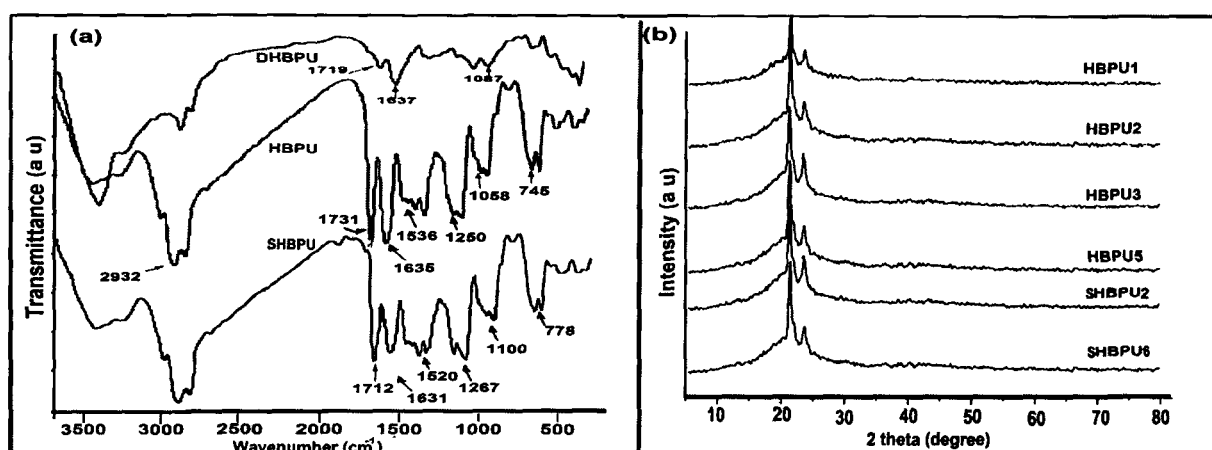


Figure 2B.1: FTIR spectra (a) of HBPU, SHBPU and degraded HBPU (DHBPU) and XRD patterns (b) of HBPU and SHBPU

2B.3.3 XRD study

XRD analysis confirmed the presence of crystalline phases in the prepared PU. The positions of the diffraction peaks at $2\theta = 21.2^\circ$ and 23.4° are due to PCL crystal structure and the position of which remained unchanged with variation of PE content in the structure of HBPU (Figure 2B.1b).⁷ The intensity of the peaks only varied slightly. Thus, XRD patterns of the polymer showed that the increased wt.% of the multifunctional unit as well as the presence of MG moiety has no significant effect on the crystallinity of the soft segment.

2B.3.4 NMR study

The structures of bio-based HBPU and SHBPU were supported by NMR study (Figure 2B.2(a-d)). ^1H NMR spectral analysis of MG based HBPU confirmed the formation of bio-based HBPU architecture and indicated the formation of linear, dendritic and terminal units in the HB structure (Figure 2B.2a). The peaks at δ (ppm) = 4.04, 4.01, 4.00 and 3.98 are due to the

presence of tetra-, tri-, di-, and mono-substituted pentaerythritol, respectively.¹⁶ The DB was calculated by the same method as mentioned in section 2A.3.4 and found to be 0.76 for HBPU2. ¹H NMR spectral analysis of SHBPU2 without MG also confirmed the formation of a HB structure, with a DB of 0.6. Different peaks in ¹H NMR of SHBPU are presented in **Figure 2B.2b**. Different peaks that were observed for different C-atoms in the ¹³C NMR spectrum of HBPU with and without MG moiety are represented in **Figure 2B.2(c and d)**.

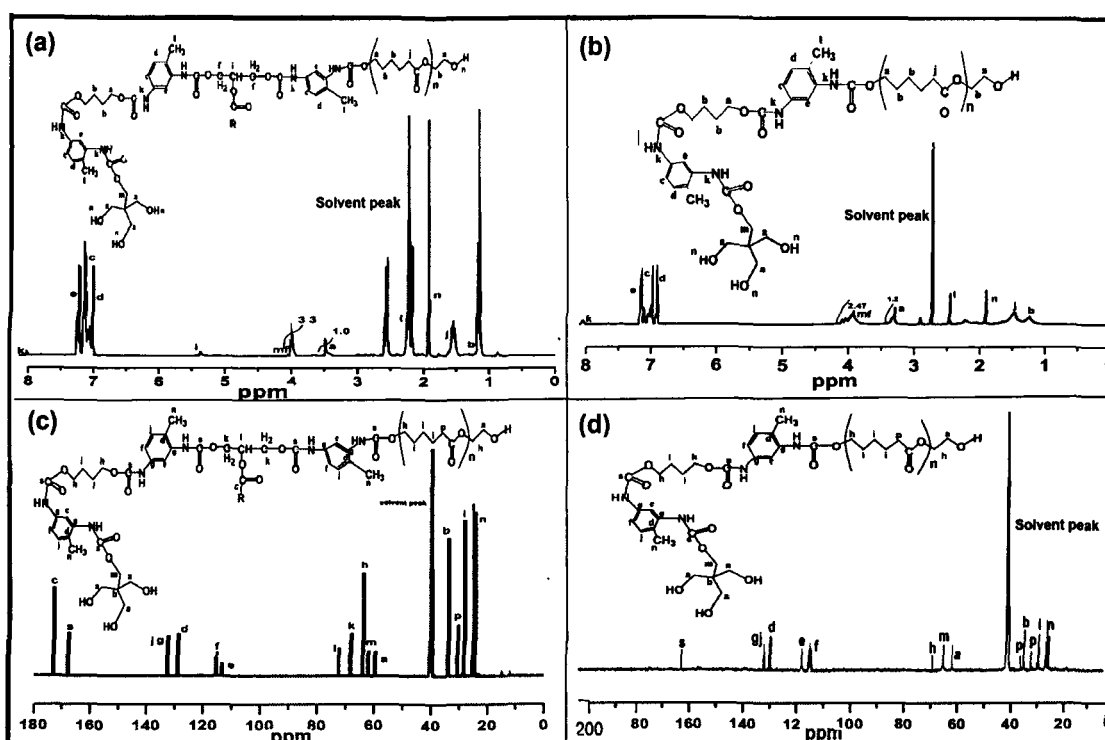


Figure 2B.2: ¹H NMR (a and b) and ¹³C NMR (c and d) spectra of HBPU and SHBPU

2B.3.5 SEM study

SEM images of MG based HBPU are shown in **Figure 2B.3(a and b)**. SEM micrographs revealed an inhomogeneity in the structure of HBPU due to the presence of soft and hard segments. This resulted in a rough surface with uniformity in the distribution of the different domains in all the cases. As the amount of hard segment in the synthesized PU was almost the same, so no major difference in surface morphology was observed from SEM study. The rough surfaces of PU could provide/mimic the native micro environment of the cells by supporting the adherence and proliferation of cells. Similarly, SEM images of the *in vitro* degraded HBPU after

7, 15, 30, 45 and 60 days are represented in **Figure 2B.3(c-f)**. SEM images suggest gradual degradation of HBPU as their incubation period in PBS increased up to 60 days. The degradation of PU was started by developing cracks and grooves in their macromolecular matrix which further progressed. Subsequently, pores were formed within the structure further accelerating the degradation process. Furthermore, to examine the effect of vegetable oil on the degradation rate of the polymer a comparative study was done up to 20 days with HBPU and SHBPU. SEM images witnessed less surface erosion and lower degradation in SHBPU without MG (**Figure 2B.3 (g-i)**).

In addition to that, **Figure 2B.4** presents the SEM images of porous HBPU and SHBPU. It was observed that almost spherical interconnected pores were formed within the matrix of PU. The size of the pores was within the range of 100-252 μm . Consequently, this three-dimensional interconnected porous HBPU structure has the potential to be used as a biodegradable scaffold that facilitates cells adhesion and proliferation by easy intaking of nutrients and outgoing of waste products. Such interconnected networks also aid in neo-vascularization at the damaged area and could upregulate the tissue regeneration process.

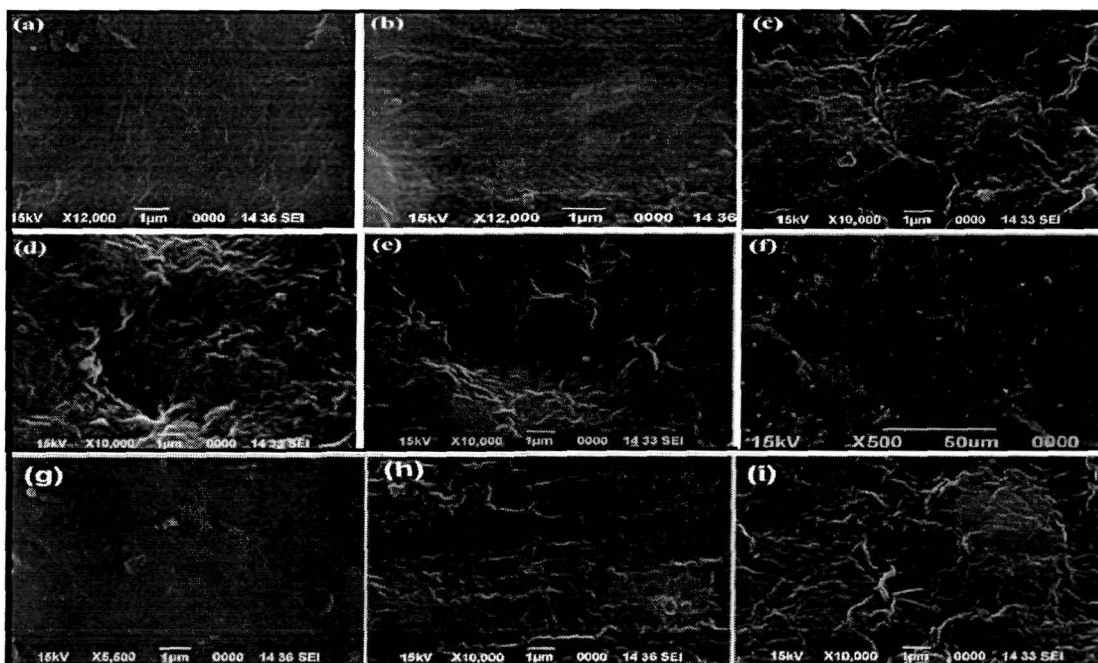


Figure 2B.3: Representative SEM images of HBPU (a and b), degraded HBPU matrix (c-f) at 15, 30, 45 and 60 days and degraded SHBPU (g-i) at 7, 15 and 20 days of degradation study

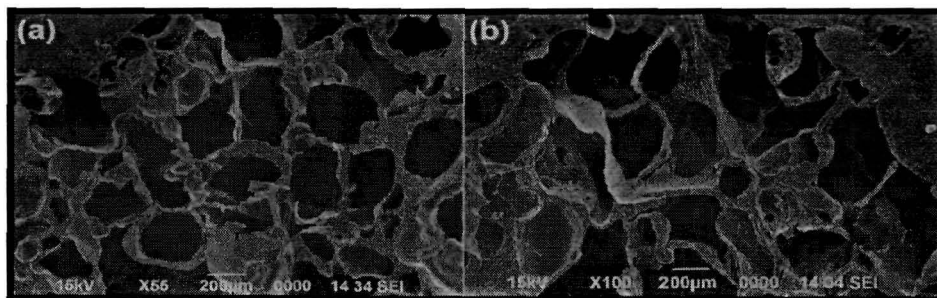


Figure 2B.4: Representative SEM images of porous HBPU (a) and SHBPU (b)

2B.3.6 Mechanical properties

The tensile strength of the polymer tends to be enhanced with the increase in wt.% of B₄ unit due to the formation of compact branched structure (**Table 2B.2**). This may lead to the increase in M_w and increase of intermolecular attractions between –NH and –C=O through H-bonding, polar-polar interaction, etc.⁷ It can be assumed that a combination of increased branching and attractive interactions renders the structure more compact. Moreover, it was observed that mechanical performance improved with increased content of PE in both HBPU and SHBPU. Thus, HBPU5 has the highest tensile strength of (27.38±0.9) MPa. This huge improvement may also be due to the occurrence of some crosslinking, as it was not soluble completely even in highly polar solvents like DMF, DMSO, DMAc, etc. The EB decreased with the increased of multifunctional moiety which may be attributed to the increase of compactness of the polymer chain with such variation. Thus, HBPU1 has the highest EB value of (863±5.6)%. The impact resistance of the synthesized HBPU was more than 100 cm, as this height is the upper limit of the instrument and no damage in the film was observed up to that height. The scratch hardness of PU was found to remain almost same with the increase in the amount of PE (**Table 2B.2**). The bending test over a mandrel of diameter 1 mm indicated good flexibility of PU. This excellent flexibility of HBPU may be attributed to the long alkyl chain of MG, flexible PCL moiety and the presence of ether/ester linkages. The enhanced flexibility and the heterogeneity in the structure of PU are mainly responsible for the good performance of the synthesized polymers. The most important result in this investigation is that a little variation in content (increase or decrease) of the multifunctional moiety (PE) has a direct consequence on the mechanical properties of PU and thus these can be tuned according to the needs of different applications. Moreover, the role of vegetable oil can also be understood as it endowed the polymer with

enhanced flexibility, scratch resistance, impact resistance and EB compared to the polymer without MG moiety. This may be attributed to the flexible alkyl chain of MG as well as PCL moieties. However, SHBPU showed almost the same tensile strength as HBPU1 and HBPU2.

Table 2B.2: Mechanical properties and thermal degradation parameters of HBPU and SHBPU

Polymer code	HBPU1	HBPU2	HBPU3	HBPU5	SHBPU2	SHBPU5
Tensile strength (MPa)	21.94±0.6	23.18±0.8	25.61±0.7	27.38±0.9	24.17±0.8	25.8±0.6
EB (%)	863±5.6	750±8.3	628±7.0	599±8.0	550±6.3	499±7.5
Impact resistance (cm)	100	100	100	100	90	95
Scratch resistance (kg)	4.5±0.5	4.6±0.6	4.7±0.7	4.7±0.6	4.2±0.3	4.4±0.6
Bending (mm)	<1	<1	<1	<1	<2	<2
T _{1st ON} (°C)	240	247	252	259	263	286
T _{2nd ON} (°C)	354	365	440	455	311	331
T _{50%} (°C)	383	385	390	397	382	383
T _{90%} (°C)	492	494	497	503	462	492
Residue (wt.% 500 °C)	5	7	7.3	8.5	8	9

2B.3.7 Thermal study

The studied HBPU showed a two-step degradation pattern in the TGA thermograms (**Figure 2B.5 (a and b)**) which is in accordance to the reported literature.^{7, 18} The initial thermal decomposition temperature of bio-based HBPU was found to be increased from 240 to 259 °C with the increase in wt.% of PE. This slight increase in thermal stability might be due to similar reasons as discussed above for the tensile strength, mainly increase in molar mass and interfacial interactions. In addition, the segmental motion of the polymer chains decreased to a certain extent for the increase of secondary interactions. In case of SHBPU, initial thermal decomposition temperature was found to increase from 263 to 286 °C with the increase of PE

content. The first degradation step is assigned to the long aliphatic chain of MG and other aliphatic chains present in the structures. Therefore, it could be said that the bio-based HBPU have a lower initial degradation temperature compared to SHBPU, though the overall thermostability is good enough for the biomedical application. The next degradation step can be assigned to the degradation of the thermostable aromatic moieties and urethane bond present in the structure. The TGA results are summarized in **Table 2B.2**. Further, DSC analysis showed increased in mp from 51 to 58 °C (**Figure 2B.5c**) with the increased PE content in HBPU. SHBPU also showed a slight increase in their mp from 50 to 53 °C with the increase of the same (**Figure 2B.5d**). This is attributed to the increase of compactness and interfacial interactions, which constrained the free molecular movement of the chains.

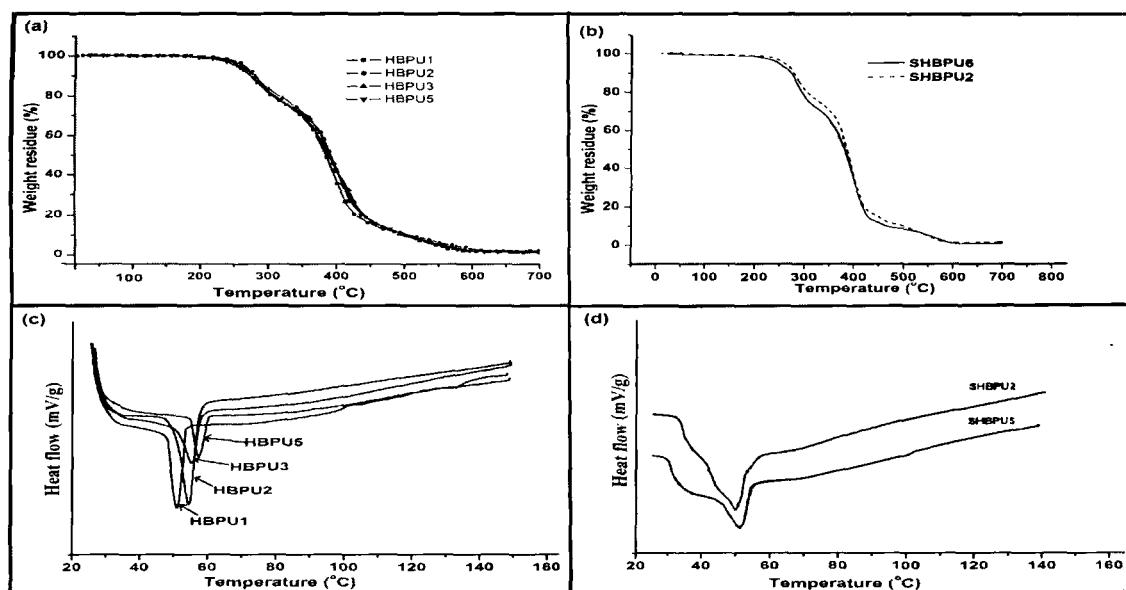


Figure 2B.5: TGA thermograms and DSC curves of HBPU (a and c) and SHBPU (b and d)

2B.3.8 Chemical resistance test

HBPU and SHBPU showed very good chemical resistance in all the studied chemical environments that includes 10% aqueous sodium chloride, 20% aqueous ethanol, 5% aqueous HCl and distilled H₂O expect in an alkaline environment of 3% NaOH. This overall trend of chemical resistance attributed to same reasons, as mentioned in section 2A.3.8 of this chapter.

2B.3.9 *In vitro* cytocompatibility

The cell viability assay suggested that both PU are cytocompatible. From **Figure 2B.6**, it can be observed that the average cell viability of HBPU with MG moiety was $\geq(92\pm 2.05)\%$ for cardiac cell line and $(\geq 85\pm 1.7)\%$ for the primary liver cells. The cell viability percentage of SHBPU was (88 ± 2.3) and $(83\pm 2.5)\%$ for cardiac and liver cell lines, respectively. Therefore, it could be said that HBPU are more compatible with cardiac cells than liver cells. Furthermore, the presence of the bio-based moiety was found to enhance the cytocompatibility of HBPU and degraded products. Thus, MG based HBPU has a high potential to be used as a scaffold material for TE. It was also observed that the increased wt.% of the multifunctional unit has no noticeable effect on the cytocompatibility of PU ($p>0.05$). The degraded sample extract have also showed $>(80\pm 1.5)\%$ viability up to 60 days of investigation. This depicted the non-toxic nature of the degraded products released from PU.

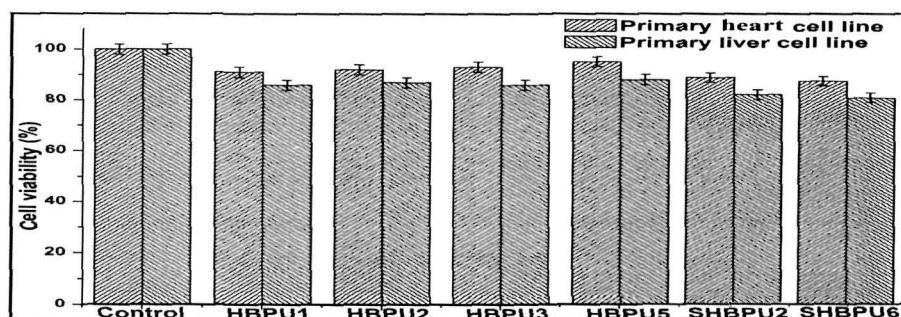


Figure 2B.6: Cell viability (%) of heart and liver cells on HBPU and SHBPU scaffold

2B.3.10 *In vitro* hemocompatibility

Hemocompatibility of HBPU, SHBPU and the degradation by-products released out of the polymers in PBS was checked by hemolytic assay (**Figure 2b.7(a and b)**). Hemocompatibility of HBPU was found to be excellent. The results obtained showed that the OD observed for MG based HBPU was almost same as that for the negative control (PBS) ($p>0.05$). The hemolytic activity of SHBPU was found to be $(5\pm 0.7)\%$, which was more ($p<0.05$) than that observed for HBPU $(3\pm 0.4)\%$. However, the hemolytic activity percentage of SHBPU is also within the compatibility range.

The hemolytic assay for the degraded by-products of HBPU with and without MG in PBS showed that they were non-toxic and compatible to the blood as they did not lyse the

erythrocytes (**Figure 2B.7a**). This hemolytic assay is crucial for any biomaterial designed to be used as a scaffold as it has to come in direct/indirect contact with blood as soon as exposed to the host's body. This fact is also applicable for the degraded/leached out products as they could be exposed to the vascular system after degradation.

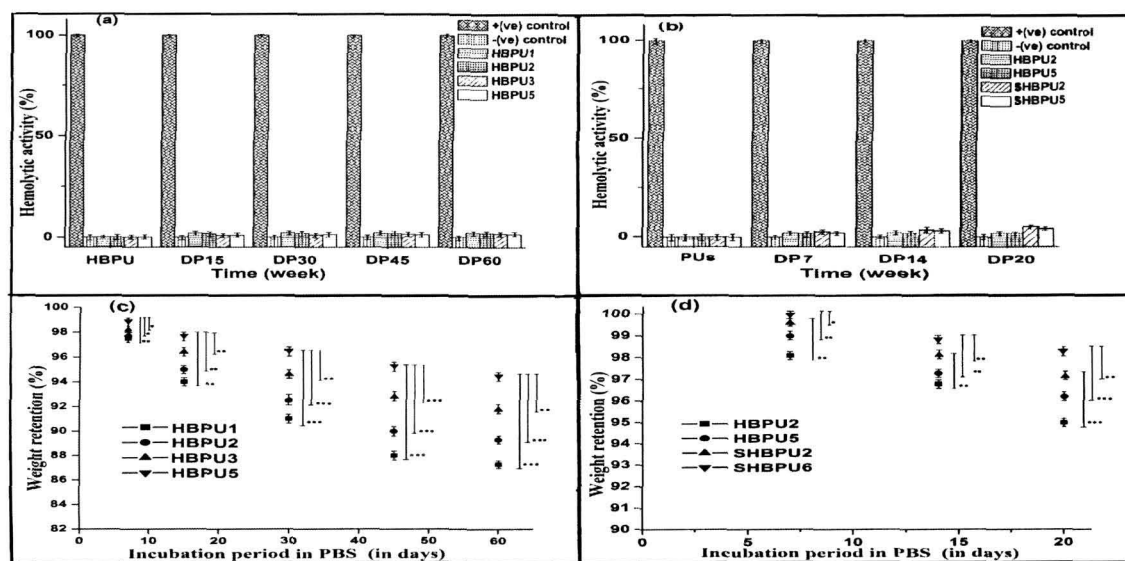


Figure 2B.7: RBC hemolytic activity (%) of HBPU and the degraded by-products (DP) after 15, 30, 45 and 60 days (a) as well as of SHBPU and the degraded by-products (DP) after 7, 15 and 20 days (b), weight retention (%) of HBPU (c) and SHBPU (d) during degradation study (* $p > 0.05$, ** $p < 0.05$ and *** $p < 0.001$)

2B.3.11 *In vitro* biodegradation

The retention of wt% of PU plotted against the incubation period of polymers in PBS is shown in **Figure 2B.7c**. It can be observed from the figure that the weight loss decreased with the increased wt.% of B₄ component. The change in pH of PBS incubated with the polymer after three days indicated an initial induction period prior to degradation. The rate of degradation for HBPU1 was highest among HBPU2, HBPU3 and HBPU5 as analyzed by the mass loss of the different PU and by the end of 8 weeks, HBPU5 had the maximum weight retention percentage ($p < 0.001$). Thus, the synthesized polymers have tunable degradation rate as supported by the biodegradation study. In the comparative study between HBPU and SHBPU up to 20 days of investigations proved the predominant role of the vegetable oil in enhancing the biodegradation

($p < 0.001$) of the synthesized polymer as shown in **Figure 2B.7d**. It is also pertinent to mention here that degradation of polyurethane or any other polymer in PBS, without using enzyme is reported to be very slow with mass loss of 3-15 % (in 2-3 months) and considered to be good under such *in vitro* physiological condition (without enzymes). It is due to the fact that degradation inside body is a result of the combined effect of enzymatic action, peroxides, salts, catalytic activity and action of the immune cells. Further, faster degradation of polymer by hydrolysis is generally takes place after the initial induction period which is characterized by uptake of fluid by the polymer and causing dimensional instability by swelling the polymeric chain. This is followed by breaking up of bonds, reduction in molecular weight and mass loss.

The degraded products in PBS after 30 days were characterized by FTIR. For the degradation products, two bands at 1085 and 1639 cm^{-1} (**Figure 2B.1a**) were observed for -C-O- stretching vibration as in alcohols/carboxylic acids and asymmetric stretching vibration of phosphate salt of carboxylic acid.³² This implies that the ester bonds present in the PCL units of HBPU structure were hydrolyzed and the degradation products leached out from the matrix into the PBS media. Again, by comparing the FTIR bands of degradation products with that of pristine polymer, it was found that the band intensity ratio of carbonyl to -C=C decreased. This result further suggested the hydrolysis of the ester linkages of the bio-based (MG of *Helianthus annuus*) and PCL moieties present in the HB structure. Further, no band corresponding to the aromatic moiety of toluene diamine was appeared in the spectra, thus revealing the non-toxic nature of the studied HBPU.

2B.3.12 *In vivo* immunocompatibility

The specific immune response as well as acute phase response function by regulating a complex cytokine and anti-cytokine network involving particularly interferon gamma, IFN-gamma, TNF, IL-1, and IL-6.^{33, 34} IL-6 and TNF- α are the two major pro-inflammatory cytokines that are responsible for the early response against any foreign body encountered.³⁴ The expression level of these cytokines after post-implantation compared to that of control is a measure of the compatibility/acceptance of the implant by the host's system. The concentration of the cytokines (IL-6 and TNF- α) in Wistar rats for both control and treated was detected by ELISA after comparing it with the standard curve for IL-6 and TNF- α , respectively (regression analysis). The average of IL6 and TNF- α levels in the serum of the treated group were found to be (8 \pm 2.3) and

(12.5±3.5) pg/mL respectively for HBPU. The results were comparable to the values obtained for the control rats (IL-6 = (6±3.0) and TNF- α = (13.2±3.6) pg/mL. Whereas, for SHBPU treated group, the IL-6 and TNF- α levels in the serum of rats were found to be (10±3.1) and (16.6±2.5) pg/mL respectively. Thus, it can be emphasized from the result that bio-based HBPU are more immunocompatible in the host system than SHBPU. Thus, this present investigation demonstrated that the bio-based moiety played a significant role to enhance the immunocompatibility of HBPU as no immune response was elicited on post-implantation. There was also no cardinal sign i.e. heat, redness, swelling or loss of function at the implantation site. Thus, it could be said that the synthesized HBPU are immunocompatible which may be attributed to their biocompatible surface as well as bulk chemistry.

2B.3.13 Alkaline phosphatase activity test

ALP is an enzyme that catalyzes the synthesis and the hydrolysis of ester phosphorous acid in alkali environment. Phosphorization and dephosphorization are the most important metabolic processes and therefore, ALP has a key role in these processes.. Phosphatases are primarily intracellular enzymes and their concentration in plasma increases drastically only when a larger number of the cells are damaged or during synthesis of enzyme.³⁵ ALP is found in all the tissues and organs, especially in mucous membrane of duodenum, bones, gristle, liver, kidneys, prostate and spleen. In this experiment no significant increase or decrease in concentration of ALP was observed in the implanted rats after 7 to 15 days ($p>0.05$). The results for the control and the treated animals (for both HBPU and SHBPU) were observed in the range of (86.9±4.3) to (92±3.2) U/L. The result obtained for the treated animals was comparable to that of observed for the control animal. Therefore, this biochemical study suggests that the implanted PU film did not damage the cells or induced any other abnormality.

2B.3.14 Histopathological study

The representative optical micrographs of liver, kidney, skin and heart tissue of the control and the treated animals after 15 days of post-implantation are shown in **Figure 2B.8**. The heart sections of both the control and HBPU treated group is shown in **Figure 2B.8 (a₁ and a₂)**. No difference in cellular arrangement of heart was observed for treated groups compared to that of the control group. Kidney section was also found to possess the similar cellular arrangement like

the control one (**Figure 2B.8 (b₁ and b₂)**) with clear visible capsules and ducts. The liver section (**Figure 2B.8c₁**) of the control and HBPU treated Wistar rats showed regular cellular architecture along with central vein with no damage or abnormal tissue architecture. The same result was also observed for the skin tissue (**Figure 2B.8 (d₁ and d₂)**). Therefore, the histopathological study suggested that the bio-based HBPU is tissue-compatible and it did not adversely affect the organs as well as functions of the animals under this study. Similarly, the histopathological study of SHBPU treated group showed no significant difference in cellular architecture and organization of the major organs as shown in **Figure 2B.8 (a₃, b₃, c₃ and d₃)**.

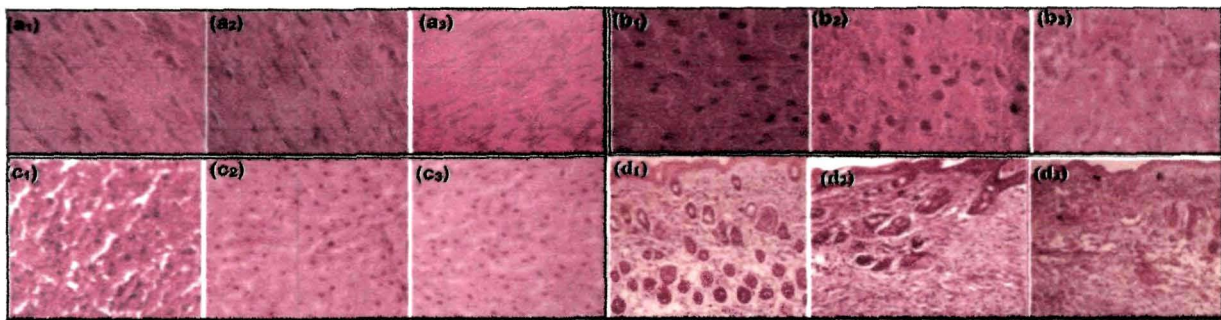


Figure 2B.8: Microscopic view of representative histological sections of heart (a₁, a₂ and a₃), kidney (b₁, b₂ and b₃), liver (c₁, c₂ and c₃) and skin (d₁, d₂ and d₃) [subscript 1, 2 and 3 indicates control, HBPU and SHBPU treated rats, respectively]

2B.3.15 In vivo cell adherence and proliferation

It was observed (**Figure 2B.9**) that the cells were firmly adhered to the implanted films and uniformly distributed. SEM images suggested that the bio-based HBPU supported higher cellular adherence and proliferation compared to SHBPU.

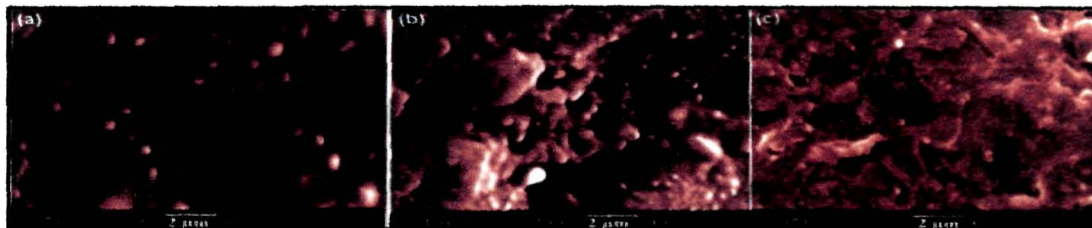


Figure 2B.9: SEM images of skin cells adherence and proliferation on HBPU matrix after 15 (a) and 30 (b) days as well as on SHBPU matrix after 15 days (c) of post-implantation

It depicted the role of long alkyl chain of MG, in improving the cellular adherence. Thus, bio-based HBPU provided the cells with a favorable environment mimicking the ECM and supported cellular adherence, growth and proliferation.

2B.4 Conclusion

In the present subchapter, vegetable oil based HBPU containing PCL soft segments and different wt.% of PE, a B₄ branching unit were successfully synthesized. The *in vitro* biodegradation study recommended that HBPU were biodegradable and they degraded into non-toxic by-products. The performance like thermo-mechanical properties and biodegradation of the synthesized PU can be tailored by subtle variations of the content of the branching unit. Above all, the synthesized HBPU were found to be biocompatible, immunocompatible, hemocompatible as well as supported the adherence and proliferation of the cells. It was also found that the incorporation of the vegetable oil moiety in HBPU enhanced various properties compared to SHBPU (without MG). Furthermore, micro-porous structures ideally suited as scaffolds can be prepared from HBPU using a porogen. This study demonstrated for the first time that *Helianthus annuus* oil based HBPU with a combination of good mechanical, thermal, chemical and biological attributes could serve as a prospective “scaffold” in the niche of TE or implantable biomaterial.

Reference

1. Lligadas, G. *Biomacromolecules* **11** (11), 2825--2835, 2010.
2. Xia, Y., & Larock, R.C. *Green Chem.* **12** (11), 1893--1909, 2010.
3. Tu, Y.C., et al. *J. Appl. Polym. Sci.* **111** (3), 1311--1317, 2009.
4. Karak, N., et al. *J. Appl. Polym. Sci.* **112** (2), 736--743, 2009.
5. Karak, N., et al. *Macromol. Mater. Eng.* **295** (2), 159--169, 2010.
6. Zhou, Y., et al. *Adv. Mater.* **22** (44), 4567--4590, 2010.
7. Deka, H., & Karak, N. *Prog. Org. Coat.* **66** (3), 192--198, 2009.
8. Abdelrehim, M.A., et al. *J. Polym. Sci. Part A: Polym. Chem.* **42** (12), 3062--3081, 2004.
9. Kricheldorf, H.R., & Schwarz, G. *Macromol Rapid Commun.* **24** (5-6), 359--381, 2003.
10. Reichelt, S., et al. *Colloids Surf. B* **69** (2), 169--177, 2009.
11. Dutta, N., et al. *Prog. Org. Coat.* **49** (2), 146--152, 2004.

12. Choudhury, R.B.R. *J. Am. Oil Chem. Soc.* **39** (8), 345--347, 1962.
13. Serdarevich, B., & Carroll, K.K. *J. Lipid Res.* **7** (2), 277--284, 1966.
14. Deka, H., et al. *Carbon*, **48** (7), 2013--2022, 2010.
15. Lee, H.S., et al. *Macromolecules* **20** (9), 2089--2095, 1987.
16. Kricheldorf, H.R., & Behnken, G. *Macromolecules* **41** (15), 5651--5657, 2008.
17. Prisacariu, C. *Polyurethane Elastomers. From Morphology to Mechanical Aspects*, Springer Verlag, Wien, 2011.
18. Javni, I., et al. *J. Appl. Sci.*, **77** (8), 1723--1734, 2000.
19. Krol, P. *Prog. Mater. Sci.* **52** (6), 915--1015, 2007.
20. Mohan, S.K., & Srivastava, T. *J. Biochem. Tech.* **2** (4), 210--215, 2010.
21. Dutta S., & Karak, N. *Polym. Int.* **55** (1), 49--56, 2006.
22. Kalita, H., & Karak, N. *Polym. Eng. Sci.* **52** (11), 2454--2461, 2012.
23. Chan-Chan, L.H., et al. *Acta Biomater.* **6** (6), 2035--2044, 2010.
24. Lamba, N.M.K. Woodhouse, K.A. & Cooper, S.L. *Polyurethane in Biomedical Application*, CRC Press, Boca Raton, 1997.
25. McKee, M.G., et al. *Prog. Polym. Sci.* **30** (5), 507--539, 2005.
26. Gao, C., & Yan, D. *Prog. Polym. Sci.* **29** (3), 183--275, 2004.
27. Abdelrehim, M.A., et al. *J. Polym. Sci. Part A: Polym. Chem.* **43** (15), 3376--3393, 2005.
28. Nam, Y.S., et al. *J. Biomed. Mater. Res.* **53** (1), 1--7, 2000.
29. Mitry, R.R., et al. *Cell Transplant.* **12** (1), 69--74, 2003.
30. Adhikari, R., et al. *Biomaterials* **29** (28), 3762--3770, 2008.
31. Nair, D.G., et al. *Biochem. J.* **402** (1), 93--104, 2007.
32. Guelcher, S.A., et al. *Biomaterials* **29** (12), 1762--1775, 2008.
33. Dinarello, C.A., et al. *J. Exp. Med.* **163** (6), 1433--1350, 1986.
34. Rihovi, B. *Adv. Drug Delivery Rev.* **21** (2), 157--176, 1996.
35. Stojanovic, D., et al. *Lucr. St. Med. Vet.* **XL**, 736--745, 2007.

Chapter 3

***Helianthus annuus* oil based hyperbranched polyurethane/Fe₃O₄ nanocomposite as an implantable material**

Highlights

This chapter demonstrates the fabrication of magneto-thermoreponsive bio-based HBPU/Fe₃O₄ NC with different wt.% of Fe₃O₄ by *in situ* polymerization technique. The study showed good interfacial interactions between HBPU and well-dispersed superparamagnetic Fe₃O₄ with an average diameter of 7.65 nm. Incorporation of Fe₃O₄ in HBPU improved the thermo-mechanical properties along with shape-memory behavior of the pristine HBPU. Interestingly, HBPU acquired antibacterial activity and magnetic property upon the incorporation of Fe₃O₄, which are very important for such implantable materials. The biocompatibility of NC and its degraded products was also verified by *in vitro* hemolytic activity and MTT assay. In addition, the *in vivo* biocompatibility and non-immunological behavior of NC after subcutaneous implantation in Wistar rats were also established. Thus, this chapter demonstrates the potentiality of this NC as thermally and magnetically controlled shape memory biomaterial.

Parts of this chapter is published in

Das, B., Mandal, M., Upadhyay, A., Chattopadhyay, P., Karak, N. *Biomed. Mater.* **8** (3), 035003--035015, 2013.

3.1 Introduction

Externally triggered shape memory biomaterial has gained immense significance as a catheter, clot remover, drug carrier, stent, scaffold, etc.^{1, 2} The exquisiteness of such biomaterials is that they can be inserted/implanted with minimal surgical incision which minimizes foreign infection. Further, their in-time monitoring and positioning are possible by using external stimuli.¹⁻³ In this avenue, the magnetic nanomaterial is an exceptionally strong candidate as a smart biomaterial. The magnetite, Fe_3O_4 is preferable over other iron oxides due to its proven biocompatibility and superparamagnetic nature.^{1, 4, 5} This superparamagnetic nanoparticle exhibits a single domain character. Moreover its mobility could be manipulated from outside of the host body during *in vivo* applications. These outstanding properties placed Fe_3O_4 in a leading precinct for many challenging applications like drug delivery, MRI, hyperthermia, TE, magnetic catheter, shape memory material, clot remover/stent and so on.⁴⁻⁸ However, the major problems associated with bare Fe_3O_4 nanoparticles are their poor stability and tendency of agglomeration, which resulted in their low performance. In this context, the incorporation of these nanoparticles into a suitable polymeric matrix is a right proposition in the current scenario of nano-biotechnology.

This fabricated Fe_3O_4 /polymer NC possesses double benefits. Polymer provides structural support and functionalizes the Fe_3O_4 nanoparticles, thereby increasing their dispersibility as well as stability.⁹ In turn; Fe_3O_4 imparts magnetic property and antibacterial activity to the polymer as well as aids to augment the other desired biological properties. In this context, bio-based HBPU (with 5 wt.% of PE) with attractive biocompatibility, biodegradability and good physico-mechanical properties along with other added advantages over conventional PU (as mentioned in Chapter 2) was selected as the matrix for the incorporation of magnetite, Fe_3O_4 . Furthermore, the presence of the hard and soft segmental structures in HBPU has bestowed this polymer with shape memory attribute.¹⁰ Shape memory polymer can regain its original shape from a fixed deformed shape on exposure of a suitable external stimulus such as light, heat, electric and magnetic field, etc. Thus, it has been projected as a stimulus responsive biomaterial with plethora of advantages in the biomedical realm.^{10, 11} Moreover, HB polymer with highly branched morphology, intra-molecular nanocavities, high surface functionalities and good compatibility has shown to provide good interaction, encapsulation and homogenous dispersion of the nanoparticles.¹² Thus, HBPU and Fe_3O_4 based NC can act as a smart biomaterial and its shape can be controlled by using external stimuli such as heat energy, magnetic field, etc. Though

literature reported the linear and HB PU/Fe₃O₄ NC with improved properties as non-contact shape memory materials^{13, 14} but bio-based HBPU/Fe₃O₄ NC is not well explored in the biomedical domain.

Therefore, the comprehensive biological aspects of the bio-based HBPU/Fe₃O₄ NC as a shape memory biomaterial were reported, in this chapter to establish the efficacy of NC in biomedical realm. The dose dependent effect of Fe₃O₄ on the pivotal performance including antibacterial activity, shape memory effect, thermo-mechanical attributes, biodegradability and biocompatibility was also studied to establish this NC as a potential smart implantable material.

3.2 Experimental

3.2.1 Materials

Chemicals such as TDI, PCL, BD, PE, *Helianthus annuus* oil and solvents like xylene, methanol, DMSO and DMAc for the synthesis of HBPU and FNC were of same specification as elaborated in section 2A.2.1 of Chapter 2. The materials for biological tests like DMEM, FCS multi-well culture plates, K3 EDTA tubes and vacuum blood collection tubes were same as discussed in section 2B.2.1 of Chapter 2.

Iron (II) chloride tetra hydrated (FeCl₂.4H₂O) was procured from Merck, Germany. Its minimum assay is 99.0 % and M_w is 198.83 g/mol. It was used as received, for the preparation of Fe₃O₄ nanoparticle.

Iron (III) chloride anhydrous (FeCl₃) was purchased from Merck, Germany. Its minimum assay is 98% and M_w is 162.21 g/mol. It was also used as received, for the preparation of Fe₃O₄.

Ammonia solution was obtained from Qualigens Fine Chemicals, Ltd. India. Its concentration is 30% and specific gravity is 0.89%. It was used as an alkali during the preparation of Fe₃O₄ nanoparticles.

Animal

The male Wistar rats (weighing 200 to 250 g) were obtained from the same breeder and housed properly as mentioned in section 2B.2.1 of Chapter 2. All animal experimental protocols were performed according to the “Principles of Laboratory Animal care” (NIH publication 85-23, revised 1985) as described in section 2B.2.1 of Chapter 2.

3.2.2 Instrumentation

The physico-chemical structural and thermal analyses were recorded by using XRD, FTIR and UV-visible spectroscopic techniques, as well as TGA and DSC as stated in section 2A.2.2 of Chapter 2. The morphological studies of HBPU, NC and degraded products were carried out by the same SEM instrument as described in section 2A.2.2. Ultrasonicator used for the dispersion of the nanotubes was Heishler, Model No. 200S, Germany operating at 60% of amplitude with a half cycle power input for 10 min at 24 kHz and acoustic power density of 460 W/cm². The dispersion of Fe₃O₄ in FNC was analyzed by using a JEOL, high resolution TEM, Model TEM2100, Japan, at an operating voltage of 200 kV. The magnetic properties of NC and nanoparticles were studied by a vibrating sample magnetometer (VSM, Lakeshore 7410) at room temperature, in the range +20,000 G to -20,000 G. The mechanical performance of the samples was performed using UTM as per the ASTM D412-51T, scratch hardness tester and falling weight tester as mentioned in section 2A.2.2 of Chapter 2. Elastic modulus of the samples was evaluated from the slope of the stress-strain curve in the elastic region. The bending test for the samples was performed by the same protocol as described in section 2A.2.2 of Chapter 2.

3.2.3 Methods

3.2.3.1 Preparation of Fe₃O₄

Fe₃O₄ nanoparticles were prepared by co-precipitation method as described elsewhere.¹⁵ Briefly, the aqueous solution of FeCl₂ (0.79 g) and FeCl₃ (1.29 g) in 1:2 mole ratio was prepared. Under continuous mechanical stirring at room temperature (ca 25 °C), ammonia solution was added dropwise to the salts solution, until the color changed to black at pH 11-12. The whole process was done under an inert atmosphere. Then, the prepared nanoparticles were allowed to precipitate completely. The precipitate was separated, washed several times with distilled water and finally dried at 45 °C in a vacuum oven for 24 h.

3.2.3.2 Preparation of nanocomposites

HBPU was prepared by using the similar strategy as reported earlier in section 2A.2.3.2 of Chapter 2, using A₂+B₂+B₄ approach. The hydroxyl terminated PU pre-polymer was prepared exactly in the same protocol as stated in section 2A.2.3.2. Then in the second step, required amount of branch generating tetra-functional unit, PE was added along with the TDI to maintain

the overall NCO/OH ratio equal to 1 and reacted for ~ 2 h at (77 ± 2) °C. However, to prepare NC, different amount of Fe₃O₄ nanoparticles (5, 10, 15 wt.%) were dispersed in DMAc by mechanical stirring (3-4 h) followed by ultrasonication (30 min) and were added to the reaction mixture in the second step, separately. NC mixtures were mechanically stirred vigorously till the completion of the reaction. Further, the reaction mixture was cooled down to room temperature and the whole mixture was transferred to a sample bottle in each case and subjected to ultrasonication (~ 30 min) to obtain homogenous dispersion of the nanoparticles into the matrix. All the above reactions were carried out by maintaining the same reaction parameters as described in section 2A.3.2.2 of Chapter 2. Then, the prepared HBPU/Fe₃O₄ NC coded as FNC were cast into films on different inert substrates and designated as FNC5, FNC10 and FNC15 for 5, 10 and 15 wt.% of Fe₃O₄, respectively.

3.2.3.3 *In vitro* degradation study

The *in vitro* degradation study was carried out according to ASTM standard method F 1635-04 as discussed in section 2B.2.3.3 of Chapter 2. For this study, the ratio of total surface area of the film (six replicates) to volume of the PBS solution was approximately equal to $2.08 \text{ cm}^2/20 \text{ cm}^3$. Films were taken out from the media at regular intervals of 7th, 15th, 30th and 60th days of test, rinsed with deionized water, wiped and vacuum dried to determine the weight retention percentage. The toxicity analysis of the degraded/leached out products was also performed as described below.

3.2.3.4 *In vitro* cytocompatibility assay

The single cells were isolated by collagenase reperfusion method from liver and heart of Wistar rat and culture was established as elaborated in section 2B.2.3.4 of Chapter 2. The cell viability percentage in direct contact with the prepared NC films and Fe₃O₄ nanoparticles were investigated by using MTT as mentioned in section 2B.2.3.4 of Chapter 2.

3.2.3.5 *In vitro* hemolytic activity assay

The *in vitro* hemolytic activity of FNC and degraded by-products (after 7, 30, 45 and 60 days of incubation in PBS) was evaluated by the same procedure as elaborated in section 2B.2.3.5 of Chapter 2.

3.2.3.6 Shape memory behavior study

The shape recovery of FNC and HBPU was measured by stretching method as mentioned in literature.¹⁶ Briefly, the samples (1 cm ×4 cm×0.2 mm, three replicates) were heated at a specified temperature (45 °C) for 5 min and stretched to double the original length (l_0) and the deformed length (8 cm) was denoted as (l_1). Immediately, samples were transferred in the ice water bath (2-3 °C) for 5 min and the retention length was measured as l_2 . The cooled samples were heated to the same temperature (5 min each) and the recovered length (l_3) was measured. The retention percentage and recovery percentage were calculated by the following equations at different temperatures.

$$\text{Retention (\%)} = [(l_2 - l_0) / l_0] \times 100 \text{ ----- (3.1)}$$

$$\text{Recovery (\%)} = [(l_1 - l_3) / l_0] \times 100 \text{ ----- (3.2)}$$

3.2.3.7 Antibacterial activity assay

The samples were individually tested against a panel of microorganisms namely *Staphylococcus aureus* and *Klebsiella pneumonia*. The antibacterial test was performed as described elsewhere¹⁷ after some modification (use of Muller Hinton broth as culture medium for bacteria instead of Nutrient broth). Antimicrobial activity of the samples was determined by the agar-well diffusion method. All the microorganisms mentioned above were incubated at 37 °C for 24 h by inoculation into Mueller Hinton broth. The culture suspensions were prepared and adjusted by comparing against 0.4–0.5 Mc Farland turbidity standard tubes. Mueller Hinton Agar (20 mL) was poured into each of the sterilized Petri dishes (10 mm×90 mm) and the different bacteria were homogeneously inoculated in it, separately. For antibacterial test, the samples were dissolved in DMSO (for easier diffusion) and filtered through a 0.22 μm membrane filter. The prepared samples namely Fe₃O₄, HBPU and FNC were taken into the wells (6 mm) in the agar plates directly and the bacteria were incubated at 37 °C for 24 h. After incubated period, the inhibition zone for the studied samples was measured. Study was performed in triplicates and ampicillin (50 μg) was used as the positive control.

3.2.3.8 Histopathological study

The subcutaneous implantation of FNC15 (1 mm×1 mm×~0.3 mm) on Wistar rats (three animals) was performed using the same procedure as mentioned in subchapter 2B.2.3.6 of

Chapter 2. After 30 days of implantation, the histopathological evaluation of skin, heart, liver and kidney (collected from control and treated rats) was done following the same steps as described in section 2B.2.6 of Chapter 2. The sections were stained with hematoxylin and eosin stain.

3.2.3.9 Cytokine analysis

The cytokine (IL-6, IL-2 and TNF- α) analysis of treated and control rats was done by using the same test kit as discussed in section 2B.2.3.7 of Chapter 2. The same procedure was used as discussed in section 2B.2.3.7 for collecting the blood from the control (without any implantation) and the treated rats implanted with FNC15 and HBPU, respectively.

3.2.3.10 Statistical analysis

Statistical analysis was done similarly as mentioned in section 2A.2.3.5 of chapter 2.

3.3 Results and discussions

3.3.1 Preparation of nanocomposites

The fundamental endeavor for the preparation of NC is the homogenous dispersion of the nanoparticles into the macromolecular matrix and utilization of beneficial qualities of these two phases in the combined system. Therefore, the nanoparticles must be well dispersed in a minimal amount of organic solvent prior to its addition into the reaction mixture of HBPU in the final stage of the polymerization process. Otherwise, agglomeration of the nanomaterials into the matrices may deteriorate the performance of FNC compared to that of the pristine polymer. The main advantage of *in situ* polymerization is the uniform mixing of the nanoparticles in the pre-polymer due to the low viscosity of pre-formed polymer unlike other techniques (mentioned in Chapter 1). Furthermore, easy breaking up of agglomerates using high shear device like ultrasonication resulted in a homogenous dispersion of the nanoparticles in the matrix. Further, highly interactive Fe₃O₄ nanoparticles aid in good interfacial interaction with HBPU matrix owing to their structural features and high surface area. The stabilization of dispersed Fe₃O₄ is due to the possible interaction of it with unique structural geometry of HBPU as shown in **Scheme 3.1**:

Figure 3.1b represented the UV-visible spectrum of Fe₃O₄. The peak observed at 385-397 nm is due to the absorption and scattering of light by Fe₃O₄.¹⁹ Thus, FTIR and UV studies confirmed the formation of Fe₃O₄ and also the presence of characteristic peaks of PU and Fe₃O₄ in NC.

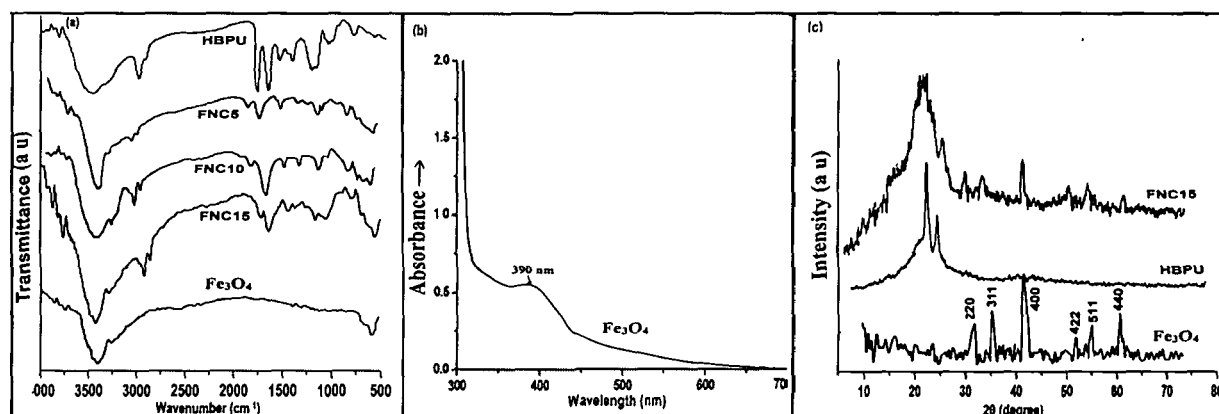


Figure 3.1: FTIR spectra (a) of HBPU, NC and Fe₃O₄, UV spectrum of Fe₃O₄ (b) and XRD patterns (c) of Fe₃O₄, HBPU and FNC15

3.3.3 XRD study

To study the crystallographic nature and the interaction of Fe₃O₄ with HBPU, the XRD analysis was performed as shown in Figure 3.1c. The peaks obtained for Fe₃O₄ are marked by their indices (220), (311), (400), (422), (511) and (440). These peaks clearly suggested that the pure Fe₃O₄ nanoparticles were successfully prepared.²⁰ HBPU showed two peak at 2θ = 21.2° and 23.4° which corresponds to the crystalline peaks for PCL present as already stated in section 2A.3.3 of Chapter 2. XRD pattern of FNC suggested the presence of both Fe₃O₄ and PU in the system. FNC retained the characteristic peaks of nanoparticles and HBPU. Noticeably, there was broadening of the peak value corresponding to PCL moieties which may be due to the influence of Fe₃O₄ as they were well dispersed throughout the matrix. The size of the Fe₃O₄ was estimated by using Scherrer's formula as given below:

$$D = 0.9\alpha / \beta \cos\theta \text{ -----(3.3)}$$

where D is the crystallite size in nm, α is the radiation wavelength (0.154 nm for CuKα), β is the bandwidth at half-height of the highest peak in radian and θ is the diffraction peak angle (2θ =

42.3°).²¹ From the equation, the size of the nanoparticles was found to be 11.16 nm, which is in good agreement with the TEM result.

3.3.4 SEM and TEM studies

SEM images of FNC and HBPU as shown in **Figure 3.2(a and b)** indicate the well dispersion and distribution of Fe₃O₄ into the HB structure of the polymer matrix. The SEM micrographs revealed inhomogeneity in the surface morphology of FNC and HBPU, which is related to the phase separation behavior of PU. However, the estimation of particle size was difficult from the SEM micrograph and hence TEM study is required.

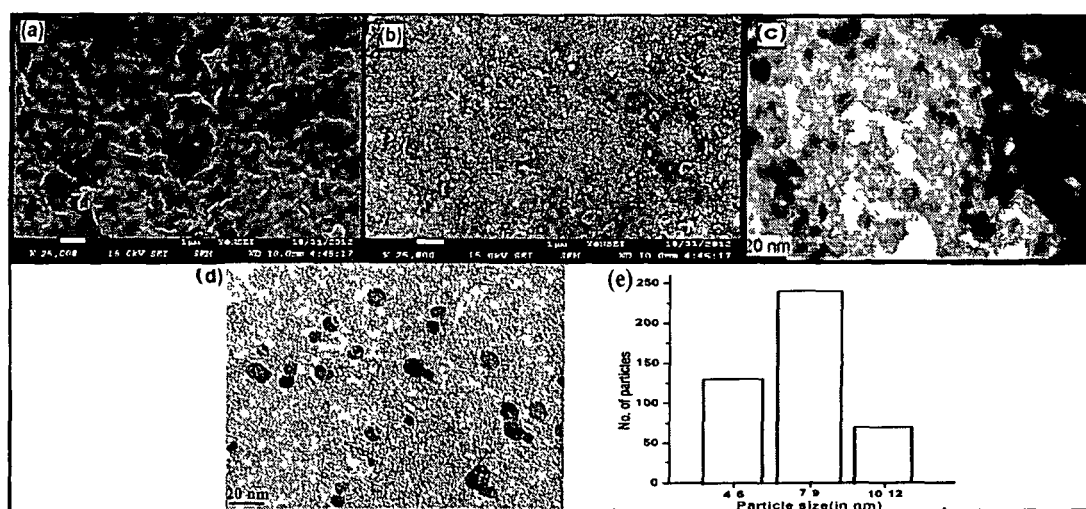


Figure 3.2: Representative SEM images of HBPU (a) and FNC (b), TEM images of Fe₃O₄ (c) and FNC (d) as well as histogram (e) for particle size distribution of Fe₃O₄

TEM images (**Figure 3.2c and d**) confirmed the formation of Fe₃O₄ and the uniform dispersion of Fe₃O₄ into HBPU with an average particles size of 7.65 nm. The histogram in **Figure 3.2d** represents the narrow particle size distribution with spherical shape particles of size 7-9 nm (measured by using Fiji software) of Fe₃O₄ nanoparticles in HBPU. Thus, TEM study confirmed the role of HBPU matrix in even distribution and stability of Fe₃O₄ in the macromolecular structure. The presence of globular void structure and high surface functionality are responsible for efficient interaction and encapsulation of these nanoparticles within the matrix.

3.3.5 Mechanical properties

A material intended to be used as a biomaterial for multifaceted applications especially as catheter, stent or implant must possess sufficient mechanical properties to withstand the internal strain and load. The key requirements are adequate tensile strength, elastic modulus, flexibility and EB. In this context, prepared FNC showed good mechanical properties (Table 3.1). Moreover, the tensile strength tends to increase with increase in Fe_3O_4 content in FNC. The role of nanoparticles for the enhancement of mechanical properties is thus well understood. The mechanical performance of FNC was found to be better than earlier reported Fe_3O_4 based PU NC.^{18, 22} Improved tensile strength and elastic modulus of FNC is due to the high surface area of the nanoparticles and the strong interaction between the nanoparticles and HBPU owing to HB morphology that facilitates the efficient transfer of the applied strain. Meanwhile, EB decreased due to the molecular restriction of the movement of polymer chains owing to better interfacial interactions. However, the long alkyl chain of MG and PCL moiety offered sufficient flexibility to the prepared system. Thus, FNC possesses adequate mechanical properties that are required for polymeric biomaterials.

Table 3.1: Mechanical properties of FNC and HBPU

Sample code	Tensile strength (Mpa)	Elastic modulus (MPa)	EB (%)	Scratch hardness (kg)	Impact resistance (cm)	Bending (mm)
FNC5	29±0.43	30±0.75	735± 5.70	6.8±0.8	>100	<1
FNC10	31±0.9	36±0.53	662±7.19	7.0±1.14	>100	<1
FNC15	34±1.02	40±1.01	574±4.12	8.0±0.3	>100	<1

3.3.6 Thermal study

TGA thermograms as presented in Figure 3.3a indicate that the initial degradation temperature of NC was higher than that of the pristine HBPU. The initial degradation temperature increased with the increasing content of thermostable Fe_3O_4 in FNC. This is due to the absorption of supplied heat and heat insulating nature of the nanoparticles. Further, the thermal degradation results

suggested that once the thermolabile aliphatic moieties and secondary bonds started to degrade, the degradation process of FNC was accelerated by the accumulated heat of Fe_3O_4 .²³ The increase in char residue of FNC with the increased in Fe_3O_4 content in HBPU is due to the increased amount of non-combustible Fe_3O_4 . Moreover, the thermal stability of FNC was found to be higher than reported by Deka et al. based on *Mesua ferrea* oil based HBPU/ Fe_3O_4 -polyaniline NC.²²

From the DSC curves (**Figure 3.3b**) it was found that the crystalline mp (50-56 °C) as well as T_g (14-16 °C) of FNC increased with the increase in wt.% of Fe_3O_4 . The augmentation of these values is due to the restricted motion of the polymer chains due to the good interaction of Fe_3O_4 with the functionalities present in HBPU matrix.²³

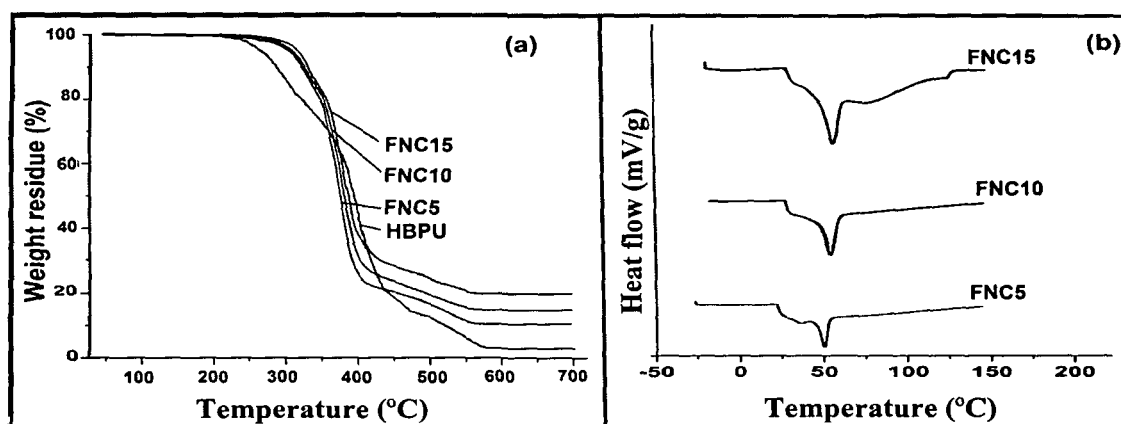


Figure 3.3: TGA thermograms (a) of HBPU and FNC and DSC curves (b) of FNC

3.3.7 Magnetic behavior of Fe_3O_4 and nanocomposites

The magnetic behavior of the prepared Fe_3O_4 and FNC are shown in **Figure 3.4(a and b)**. It was observed that bare Fe_3O_4 as well as FNC exhibited superparamagnetic like behavior. The saturation magnetization value of FNC (7-12 emu/g) was found to be lower than the Fe_3O_4 nanoparticles (48 emu/g). The increased value is assigned due to the particle-polymer interfacial interaction.^{24, 25} The low coercive force (10 Oe) indicates the superparamagnetic like behavior of the nanoparticles. The coercivity of FNC was 44-49 Oe which was higher than that of the bare nanoparticles. This trend is due to decrease in inter-particles dipolar interactions of FNC with a good dispersion of very narrow-domain Fe_3O_4 , consistent with particle-loading-dependent

coercivity in nanoparticles assembly. It has been observed that an increase in the stability of the particles leads to a decrease in toxicity.²⁶ Low coercive force prevents aggregation of the particles prior to superimposition of the field. As a result, these nanoparticles and NC seem to be ideal for biomedical uses.

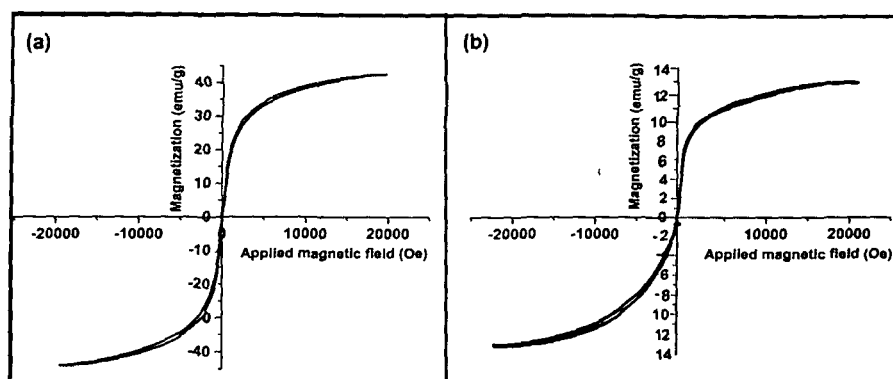


Figure 3.4: Hysteresis loop of Fe₃O₄ (a) and FNC15 (b)

3.3.8 Study of shape memory behavior

To use FNC as a thermo-responsive smart biomaterial, shape recovery and shape retention percentages were determined. The prepared FNC showed excellent shape recovery ranging from (97±1.5)% to 100% (at 45 °C). The value increased as the content of Fe₃O₄ increased in FNC (**Figure 3.5a**). However, HBPU showed only (95±2.1)% shape recovery. Thus, the formation of NC improved the shape recovery of pristine polymer and moreover, increased doses of Fe₃O₄ have a positive effect on the shape recovery percentages of FNC. Similarly, FNC15 showed the maximum shape retention percentage of (85±2.0)%, whereas FNC10 and FNC5 showed (72.5±3.0)% and (67±1.0)% of shape retention, respectively. Again, HBPU exhibited the lowest shape retention of (60±2.5)%. The enhanced shape memory effect of FNC is due to the increase of internal store energy of the polymer matrix resulted from the strong interactions of the nanoparticles with the polymer chains. Further, with the increase of the surface area such interactions also increased that enhanced the shape memory effect of FNC in dose dependent manner. This is also correlated to the increase in degree of crystallinity. The increased crystallinity on incorporation of Fe₃O₄ (as suggested from the increase of enthalpy) may be resulted in increment of unlocked oriented chains, which in turn improved the shape recovery.¹¹ The macroscopic shape memory effects of HBPU and FNC are shown in **Figure 3.5a**.

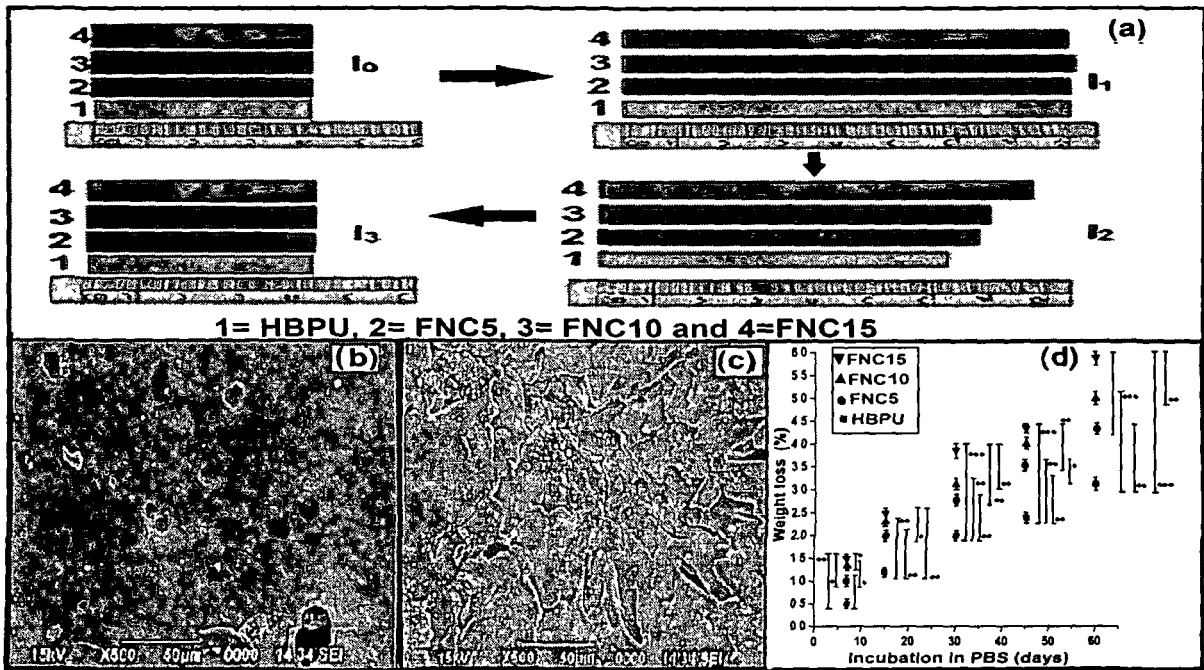


Figure 3.5: Representing the thermo-responsive shape memory behaviors (a) of HBPU and FNC, SEM images of degraded FNC after 15 (b) and 60 (c) days as well as *in vitro* degradation (d) of HBPU and FNC in terms of weight loss (%) against their incubation period (*p > 0.05, **p < 0.05 and ***p < 0.001)

3.3.9 *In vitro* biodegradation study

SEM images of the degraded FNC15 after 15 and 60 days are presented in the **Figure 3.5(b and c)** which indicated the gradual degradation of the film incubated in PBS (pH 7.4). The percentages of weight loss of FNC and HBPU against their incubation period in PBS showed that FNC degraded faster than HBPU ($p < 0.05$) as represented in **Figure 3.5d**. The weight loss of FNC film in the 1st week is mainly due to the leaching out of a few loosely attached Fe₃O₄ nanoparticles. The presence of Fe₃O₄ in the matrix resulted in enhanced degradation as the fluid can come in close proximity with polymeric chain owing to the favorable structural features of FNC system. Initial swelling suggested the absorption of water by FNC films, however with time the hydrolysable polymeric chain in the surface/bulk of FNC started to degrade by hydrolytic cleavages. This can be attested from the SEM images, which depict the formation of pores, surface cracking and erosion of FNC film in PBS (**Figure 3.5c**). Thus, more Fe₃O₄ content may facilitate more hydrolytic degradation of FNC compared to HBPU. Thus, it could be presumed

that under *in vivo* physiological milieu, the degradation become much faster owing to the interplay of body fluid containing different types of enzymes accompanied by other functional mechanisms of the host.

3.3.10 Antibacterial activity

Biomaterials for internal use such as catheter, scaffold or any other blood contacting devices must possess antimicrobial activity and protection against the biofilm formation by microbes like *Staphylococcus aureus* and *Klebsiella pneumoniae*. These bacteria are the most common human pathogens²⁷ and are related to wound or postoperative and prosthetic infections (occurs during the use of catheters, endotracheal tubes, and other biomaterials).²⁸⁻³⁰ HBPU showed no antibacterial activity as it has rough surface with ester/ether linkages which aids in the bacterial adhesion and growth (as discussed in Chapter 2). However, Fe₃O₄ showed zones of inhibition of 13±0.65 mm and 11±0.41 mm against *Staphylococcus aureus* and *Klebsiella pneumoniae*, respectively. Interestingly, FNC exhibited antibacterial activity with zone of inhibition of 14±0.25 mm and 13±0.24 mm, respectively as shown in **Figure 3.6(a and b)**. Thus, incorporation of Fe₃O₄ endowed antibacterial activity to HBPU and this activity increased with the increase of Fe₃O₄ content ($p < 0.001$) and noticeably FNC has higher antibacterial activity in comparison to bare Fe₃O₄ ($p < 0.05$). This reflected the prominent role of HBPU in stabilizing the nanoparticles (as evident from above studies), which resulted in higher surface area of Fe₃O₄ and better interaction with the bacteria to act upon. The antibacterial activity of Fe₃O₄ is assigned due to the generation of ROS which could damage the proteins and DNA of the bacterial cells without harming the human cells.³⁰

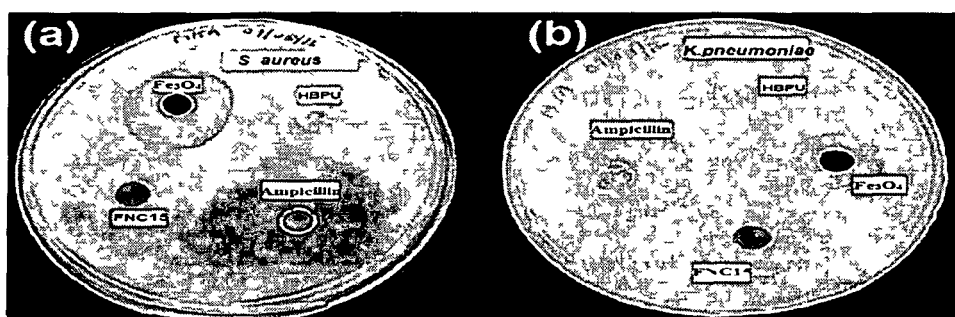


Figure 3.6: Representing the antibacterial activity of Fe₃O₄, HBPU and FNC15 against *Staphylococcus aureus* (a) and *Klebsiella pneumoniae* (b)

3.3.11 *In vitro* cytocompatibility and hemocompatibility

The cell viability assay with primary liver and cardiac cells confirmed the cytocompatibility of FNC. From **Figure 3.7a**, it can be observed that the cell viability of HBPU was $(92\pm 3.2)\%$ and $\geq(85\pm 2.0)\%$, while FNC showed $\geq(97\pm 2.5)\%$ and $\geq(94\pm 1.9)\%$ for primary cardiac and liver cells, respectively. However, Meenach et al. reported less than 90% cell viability of Fe_3O_4 based poly(N-isopropylacrylamide) NC.³¹ The comparatively better cytocompatibility of FNC is mainly due to the presence of biocompatible HBPU matrix, the bio-based moiety and well dispersed nanostructure. Moreover, Fe_3O_4 are biocompatibility and its nanostructural form provided better structural support and anchorage substrate to the cells to proliferate. Further, FNC and HBPU did not show any hemolytic activity. The hemolytic percentages of FNC were in the range of (4.3 ± 2.6) to $(5\pm 0.3)\%$, whereas for HBPU, it was $(3.0\pm 0.3)\%$ as represented in **Figure 3.7b**. Thus, incorporated FNC did not adversely affect the survivability of erythrocytes.

After 60 days of *in vitro* degradation study, the degraded products showed non-toxic nature with $>(80\pm 2.1)\%$ cell viability as evaluated by cell viability assay. Literature reported that Fe_3O_4 degrades into iron and oxygen and it is supposed to happen in intracellular lysosomes of macrophages according to natural Fe pathways.³² Thus, it is regulated by the Fe pathway of the body system without hampering the regular body mechanism.²⁵ Therefore, Fe_3O_4 can be degraded *in vivo* and found to be non-toxic to the organism up to a level of $100\ \mu\text{g/mL}$, as shown by *in vitro* cell viability study in literature.^{25, 33} PU matrix also degraded into non-toxic and easily metabolized products because of the presence of compatible urethane linkages that are acceptable to the body system. However, it is pertinent to mention about the toxicity aspect of TDI used in PU preparation.³⁴ Although, reports showed that TDI based PU has no acute toxic effect on the lungs isolated from guinea pig.³⁵ In Chapter 2 also, it was observed that TDI based HBPU and the degraded products had no toxic effect on Wistar rat. Moreover, FTIR spectrum of degraded products of HBPU (Chapter 2) suggested the absence of such toxic component (toluene diamine) after degradation. Therefore, the overall degraded product of FNC found to be non-toxic. The non-toxic nature of the leached/degraded products was also evaluated by hemolytic assay, which exhibited hemolytic activity of $<5\%$ as presented in **Figure 3.7b**.

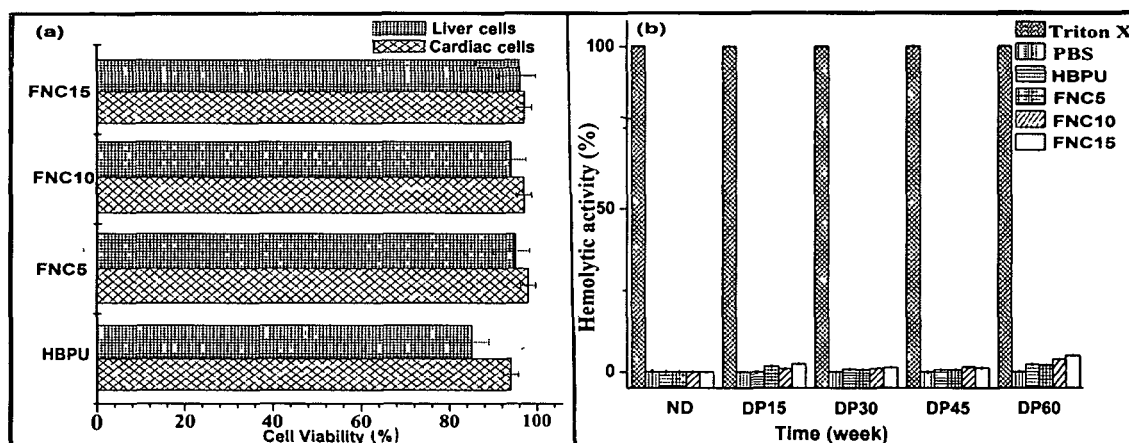


Figure 3.7: The cell viability percentage (a) of the liver and heart cells and hemolytic activity (b) of HBPU, non-degraded FNC (coded as ND) and the degraded by-product after 15 (DP15), 30 (DP30), 45 (DP45) and 60 (DP60) days of *in vitro* biodegradation study

3.3.12 Histopathological study

Histopathological study confirmed the *in vivo* biocompatibility of FNC on post-implantation. **Figure 3.8** clearly suggested that FNC had no negative effect on the major organs like kidney, skin, liver and heart of the Wistar rats. The representative kidney section had shown the normal cellular arrangement with prominent capsules, podocytes and vascular pole without any damages. The representative histological section of the skin presented normal cellular arrangement with well distinguished epidermis and dermis with visible blood vessel and other cell types. The liver section also demonstrated normal cellular organization with distinct central veins and sinusoids, similarly the representative heart section witnessed normal architecture without any cellular damages or necrosis. These observations were in accordance to the results shown in section 2B.3.14 of Chapter 2 for HBPU and same as the control tissues. Thus, this endorsed the biocompatibility of FNC for biomedical purposes.

3.3.13 *In vivo* immunocompatibility

Histopathological study was further supported by other *in vivo* analyses that confirmed no adverse effect of FNC on the treated animals. Cytokine analysis revealed the insignificant inflammatory response of FNC by the treated Wistar rats on post implantation ($p > 0.05$). The implantation site in the vertebral region witnessed no cardinal sign or local infection. The

cytokines level viz., IL-6 and TNF- α was evaluated on the sera of the sacrificed rats (control, HBPU and FNC15 implanted rats) after one month of post-implantation which demonstrated no inflammatory response. IL-6 was found to be (6 \pm 2.3), (10 \pm 3) and (8 \pm 2.1) pg/mL, while TNF- α were found to be (13.2 \pm 3.6), (12.5 \pm 3.5) and (13.0 \pm 0.2) pg/mL in control, HBPU and FNC15 implanted rats, respectively. IL-6 and TNF- α are the two active pro-inflammatory cytokines responsible for eliciting immune response against any material identified as a foreign material by the host body system including polymeric biomaterial. Therefore, this present study supported the non-immunogenic behavior of the implanted FNC film as well.

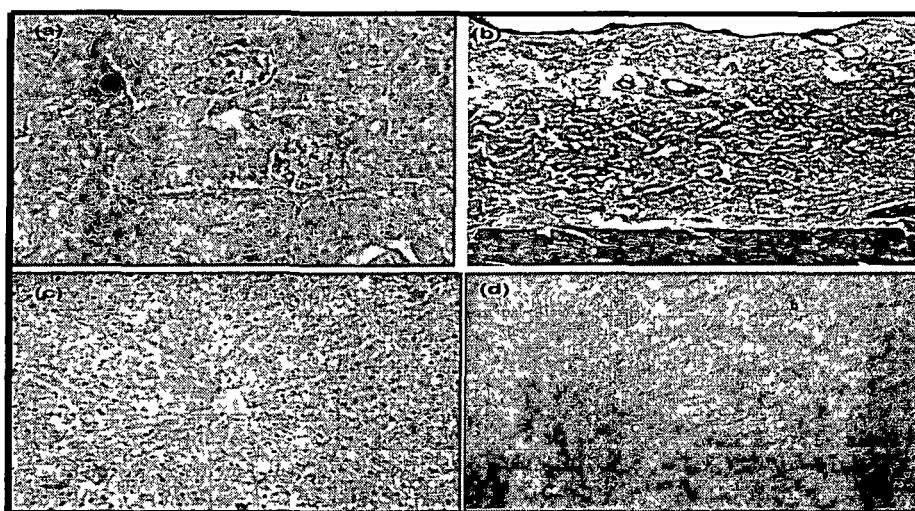


Figure 3.8: Microscopic view of representative histological sections of kidney (a), skin (b), liver (c) and heart (d) of FNC implanted rat

3.4 Conclusion

This study reported the successful preparation of NC from bio-based HBPU and Fe₃O₄ nanoparticles. FNC showed a superparamagnetic like behavior along with enhanced biodegradation, biocompatibility, antimicrobial activity and shape recovery effect compared to the pristine HBPU. The HB structure led to the uniform dispersion of Fe₃O₄ by preventing the agglomeration and providing stability of the later owing to the unique branched architecture and high surface functionalities. Fe₃O₄ content had direct effect on enhancement of many desired properties of FNC. FNC showed adequate thermo-mechanical and improved biological aspects which recommended this material as a potential implantable biomaterial. It may also find avant-

garde applications as a thermally and magnetically controlled smart biomaterial which could open up a new avenue in biomedical research.

Reference

1. Nitin, S., et al. *Soft Matter* **6** (11), 2364--2371, 2010.
2. Roy, I., & Gupta, M.N. *Chem. Biol.* **10** (12), 1161--1171, 2003.
3. Furth, M.E. *Biomaterials* **28** (34), 5068--5073, 2007.
4. Kim, D.K., et al. *Scripta. Mater.* **44** (8), 1713--1717, 2001.
5. Mihaiescu, D.E., et al. *Biofabrication* **5** (1), 015007--015017, 2013.
6. Zeng, X.B., et al. *Int. J. Nanomed.* **7**, 3365--3378, 2012.
7. Li, Z., et al. *Biomed. Mater.* **5** (6), 065010--065019, 2010.
8. Arya, A., et al. *Pacing Clin. Electrophysiol.* **31** (5), 597--603, 2008.
9. Konwarh, R., et al. *Colloids Surf. B* **81** (2), 578--586, 2010.
10. Deka, H., et al. *Carbon* **48** (7), 2013--2022, 2010.
11. Ajili, S.H., et al. *Acta Biomater.* **5** (5), 1519--1530, 2009.
12. Zhou, Y., et al. *Adv. Mater.* **22** (41), 4567--4590, 2010.
13. Ashjari, M., et al. *J. Inorg. Organomet. Polym.* **20** (2), 213--219, 2010.
14. Cai, Y., et al. *J. Appl. Polym. Sci.* **127** (1), 49--56, 2013.
15. Bumb, A., et al. *Nanotechnology* **19** (33), 335601--335607, 2008.
16. Deka, H., & Karak, N. *J. Appl. Polym. Sci.* **116** (1), 106--115, 2010.
17. Turkoglu, A., et al. *Food Chem.* **101** (1), 267--273, 2007.
18. Guo, Z., et al. *Nanotechnology* **18** (33), 335704--335712, 2007.
19. Rahman, O.U., et al. *Mater. Chem. Phys.* **132** (1), 196--202, 2012.
20. Sun, J., et al. *J. Biomed. Mater. Res. A* **80** (2), 333--341, 2007.
21. Welham, N.J. *J. Mater. Res.* **15** (11), 2400--2407, 2000.
22. Deka, G., et al. *J. Macromol. Sci., Pure Appl. Chem.* **46** (11), 1128--1135, 2009.
23. Guo, Z., et al. *Compos. Sci. Technol.* **68** (6), 1513--1520, 2008.
23. Jin, S.H., et al. *Compos. Sci. Technol.* **67** (15-16), 3434--3441, 2007.
24. Zhang, D., et al. *Phys. Rev. B* **58** (21), 14167--14170, 1998.
25. Guo, Z., et al. *J. Appl. Phys.* **101** (9), 09M511--09M513, 2007.
26. Singh, N., et al. *Nano. Rev.* **1**, 5358--5373, 2010.

27. Hassan, M.S., et al. *J. Biomed. Nanotechnol.* **8** (3), 394--404, 2012.
28. Tran, N., et al. *Int. J. Nanomed.* **5**, 277--283, 2010.
29. Harris, L.G., et al. *Biomaterials* **25** (18), 4135--4148, 2004.
30. Touati, D., *Arch. Biochem. Biophys.* **373** (1), 1--6, 2000.
31. Meenach, S.A., et al. *J. Biomed. Mater. Res A* **91** (3), 903--909, 2009.
32. Anzai, Y., et al. *Radiology* **228** (3), 777--788, 2003.
33. Karlsson, H.L., et al. *Chem. Res. Toxicol.* **2** (9), 1726--1732, 2008.
34. Hafeman, A.E., et al. *Pharm. Res.* **25** (10), 2387--2399, 2008.
35. Lastbom, L., et al. *Scand. J. Work Environ. Health* **29** (2), 152--158, 2003.

Chapter 4

***Helianthus annuus* oil based hyperbranched polyurethane/MWCNT nanocomposite as a scaffold for bone tissue engineering**

Highlights

This chapter demonstrates the importance of MWCNT/HBPU NC as a scaffold for bone TE. It also describes the formation of stable HBPU NC with carboxyl functionalized MWCNT. MWCNT based NC showed dramatic improvement in mechanical properties compared to the pristine HBPU. Most importantly, this chapter reveals that MWCNT based NC with interconnected pores size (200-330 μm) showed better proliferation and adherence of osteoblast (MG63) cells compared to HBPU. The hematological, histological and immunological indices of toxicity suggested the safety potential of the prepared NC and its degraded products within the tested animal. Moreover, the cytokines (viz. IL-6 and TNF- α) detection, MTT assay and anti-hemolytic assay boosted the non-toxic behavior of this NC. Thus, this chapter forwarded this NC as a suitable scaffold material for bone TE.

Parts of this chapter is published in

Das, B., Chattopadhyay, P., Mishra, D., Maiti, T.K., Maji, S., Narayan, R., & Karak, N. *J. Mater.*

Chem. B 1, 4115--4126, 2013.

4.1 Introduction

PU based scaffolds are abundantly reported in literature for orthopedic applications.¹ However, the problems associated with PU scaffolds are their insufficient mechanical strength and structural characteristic to match the basic biomechanical and biochemical requirements for their proper functioning.² There is also a problem associated with the gradual loss of mechanical properties of the implanted polymer on post-degradation.³⁻⁵ These mechanical setbacks can lead to fatigue failure. So, the impediment of PU based scaffold can be overcome by employing the concept of nanotechnology with the amalgamation of efficient nanostructure into PU. NC can offer sufficient strength, flexibility and surface area. It can also imitate the natural ECM consisting of micro- and nano-sized structures,⁶ which direct the cells behavior.⁷ Thus, the presence of nano/micro size structure in PU system is beneficial for mimicking the natural ECM.

Literature illustrated the importance of MWCNT in bone TE.⁸ The magic of MWCNT lies on its high aspect ratio, mechanical strength, thermal stability, excellent electrical and biological properties.^{9, 10} MWCNT not only enhances the performance of polymers, but it can also be used in biological domains as a drug delivery system, diagnostic or therapeutic agent and so on.¹¹ Nano-tubular structure of MWCNT can emulate the role of collagen, thereby providing mechanical integrity to a damaged or lost bone region.¹² It is reported that MWCNT is bioactive and hence influences the bio-interfacial interaction. Narita et al. also reported that MWCNT accelerate the osteogenesis process, mainly by inhibiting osteoclastic differentiation and *in vivo* bone resorption.¹³

However, it is pertinent to mention about the toxicity aspect associated with MWCNT, though literature reported that nanotubes in association with the polymers are not toxic.¹⁴ Further, proper functionalization can down-regulate the immunogenic nature of MWCNT within the host. Moreover, reports claimed that -COOH functionalized MWCNT can boost the growth and crystallization of HA if proper stimulated conditions are provided, and thereby helping bone regeneration.^{4, 15} Liu et al. reported that carboxylated nanotubes can be degraded by a phagolysosomal stimulant.¹⁶ Thus, the significance of covalent functionalization of nanotubes is justified for its biomedical application. Again, the presence of such -COOH groups on the surface of MWCNT is very essential for the formation of stable NC. Large number of surface end groups like -OH, -NH and -C=O groups of HBPU can readily interact with the

functionalized MWCNT and the compatibility between these two phases is thus improved. Better the interfacial interaction between the nanomaterials and matrix, better is the performance of NC.

In this context, covalently functionalized MWCNT (using mild KMnO_4 oxidative method) may be used as the suitable nanomaterial to prepare the desired NC. Further, preferable bio-interfacial attributes of the bio-based HBPU with fascinating cell adherence aptitude (as mentioned in Chapter 2) and good interfacial interaction with nanostructure (as stated in Chapter 3) forwarded this polymer as the matrix to prepare MWCNT based NC. To examine the toxicity of MWCNT in this NC, the bio-interfacial interaction, immunocompatibility, hematological parameters and other aspects related to post-implantation syndrome were performed. Finally, to judge the suitability of this NC as a bone tissue scaffold, the adherence and proliferation of mammalian MG63 osteoblast cell line on this NC were also scrutinized.

4.2 Experimental

4.2.1 Materials

Chemicals such as TDI, PCL BD, PE and *Helianthus annuus* oil for the synthesis of HBPU and solvents like xylene, methanol and DMAc were of same specification as elaborated in section 2A.2.1 of Chapter 2. MWCNT was purchased from Iiljin Nanotech, Korea with diameter 10-15 nm and length of 20 μm . The purity of MWCNT is $\geq 95\%$. The materials for biological tests like DMEM, FCS, multi-well tissue culture plates, K3 EDTA tubes and vacuum blood collection tubes were of same specification as described in section 2B.2.1 of Chapter 2. Alamar blue was bought from Life Technologies, USA.

Potassium permanganate (KMnO_4) was purchased from S.D. Fine Chemical Ltd., Mumbai. It mp is 240 $^\circ\text{C}$, density is 2.73 g/mL and M_w is 158.03 g/mol. It was used as a mild oxidizing agent for the functionalization of MWCNT.

Cetyltrimethylammonium bromide (CTAB) was bought from Merck, India. It has mp in the range 237-243 $^\circ\text{C}$ and M_w is 364.45 g/mol. It was used as a surfactant to functionalize MWCNT.

Dichloromethane (DCM) was purchased from Sigma-Aldrich with $\geq 99.8\%$ minimum assay. It bp is 39.8-40 $^\circ\text{C}$ mmHg, mp is -97 $^\circ\text{C}$ and density is 1.32 g/mL at 25 $^\circ\text{C}$. It was used after distillation to disperse MWCNT..

Acetic acid was obtained from Merck, India. It is a colorless liquid with M_w 60.05 g/mol and density 1.05 g/mL. Its mp is 16.5 °C and bp is 118.1 °C. It was used as an auxiliary chemical in the functionalization of MWCNT.

Hydrochloric acid was purchased from Merck, India and used as received. Its F_w is 36.45 g/mol, minimum assay is 36-38%. It was used in the functionalization process of MWCNT.

Animal

Male Wistar rats weighing 200 to 250 g were acquired from the same breeder and housed properly as mentioned in section 2B.2.1 of Chapter 2. All animal experimental protocols were performed according to the “Principles of Laboratory Animal care” (NIH publication 85-23, revised 1985) as described in section 2B.2.1 of Chapter 2.

4.2.2 Instrumentation

Physico-chemical structural analyses were recorded by using XRD, FTIR and UV-visible spectroscopic techniques as described in section 2A.2.2 of Chapter 2. The morphological studies of NC, porous NC and degraded products were carried out by the same SEM and HRTEM instruments as described in section 2A.2.2 of Chapter 2 and section 3.2.2 of Chapter 3, respectively. The nanotubes were dispersed with the help of a ultrasonicator under the same operating conditions as mentioned in section 3.2.2 of Chapter 3. The mechanical performance of the materials was evaluated using UTM as per the ASTM D412-51T, scratch hardness tester, falling weight impact tester and bending test as mentioned in section 2A.2.2 of Chapter 2. Elastic modulus of the samples was evaluated from the slope of the stress-strain curve in elastic region. Toughness of NC was calculated from the total area under the stress-strain curve.

4.2.3 Methods

4.2.3.1 Functionalization of MWCNT

MWCNT was functionalized by using an oxidizing agent, potassium permanganate as mentioned in literature.¹⁷ In brief, MWCNT was dispersed in DCM by ultrasonication in the presence of CTAB. Then, the required amount of potassium permanganate was added slowly (2 h) under constant stirring followed by the addition of acetic acid. The reaction was continued for 48 h at room temperature. Then, the reaction mixture was washed with dilute hydrochloric acid, until the

disappearance of pink color. The washing was continued with distilled water to neutralize the pH followed by washing with acetone and finally vacuum dried at 45 °C for 2 days. The functionalized MWCNT was coded as f-MWCNT.

4.2.3.2 Preparation of nanocomposites

The *Helianthus annuus* oil based HBPU was prepared as described in section 2A.2.3.2 of Chapter 2 by pre-polymerization technique using the A₂+B₂+B₄ approach. In the first step, hydroxyl terminated pre-polymer was prepared from TDI, BD, MG and PCL by using xylene as the solvent. Then in second step, rest amount of TDI and the branching unit, PE were added (by maintain NCO/OH=1) and reacted for 2 h at 77±2 °C. Further, the required amount (0.5, 1.5 and 3.0 wt.%, separately) of well dispersed f-MWCNT (dispersion was done in DMAc by mechanical stirring followed by ultrasonication) was added into the reaction mixture. The reaction was continued till the disappearance of free NCO group as tested by FTIR spectroscopy. HBPU/f-MWCNT NC (MNC) were coded as MNC0.5, MNC1.5 and MNC3.0 for 0.5, 1.5 and 3.0 wt.% of f-MWCNT, respectively.

Porous MNC was fabricated by using the same gas foaming porogen method as discussed in section 2B.2.3.2 of Chapter 2. Porosity of the scaffold was determined by the direct method. In brief, volume of the scaffold material obtained from its dimensions was subtracted from the neat volume of the porous scaffold (calculated from its mass and density). Then, the pore volume and hence porosity of the scaffold was determined.

4.2.3.3 *In vitro* degradation study

In vitro degradation study was carried out according to the ASTM standard method F 1635-04 as discussed in section 2B.2.3.3 of Chapter 2. The films were taken out from the media at a regular interval of 15, 30, 60 and 120 days of test, rinsed with deionized water and wiped. These degraded by-products were coded as DMNC15, DMNC30, DMNC60 and DMNC120, respectively. The degraded films were further dried under vacuum for 4 days at 40 °C to determine the weight retention percentage. Toxicity of the degraded/leached products was estimated by MTT assay and hemolytic activity assay.

4.2.3.4 *In vitro* cytocompatibility assay

The single cells were isolated by collagenase reperfusion method from the heart of Wistar rat as mentioned in section 2B.2.3.4 of Chapter 2. The cell viability percentages of the heart cells in direct contact with the prepared films, degraded/leached products and the nanotubes were investigated by using MTT assay as described in section 2B.2.3.4. of Chapter 2.

4.2.3.5 *In vitro* hemolytic activity assay

In vitro hemolytic activity of MNC and degraded by-products (at 15, 30, 60 and 120 days of incubation) was evaluated by the same procedure as elaborated in section 2B.2.3.5 of Chapter 2.

4.2.3.6 Osteoblast adhesion assay

Indirect cell counting method was employed for osteoblast adhesion test on HBPU and MNC3.0 substrates. Briefly human osteoblast cell line, MG63 was cultured in DMEM complete medium comprising of 10% FCS in a humidified incubator set to deliver 37 °C temperature and 5% CO₂ environment. MG63 cells (1×10⁵) were seeded onto 1 cm×1cm×0.5 cm porous MNC and HBPU. Similar numbers of cells were also seeded onto 1 cm×1cm×0.5 cm cut outs of polystyrene coated tissue culture plate, which served as the control. The cell seeded sheets were placed in cell non-adhesive culture plates followed by their transfer to the incubator. The plates were incubated for different time intervals wherein the unadhered cells were collected and counted under a phase-contrast microscope with the help of a Neuber's hemocytometer. The numbers of unadhered cells were subtracted from the original number of seeded cells in order to obtain the number of adhered cells (equation 4.1).

$$N_{\text{adhered cells}} = N_{\text{seeded cells}} - N_{\text{unadhered cells}} \text{ ----- (4.1)}$$

4.2.3.7 Osteoblast proliferation assay

MG63 human osteoblast cell line was used for osteoblast cell proliferation study on the polymeric substrates by applying Alamar blue assay.¹⁸ Briefly, 20 μL of MG63 cells (containing 1×10⁴ cells) suspension was applied on different polymeric substrates and control sheets (1 cm×1cm×0.5 cm size) and incubated in a humidified CO₂ incubator (37 °C and 5% CO₂) for 3 h before flooding with complete DMEM medium with 10% FCS. Incubation was continued for 7 days with change of media at every alternate day. For the Alamar blue assay, the working

solution was prepared by adding 10% alamar blue solution in incomplete DMEM medium (without FCS) separately and this working solution was added to the cells by replacing the old media followed by incubation at 37 °C in 5% CO₂ incubator for 4 h period. After incubation, supernatants were collected from the culture media and OD were taken at 570 nm and 600 nm. The calculations were carried out according to the manufacturer's instructions.

4.2.3.8 Hematological parameters of rats post-implantation

The subcutaneous implantation of MNC (MNC3.0) and HBPU (dimension 1 mm×1 mm×~ 0.3 mm) on Wistar rats were performed in two groups of rats (three animal in each group), separately using the same procedure as mentioned in section 2B.2.3.6 of Chapter 2. The blood parameters of Wistar rats before and after implantation (with MNC and HBPU) were checked by hematology analyzer (manufactured by Melet Schloesing Laboratory, France, Model No MS4-5). Blood was withdrawn retro-orbitally from the orbital sinus nerve in K3 EDTA tubes at regular intervals (at 1st, 7th, 30th and 60th days of post-implantation). Finally, the blood samples were subjected to hematology analyzer. The analysis was done in triplicate in each case.

4.2.3.9 Histopathological study

After 45 days of post-implantation, the histological evaluation of brain, skin, heart, liver and kidney (collected from control and treated rats) was done by following the same steps as described in section 2B.2.6 of Chapter 2 and stained with hematoxylin and eosin stain. The stained sections were then observed under light microscope.

4.2.3.10 Cytokine detection

Blood was collected in a vacuum blood collection tubes by the same procedure as described in above 2B.2.3.7 of Chapter 2, from the control (without any implantation) as well as MNC (MNC3.0) and HBPU implanted rats. The collected blood was allowed to stand still for 6 h and then centrifuged at 4500 rpm for 10 min to separate the serum. Finally, cytokine (IL-2 and TNF- α) analysis in the serum of treated and control rats was done by using the same procedure as discussed in section 2B.2.3.7 of Chapter 2.

4.2.3.11 Statistical analysis

Statistical analysis was done similarly as mentioned in section 2A.2.3.5 of chapter 2.

4.3 Results and discussions

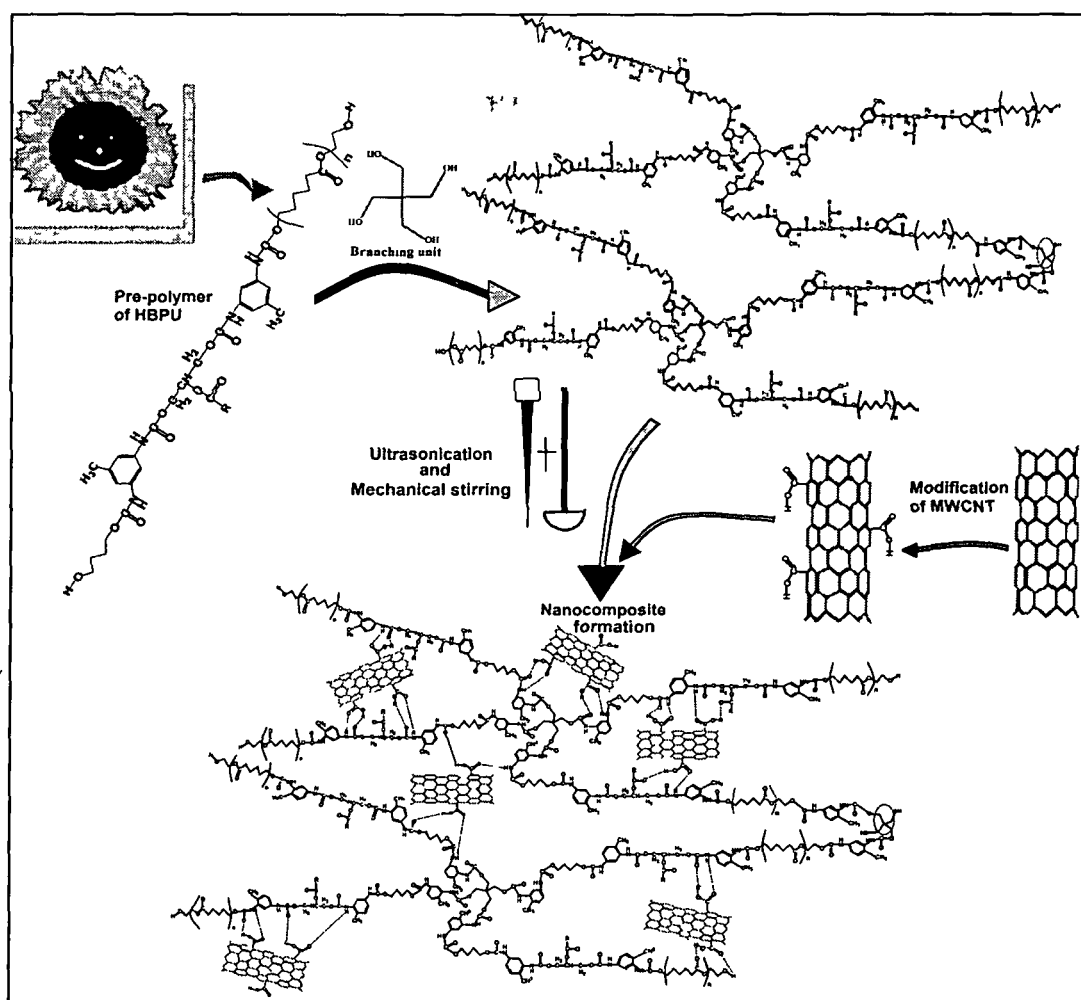
4.3.1 Preparation of nanocomposite

The extent of interaction between the polymer and the nanotubes depends on the level of dispersion of the nanotubes and functional groups present in the matrix. The homogenous dispersion relies on the method of NC formation, nature of polymer, surface functionalities, the degree of modification and mainly the compatibility between the polymeric matrix and nanomaterial.¹⁹ Among all the available methods, *in situ* polymerization is the best as it leads to the homogenous mixing of the nanotubes into the matrix. This is due to be continuous increment in the viscosity with the progress of the polymerization process. Herein, the nanotubes were forced to well disperse in HBPU matrix by *in situ* polymerization method. The expanded branched structure with large surface functionalities and good compatibility with other systems resulted in excellent interaction and homogenous dispersion of the functionalized nanotubes within the polymer chains. This was further witnessed by the different characterization and morphological studies, as presented in the next section. Furthermore, the use of vigorous mechanical stirring and ultrasonication also enhanced the distribution of the nanotubes within HBPU. The preparative protocol and the probable interactions between HBPU and the nanotubes are shown in **Scheme 4.1**.

4.3.2 FTIR study

Figure 4.1a represents the FTIR spectra of the pristine MWCNT, f-MWCNT, HBPU and MNC. The appearance of the FTIR band at around 1734 cm^{-1} (-C=O) as well as increased intensity of the -OH band ($\sim 3400\text{ cm}^{-1}$) in the spectrum of f-MWCNT along with the presence of characteristic band of MWCNT (near 1630 and 1475 cm^{-1}) confirmed the appearance of the carboxylic group on f-MWCNT after oxidation. The presence of such groups on f-MWCNT conferred its dispersibility on aqueous and non-aqueous solvent. **Figure 4.1a** revealed the co-existence and finer interaction between the polymer and nanotubes owing to the presence of -COOH group in f-MWCNT and surface functionalities like -COO , -NH and -OH in HBPU. The characteristic bands of the urethane linkage were observed in the spectrum of HBPU at 1719 ,

1530 and 1067 cm^{-1} corresponding to the $-\text{C}=\text{O}$ stretching vibration, $-\text{NH}$ bending vibration and for $-\text{O}-\text{C}=\text{O}$ stretching vibration of urethane/ester linkages, respectively. Moreover, lowering of the absorption frequency of $-\text{C}=\text{O}$, $-\text{NH}$ and $-\text{OH}$ bonds (at 1707, 1520 and around 3300 cm^{-1} , respectively) in the spectrum of MNC compared to HBPU was observed (**Figure 4.1a**). These suggested more hydrogen bonded such groups in MNC compared to HBPU due to the interactions between the matrix and nanotubes, which might have influenced the phase separation behavior of MNC as well.



Scheme 4.1: Diagram representing the preparation of MNC

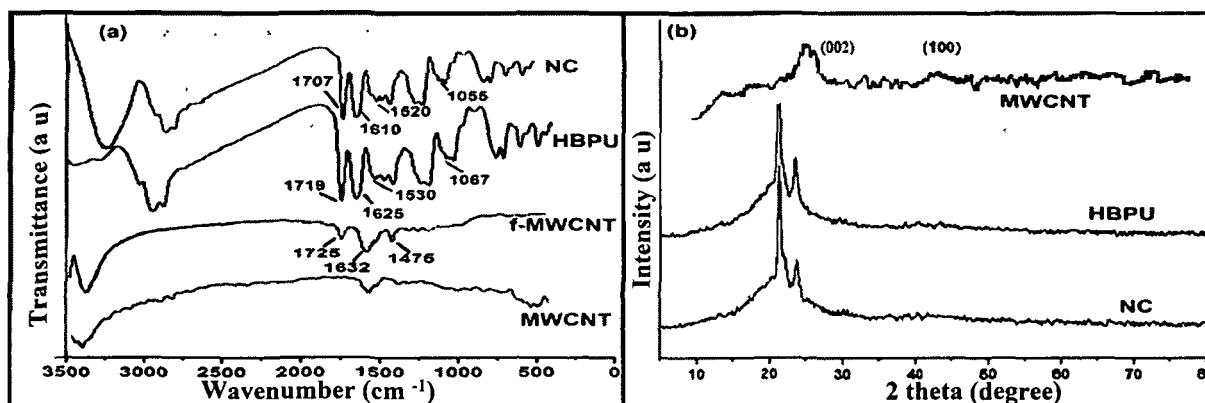


Figure 4.1: FTIR spectra (a) and XRD diffractograms (b) of MWCNT, HBPU and MNC

4.3.3 XRD study

XRD diffractograms of f-MWCNT, HBPU and MNC are shown in **Figure 4.1b**. The XRD pattern of f-MWCNT showed their characteristic peaks at $2\theta = 26.2^\circ$ and 43.1° which are assigned to the (002) and (100) planes of carbon atom.²⁰ XRD diffractogram of HBPU showed the characteristic peaks at $2\theta = 21.2^\circ$ and 23.4° owing to the lattice plane corresponding to (110) and (200) of PCL crystal and the position of which remained unchanged in the XRD diffractogram of MNC. However, higher intensity of the peaks in MNC corresponding to PCL crystal is due to the nucleating effect of f-MWCNT as supported by many literatures.^{9, 21}

4.3.4 SEM and TEM studies

Figure 4.2 represents the SEM micrographs of the non-porous and porous MNC, respectively. It was observed that interconnected pores were generated by the gas foaming method and these pores were evenly distributed throughout the matrix. The pores size of the scaffold ranges from 200-330 μm with porosity of 39.53% and thus the fabricated scaffold is appropriate for osteoblast proliferation and nutrient exchange. However, from SEM images the distribution of nanotubes in the matrix could not be observed. Therefore, the detailed morphological feature of MNC was studied from the HRTEM images (**Figure 4.3(a and b)**). HRTEM images showed that the nanotubes were well dispersed and remained embedded into the polymeric matrix and there is an excellent orientation of the nanotubes throughout the matrix with the average inner and outer diameter equals to 3.65 and 16.9 nm, respectively. This high level of interfacial interaction and absence of agglomeration was achieved due to the presence of different surface

functionalities in HBPU and functionalized MWCNT, which resulted in higher wetting of f-MWCNT by the polymer chains and excellent interfacial contact. Furthermore, the well dispersed f-MWCNT may result in the improved performance of MNC.

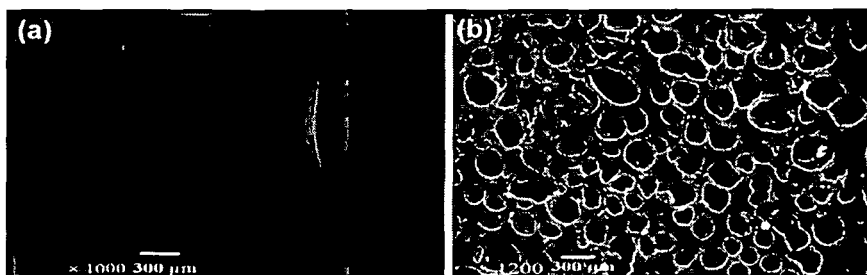


Figure 4.2: Representative SEM images of MNC (a) and porous MNC (b)

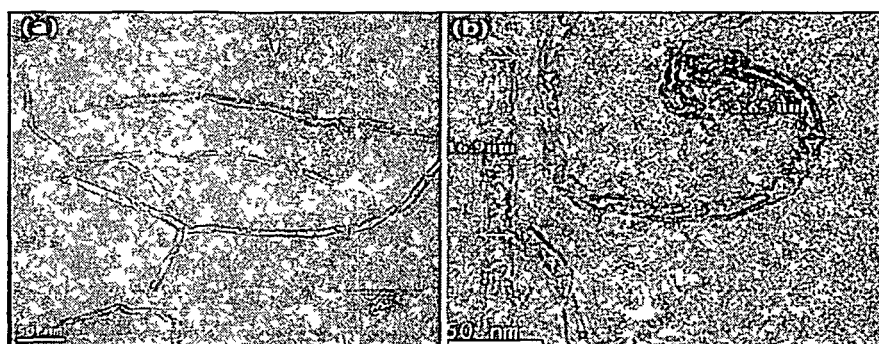


Figure 4.3: Representative TEM images of MNC (a and b).

4.3.5 Mechanical properties

The enhancement of mechanical strength is one of the vital reasons for preparation of CNT based PU NC to match the basic biomechanical properties of the bone tissue. The incorporation of the nanotubes dramatically improved the tensile strength of the virgin polymer by approximately two fold (**Table 4.1**). However, this compensated with decreased EB. A low dose of 0.5 wt.% of f-MWCNT had drastically improved the strength of MNC to (36.98 ± 1.8) from (26.93 ± 2.0) MPa of pristine HBPU. The scratch hardness (4.6 ± 0.7 to 7.8 ± 1.1 kg) also improved compared to the pristine polymer (**Table 4.1**). Similarly, the strength of MNC increased from (36.98 ± 1.8) to (47.6 ± 3.3) MPa with the increase in the wt.% (0.5-3.0) of nanotubes, whereas the EB decreased from 673 to 550% for the same (**Table 4.1**). Furthermore, the degraded MNC3.0 after 60 days of incubation showed decrease in performance which is quite obvious owing to the surface erosion

as well as hydrolysis of hydrolysable chemical linkages in MNC. The mechanical properties of pristine as well as MNC are given in **Table 4.1**, whereas the stress-strain profiles of them are shown in **Figure 4.4a**. These mechanical properties of MNC were sufficient for using it as a polymeric scaffold for supporting the growth of bone cells enduring the repeating load and pressure.²² MNC showed semi-crystalline polymeric behavior. The toughness and the elastic modulus were found to be enhanced with f-MWCNT content (**Table 4.1**). The outstanding properties of MNC are due to the efficient and uniform transfer of stress/load applied on them to the dispersed nanotubes with high surface area and high rigidity. The mechanically tough nanotubes thus improved the load bearing potential of the pristine HBPU and made it suitable for the destined application of bone TE with required biomechanical properties.

Table 4.1: Mechanical properties of HBPU and MNC

Sample code	Tensile strength (MPa)	EB (%)	Toughness	Elastic modulus (MPa)	Scratch hardness (kg)	Impact resistance (cm)	Flexibility (mm)
HBPU	26.93±2.0	600 ±9.2	12767	30± 0.32	4.6±0.7	100	< 1
MNC0.5	36.98±1.8	673± 9.3	18427	48±0.78	5.7±1.3	100	< 1
MNC1.5	40.01± 2.5	610± 8.8	19181	53±1.03	6.3±0.7	100	< 1
MNC3.0	47.60±3.3	547± 9.0	19440	59 ±0.98	7.9±1.1	100	< 1
DMNC60	39.04± 1.6	450± 8.4	17729	41± 1.03	4.8±1.2	90	< 2

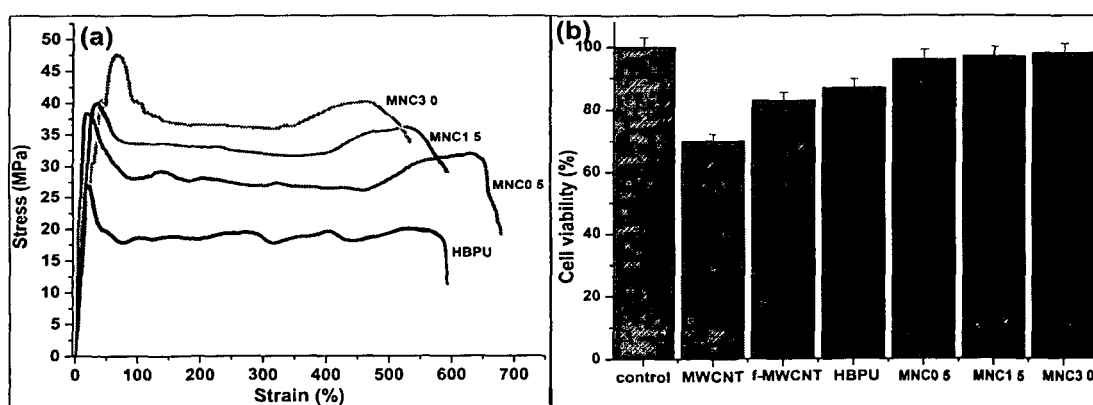


Figure 4.4: Stress-strain profiles (a) of HBPU and MNC as well as cell viability % (b) of heart cells on HBPU and MNC scaffolds

4.3.6 *In vitro* cytocompatibility

The cytocompatibility of the pristine MWCNT, f-MWCNT, HBPU, MNC and degraded MNC was analyzed by MTT assay and the cell viability percentages is presented by bar diagram in **Figure 4.4b**. The unmodified MWCNT showed less than $(70\pm 3.7)\%$ of cell viability suggesting its toxicity to the heart cells; however f-MWCNT showed good cytocompatibility to heart cells with $(83\pm 3.0)\%$ of cell viability. HBPU as well as MNC showed excellent cell viability as observed from **Figure 4.4b**. Thus, the study demonstrated better compatibility of MNC than HBPU ($p < 0.05$) and also suggested that toxic effect of MWCNT was neutralized upon unison with the matrix as well as on functionalization. Moreover, the porous HB macromolecule with nano-dimensional evenly distributed f-MWCNT enhanced the cells proliferation and escorted the cellular behavior positively by mimicking the natural mesh of ECM. The positive feedback due to the presence of nanostructure in MNC is clearly understood from **Figure 4.5(a and b)**. It indicated that higher numbers of cells were adhered on MNC film compared to that of HBPU. The degraded product up to 120 days of degradation exhibited non-cytotoxicity. This demonstrated that MNC degraded into body compatible by-products, however a detailed toxicity study on the degraded/released product for longer duration is must.

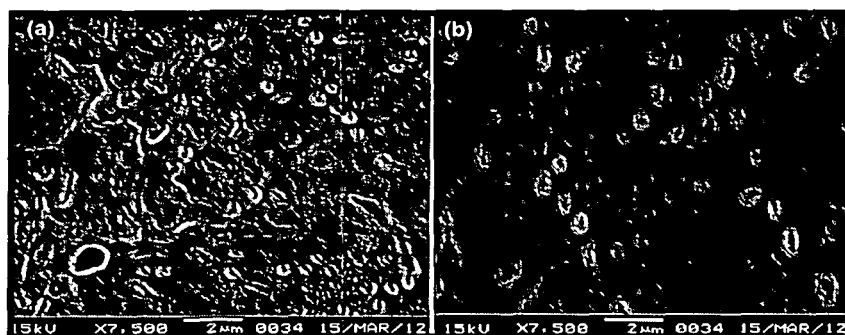


Figure 4.5: Cell adherence on representative MNC (a) and HBPU (b) scaffolds

4.3.7 *Analysis of hematological parameters*

The hematological study demonstrated the blood parameter of an organism. White blood cell or leukocytes are the cells of the immune system involved in defending the body against the infectious diseases and foreign materials. The numbers of leukocytes in the body is often determinant of harmful effect relating to foreign materials and diseases.²³ The data obtained

through the study before and after implantation of MNC and HBPU in rats are represented in **Table 4.2**. The rats without implantation showed the values within the normal range. However, the hematological parameters on post-implantation at a interval of 1, 7, 30 and 60 days demonstrated minute variations (**Table 4.2**) which are quite obvious.

Table 4.2: Hematological parameters of Wistar rats before and after implantation

Cell types	Before implantation		Hematological parameters							
			Post implantation (days)							
	MNC	HBPU	1		7		30		60	
MNC			HBPU	MNC	HBPU	MNC	HBPU	MNC	HBPU	
WBC	4.5±0.3	5.1±0.5	6.2±0.2	6.9±0.3	5.5±0.4	6.1±0.3	6.6±0.4	6.7±0.2	4.4±0.2	5.1±0.3
LYM	75±3.4	73±2.9	76±3.2	77±4.2	78±3.0	79±3.8	81±2.5	9±3.7	84±4.2	85±4.3
MON	6.3±1.2	4.8±0.7	3.8±1.0	2.1±0.5	10±1.5	7±2.3	3.7±0.3	5.6±0.7	2.8±0.2	3.7±0.4
NEU	15±2.0	17±1.5	20±2.3	18±1.0	11±2.9	10±1.5	15±1.8	13±1.2	12±0.8	10±1.0
EO	3.3±0.3	4.9±0.6	0.2±0.01	2.8±0.3	0.7±0.03	3.9±0.5	0.6±0.1	2.3±0.3	1.2±0.2	0.9±0.2
BA	0.1	0.0	0.0	0.0	0.0	0.1	0.0	0.0	0.0	0.0
RBC	7.6±1.9	8.2±1.5	7.3±0.5	7.5±1.5	7.6±1.2	7.9±2.0	7.7±1.5	7.9±1.6	7.7±1.0	7.9±1.9
MCV	52±3.0	65±3.2	63±1.8	62±3.0	62±1.5	62±2.9	61±1.6	64±0.8	60±2.2	63±2.5
HcT	29±0.9	28±2.0	28±2.4	26±0.7	22±0.9	26±1.5	29±2.0	27±0.9	31±2.1	27±3.0
RDW	11±0.5	11±1.0	14±1.5	10±0.6	16±0.9	12±1.0	13±0.8	11±0.8	12±1.2	11±0.5
Hb	11.9±1.2	11.7±1.1	11.4±0.3	11.2±1.2	11.8±1.5	11.1±0.2	11±2.0	11.2±1.2	12.0±0.9	11.0±1.4
TCR	691±5.0	700±3.6	700±4.5	810±4.9	600±3.9	788±5.5	690±7.1	750±5.5	610±5.0	742±4.7
MPV	7.3±2.1	8.4±0.8	8.0±1.1	9.2±0.9	7.7±1.3	8.6±0.5	7.9±2.2	8.5±0.5	8.0±1.3	8.4±2.0
Pct	0.5±0.01	0.4±0.02	0.6±0.01	0.7±0.02	0.3±0.02	0.6±0.01	0.4±0.1	0.5±0.01	0.3±0.05	0.5±0.03
PDW	12±2.3	11±1.9	14±0.8	17±2.5	13±1.3	16±0.7	12±2.9	15±1.4	12±0.4	15±0.8

WBC=White blood cell (3.0-12 m/mm³); LYM= lymphocyte (65-85%); MON= Monocyte (0-5%); NEU=Neutrophile (9-34%); EO= Eosinophil (0-6%); BA= Basophil (%); RBC= Red blood cells (7-10 M/mm³); MCV= Mean corpuscular Volume (65-70 fl); HcT=Hematocrit (30-39%); RDW= Red blood cell distribution width (8-12); Hb= Hemoglobin (11-18 g/dl); TCR=T-cell receptor (500-1300 m/mm³); MPV=Mean Platelet Volume (6-1- fl); Pct=Plateletcrit (%); and PDW= Platelet distribution width (12-18).

In this study, leukocytes count post 1st day of implantation was observed to increase in both MNC and HBPU treated rats as compared to the control ($p < 0.001$) (but within the normal range). Further, no inflammatory response viz. swelling, redness or rise in temperature was observed nearby the implantation site. After 7th day of post-implantation, the leukocytes count decreased and minute increase in the macrophage (matured monocytes) and neutrophils levels were observed ($p < 0.05$), however without any cardinal sign. The raise in macrophage level was within the normal range. Moreover, no significant difference was observed between MNC and HBPU treated groups ($p > 0.05$). Thus, these findings suggested the immunocompatibility of MNC as well as HBPU as supported by the literature.²⁴ The variation in such parameters is due to sudden encounter of the host with the foreign material and surgery. Noticeably, sudden rise in the immune cells count was observed after approximately one month of implantation in all the treated groups. This may be due to the release of leachable substances or induction of degradation of the film within the host system. During that period, the implantation site was intensely observed for inflammatory response. However, the absence of inflammatory sign and neutralization of the immune response within 6-7 days, further confirmed the non-toxic nature of the degraded product as well as the released product(s) in the body of the treated rats. These results are in accordance with the *in vitro* cytotoxicity results of MNC, degraded MNC and degraded by-products. Furthermore, non-toxic nature of MNC, degraded and the released products including HBPU upto 60 days of test was confirmed from the other blood parameters that includes plateletcrit, red blood cell (RBC) count, RBC distribution width, etc. of the treated animal as presented in **Table 4.2**.

4.3.8 *In vitro* hemocompatibility

The blood-material interaction is a very crucial phenomenon after implantation.²³ The *in vitro* hemocompatibility assessment of MNC, degraded products as well as released product(s) of MNC incubated in PBS buffer was done in direct contact with the blood cells and the results are represented in **Figure 4.6a**. Both MNC and HBPU exhibited $\sim(2.5 \pm 0.005)\%$ of hemolytic activity, whereas for the degraded/released product(s) the hemolytic activity varies in the range of (3 ± 0.023) to $(3.5 \pm 0.04)\%$ up to 120th days of incubation. Thus, the overall result at different time intervals illustrated the anti-hemolytic activity of the prepared MNC as well as the degraded products, which was further in accordance with the *in vivo* results.

4.3.9 *In vivo immunocompatibility*

IL-6 and TNF- α ²⁵ can be detected in the peripheral blood of the recipient on exposure to the biomaterials and are crucial indicator of immunocompatibility, as already mentioned in previous chapters.²⁶ The graph presented in **Figure 4.6b** suggested that the level of these cytokines (IL-6 and TNF- α) is within the safety zone as compared to the control rats. The minute increased concentration (5 ± 0.047) pg/mL in the cytokines level post-implantation is due to the surgical incision as well as related biological healing process. None of the treated groups were found to express abnormal increase in the cytokine concentration. Hence, these results suggested that the tested materials were accepted by the host animals.

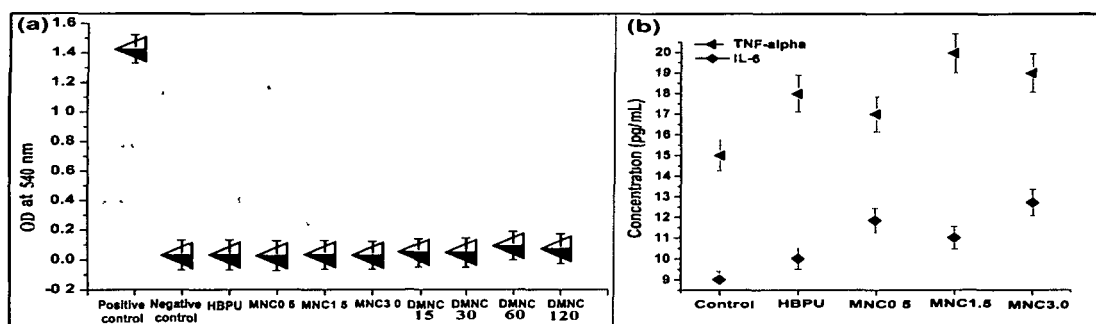


Figure 4.6: Representing the anti-hemolytic activity % (a) of control, HBPU and MNC as well as cytokine expression (b) in HBPU and MNC treated animals as well as in the control group

4.3.10 *Adhesion and proliferation of MG63 cells*

MG63 osteoblast cell adhesion test revealed that in all the cases the threshold cellular adhesion reached at ~ 3 h of time period (**Figure 4.7a**). However, the degree of adhesion varied when control and polymeric films were compared. Control experiment showed about 9.5×10^4 cells out of 10×10^4 cells adhered at ~ 3 h time, which can be considered as $(95 \pm 3.2)\%$ adhesion. In case of HBPU and MNC (MNC3.0), maximum cell adhesion varied from 80-85% as shown in the **Figure 4.7a**. The initial cell adherence potential of MNC3.0 was higher than HBPU ($p < 0.001$). However, at maximum adhesion time the difference between them was reduced ($p < 0.05$). Initial cell adhesion at 15 min time on MNC3.0 was $(50 \pm 4.2)\%$, whereas HBPU showed only $(37 \pm 2.9)\%$ of cell adhesion. The results indicated that MNC has good osteoblast adherence capability though the result was slightly lower than the control at 500 min. However, it is

noteworthy that the presence of f-MWCNT enhanced this vital biological property of NC, which befits it as a scaffold material.

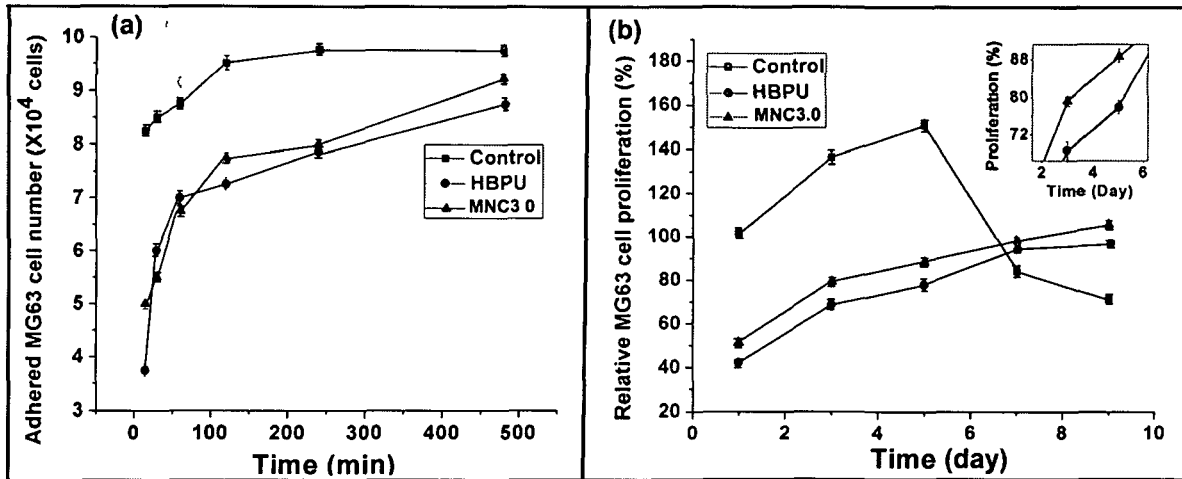


Figure 4.7: MG63 cells adhered (a) against time (min) on control, HBPU and MNC3.0 as well as MG63 cells proliferation % (b) against day of incubation on HBPU and MNC3.0

Furthermore, osteoblast proliferation data are shown in **Figure 4.7b**. MG3 cell proliferation on the control film was reached up to a maximum value of ~140% within 5 days of test, though the same was 100% even in the first day. However, the proliferation gradually reduced after 6th day as revealed by the Alamar blue based viability experiment. On the other hand, HBPU and MNC were lagging with only $\sim(40\pm 2.0)$ and $(50\pm 2.8)\%$ proliferation, respectively in the 1st day of test. MNC3.0 reached 100% cell proliferation at 9th day, whereas HBPU showed less than $(90\pm 2.7)\%$. Moreover, the initial osteoblast proliferation on MNC3.0 was maintained 1.2 fold higher than that of pure HBPU up to 5th day of test ($p < 0.05$). Nevertheless, the osteoblast proliferation pattern was much different in control and treated systems. In control proliferation rate after attaining the highest proliferation at 5th day, whereas in MNC treated culture, the trend was eye catching as proliferation of MG63 cells kept on increasing at the maximum studied time. The results suggested that MG63 initially taken time to acclimatize them with MNC and finally geared up by getting the suitable supporting matrix. This higher proliferation rate in MNC may be accounted by better osteoblast adhesion on them compared to HBPU. Thus, the presence of MWCNT in MNC has a potent role in enhancing the

bioactivity of synthetic polymers. These observations are supported by literature, as Hirata et al. also showed improved MC3T3-E1 cells adherence and proliferation on collagen honeycomb scaffold on inclusion of MWCNT.²⁷ Moreover, the porous ultrastructure in both MNC and HBPU helped in supporting the growth of MG63 cells up to a longer period. Hence, the overall results suggest that NC could be referred to as osteoconductive material, as it served to perpetuate the growth of osteoblast cell. Thus, the presence of bioactive nanostructure in the biocompatible porous HBPU provided a natural mesh of ECM to the MG63 cells to proliferate.

4.3.11 Histopathological study

Histopathological study is the microscopy observation of cells and tissues. Any change in the normal architecture of an organ is directly related to the occurrence of some diseases, presence of toxic material, severe infection, wound and so on. The representative histological sections of each group is shown in Figure 4.8. MNC film (MNC3.0) implanted within the rats showed no adverse effects on the morphology of the brain, liver, heart, kidneys and skin as shown in **Figure 4.8a-e**. Thus, the microscopic observation of these major organs in treated group demonstrated the non-toxic and safety aspect of the prepared MNC.²⁸ Furthermore, a similar result was also observed for HBPU treated rats with no ill effect on the morphology of the major organs (**Figure 4.8a₁- e₁**) as supported by the results of section 2B.3.14 of Chapter 2.

The representative brain section demonstrated normal architecture with well visualized ganglion cells and nerve cells (**Figure 4.8(a and a₁)**). Similarly, the liver sections of the treated rats showed to have normal cellular organization as represented in **Figure 4.8(b and b₁)**) with well visualized hepatocytes, portal vein, distinct central veins and sinusoids. The derived histological sections of the kidney (**Figure 4.8(c and c₁)**) from implanted rats with MNC3.0 and HBPU film after 45 days of post-implantation showed a normal appearance of the renal capsules and tubules. **Figure 4.8(d and d₁)**) represent well distinguished intercalated disc, nuclei and muscle fiber of representative heart section without any dead cells. Moreover, skin section from the implanted site after 45 days of implantation showed well distinguished intercalated disc, nuclei and muscle fiber without any dead cells. Similarly, skin section (**Figure 4.8(e and e₁)**) from the implanted site after 45 days of implantation exhibited normal cellular arrangement of different layers with complete re-epithelialization along with the appearance of prominent blood vessel. However, compared to that of the skin section (implantation site) of HBPU treated rats,

the neo-vascularization in MNC3.0 treated group was better with more compact collagen formation as observed from **Figure 4.8(e and e₁)**. This suggested that MNC possess structural benefits over HBPU that enhanced the re-epithelialization process at the surgical site.

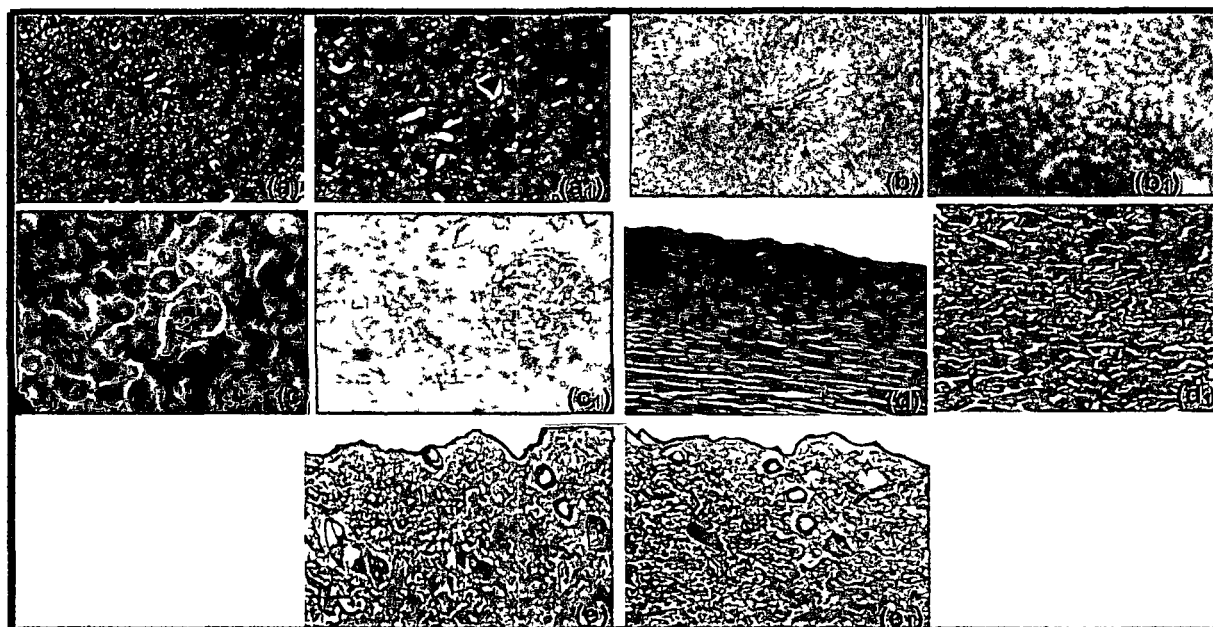


Figure 4.8: Microscopic view of representative histological sections of brain (a and a₁), liver (b and b₁), kidney (c and c₁), heart (d and d₁) and skin (e and e₁) of Wistar rat implanted with MNC3.0 (a-e) and HBPU (a₁-e₁)

4.3.12 In vitro biodegradation study

The union of biodegradability (as evaluated by time dependent weight loss of MNC film in PBS and morphological changes, **Figure 4.9**) with the aforementioned positive attributes of MNC revealed the potency of the studied material as an advanced biodegradable scaffold. The progressive morphological changes of MNC during degradation are shown in **Figure 4.9(a-c)**. It was observed from the images that there was gradual surface erosion on MNC film. Thereafter, there was surface cracking, development of random pores and fractures throughout the NC matrix. The weight retention percentage by the samples against the time of incubation is shown in **Figure 4.9d**. The differences in the secondary intra/inter-molecular interactions between polymer and nanotubes with the increase in amount of f-MWCNT resulted in the observed differences ($p < 0.05$) in their degradation rate. Furthermore, by choosing the appropriate

compositional parameters and f-MWCNT content, the biodegradation properties can be tailored as suggested by this study.

The biodegraded products are non toxic as tested by different studies; discussed above. Therefore MNC, leachable substances as well as degraded products are supposed to be safe to the patient. The evidence of the biodegradation of TDI based polyurethane in physiological condition into non-toxic products are reported by many researchers^{9, 29} including our earlier studies in Chapter 2 and Chapter 3. Moreover degradation of CNT by horse redox peroxidase/H₂O₂ over the period of several weeks was also provided by literature.³⁰ It is therefore appealing to speculate that other peroxidases present in the body system may be effective in oxidative degradation of CNT. Augmentation of these catalytic biodegradation pathways may be influential in avoiding the *in vivo* toxic effect, as presumed by many studies.³¹

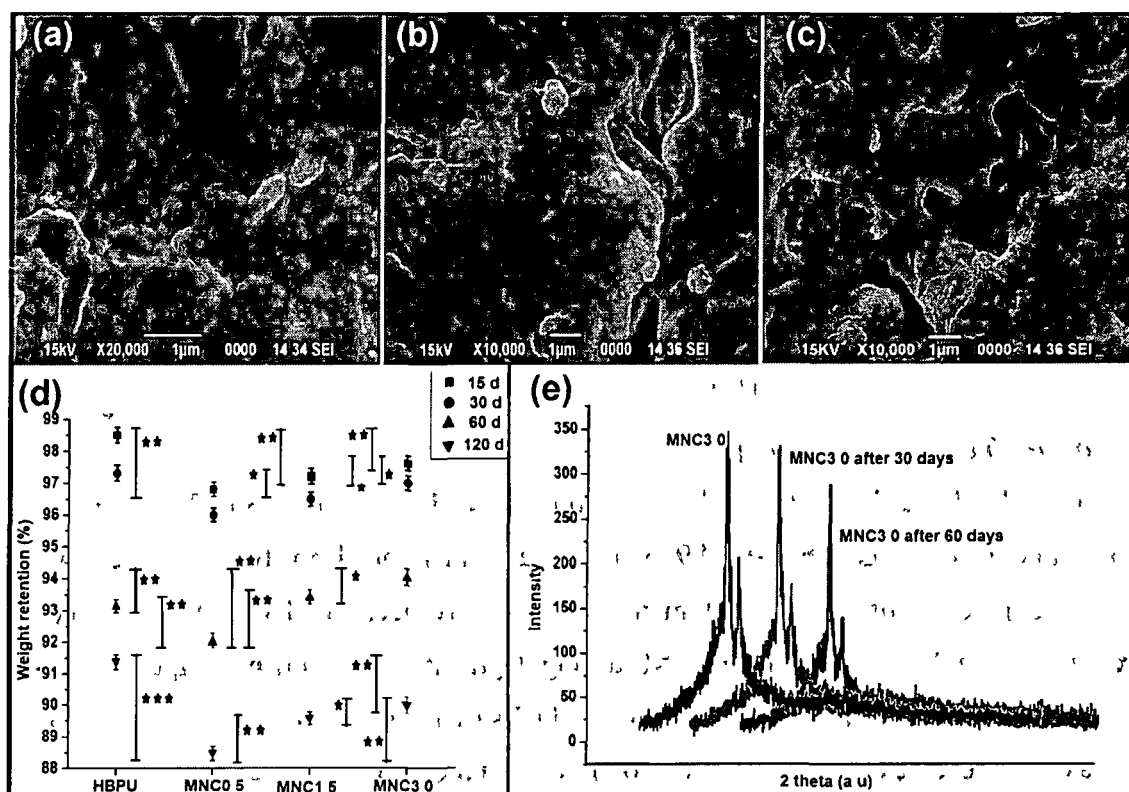


Figure 4.9: SEM images (a-c) showing the morphological changes during progressive degradation of representative MNC film, the weight retention % (d) of NC against their incubation period in PBS at regular interval (* $p > 0.05$, ** $p < 0.05$ and *** $p < 0.001$) and XRD diffractograms (e) of degraded MNC3.0

The degradation of HBPU was suggested (as mentioned in Chapter 2) to occur by the gradual breaking of the ester linkages present in PCL and MG moieties, and other secondary interactions in the *in vitro* physiological environment. Moreover, the hydrolysis of ester linkages of PCL present in MNC was confirmed by the XRD diffractograms of the degraded NC. **Figure 4.9e** showed gradual decreased in the peaks intensity corresponding to the PCL crystal post-degradation, which thus verifies our earlier result.

4.4 Conclusion

HBPU and f-MWCNT based NC was demonstrated as a potent scaffold for bone TE. MNC based scaffold approved the safety potency and non-toxic behavior as demonstrated by various biological studies. The hematological parameters, cytokine profiles and histopathological studies after subcutaneous implantation in Wistar rats established the immunocompatibility and the excellent biocompatibility of MNC. The enhanced cell proliferation on MNC compared to the HBPU revealed the important role of macro as well as nano structural elements to mimic the native cellular environment to the cells to grow naturally on the artificial scaffold. The incorporation of f-MWCNT into HBPU dramatically improved the mechanical performance of MNC in a dose dependent manner. Moreover, compared to the control study, MNC3.0 supported the proliferation of MG63 for longer period of time. Further, the enhanced adherence of MG63 cells on MNC accords for its scaffold application. Thus, MNC with interconnected porous structure, adequate mechanical properties, biodegradability and osteoconductivity stands as an ideal scaffold in bone TE. However, prior to actual application the *in vivo* assessment of bone/cartilage tissue growth on this scaffold must be performed.

Reference

1. Liu, X., & Ma, P.X. *Ann. Biomed. Eng.* **32** (3), 477--486, 2004.
2. Zych, E.S., et al. *Acta. Physica Polonica A* **121** (2), 518--521, 2012.
3. Jasty, M.J., et al. *J. Bone Joint Surg. Am.* **68** (6), 912--919, 1986.
4. Glant, T.T., et al. *J. Bone Miner. Res.* **8** (9), 1071--1079, 1993.
5. Derbyshire, B., et al. *Med. Eng. Phys.* **16** (3), 229--236, 1994.
6. Rogel, M.R., et al. *J. Mater. Chem.* **18** (36), 4233--4241, 2008.
7. Chen, X., et al. *J. Am. Chem. Soc.* **128** (19), 6292--6293, 2006.

8. Jell, G., et al. *J. Mater. Chem.* **18** (16), 1865--1872, 2008.
9. Deka, H., et al. *Carbon* **48** (7), 2013--2022, 2010.
10. Sweetman, L.J., et al. *J. Mater. Chem.* **18** (44), 5417--5422, 2008
11. Mendes, G.R., et al. *J. Mater. Chem. B* **1** (4), 401--428, 2013.
12. Zhao, B., et al. *Chem. Mater.* **17** (4), 3235--3241, 2005.
13. Narita, N., et al. *Nano Lett.* **9** (4), 1406--1413, 2009.
14. Tabet, L., et al. *Part. Fibre Toxicol.* **8** (3), 1--13, 2011.
15. Li, X., et al. *Biomaterials* **33** (19), 4818--4827, 2012.
16. Liu, X., et al. *Carbon* **48** (7), 1961--1969, 2010.
17. Konwar, U., et al. *Adv. Sci. Lett.* **16** (1), 265--273, 2012.
18. Byth, H.A., et al. *Phytochem. Anal.* **12** (5), 340--346, 2001.
19. Karak, N. *Fundamentals of Polymers: Raw Materials to Finish Products*, PHI Learning Private Limited, New Delhi, 2009.
20. Pramanik, S., et al. *Carbon*, **55**, 34--43, 2013.
21. Sahoo, N.G. *Compos. Sci. Technol.* **67** (9), 1920--1929, 2007.
22. Razak, S.I.A., et al. *Int. J. Basic Appl. Sci.* **12** (1), 31--49, 2012.
23. Anderson, J.M., et al. *Semin. Immunol.* **20** (2), 86--100, 2008.
24. Kang, B.C., et al. *Exp. Anim.* **54** (1), 37--52, 2005.
25. Dinarello, C.A., et al. *J. Exp. Med.* **163** (6), 1433--1450, 1986.
26. Perlmutter, D.H., et al. *J. Clin. Invest.* **78** (5), 1349--1354, 1986.
27. Hirata, E., et al. *J. Biomed. Mater. Res. Part B Appl Biomater.* **90B** (2), 629--634, 2009.
28. Su, B., et al. *Biochem. Pharmacol.* **1** (7), e106--116, 2012.
29. Lamba, N.M.K. Woodhouse, K.A. & Cooper, S.L. *Polyurethane in Bio-medical Application*, CRC Press, Boca Raton, 1997.
30. Kagan, V.E., et al. *Nat. Nanotechnol.* **5** (5), 354--359, 2010.
31. Armentano, I., et al. *Polym. Degrad. Stab.* **95** (11), 2126--2146, 2010.

Chapter 5

***Helianthus annuus* oil based hyperbranched polyurethane/Fe₃O₄ decorated MWCNT nanocomposite as a wound healing material**

Highlights

This chapter deals with the preparation of an antibacterial wound healing NC based on HBPU and Fe₃O₄ decorated MWCNT nanohybrid. The nanohybrid was prepared by a non-covalent approach employing *in situ* generation of Fe₃O₄ nanoparticles in the presence of MWCNT. The dressing patch of this HBPU/nanohybrid NC showed excellent *in vivo* wound healing potency in albino mice with enhanced wound closure rate, as evident from circular excision experiment. This chapter also provides a comparative study in terms of drug (gentamicin sulfate) loading efficacy, antibacterial activity, mechanical performance, fluid handling capacity and moisture vapor permeability for HBPU and its NC with nanohybrid, Fe₃O₄ and f-MWCNT. The nanohybrid based NC exhibited the best performance along with hemocompatibility and non-immunogenic attributes. Thus, this chapter verifies the vital role of structural variation and surface properties of such materials at the bio-interface. In addition, nanohybrid based NC showed excellent controlled over drug release for a period of >72 h. Thus, this NC holds strong potential as an antibacterial wound healing material with controlled drug release aptitude.

Parts of this chapter is published in

Das, B., Chattopadhyay, P., Upadhyay, A., Gupta, K., Mandal, M., Karak, N. *New J. Chem.*
DOI: 10.1039/C4NJ00732H, 2014.

5.1 Introduction

Efficient healing of wounds especially, the chronic wound due to burns, diabetes mellitus and ulcer necessitates the use of a suitable wound healing material/dressing with controlled growth factor or drug releasing ability. PU is extensively used as the most preferred wound healing material and potent drug carrier.^{1, 2} Different types of PU wound dressing, both individually and in combination with other systems are used commercially.^{1, 2} The reasons for using PU as a wound healing material include its good barrier properties, especially high oxygen permeability, high moisture vapor transmission rate, excellent blood compatibility and most importantly enhanced rate of epidermal resurfacing as well as collagen production.¹ Moreover, the biocompatibility, biodegradability (into non-toxic by-products) and segmental structure of PU attested its utility as a controlled drug delivery vehicle.^{1, 2} However, PU is susceptible to bacterial infection and inefficient to absorb wound exudates.³ Consequently, extensive researches are going on to develop advanced wound healing materials, especially existing materials with improved performance. The vital criteria encompass accelerated wound healing process with optimal moist environment, bacterial resistive surface and controlled release of drug/active biological agents.^{3, 4}

These properties could be achieved by proper modification of the existing materials through incorporation of appropriate agents, formation of composite and blending with other materials.^{5, 6} In this venture, polymer NC contributes significantly to design advanced wound healing material by incorporating the suitable nanomaterials.⁶ In fact, Ag nanoparticles have been incorporated in PU matrix, but the related side effects at the bio-interface⁷ (as mentioned in section 1.5.3.1 of Chapter 1) are the major drawbacks. Thus, design of an efficient antibacterial wound healing material with biocompatibility and controlled drug release aptitude is the prime requisite in healthcare research. In this context, *Helianthus annuus* oil modified HBPU based healing material would be an exciting idea as this biocompatible polymer supported the adherence and proliferation of skin cells (as evident from Chapter 2). Moreover, Chapters 3 and 4 also projected HBPU as a suitable matrix that leads to good interaction, uniform dispersion and stability to the nanomaterials. Moreover, the competence of HBPU NC at interface with the biological system can also be ascertained from literature.^{8, 9}

Further, the importance of MWCNT at bio-interface and its similarities to collagen, an important component of wound healing process has already been stated in Chapter 4.¹⁰ However

the surface inertness, toxicity and lack of dispersibility of MWCNT demand for its functionalization by covalent and non-covalent approaches.¹¹⁻¹⁴ Decoration of the surface of MWCNT by Fe₃O₄ nanoparticles is also gaining lots of impetus in biomedical applications like drug delivery, MRI, hyperthermia, TE and so on.¹⁵⁻¹⁷ The nanohybrid exhibited prolific effect on biocompatibility, microbicidal and biofilm inhibition activities as well as drug targeting. Further, MWCNT possesses bactericidal effect as well.¹² However, the potentiality of Fe₃O₄-MWCNT nanohybrid and its HBPU based NC as a wound healing material is yet to be explored. Different strategies are reported to obtain such nanohybrid. These include solvothermal synthesis of Fe₃O₄ on the surface of CNT by *in situ* technique, non-covalent decoration with pre-formed nanoparticles and covalent grafting on nanotubes by amidation or acid treatment.^{17, 18} Interestingly, in this investigation nanohybrid was prepared by using a facile non-covalent approach by employing a greener tool like ultrasonication.

Under the above background, NC of HBPU/nanohybrid was investigated as a novel healing material with drug releasing ability. The bio-physical interfacial attributes like mechanical performance, fluid retention, vapor permeability, drug loading efficiency (using gentamicin sulphate as a model drug) and *in vivo* wound healing potential of nanohybrid based NC were probed into. Simultaneously, MWCNT based NC (MNC) and Fe₃O₄ based NC (FNC) were also studied for comparison purpose. Thus the roles of nanostructure, interfacial interactions of nanomaterial with matrix and their surface properties on the performance of NC were investigated.

5.2 Experimental

5.2.1 Materials

Chemicals such as TDI, PCL BD, PE and *Helianthus annuus* oil for the synthesis of HBPU and solvents like xylene, methanol, DMSO and DMAc were of same specification as elaborated in section 2A.2.1 of Chapter 2.

FeCl₂.4H₂O, FeCl₃ and ammonia solution used for the preparation of Fe₃O₄ nanoparticles were of same specification as described in section 3.2.1 of Chapter 3.

MWCNT, KMnO₄, CTAB, acetic acid, hydrochloric acid and DCM used for the covalent functionalization of MWCNT were of same specification as given in section 4.2.1 of Chapter 4.

Gentamicin sulfate was purchased from Sigma-Aldrich, Germany. It is water soluble (50 $\mu\text{g}/\text{mL}$ of water) and stored at 2-8 $^{\circ}\text{C}$.

The other items used in biological tests like DMEM, multi-well culture plates, K3 EDTA and vacuum blood collection tubes were same as mentioned in section 2B.2.1 of Chapter 2.

Animal

The male Wistar rats (200-250 g, 7-8 weeks old) and albino mice (20-30 g, 4 weeks old) were procured from the same breeder and housed properly as mentioned in section 2B.2.1 of Chapter 2. All animal experimental protocols were performed following the same protocol as mentioned in section 2B.2.1 of Chapter 2.

5.2.2 Instrumentation

Physico-chemical structural analyses were recorded using the XRD, FTIR and UV-visible spectroscopic techniques as described in section 2A.2.2 of Chapter 2. The morphological studies of NC, porous NC and degraded products were carried out by the same SEM and HRTEM instruments as described in section 2A.2.2 of Chapter 2 and section 3.2.2 of Chapter 3, respectively. Dispersion of nanomaterials was done with the help of the same ultrasonicator under similar operating conditions as mentioned in section 3.2.2 of Chapter 3. Mechanical properties of the materials were measured using UTM as per the ASTM D412-51T, scratch hardness tester and falling weight impact tester by following the same procedure as mentioned in section 2A.2.2 of Chapter 2.

5.2.3 Methods

5.2.3.1 Preparation of Fe_3O_4 -MWCNT nanohybrid

Fe_3O_4 nanoparticles decorated MWCNT were prepared by a single pot reaction as described elsewhere¹⁸ with a little modification. Instead of chemically oxidized MWCNT, the decoration of as received pristine MWCNT was done (**Scheme 5.1**). At first, $\text{FeCl}_2 \cdot 4\text{H}_2\text{O}$ (0.596 g) and anhydrous FeCl_3 salts (0.974 g) in 1:2 mol ratio were taken in water and stirred at room temperature (ca. 25 $^{\circ}\text{C}$). The required amount of MWCNT (0.067 g) was dispersed in water under mechanical stirring for 1 h followed by ultrasonication for 20 min. The partially dispersed MWCNT were immediately added to the above aqueous solution and stirring was continued for

about 1 h at room temperature (ca. 25 °C). Finally, aqueous ammonia solution was added dropwise to the mixture until the color of the mixture turned black (pH 11-13). This resulted in the *in situ* generation of Fe₃O₄ nanoparticles on the surface of MWCNT. The entire reaction was carried out under an inert atmosphere.

In addition, Fe₃O₄ nanoparticles were prepared by co-precipitation method as mentioned in section 3.2.3.1 of Chapter 3 for the fabrication of FNC. The functionalization of MWCNT was done by exactly the same protocol as elaborated in section 4.2.3.1 of Chapter 4.

5.2.3.2 Preparation of nanocomposites

The preparation protocols for HBPU was exactly same as elaborated in section 2A.2.3.2 of Chapter 2 using the A₂+B₂+B₄ approach. Moreover, NC were prepared by *in situ* technique as elaborated in section 3.2.3.2 of Chapter 3. The –OH terminated pre-polymer of HBPU was prepared similarly as mentioned in Chapter 2. Pre-polymer was then reacted with requisite amount of PE and TDI, so that overall NCO/OH ratio was equal to 1. The reaction mixture was heated to (77±3) °C for 2 h. Then, Fe₃O₄-MWCNT nanohybrid was dispersed in DMAc and added into it at different wt.% (5, 10 and 15) in the second step, separately to obtain nanohybrid based NC (designated as NNC). NNC obtained with 5, 10 and 15 wt.% of nanohybrid were coded as NNC1, NNC2 and NNC3 respectively. Then, the reaction was continued at the same temperature to complete the reaction. For comparative study, FNC and MNC were also prepared, by following the same protocol as described in the sections 3.2.3.2. and 4.2.3.2 of Chapters 3 and 4, using Fe₃O₄ and f-MWCNT, respectively. HBPU and all NC were cast on the different substrates for further testing and analyses.

5.2.3.3 Preparation of porous samples

The porous NC and HBPU were obtained by a gas foaming porogen method as mentioned in section 2B.2.3.2 of Chapter 2.

5.2.3.4 Fluid handling capacity

The fluid handling capacity of HBPU, NC and the control dressing (ActivHeal[®], from Advance Medical Solution) in direct contact with the fluid for both porous and non-porous samples were evaluated by the 'Surgical Material Test Laboratory, test method TM-65 with little

modification.¹⁹ An appropriate volume of a solution of sodium chloride and calcium chloride with 2.5 mmol/L calcium ions and 142 mmol/L sodium ions (equivalent to chemical composition of serum and wound fluid) was prepared. The prepared fluid was added to a container and the sample (0.276 mm thickness, three replicates) was fitted on the mouth of the container in such a way so that the sample remained in contact with the fluid. The mouth of the container was sealed tightly so that moisture vapor could come out only through the sample membrane. Then, the weighed container was incubated at temperature (37±2) °C under relative humidity of <20%. The container and the sample were weighed at regular intervals of 24, 48 and 72 h and the average value obtain at each test was calculated.

5.2.3.5 Moisture vapor permeability

The moisture vapor permeability test of the samples was evaluated by the same procedure as described above in section 5.2.3.4 of this chapter. However, a sufficient gap between the fluid and the sample was maintained. The weight loss of the fluid was calculated at regular intervals of 24, 48 and 72 h. The average value of three tests was taken in each case.

5.2.3.6 Loading of gentamicin sulfate and *in vitro* drug release profile study

The porous samples of NC and HBPU (each with three replicates) were incubated in gentamicin sulfate solution (0.01 mg/mL) at room temperature (ca. 25 °C) for 12 h. Then, the samples were rinsed with water to wash out the drug molecules that were loosely adhered on the surface of the samples.²⁰ To determine the drug loading efficiency of the samples, the remaining concentration of the drug in the incubation media was measured photometrically (at 340 nm) by comparing with the standard curve of gentamicin sulfate at interval of 1, 3, 10 and 12 h. The drug loading efficiency percentage was calculated using the equation 5.1.

$$\text{Drug loading efficiency (\%)} = (T_o - T_n) / T_o \times 100 \dots\dots\dots (5.1)$$

where, T_o = total amount of drug and T_n = amount of free drug in medium.

The release pattern of drug from each sample was studied as described elsewhere with little modification.²¹ The drug loaded samples were immersed in 20 mL of PBS (pH-7.4) in glass containers. The containers were placed in an incubator at 37 °C and the release profile of the drug was monitored up to 72 h. An amount of 2 mL of medium was taken from the container at interval of 3, 6, 12, 24, 36, 48 and 72 h and then the same quantity of fresh buffer solution was

added into the each container to maintain the total volume same. The collected medium was analyzed by UV-visible spectroscopy to record the absorption intensity of the drug molecule and concentration of the released drug in PBS buffer was measured photometrically by comparing with the standard curve of gentamicin sulfate.

5.2.3.7 Antibacterial activity assay

HBPU, NNC, FNC and MNC with and without loaded drug as well as the drug eluted from NNC at different time intervals (12, 24, 48 and 72 h) were individually tested against Gram negative and Gram positive bacteria, namely *Klebsiella pneumonia* and *Staphylococcus aureus*. The test was done in triplicates. The antibacterial test was carried out as described in section 3.2.3.7 of Chapter 3 by agar well diffusion method. However, in this study gentamicin sulphate (10 µg/mL) was used as the positive control.

5.2.3.8 *In vitro* cytocompatibility study

The single cells were isolated by collagenase reperfusion method from the heart of Wistar rat as mentioned in section 2B.2.3.4 of Chapter 2. The cell viability percentages of the heart cells in direct contact with the sample and sample extract were evaluated using MTT assay using the same protocol as described in section 2B.2.3.4 of Chapter 2. Porous NC samples (1 mm×1 mm ~0.206 mm), MWCNT and Fe₃O₄-MWCNT nanohybrid were placed into the wells of culture plate and the cell viability was evaluated in triplicates.

5.2.3.9 *In vitro* hemolytic activity assay

The *in vitro* hemolytic activity of NC and degraded by-products (after 7, 30, 45 and 60 days of incubation) was evaluated by the same procedure using three replicates as elaborated in section 2B.2.3.5 of Chapter 2 by the following equation as given below.

$$\text{Hemolytic \%} = \left[\frac{(\text{Sample OD} - \text{Blank OD})}{\text{Positive control OD}} \right] \times 100 \text{ -----(5.2)}$$

5.2.3.10 Hematological parameters of rats post-implantation

The subcutaneous implantation of NNC in three replicates (dimension, 1 mm×1 mm×~ 0.3 mm) on Wistar rats was performed as mentioned in section 2B.2.3.6 of Chapter 2. The hematological parameters at regular intervals for a period of 1 month was measured in the blood of the treated

rats using the same procedure as mentioned in section 4.2.3.8 of Chapter 4. Again, the cytokine expression viz IL-6 and TNF- α level in the serum of treated and control groups was evaluated using ELISA kit as per the manufacturer instructions' as elaborated in 2B.2.3.7 of Chapter 2.

5.2.3.11 Circular excision experimental model and wound contraction rate analysis

Circular excision experiment was done by following the same protocol as described in literature to evaluate the wound healing potentiality of NNC.²² In brief, skin wounds were carefully created on the dorsal surface of the mice up to a depth (1.5 cm \times 1.5 cm \times ~2.0 mm) of loose subcutaneous, after disinfection. The mice were divided into three groups randomly consisting of three animals: untreated (A), standard treated (B) and NNC treated (C). The patches of standard and NNC were placed over the wound and the progressive changes of wounded area until complete epithelialization were photographed (Nikon Coolpix-S3000 camera) at every alternative days of testing. All wound images were analyzed and changes in wound size of mice were evaluated as wound percentage contraction by using equation 5.3.

$$\text{Wound contraction percentage} = [(A_0 - A_n) / A_0] \times 100 \dots \dots \dots (5.3)$$

where, A_n : wound area on n^{th} day, and A_0 : original wound area.

Further, half of the above animals were sacrificed on 10th post-operative day and wound granulation tissue harvested for histopathological examinations by staining with Masson's trichrome as well as hematoxylin and eosin stain. The tissues were examined under light microscope.

5.2.3.12 Statistical analysis

Statistical analysis was done as mentioned in section 2A.2.3.5 of chapter 2.

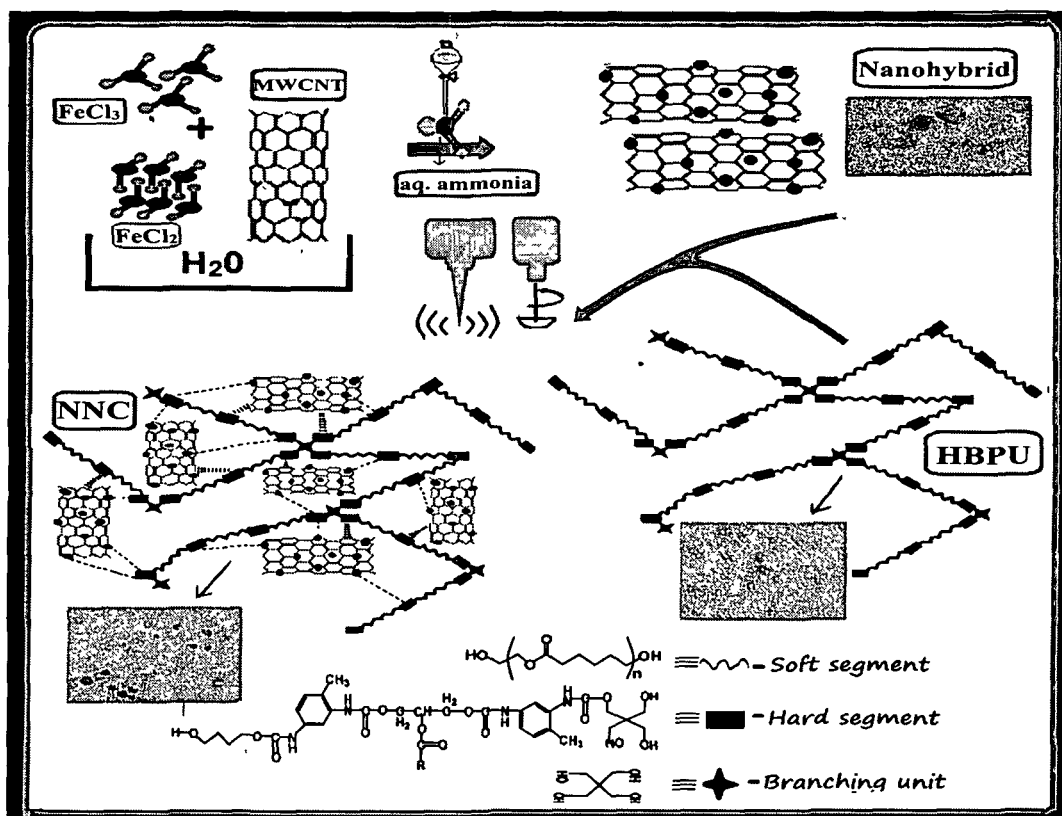
5.3 Results and discussions

5.3.1 Preparation of nanohybrid and nanocomposites

Pristine MWCNT was decorated to obtain Fe₃O₄-MWCNT nanohybrid by a simple single pot process. Fe₃O₄ nanoparticles were formed in the presence of MWCNT and they simultaneously decorated the surface of the tubes as evident from the FESEM and TEM images (as elaborated in section 5.3.4 underneath). The decoration of the tubes by Fe₃O₄ nanoparticles was achieved due to the generation of large surface area by the debundling of MWCNT on the exposure of

sonication and mechanical shear force. The high surface energy and van der Waals interactions aid in the anchorage of Fe_3O_4 on the wall of MWCNT. Moreover, the presence of absorption sites (dangling bond) on MWCNT, further facilitated the nucleation of Fe_3O_4 on MWCNT surface.^{11,23}

Furthermore, NC were prepared by using *in situ* polymerization reaction technique, as it leads to the uniform dispersion of the nanomaterial into HBPU matrix due to the simultaneous polymerization process in presence of nanomaterial. The probable interactions between the Fe_3O_4 -MWCNT nanohybrid and the matrix are shown in **Scheme 5.1**. The possible π - π interaction between the aromatic moieties of TDI with the graphitic delocalized π -electrons of MWCNT and interaction of $-\text{C}=\text{O}$ and $-\text{NH}$ of the urethane linkages with $\text{Fe}-\text{O}$ and $-\text{OH}$ of H_2O adsorbed by Fe_3O_4 resulted in good interfacial interaction between them.



Scheme 5.1: Diagram for the preparation of Fe_3O_4 -MWCNT nanohybrid and NNC

5.3.2 FTIR study

FTIR spectra of Fe_3O_4 , MWCNT, nanohybrid, HBPU and NC are presented in **Figure 5.1a**. MWCNT showed their characteristic bands at around 1630 and 1425 cm^{-1} assigned to the $-\text{C}=\text{C}$ bond and IR phonon mode of MWCNT.^{8, 12} Fe_3O_4 showed its characteristics band at 555 cm^{-1} assigned to the stretching vibration of $\text{Fe}-\text{O}$ bond of Fe_3O_4 and the band around 3430 cm^{-1} represented the stretching vibration of $-\text{OH}$ of H_2O that were absorbed by Fe_3O_4 , as described in section 3.3.2 of Chapter 3. From **Figure 5.1a**, it was observed that the nanohybrid retained the characteristic bands for both Fe_3O_4 and MWCNT, though little blue shiftings in the band positions were observed. The interaction between them resulted in the blue shift of the bands corresponding to $-\text{C}=\text{C}$ backbone (from 1630 to 1610 cm^{-1}) as well as $\text{Fe}-\text{O}$ bond (from 555 to 545 cm^{-1}). Furthermore, FTIR spectrum of NNC confirmed the presence of the characteristic bands corresponding to HBPU and the nanohybrid. Similarly, the FTIR spectra of FNC and MNC as presented in **Figure 5.1a**, confirmed the presence of the respective components in NC. In all the cases, shifting of bands to lower frequencies for $-\text{C}=\text{O}$, $-\text{NH}$ and $-\text{OH}$ in NNC, FNC and MNC compared to the corresponding bands in the spectrum of HBPU were observed as shown in **Figure 5.1**. These shifting are due to the interaction of the functionalities present in the nanomaterial with $-\text{C}=\text{O}$, $-\text{NH}$ and $-\text{OH}$ groups as well as aromatic moieties present in HBPU. The presence of large number of such surface functionalities in HBPU had facilitated good interactions with the respective nanomaterial.

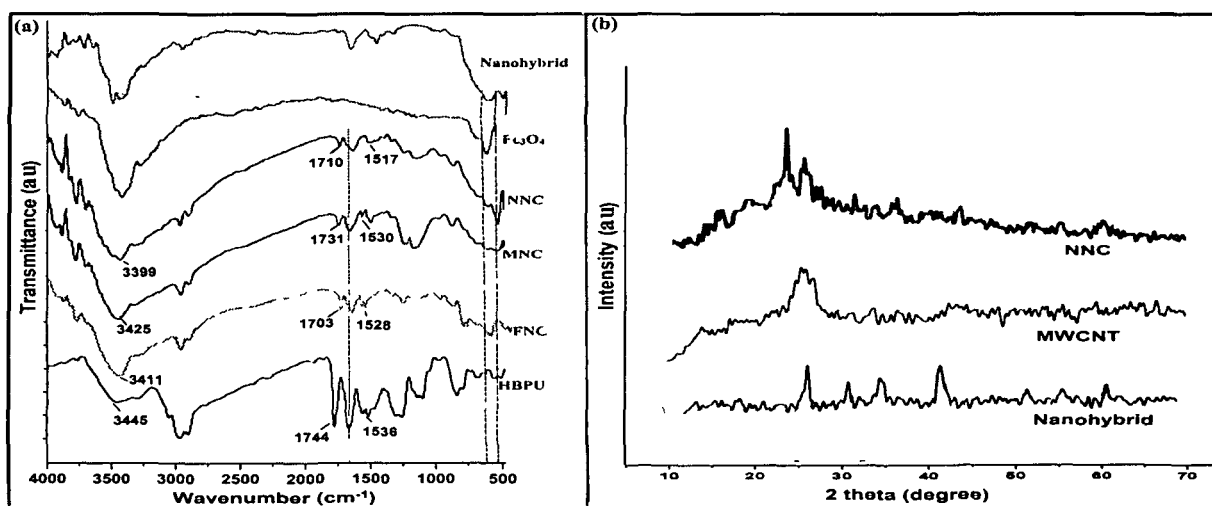


Figure 5.1: FTIR spectra (a) and XRD diffractograms (b) of nanomaterials, NC and HBPU

5.3.3 XRD study

XRD patterns of the samples are presented in **Figure 5.1b**. The characteristic peaks of MWCNT was observed at $2\theta = 26.2^\circ$ and 43.1° which are assigned to the (002) and (100) planes of carbon.^{8, 11} and the characteristic peaks of PCL moiety present in HBPU and NC were observed at $2\theta = 21.4^\circ$ and 23.2° .^{8, 22} Fe_3O_4 nanoparticles showed their characteristic peaks corresponding to the indices (220), (311), (400), (422), (511) and (440) (as shown in **Figure 3.1c** of Chapter 3). The peaks observed for Fe_3O_4 -MWCNT nanohybrid are shown in **Figure 5.1b**, which confirmed the presence of characteristic peaks for both Fe_3O_4 and MWCNT suggesting the formation of the nanohybrid. It was observed in the XRD diffractogram of NNC that the nanomaterials influenced the crystallinity of PCL. The characteristic peaks of Fe_3O_4 were observed in the diffractogram of NNC, however the peaks were not sharp that may be due to the masking effect by the polymer.

5.3.4 SEM and TEM studies

It was also observed by FESEM and TEM images (**Figure 5.2**) that there was well dispersion and distribution of the nanohybrid within the matrix. The presence of large number of surface functional groups with unique structural geometry of HBPU privileged the strong interaction between the matrix and the nanohybrid (**Figure 5.2**). It was observed that nearly uniform sizes of Fe_3O_4 nanoparticles with an average size of 11 nm (range of 8.8-12 nm) decorated the wall of MWCNT and were well distributed along the tubes. **Figure 5.2(c and d)** also represents the FESEM images of FNC and MNC that witnessed homogenous dispersion and well distribution of the nanomaterials on PU matrix.

SEM images of the representative porous NNC3 and drug loaded porous NNC3 are shown in **Figure 5.3(a-d)**, which suggested that drug particles (size in μm) were adsorbed on to the surface of NNC as well within the pores. The gentamicin sulfate mainly remained in agglomerated state with size in the μm range, whereas the particle size of Fe_3O_4 was in nano meter range (~ 11 nm) as supported by HRTEM analysis. Thus, their size difference was the determinable factor in the SEM analysis that ascertained the adsorption of drug on the matrix. Moreover, by comparing the SEM images of NNC with and without drug loaded (**Figure 5.3**), the adsorption of drug by matrix became more prominent. The porous structure, high surface area, large number of surface functionalities and nanohybrid facilitated the efficient adsorption of drug on NNC matrix.

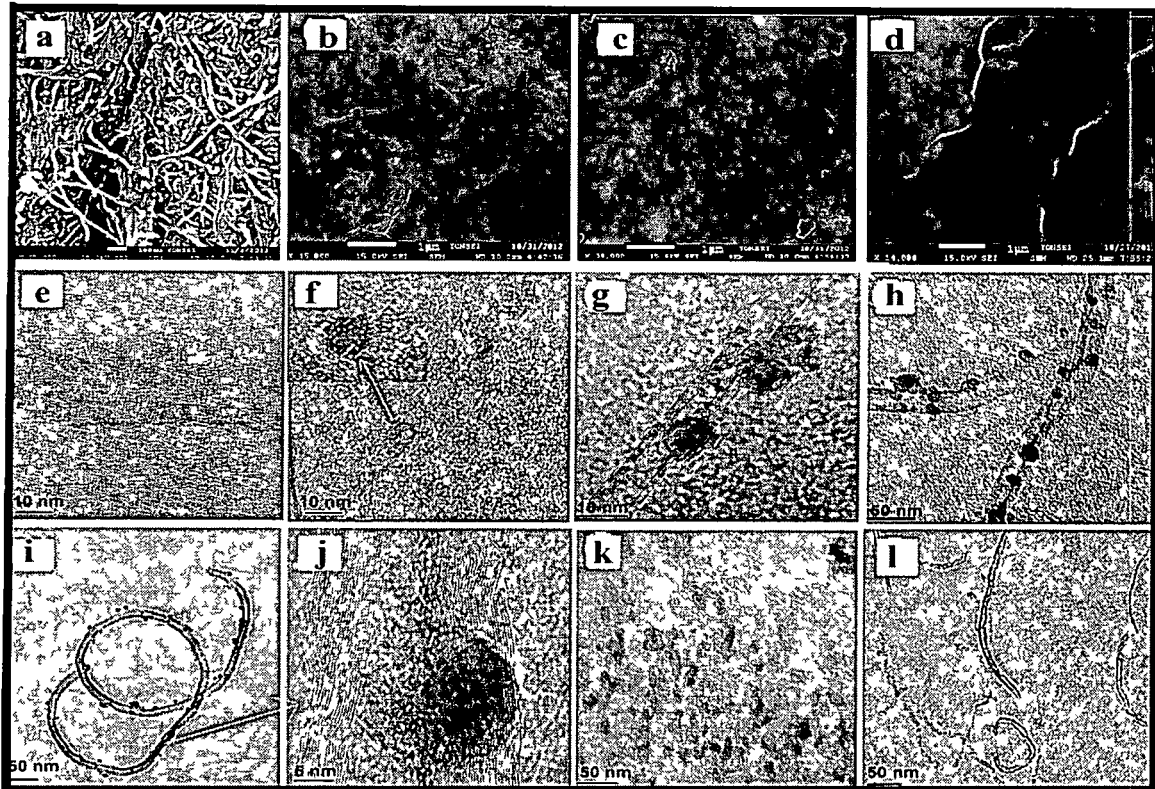


Figure 5.2: FESEM images of Fe₃O₄-MWCNT nanohybrid (a), NNC (b), FNC (c) and MNC (d) as well as TEM images of MWCNT (e), Fe₃O₄-MWCNT nanohybrid (f and g), NNC (h- j at different magnifications), FNC (k) and MNC (l)

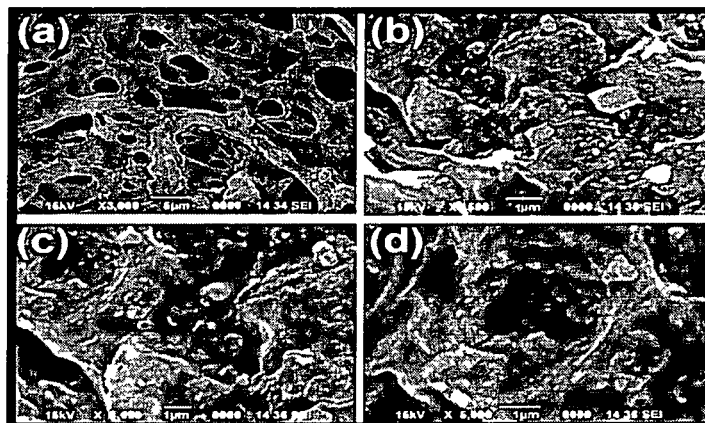


Figure 5.3: Representative SEM images of porous NNC3 (a) and drug loaded porous NNC3 (b), NNC2 (c) and NNC1 (d)

5.3.5 Mechanical properties

The data for mechanical properties for HBPU and NC are given in **Table 5.1**. NC showed better mechanical strength compared to the pristine polymer. Among all NC, NNC showed the highest tensile strength, whereas FNC exhibited the lowest strength. Moreover, it was observed that with the increase in wt.% of nanohybrid, the strength was found to be increased (**Table 5.1**). The enhanced tensile strength of NNC is due to the presence of MWCNT with layered structure and excellent mechanical strength along with highly interactive Fe_3O_4 which facilitated better interaction with the matrix and better transmission of the external tensile load from the matrix to the nanohybrid due to the interfacial shear stress.²⁴ Moreover, with the increase in wt.% of nanohybrid, such interaction and load transmission increased, which further improved the strength. MNC showed better strength compared to FNC as MWCNT has higher aspect ratio compared to Fe_3O_4 along with the layered structure of the former. Consequently, EB decreased for NNC with increased in nanohybrid content due to the restricted molecular movement as inter and intra-molecular interactions increased. However compared to FNC, the elongation was better for NNC due to the presence of MWCNT which can withstand considerable amount of strain before breaking along the direction of tube. MNC showed the highest elongation compared to NNC and FNC. The flexibility was good for NC and the presence of different types of nanomaterial in NC showed insignificant influence on the bending properties. The observed impact resistance and scratch hardness of NC and HBPU are given in **Table 5.1**. The mechanical performance of the studied NC was better compared to the reported similar types of NC.¹⁸ The results suggested that NNC has superior performance over the other two NC as well as other reported nanohybrid based NC system.¹⁸ This is due to the conjointing effect of mechanically strong MWCNT and Fe_3O_4 nanomaterials. However, for the porous samples, the mechanical strength decreased and the decreased in value was mainly related with the porosity (40-45 %).

5.3.6 Fluid handling capacity and moisture vapor permeability

The fluid handling capacity of a material is the sum of the retained weight of test solution and the weight of fluid lost through transmission as a vapor through it.¹⁹ Fluid handling capacity of the control, HBPU, MNC, FNC and the three compositions of NNC against different time intervals are presented in **Figure 5.4a**. It was observed that the ability to absorb moisture by NNC was comparable to that of the control system. FNC and MNC showed lesser fluid retention ability as

Table 5.1: Mechanical properties of HBPU and its NC

Sample code	Tensile strength (MPa)	EB (%)	Scratch hardness (kg)	Impact resistance (cm)	Flexibility (dia., mm)
HBPU	27.15 ± 0.7	590 ± 8.2	4.6 ± 0.3	100	<1
FNC	34.0 ± 0.9	574 ± 4.1	7.0 ± 0.1	100	<1
MNC	44.0 ± 1.0	700 ± 9.8	7.4 ± 0.2	>100	<1
NNC 1	52.0 ± 1.7	650 ± 10.0	7.8 ± 0.3	>100	<1
NNC 2	55.3 ± 0.9	610 ± 8.0	8.0 ± 0.3	>100	<1
NNC 3	59.0 ± 0.8	550 ± 8.5	8.5 ± 0.2	>100	<1

compared to NNC ($p < 0.05$), however FNC and MNC both exhibited better fluid handling capacity than HBPU. Therefore, it can be inferred that NNC due to the presence of nanohybrid, has compositional as well as structural benefits over the other three systems which improved the fluid handling capacity of the material. NC absorbed more amount of fluid compared to HBPU due to the presence of larger number of functional groups, hydrophilic nature of Fe_3O_4 and larger surface area. Moreover, the handling capacity was found to be better for porous system, compared to that of the non-porous one, in each samples. The enhanced fluid retention ability of NNC is beneficial as it can retain the huge amount of exudates that are produced from third degree burn, ulcer, donor site, etc.

Furthermore the moisture vapor permeability results, when the samples were not placed in direct contact with liquid (**Figure 5.4b**) showed that the porous systems have better permeability than the non-porous one, which is quite obvious. However, the rate of moisture vapor evaporation was in appropriate balance between removal of excess of exudates as well as to provide moist environment to the wound site. The permeability was found to be higher for NC with direct contact of the fluid than NC without contact (**Figure 5.4(a and b)**). It implies that they could provide a moist wound healing environment for dry wounds as well. Interestingly, NNC showed the best performance compared to other studied materials. They possess almost comparable fluid handling and moisture permeability ability like the control system. This result

suggested NNC as a suitable wound healing material as they could provide an optimal moist environment, thereby speeding up the normal tissue healing process.

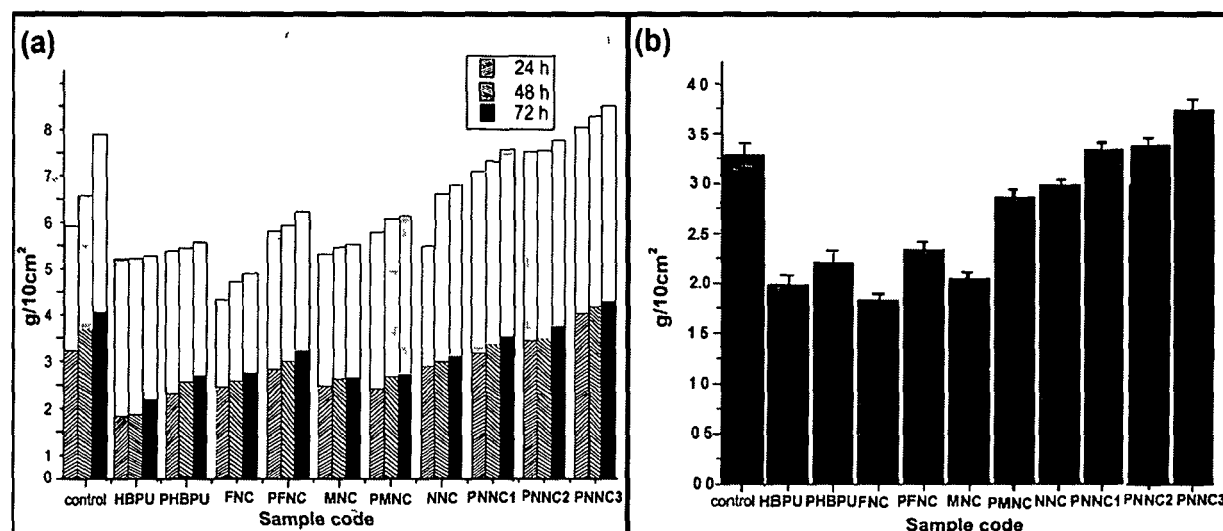


Figure 5.4: Representing the fluid handling capacity (a) (light brown indicated the moisture vapor permeability when materials are in direct contact with the fluid) and moisture vapor permeability (b) of HBPU, porous HBPU (PHBPU), FNC, porous FNC (PFNC) MNC, porous MNC (PMNC), NNC and porous NNC (PNNC1, PNNC2 and PNNC3)

5.3.7 Drug loading efficacy of NC and *in vitro* controlled release profile

The drug loading efficiency of different samples was evaluated. It was observed that pristine polymer has the lowest drug loading efficiency of (53.0±3.6)%. FNC and MNC showed comparable ((56.0±1.3)% and (59.0±1.0)%, respectively) drug loading efficiency, which was better than HBPU ($p < 0.05$). However, NNC exhibited the highest loading efficiency of (79.3±4.1)% ($p < 0.001$). Superior loading efficiency of NNC is due to better interaction of the nanohybrid (present in NNC) with the drug molecule. Along with higher surface area, their structural features aid in the absorption of more drug²⁵ into NNC compared to other NC due to the synergistic effect of both Fe₃O₄ and MWCNT. The results further suggested that the loading efficiency enhanced to (83.5±1.5)% (NNC3) from (79.3±4.1)% (NNC1) with the increase in wt.% of the nanohybrid. Hence, the surface structure and compositions played a significant role in enhancing the drug loading efficiency of NC.

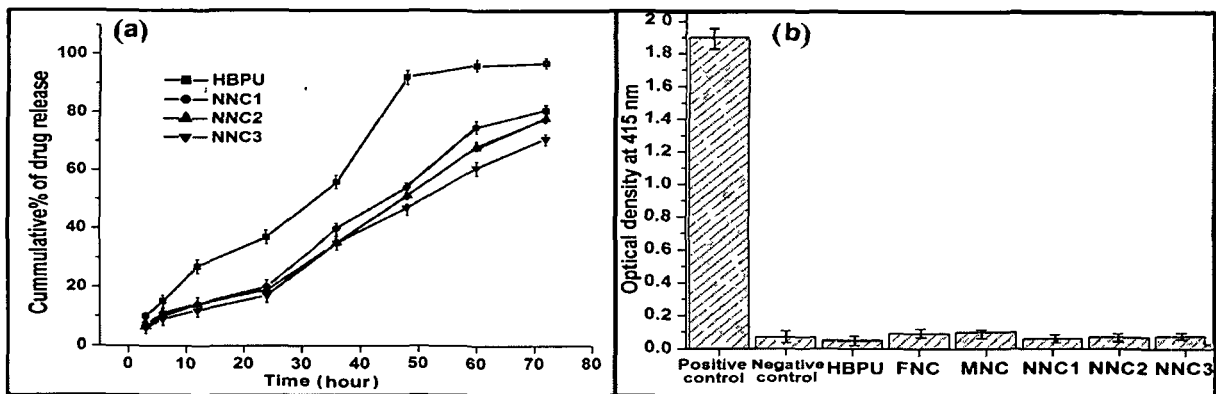


Figure 5.5: Representing the cumulative drug release profile (a) of HBPU and NNC and anti-hemolytic activity % (b) of HBPU, NC and the control system

The *in vitro* controlled release profile was checked only for NNC (**Figure 5.5a**) as they illustrated the best drug loading efficiency compared to the other NC. However, the controlled release profile of HBPU was also studied for comparison purpose. An initial burst effect in drug release was observed for HBPU, whereas NNC showed a minimal burst effect ($p < 0.05$). Over the period of 24 h, the cumulative % of gentamicin sulfate released from HBPU was $(37 \pm 2.6)\%$ and for NNC it was 16-19%, showing that NNC aid to release the drug in a more controlled manner than HBPU. In the initial 36 h, the loosely associated drug was eluted from the surface by dissolution. After 36 h onward NNC provided more controlled and matrix driven release of the drug mainly by diffusion and dissolution.²⁶ There was gradually increase in the concentration of gentamicin sulfate in the elution as measured photometrically and the absorbance band for drug increased with time. Up to 48-60 h, the drug released maximum for HBPU ($96 \pm 2.0\%$) which remained constant up to 72 h. For NNC the maximum drug released was 71-81% at ~72 h (**Figure 5.5a**). The loaded drug did not release out completely within the studied period of 72 h, as the rest amount of drug remained entrapped within the matrix that may gradually elute out in due course of time. However, the varying wt.% of nanohybrid in NNC showed slight variation in the release profile of the drug ($p > 0.05$). *In vitro* study showed that NNC released drug in a much controlled manner compared to HBPU. The prolong action as well as sustained release of the drug/growth factor are two important aspects of healing material to prevent infection and accelerated re-epithelialization at the wound site. This investigation thus emphasized that the formation of NC improved the control release profile of the pristine polymer profoundly. This is

due to the greater and stronger interactions among the drug, nanohybrid and the matrix in NNC, which controlled the overall drug release rate. Thus, this study with the model drug revealed that NNC can also be used as a carrier for drugs like pain killer, antibiotic, growth factors or other supplements that can aid in faster healing process.

5.3.8 *In vitro* cytocompatibility and hemocompatibility

The studied samples showed more than 90% cell viability of heart cells in presence of HBPU, Fe₃O₄-MWCNT and NC. The cell viability of MNC (94±1.0)%, FNC (96±1.6)% and NNC (with varied wt.% of nanohybrid) 98-99% was observed. The extract of NC also showed more than (85±2.9)% of cell viability. Fe₃O₄-MWCNT nanohybrid exhibited (91±2.4)% cell viability, whereas MWCNT showed only (77±3.0)%. This findings suggested that the formation of nanohybrid and hence NC directly influenced the biocompatibility of the studied material. The *in vitro* hemolytic test with erythrocytes also revealed hemocompatibility of NC. **Figure 5.5b** represented the hemolytic activity of all the NC and HBPU. It was observed that NNC showed the lowest hemolytic activity compared to that of pristine HBPU and other NC ($p < 0.05$). Between FNC and MNC, the later showed slightly higher hemolytic activity compared to the former, though both were within the safety range. The result of hemolytic activity assay confirmed that neither NC nor the leached out products had any detrimental effect on the survivability of the erythrocytes. Furthermore, the cytocompatibility assay also proved the non-toxic nature of the studied materials. Herein, the amalgamation of the nanostructured elements and the macromolecular HBPU matrix provided the native physiological environment to the cells to retain their normal functions. Thus, these approved the suitability of the prepared NNC in advanced biomedical platform.

5.3.9 *Antibacterial activity assay*

Bacterial infection and adhesion is one of the most difficult problems in biomedical domain. It can delay the wound healing process and deteriorate the wound condition with excessive pain, bad odor as well as swelling.²⁷ Therefore, bactericidal material is very effectual to prevent the infection at the wound site. *Staphylococcus aureus* and *Klebsiella pneumonia* are the most widespread human pathogens that are related to many infections associated with wounds. In this

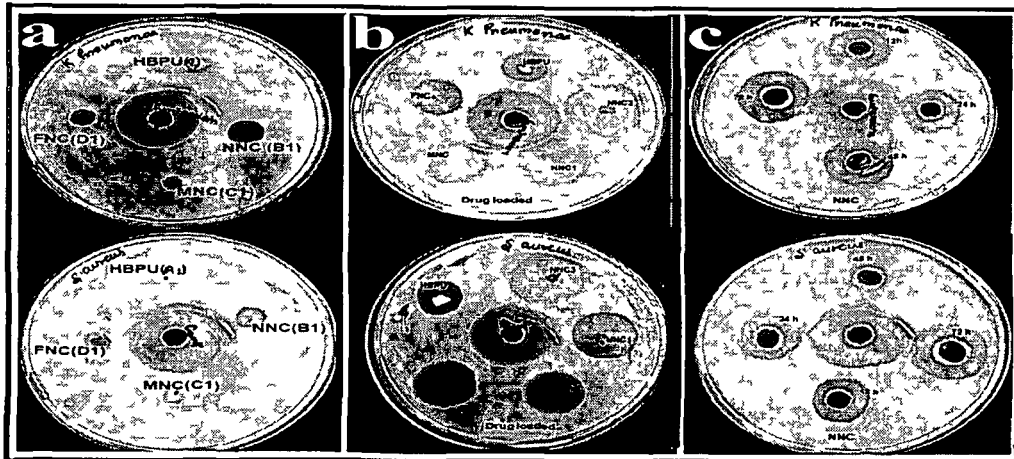


Figure 5.6: Representative antibacterial activities of (a): HBPU (A₁), NNC (B₁), MNC (C₁) and FNC (D₁), (b): drug loaded HBPU, NNC, MNC and FNC as well as (c): drug eluted from NC at different interval of 12, 24, 48 and 72 h against *Klebsiella pneumonia* and *staphylococcus aureus*

context, the antibacterial activity was tested on studied materials in three sets of experiments. The first set consisted of the porous HBPU and studied NC. The second set consisted of drug loaded porous HBPU and drug loaded NC. The antibacterial activity of the samples was evaluated by agar gel diffusion method by measuring the diameter of the zone of inhibition (the clear region in the agar plate where the bacteria cannot grow) against the tested bacterial strains. HBPU did not show any zone of inhibition as indicated by **Figure 5.6a**, therefore HBPU has no antibacterial activity. However, it was observed that NNC, MNC and FNC exhibited good antibacterial activity against the same strain of bacteria with distinct zone of inhibition (**Figure 5.6a**). It has been reported in literature including our own study as mentioned in Chapter 3 that Fe₃O₄ has antibacterial activity and also provided sufficient antibacterial activity to NC.²⁸ Similarly, MWCNT has antibacterial activity by destroying the plasmid DNA of the bacteria.¹¹ The measured zone of inhibition was the highest for NNC (16±0.54 mm) compared to FNC and MNC (14±0.3 and 11±1.0 mm, respectively) against *Klebsiella pneumonia* (p<0.05). This suggested a synergistic antibacterial activity of MWCNT and Fe₃O₄ in NNC. Moreover, NC showed a bacterial resistant surface. In the second set of test, it was observed that compared to the other two NC and HBPU, NNC exhibited higher zone of inhibition (p<0.05) (**Figure 5.6b**). This is in good agreement with the drug loading efficacy result, as NNC showed higher drug loading ability than the other samples. The third set of experiment revealed the antibacterial

activity of the drug released in PBS from NNC at different time intervals (12, 24, 48 and 72 h) which showed that the zone of inhibition increased with the increased period of incubation ($p < 0.001$) and the activity of drug was not hindered on interaction with the polymer. Noticeably, no bacterial growth was observed on the surface of NNC (with or without the adsorbed drug). Thus, NNC stands as a bacterial resistant surface by itself. However, for continuous microbial attack on the surrounding wound area, loading of drug can prevent infection and could accelerate the wound healing process.

5.3.10 Analysis of hematological parameters

The hematological parameters, . at regular intervals for the duration of 30 days were checked in Wistar rats before and after exposure to NNC. The data of hematological parameters are presented in **Table 5.2**. An increase in the count of neutrophils on 1st day of treatment was observed ($p < 0.05$), which was soon replaced by increased monocytes count as revealed on 3rd day. The monocytes matured to macrophages which played a dominant role to phagocytize bacteria and cell debris.³ The leukocytes and platelet count was also increased due to the surgery, implanted foreign material and the subsequent defense and healing mechanism of the host. However with due course of time, gradually normalization in the blood cells count with no significant difference between NNC3 treated and control groups was observed ($p > 0.05$). Moreover, result of post 7 days of implantation suggested that the macrophage count decreased ($p < 0.001$), which eventually facilitated the proliferation phase with no adverse effect of NNC3 on the treated rats. The lack of inflammatory response in the host animal at the implantation site demonstrated the safety aspect of NNC in the host biological environment. The other blood cells parameters like RBC count, distribution width, platelet count and others as presented in **Table 5.2** are within normal range with slight variations ($p > 0.05$).

Furthermore, the cytokine expression in the treated group showed that the level of TNF- α and IL-6 were (11.0 ± 0.3) and (9 ± 0.27) pg/mL, respectively after 30 days of post implantation. This observation was comparable with the results of the control group as mentioned in the previous chapter ($p > 0.001$). This study thus revealed the hemocompatible and non-immunogenic nature of NNC, which is required for such blood contact applications.

Table 5.2: Hematological parameters of Wistar rats upon exposure to NNC

Cell type*	Normal range	Before implantation	Hematological parameter				
			Post-implantation day(s)				
			1	3	7	15	30
WBC	3.0-12 m/mm ³	4.02±0.53	6.23±1.1	5.52±0.5	5.5±1.0	4.93±0.3	4.43±0.2
LYM	65-85%	74.2±2.4	74.0±2.2	78.0±1.1	81.9±0.4	75.2±1.5	75.0±0.9
MON	0.0-5.0%	4.3±0.34	3.8±0.6	10.0±1.2	8.0±1.0	4.4±0.9	4.6±0.5
NEU	9.0- 34.0	17.1±0.5	23.0±1.1	11.1±1.0	10.1±0.9	16.1±2.0	15.9±0.4
EO	0.0-6.0%	4.3±1.4	0.2±0.04	0.7±0.1	0.1±0.02	4.3±0.89	4.5±1.0
RBC	7-10 M/mm ³	8.03±1.1	7.9±0.6	8.0±0.41	8.17±1.1	8.17±1.0	8.19±0.5
MCV	65-70 fl	53.1±2.4	59.2±1.6	61.3±1.5	55.9±0.7	55.4±0.71	56.3±1.0
HcT	30-39 %	31.0±1.3	30.0±0.6	31.3±1.1	31.5±1.0	31.3±1.0	30.9±0.5
MCH	22-24 pg	22.6±0.5	23.6±0.51	23.9±1.1	22.0±0.2	21.7±1.4	23.4±0.5
MCHC	34-37 g/dl	38.6±0.61	38.5±2.0	37.2±0.6	37.3±1.0	38.3±1.23	38.9±1.0
RDW	8-12	10.9±0.4	11.3±1.21	11.6±0.4	12.0±0.3	11.7±1.5	12±1.0
Hb	11-18 g/dl	11.8±0.12	11.4±0.3	11.6±0.3	11.8±0.1	11.1±0.4	11.9±0.3
TCR	500-1300 m/mm ³	691±4.1	700±2.9	703±4.5	660±7.1	690±7.0	690±3.0
MPV	6-10 fl	8.3±1.2	8.0±0.7	7.9±0.57	8.0±0.23	7.9±0.5	8.1±1.0
Pct	0-0.37%	0.50±0.01	0.76±0.01	0.73±0.1	0.66±0.5	0.59±0.01	0.53±0.1
PDW	12-18	13.0±1.0	14.3±0.12	13.9±1.4	13.4±0.8	13.2±1.3	13.1±0.4

*WBC=White blood cell; LYM= lymphocyte; MON= Monocyte; NEU=Neutrophil; EO=Eosinophil; BA= Basophil; RBC= Red blood cells; MCV= Mean corpuscular Volume; HcT= Hematocrit; MCH=Mean Corpuscular Volume; MCHC=Mean Corpuscular Volume Concentration; RDW= Red blood cell distribution width; Hb= Hemoglobin; TCR=T-cell receptor; MPV=Mean Platelet Volume; Pct=Plateletcrit; and PDW= Platelet distribution width.

5.3.11 Histopathological study and wound contraction rate

In vivo wound healing evaluation was performed on albino mice using circular excision model. The wound contraction rate and representative histopathological images are summarized in **Table 5.3** and shown in **Figure 5.7**, respectively. The application of NNC3 and the standard patches to the wound significantly accelerated the healing process as evident by wound contraction rate ($p < 0.001$) (**Table 5.3**). Histopathological examinations also supported the findings of wound contraction as the granulation tissues were found with abundant collagen and maturing hair follicles. Moreover, more matured dermis and epidermis layers were observed in histopathological images (using hematoxylin and eosin stain) of NNC3 and standard treated mice in comparison to non-treated group.²² The slow epithelialization rate with less collagen bundles formation as well as irregular packing of collagen fibres with minor to moderate macrophage infiltration was observed in the non-treated group.²⁹ On other hand, Masson's trichrome staining showed a clear and distinct collagen layer formation with high macrophage and fibroblast density both in NNC and the standard treated groups. Further in such treated groups no ulcer or edematous area was observed. Histopathology examinations on post 10th day precisely delineated the accelerated wound healing property of NNC as well organized re-epithelialization with abundant fibroblast density, more compact collagen layering and faster keratinization with abundant mature hair follicles were present in thick matured dermis (**Figure 5.7**) in comparison to the non-treated one.

The efficient wound healing activity of NNC may be due to the combined effect of favourable bioactive environment for re-epithelialization to take place by hindering antimicrobial growth. Moreover, good fluid handling capacity and moisture vapour permeability of NNC might have provided an optimal moist environment around the wound site for accelerated healing process. Moreover, the cytocompatible NNC provided the adequate mechanical support to the cells to grow and strengthen the wound site to avoid the traumatic injury. Fe₃O₄ decorated MWCNT in NNC might have provided a native environment by mimicking the function of some vital healing components that further facilitated the wound healing process. These desired properties of NNC are due their structural and surface properties along with positive bio-interfacial attributes.

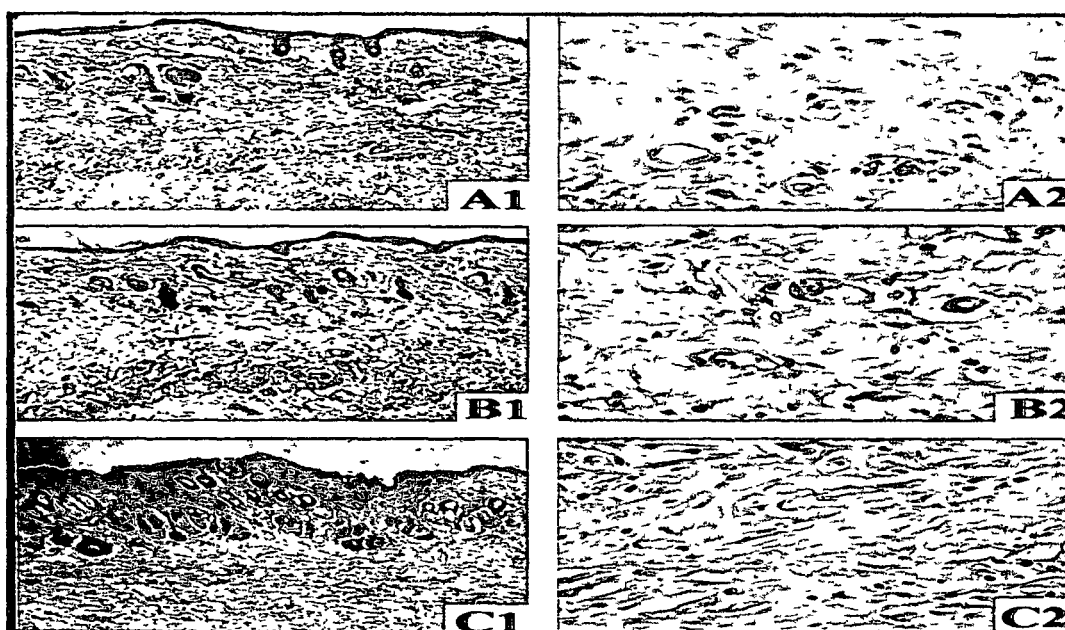


Figure 5.7: Microscopic view of the representative skin sections of non-treated (A), standard treated (B), NNC3 treated (C) animal groups showing the hematoxylin and eosin stained epidermis-dermis in A1, B1 and C1 (magnification 100×) and the dermis stained with the Masson's trichrome in A2, B2 and C2 (magnification 400×)

Table 5.3: Wound contraction rate in albino mice

Post experimental day(s)	Unhealed wound area (mm ²) ± S.D. (% wound contraction)		
	Negative Control	Standard	NNC3
0	31.27 ± 1.18	29.72 ± 1.03	29.89 ± 1.07
2	28.38 ± 1.78	26.63 ± 0.96	25.76 ± 1.29
4	26.27 ± 1.19	20.61 ± 1.07	21.03 ± 1.45
6	22.51 ± 1.47	16.20 ± 1.19	17.19 ± 2.81
8	17.68 ± 1.90	9.67 ± 1.04	10.03 ± 1.75
10	12.05 ± 2.26	3.78 ± 1.99	3.54 ± 1.42
12	8.63 ± 1.74	1.14 ± 1.01	1.63 ± 0.86
14	4.11 ± 2.04	0.00 ± 0.00	0.00 ± 0.00

5.4 Conclusion

The study investigated the preparation of a novel wound healing NC based on Fe₃O₄-MWCNT nanohybrid and bio-based HBPU with controlled drug releasing ability. Among all the studied materials, NNC showed the best physico-mechanical performance along with antibacterial activity. The fluid handling capacity and moisture vapor permeability of NNC suggested its immense potential to provide an optimal moist environment for accelerating the wound healing process. The histopathological study at the wound site confirmed that NNC accelerated the wound healing process with enhanced wound closure rate and the results were comparable with the standard system. Again, the *in vivo* hematological and cytokine studies, *in vitro* hemolytic activity and cytocompatibility assay vouched for the biocompatibility of NNC with no inflammatory response on the tested animals. Furthermore, NNC has the best gentamicin sulfate loading efficiency with controlled release of the drug from the matrix for a prolonged period. The above results indicated that NNC had structural and compositional benefits over the other two NC. Hence, it is relevant to state that a minute structural variation may result in significant difference in properties that may be vital at the bio-interface. Thus, our findings recommend NNC as a potential wound healing material with drug delivery ability to the wound site.

Reference

1. Lamba, N.M.K. Woodhouse, K.A. & Cooper, S.L. *Polyurethane in Biomedical Application*, CRC Press, Boca Raton, 1997
2. Reddy, T.T., et al. *Macromol. Symposia* **242** (1), 241--249, 2006.
3. Craven, D.E., et al. *Infect. Control* **6** (9), 361--366, 1985.
4. Rieger, K.A., et al. *J. Mater. Chem. B* **1** (36), 4531--4541, 2013.
5. Lakshman, L.R., et al. *J. Macromol. Sci., Part A: Pure Appl. Chem.* **47** (10), 1012--1018, 2010.
6. Rapulenyane, N., et al. *New J. Chem.* **37** (4), 1216--1223, 2013.
7. Fredriksson, C., et al. *Wounds* **21** (5), 116--123, 2009.
8. Deka, H., et al. *Carbon*, **48** (7), 2013--2022, 2010.
9. Deka, H., et al. *Polym. Degrad. Stab.* **95** (9), 1509--1517, 2010.
10. Tonelli, F.M.P., et al. *Int. J. Nanomedicine* **7**, 4511--4529, 2012.
11. Pramanik, S., et al. *Carbon* **55**, 34--43, 2013.

12. Zhang, Y., et al. *Macromolecules* **41** (24), 9581--9594, 2008.
13. Jin, G.P., et al. *New J. Chem.* **33** (1), 107--111, 2009.
14. He, H., et al. *Chem. Commun.* **13**, 1655--1657, 2009.
15. Masotti, A., & Caporali, A. *Int. J. Mol. Sci.* **14** (12), 24619--24642, 2013.
16. Lu, Y.J., et al. *Colloids Surf. B Biointerfaces* **89**, 1--9, 2012.
17. Lamanna, G., et al. *Nanoscale* **5** (10), 4412--4421, 2013.
18. Kalita, H., & Karak, N. *J. Nanoeng. Nanomanuf.* **3** (3), 194--201, 2013.
19. Boateng, J.S., et al. *J. Pharma. Sci.* **97** (8), 2892--2923, 2008.
20. Yan, W., et al. *Thin Solid Films* **517** (5), 1794--1798, 2009.
21. Rossi, S., et al. *J. Antimicrob. Chemother.* **54** (5), 1013--1018, 2004.
22. Upadhyay, A., et al. *J. Ethnopharma.* **146** (2), 490--494, 2013.
23. Feng, X., et al. *J. Am. Chem. Soc.* **127** (30), 10533--10538, 2005.
24. Qian, D., et al. *Appl. Phys. Lett.* **76** (20), 2868--2869, 2000.
25. Crisante, F., et al. *Eur. J. pharma. Sci.* **36** (4), 555--564, 2009.
26. Schierholz, J.M., et al. *Biomaterials*, **18** (12), 839--844, 1997.
27. Sandri, G., et al. *Eur. J. Pharm. Biopharm.* **84** (1), 84--90, 2013.
28. Tran, N., et al. *Int. J. Nanomed.* **5**, 277--283, 2010.
29. Aramwit, P., & Sangcakul, A. *Biosci. Biotechnol. Biochem.* **71** (10), 2473--2477, 2007.

Chapter 6

***Helianthus annuus* oil derived hyperbranched polyurethane/ rapeseed protein functionalized MWCNT NC as a rapid bone healing material**

Highlights

This chapter probes into the fabrication of a bioactive scaffold by exploring the splendor of rapeseed protein functionalized MWCNT and bio-based HBPU NC. MWCNT with anchored protein molecules showed incredible bioactivity/biocompatibility compared to bare MWCNT as ascertained via *in vitro* and *in vivo* studies. This NC showed enhanced osteoblast differentiation ability compared to control, HBPU and carboxyl functionalized MWCNT based NC including better cellular adhesion, spreading and proliferation. NC scaffold illustrated rapid bone neoformation on a critical sized tibial fracture gap with 90-93% filling up of the defect area within 60 days. Moreover, histopathological studies demonstrated the exact healing scenario with normal tibial architecture and marked the bioresorption of the implanted NC. This chapter also depicts the excellent biocompatibility, non-immunogenicity, osteoconductivity and cell differentiation ability of NC upon incorporation of bio-functionalized MWCNT compared to carboxyl functionalized one. The excellent bio-physiological features of this studied NC with high load bearing ability, ductility and biodegradability (into non-toxic by-products) promote it as one of the alternatives for clinical challenges as bone endoprosthesis.

Parts of this chapter is submitted for publication

Das, B., Chattopadhyay, P., Maji, S., Upadhyay, A., Dasprukasta, M., Mohanta, C.L., Maity, T.K. & Karak, N. Bio-functionalized MWCNT/hyperbranched polyurethane bionanocomposite for bone regeneration, (revision submitted)

6.1 Introduction

Bone fracture is one of the most common health related issues. It is a consequence of trauma, high mechanical stress and medical conditions such as osteoporosis, primary bone cancer, metastatic bone disease or Lobstein syndrome.^{1,2} Moreover, with mounting cases of cancer, the risk of osteolytic bone destruction due to metastatic bone disease is also alarming. Metastatic cancer cells in bony region can activate the osteoclasts, and thus patients develop a risk for pathological fracture.^{3,4} The irreparable damages require appropriate endoprosthetic replacement to restore its function. Such prostheses must be bioactive to promote and support the infiltration of bone cells/biomolecules as well as accelerate their adhesion and proliferation. For bone healing process, the formation of collagen network (hyaline cartilage or woven bone or lamellar bone) is an important process.⁵ The chondrocytes secrete collagen and proteoglycan (protein and polysaccharide) and thereby facilitating bone healing process by formation of a cartilaginous matrix. In this vein, design of advanced scaffold materials by exploration of material science, nanotechnology and protein chemistry is an exciting idea to emulate these functional healing components at bio-physiological environment.

Moreover, the significance of MWCNT and PU in bone TE is reported time and again in literatures.^{6,7} Moreover, Chapter 4 also elaborated the efficiency of MWCNT in bone TE. The structural features of MWCNT bear a resemblance to triple helical structure of the collagen fibril.⁶ Moreover high degree of porosity and high contact area of MWCNT mimic the vital characteristics of ECM.⁸ However, the surface modulation of MWCNT prior to *in vivo* utilization is a basic requirement. Functionalization of MWCNT with biomacromolecules like protein at bio-interface could effectively address the limitations of MWCNT (as discussed in previous chapters).⁹ Anchorage of protein on the surface of MWCNT is illustrated to provide biocompatibility and dispersability to the latter.⁹ The presence of hydrophobic and aromatic amino acids in proteins facilitates the non-covalent interaction with MWCNT. Notably, the exquisiteness of rapeseed proteins is not yet exploited in this field, to the best of our knowledge. It is reported that the protein isolated from rapeseed positively influences the growth and proliferation of the cells in serum free media.¹⁰ Moreover, it has good amino acid profile and low cost compared to many other peptide sequences like Arg-Gly-Asp, Gly-Arg-Gly-Asp-Ser-Pro, etc. that are routinely used in TE.¹¹ These protein hydrosylates encompass the capability to replace the protein substitute used in cell culture medium derived from animal and human

sources.¹⁰ Therefore, crude rapeseed protein (r-protein) after elimination of the non-proteinous substances like phenol, phytols, fibres, etc. could be an efficient substitute to promote cells proliferation. In this investigation, r-protein was extracted from low cost rapeseed oil press cake (industrial waste) after proper detoxification.¹² As a consequence, the exploration of r-protein for non-covalent modification of pristine MWCNT is a greener advantage, besides purging the need of acid/chemically treated MWCNT (using organic solvent). Moreover, the biological attributes of r-protein could also be scrutinized.

However, the confinement of MWCNT at a localized fracture area is necessary for its practical feasibility, minimized toxicity and improved performance.¹³ Therefore, the incorporation of MWCNT into a suitable biocompatible polymeric matrix is more effective compared to metallic or ceramic based matrices^{14, 15} (as already explained in Chapter 1). Moreover, the previous chapters approved the efficacy of oil based HBPU in biological domains including bone TE. Thus, HBPU with high surface end groups, rough surface beneficial for cellular interactions and tailorable bio-physiological attributes was chosen as the matrix for the preparation of desired NC. Moreover, vegetable oil based PU is reported to have good bone healing potency.⁷ Therefore, the incorporation of properly modified MWCNT into *Helianthus annuus* oil based HBPU may result in enhancement of such properties.

Spurred by the above mentioned prospective, this present chapter demonstrates the (a) functionalization of MWCNT with the industrial waste (oil cakes) derived r-protein, (b) evaluation of toxicity parameters of pristine MWCNT, r-protein and r-protein functionalized MWCNT (mMWCNT) in rats after administration through interperitoneal route, to ascertain the benefits of such bio-functionalization, (c) determination of *in vitro* osteoblast growth and differentiation studies to illustrate the benefits of mMWCNT based *Helianthus annuus* oil derived HBPU NC as advanced material over the chemically functionalized MWCNT/HBPU NC (MNC) and (d) exploration of the *in vivo* bone healing aptitude of the well-designed r-protein functionalized MWCNT based NC in critical sized tibial shaft defect in Wistar rat. The attributes ranging from biodegradation, immunocompatibility, biocompatibility, bone neoformation and toxicity of the neat and degraded NC at a regular basis were investigated to explore the aptness of this material as an endoprosthesis replacement.

6.2 Experimental

6.2.1 Materials

Chemicals such as TDI, PCL BD, PE, *Helianthus annuus* oil and solvents like xylene, methanol and DMAc (for the synthesis of HBPU and NC) were of same specification as described in section 2A.2.1 of Chapter 2. MWCNT was purchased from the same vendor and with similar specification as mentioned in section 4.2.1 of Chapter 4. The materials for biological tests like DMEM, FCS, alamar blue, multi-well tissue culture plates, K3 EDTA tubes and vacuum blood collection tubes were of same specification as mentioned in sections 2B.2.1 and 4.2.1 of Chapter 2 and Chapter 4. The additional reagents utilized were of reagent grade and utilized directly without further purification.

The r-protein was extracted from the pressed oil cake and the toxic components were removed using the standard protocol as reported in literature.^{12, 16} The r-protein was obtained from Department of FPT, Tezpur University, India. This was used for the non-covalent functionalization of MWCNT.

KMnO₄, CTAB, acetic acid, hydrochloric acid and DCM used for the oxidative functionalization of MWCNT were of same specification as given in section 4.2.1 of Chapter 4.

Animals

Male Wistar rats (weighing 200 to 250 g) were procured from the same breeder and housed properly as mentioned in section 2B.2.1 of Chapter 2. All animal experimental protocols were performed as described in section 2B.2.1 of Chapter 2.

6.2.2 Instrumentation

Physico-chemical structural analyses were recorded by using XRD, FTIR and UV-visible spectroscopic techniques as described in section 2A.2.2 of Chapter 2. The morphological studies of desired samples were carried out by the same SEM and HRTEM instruments as described in sections 2A.2.2 and 3.2.2 of Chapter 2 and 3, respectively. The ultrasonicator was of same specification and experiment was performed at the same operating conditions as described in section 3.2.2 of Chapter 3. The mechanical performance of the materials were done using UTM as per the ASTM D412-51T, scratch hardness tester, falling weight impact tester and bending test as described in section 2A.2.2 of Chapter 2.

6.2.3 Methods

6.2.3.1 Functionalization of MWCNT by rapeseed protein

A very simple protocol was applied to non-covalently functionalized MWCNT by r-protein using a green tool of ultrasonication, under ambient condition. A required amount of MWCNT was partially dispersed in millipore water with the help of sonication working at 24 kHz and acoustic power density of 460 W/cm^2 as well as by mechanical shear mixing. Thereafter, a required amount of protein (1:1 with respect to MWCNT) was dissolved in water and added to MWCNT under continuous stirring (using ice bath). The solution was subjected to ultrasonication for 30 min. Again, the mixture was subjected to mechanical mixing, until homogenous dispersion of r-protein functionalized MWCNT (mMWCNT) was attained.

6.2.3.2 Oxidative modification of MWCNT by carboxyl groups

MWCNT was covalently functionalized by oxidative method using KMnO_4 by using exactly the same protocol as elaborated in section 4.2.3.1 of Chapter 4.

6.2.3.3 Preparation of nanocomposites

NC was prepared by an *ex situ* technique. HBPU was prepared using an $\text{A}_2+\text{B}_2+\text{B}_4$ approach as elaborated in section 2A.2.3.2 of Chapter 2. The pre-polymer was prepared and the second step to synthesize the polymer was done by the same protocol as mentioned in section 2A.2.3.2 (under the same reaction condition). After the completion of reaction, the reaction mixture was cooled down to room temperature. The mMWCNT (dispersed in minimal amount of solvent) was then added to it under continuous mechanical stirring at room temperature (ca 25°C). The mixture was subjected to mechanical stirring for 2-3 h followed by ultrasonication under the same operating condition (section 6.2.3.1) to obtain NC and coded as PNC. PNC with 0.2, 1.0 and 2.0 wt.% of mMWCNT were assigned as PNC0.1, PNC1.0 and PNC2.0, respectively. Carboxyl functionalized MWCNT based NC (MNC) was also prepared exactly by same procedure as described in section 4.2.3.2 of Chapter 4.

Porous HBPU, PNC and MNC were fabricated using the same porogen gas foaming method as described in section 2B.2.3.2 of Chapter 2, using ammonium bicarbonate and used for *in vitro* tests. Further, sufficient amount of PNC solution was preserved in a sterilized beaker for *in vivo* study.

6.2.3.4 *In vitro* and *in vivo* biodegradation studies

In vitro degradation of the prepared samples was evaluated by a reported method according to the ASTM standard F 1635-04 method as mentioned in section 2B.2.3.3 of Chapter 2. The degradation media was 0.1 M PBS with pH (7.4±0.2) and the study was carried out for three months. The degraded samples and degraded by-product were further analyzed for their toxic effect by direct contact or non-contact cytotoxicity methods¹⁷ as described in section 2B.2.3.4 of Chapter 2. For monitoring the *in vivo* degradation of the scaffold, weighed PNC was implanted into the defect site and fate of the sample was observed at the end of experiment.

6.2.3.5 *In vitro* cytocompatibility and hemolytic activity assay

In vitro direct contact method was applied to determine the cytocompatibility of the pristine HBPU and NC films using MTT assay. Heart cells were isolated by the collagenous reperfusion method as described in section 2B.2.3.4 of Chapter 2. The cells (1×10^4) were seeded on the samples (MWCNT, mMWCNT, r-protein, PNC, MNC and HBPU) which were placed in the culture plate, separately. It was then incubated for 24, 48 and 72 h. After the incubation, cell viability was evaluated by MTT assay as mentioned in the section 2B.2.3.4 of Chapter 2. Similarly, the cytotoxicity of the leached and degraded by-product(s) was determined by elution method¹⁷ using MTT assay. This study was performed in triplicate.

Hemocompatibility of the samples (including the degraded/leached products) with mammalian erythrocytes was checked by hemolytic assay as mentioned in section 2B.2.3.5 of Chapter 2.

6.2.3.6 Osteoblast proliferation assay and cell adhesion

Osteoblast proliferation assay was performed using Alamar blue assay according to the manufacturer instruction, as elaborated in section 4.2.3.7 of Chapter 4. This test was done for HBPU, PNC, MNC and the control system. After the required period of incubation, the polymeric samples were taken out from the culture media and fixed for SEM studies. The adherence and spreading of the osteoblast cells on control, HBPU and NC substrates were then analyzed by SEM images.

6.2.3.7 *In vitro* osteoblast differentiation study

MG63 human osteoblast cell line was used for osteoblast cell differentiation study on the polymeric substrates using ALP assay kit (Span Diagnostics, Surat, India). Briefly, 20 mL (containing 1×10^4 cells) of MG63 cell suspension was applied on different polymeric substrates and the control sheets ($\sim 1 \text{ cm} \times 1 \text{ cm} \times 0.43 \text{ cm}$) and incubated in a humidified CO_2 incubator (37°C and 5% CO_2 flow) for 3 h. The cell attachment on the films was allowed before flooding with differentiating medium comprising DMEM supplement with 10% FBS, sodium beta-glycerol phosphate (10 Mm), L-ascorbic acid (50 $\mu\text{g}/\text{mL}$), and dexamethasone (100 nM). Osteoblast differentiation was determined at 3th, 6th and 9th days of test. The cells were removed from the films and lysed using lysis buffer followed by determination of ALP activity according to the manufacturer's instruction using ALP assay kit.

6.2.3.8 Tibial shaft critical sized defect model

Wister rats were anesthetized by injecting sodium phenobarbital (50 mg per kg body weight). The lateral side of right limb of the rat was shaved and disinfected using antiseptic solution (containing 10% povidone iodine and alcohol). The tibia was exposed by lateral longitudinal incision using a surgical blade. The upper skin layer and the subcutaneous layer were carefully incised so that the underlying peritoneal layer remained intact. Then, the peritoneal was stripped from the bone with intense care and a length of 6 mm was marked on the tibial shaft. The marked bone was resected with the help of a bone cutter under continuous saline irrigation.

6.2.3.9 Implantation procedure of the sticky nanocomposite

PNC solution was poured dropwise on the sterilized DMEM and the sticky PNC formed was placed immediately at the defect site such that the fracture ends get proper support. Then, the incision was closed into two layers. After proper stitching, the region was cleaned and betadine was applied to avoid infection. The rats were then housed one per cage under proper condition and they are monitored throughout the experimental period. In one group of rats, the incision was stitched without filling the gap with implant. According to the nature of defect on tibia and the treatment, animals were divided into three groups (with three animals in each group): the single side fractured, both side fractured and untreated groups and were coded as ST, BT and UT groups, respectively.

6.2.3.10 Radiographic analysis

The rats underwent standardized radiographic study immediately after the implantation as well as after 15, 22, 35, 45, 60 and 90 days to quantify the bone regeneration in all the experimental groups of rats. The radiography was done by using the X-ray machine (SEMEN) available at Assam X-ray, Tezpur, India under the proper guidance of the concerned radiologist.

6.2.3.11 Hematological parameters of rats post-implantation

Blood parameters of the three groups including the normal rats were analyzed at 2nd, 7th, 30th, 60th and 90th days of post-implantation. Blood was collected and then examined by automatic hemato-analyzer as described in section 4.2.3.8 of Chapter 4. The study was done in triplicate.

6.2.3.12 Serum biochemistry and cytokine detection post implantation

Blood was collected in a vacuum blood collection tubes and serum was separated by the same procedure described in section 2B.2.3.7 of Chapter 2. Serum biochemical parameters (kidney, liver and lipid profiles) were examined by using biochemical kits (as per as the manufactures' instruction) in Coralyzer-100 (Tulip Diagnostics Pvt. Ltd, India). Again, the cytokine expression viz IL-6 and TNF- α level was evaluated by ELISA kit as described in section 2B.2.3.7 of Chapter 2.

6.2.3.13 *In vivo* toxicity analysis of protein, MWCNT and protein functionalized MWCNT

Wistar rats were grouped into another three groups having three animals each. Then, solution (~2 mg/mL) of r-protein, MWCNT and mMWCNT in millipore water were prepared and injected into the peritoneal cavity of the rats, separately and were divided into three groups as P, M and MM-groups respectively. The animals were weighted prior to the experiment and their hematological and serum biochemical parameters were evaluated (using the same protocol as described in section 4.2.3.8 of Chapter 4 and section 6.2.3.11 of this chapter, respectively). Similarly, at 1st, 2nd, 7th, 30th, 60th and 90th days of post-administration, these parameters were again checked by collecting blood retro-orbitally. The normal food habit and behavior of the tested rats were monitored, throughout the experimental period.

6.2.3.14 Histopathological study of fractured tibia

The animals were sacrificed by cervical dislocation and tibia was carefully removed from the experimental animals (ST, BT and UT and control groups). The appropriately sized cross-sections of the tibia were washed in normal saline followed by tissue fixation in formaldehyde. The tissues were decalcified using formic acid/formaldehyde treatment.¹⁸ After complete decalcification, the tissues were treated in increasing grade of alcohol for dehydration followed by clearing in xylene. After block preparation, the tissues were sliced using microtome and stained with hematoxylin and eosin stain as well as Masson's trichrome stain. Finally, the respective tissues were observed under light microscope and analyzed.

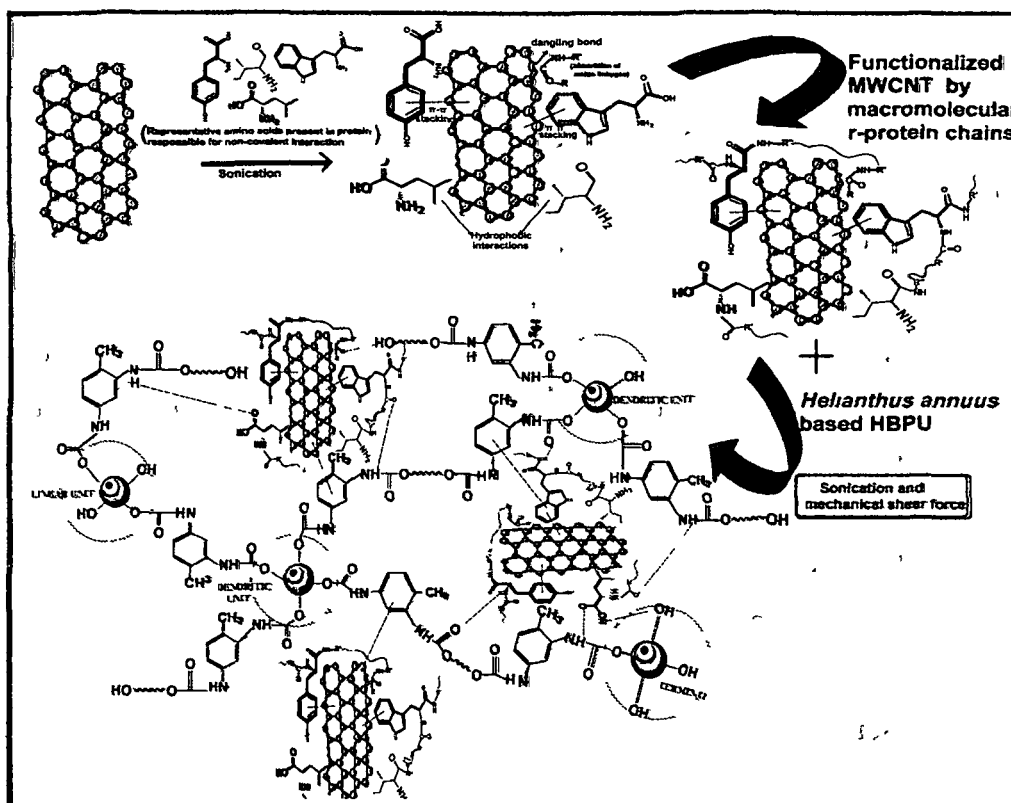
6.2.3.15 Statistical analysis

Statistical analysis was done as mentioned in section 2A.2.3.5 of chapter 2.

6.3 Results and discussions

6.3.1 Functionalization of MWCNT

The non-covalent functionalization of MWCNT was done successfully by using industrial waste derived r-protein and greener approach of ultrasonication. The implosion of cavitation bubbles during ultrasonication generates the hot spot. The temperature and the pressure generated were sufficient enough to facilitate the interactions between the protein and MWCNT. Sonication resulted in the introduction of defects and dangling bond along with debundling of MWCNT and thereby providing active site for anchorage of r-protein on its surface, as supported by literatures.¹⁹ In addition, the mechanical force leads to the homogenous distribution of the reactants. The high surface energy of MWCNT further promoted the adsorption of free r-protein moieties on its surface in order to minimize energy and attain stability. Stable and homogenous aqueous dispersion of mMWCNT was observed after functionalization. The plausible bonding between r-protein and MWCNT includes electrostatic and hydrophobic interactions.²⁰ The hydrophobic amino acids namely phenylalanine and serine contributed to the hydrophobic interaction with the hydrophobic surface of MWCNT. Aromatic amino acids contributed to the electrostatic interaction with the delocalized π -electrons of the graphitic structure of MWCNT. The presence of defect also provided the reactive site for the attachment of the amide linkages of the protein. The pictorial representation of such interactions is shown in **Scheme 6.1**.



Scheme 6.1: Representing the probable interactions between MWCNT and r-protein as well as functionalized MWCNT with HBPU matrix

6.3.2 Preparation of nanocomposites

PNC was prepared by *ex situ* technique by employing shear mixing and ultrasonication. Ambient conditions were maintained to prevent any adverse impact to the structural integrity of r-protein. The mechanical shear force and the sound energy helped in the debundling of MWCNT and disentanglement of polymeric chain. Moreover, the dispersed nanotubes were added into the polymeric reaction mixture just after completion of polymerization process. As a consequence, the polymer chains were in a state of complete dispersion and swelled in minimal amount of solvent. Subsequently, the high surface area of mMWCNT and the reactive group of r-protein can readily interact with the matrix without much hindrance. The interfacial interaction between the matrix and the nanotubes was thus very high and mMWCNT remained homogeneously distributed as depicted by TEM study, as described in section 6.3.5 of this chapter. The probable interaction between these two phases is due to the π - π interaction between

the aromatic rings of TDI (HBPU) and carbon rings of MWCNT as well as aromatic amino acids of r-protein. There are more probability of secondary interactions between the surface functionalities like -C=O , -OH and -NH of HBPU with the protein moieties (amide linkages and side chains like -COO , -NH_2 and benzene rings). **Scheme 6.1** represents the plausible interfacial interactions between the nanotubes and the matrix.

6.3.3 FTIR and UV-visible studies

The mMWCNT, r-protein and PNC were characterized by FTIR and UV-visible spectroscopic studies. r-Protein exhibited bands corresponding to amide I at 1656 cm^{-1} due to the C=O stretching vibration of peptide and amide II band at 1543 cm^{-1} allocated to the -NH bending vibration or C-N stretching vibration (**Figure 6.1a**).²¹ The bands at around 3400 cm^{-1} and 2960 cm^{-1} assigned to the primary amine and aliphatic -C-H vibration. The band at 1447 cm^{-1} was due to the protein -COO side chain.²² In the spectrum of mMWCNT (**Figure 6.1a**), along with the characteristic bands of MWCNT at 1625 and 1425 cm^{-1} (as mentioned in section 4.3.2 of Chapter 4), the appearance of similar bands corresponding to r-protein ascertained the co-existence of the two systems and their probable interactions as evident by the shifting of the band positions. Moreover, the appearance of characteristic bands corresponding to -C=O , -NH bending and O-C=O stretching vibration in PNC spectrum, confirmed the formation of urethane linkages. The blue shifting in the band position in PNC spectra (**Figure 6.1a**) as compared to the spectra of HBPU (**Figure 2B.1** of Chapter 2), indicated the probable interaction between mMWCNT and the matrix. The shifting was mainly noted in the carbonyl (1731 to 1710 cm^{-1}) and -NH bending region (1545 - 1570 cm^{-1}) along with increased intensity and broadening of band assigned to -OH and -NH overlapped band (3300 - 3400 cm^{-1}) which suggested the presence of strong interactions.

The modification of MWCNT was again confirmed through UV-visible spectroscopic study. The dispersed aqueous solution r-protein and mMWCNT solution showed characteristic UV absorbance at $\sim 280\text{ nm}$ due to the presence of r-protein (**Figure 6.1b**).²³ The protein showed this peak owing to the absorbance by aromatic amino acids (tryptophan and tyrosine) and disulphide bond of cystein. However, the absence of such absorbance in MWCNT again suggested the anchorage of r-protein on the nanotubes.

6.3.4 XRD study

XRD patterns of mMWCNT, MWCNT and PNC are represented in **Figure 6.1c**. Functionalized MWCNT retained the characteristic peaks at $2\theta = 26.2^\circ$ and 43.1° of MWCNT with little lowering of peak intensity at $2\theta = 26.2^\circ$. This may be due to the masking effect of the adhered r-protein on their surface. PNC showed the characteristic peaks at 21.4° and 23.2° due to the presence of (110) and (200) lattice planes of PCL crystals. On formation of NC, the peaks intensity increased compared to the pristine HBPU, which is supported by many literatures due to nucleating effect offered by MWCNT.

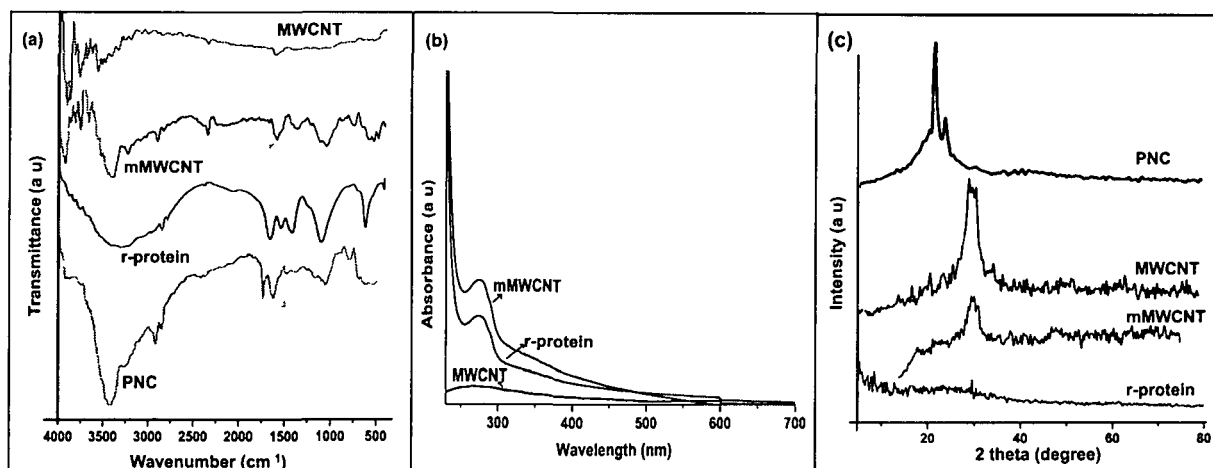


Figure 6.1: Representing the FTIR spectra (a), UV-visible spectra (b) and XRD pattern (c) of r-protein, nanomaterials and PNC

6.3.5 TEM study

HRTEM images of mMWCNT clearly indicated the surface anchorage of r-protein on MWCNT as indicated by increased roughness and thickening of mMWCNT (**Figure 6.2**). In contrast, such observation was absent in pristine MWCNT which exhibited smooth wall. Different thicknesses of r-protein (vary from 4.2 to 5.34 nm) were randomly adhered on the surface of mMWCNT (**Figure 6.2**). The average thickness of the outer wall of mMWCNT was measured to be 20.66 nm, whereas that of MWCNT was 14.23 nm. The inner and outer diameters of the nanotubes were also altered after functionalization compared to the pristine nanotube as shown in the inset of **Figure 6.2(a and b)**. These findings suggested the successful functionalization of MWCNT by r-protein.

In NC, no agglomeration was observed even at high wt.% (2 wt.%) of mMWCNT. The excellent orientation of mMWCNT into the matrix can be witnessed from TEM images as shown in **Figure 6.2(c and d)**. This suggested that mMWCNT has good interfacial interactions with the matrix. However, it is difficult to locate the presence of r-protein on MWCNT surface upon NC formation. This may be due to good compatibility between the protein and PU chains.

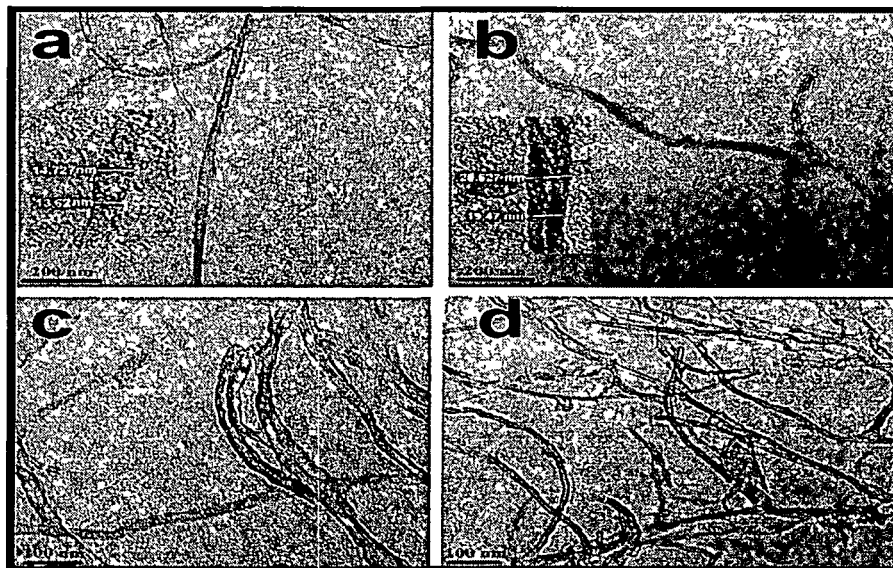


Figure 6.2: Representing the TEM images of pristine MWCNT (a), MWCNT (b), PNC0.1 (c) and PNC2.0 (d)

6.3.6 Mechanical properties

The mechanical properties like tensile strength and EB of PNC, MNC and HBPU are given in **Table 6.1**. PNC with 2 wt.% of mMWCNT content showed (55.5 ± 0.89) MPa tensile strength and the ductility improved up to $(790 \pm 7.8)\%$. In PNC with increased doses of mMWCNT, the EB decreased from (790 ± 7.8) to $(675 \pm 7.3)\%$ while tensile strength increased from (49 ± 1.03) to (55.5 ± 0.89) MPa. Again, MNC (with 2 wt.% $-\text{COOH}$ functionalized MWCNT) exhibited tensile strength of (48 ± 1.2) MPa with $(560 \pm 6.8)\%$ ductility. This superior tensile strength of PNC is due to the increased secondary intra/inter-molecular interactions and better interfacial interactions between the matrix and mMWCNT upon functionalized by r-protein as attested from the above studies. Moreover, the high aspect ratio of mMWCNT remains intact on non-covalent functionalization that allows excellent load transfer between mMWCNT and matrix. Whereas,

the decreasing trend in EB reflected the restricted molecular movements of the polymeric chains at interfacial region (due to good interaction between the two components). The scratch hardness of PNC also improved with the increased wt.% of mMWCNT and the flexibility of PNC was better than MNC. The amalgamation of tough mMWCNT and flexible fatty acid chains of MG, long segmental PCL chain and protein moieties endorsed good physico-mechanical performance of PNC. Thus, improved tensile strength, scratch hardness and impact resistance were achieved in PNC without much compromising with the flexibility of NC. The overall enhanced toughness of PNC can provide the mechanical integrity at the fractured site.

Table 6.1: Mechanical properties of PNC, MNC and HBPU

Polymer code	Tensile strength (MPa)	EB (%)	Flexibility (cm)	Impact resistance (cm)	Scratch hardness (kg)
PNC 0.1	49.0±1.03	790±7.8	<0.5	>100	8.2±0.51
PNC 1.0	52.9±0.91	710±6.0	<0.5	>100	8.5±0.32
PNC 2.0	55.5±0.89	675±7.3	<0.5	>100	9.2±0.41
MNC 2.0	48.0±1.20	553±6.8	<1.0	>100	7.8±0.10
HBPU	26.0±0.97	610±7.0	<1.0	>100	4.7±0.03

6.3.7 *In vitro* hemocompatibility and cytocompatibility

In vitro hemocompatibility study hints the viability of erythrocytes on exposure to the sample and its extract. The hemolytic (%) results of the positive control, negative control, samples and the degraded products are represented in **Figure 6.3a**. The disruption of the erythrocytes resulted in the release of some internal cellular components like hemoglobin that can be detected through UV-visible spectroscopy at 540 nm. The neat HBPU, PNC and degraded sample extracts were showed hemolytic activity within (4±0.56)% (**Figure 6.3a**). This suggested the compatibility of the studied material with erythrocytes, as the result was same as the negative control. The degraded by-products showed the same extent of anti-hemolytic activity. Notably, MWCNT showed higher hemolytic activity (12±0.98)% compared to mMWCNT (**Figure 6.3b**). This is due to the difference in surface chemistry and physical attributes of MWCNT and mMWCNT

upon functionalization. Pristine MWCNT has been reported to involve in RBC hemolysis by disturbing the membrane integrity and lead to blood coagulation.²⁴ Moreover, the r-protein exhibited good hemocompatibility and helped mMWCNT to become compatible. The reason may be the minimization of surface activity of mMWCNT that sometimes leads to uncontrolled aggregation of biomolecules on its surface at bio-interface.¹³ Moreover, it may help to evade MWCNT from negative feedback from immune cells and thereby improving the tissue tolerance.²⁵

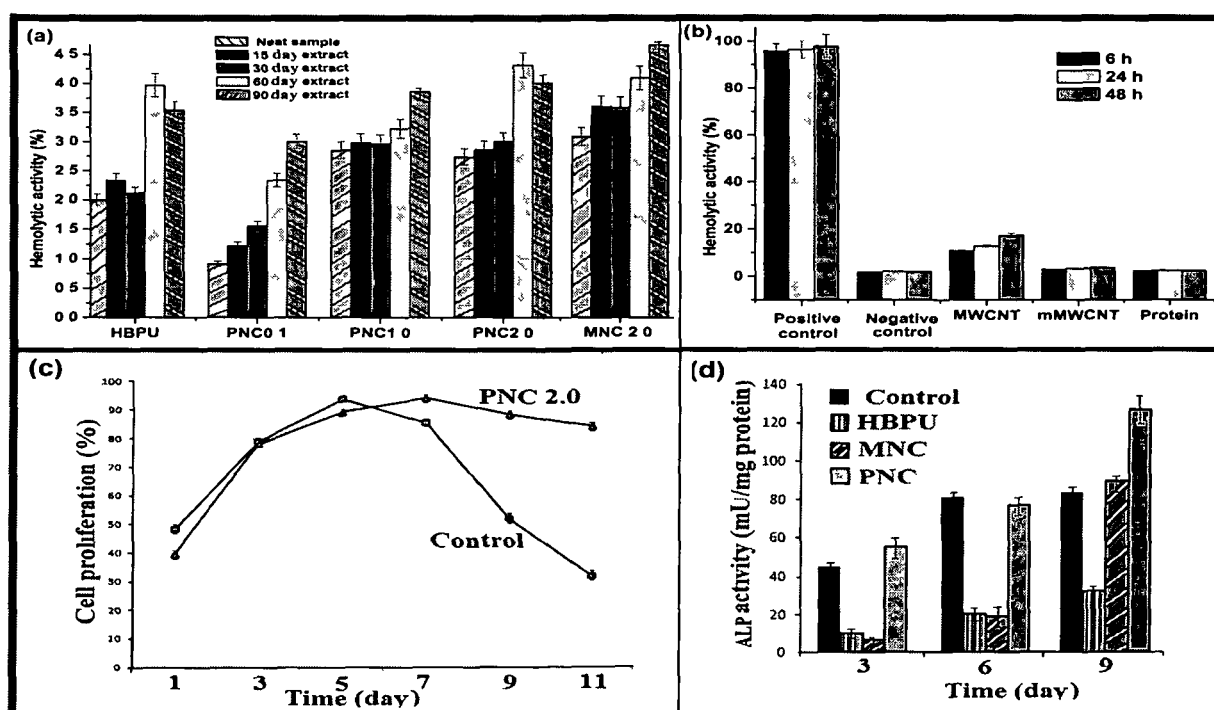


Figure 6.3: Hemolytic activity % (a) of HBPU, PNC and their degradation products as well as of r-protein, MWCNT and mMWCNT (b), MG63 cell proliferation (c) on PNC scaffold and the control as well as MG63 cells differentiation (d) on PNC, MNC, HBPU scaffolds and the control

The cytocompatibility assessment of PNC and MNC showed more than 97-99% of heart cells viability. HBPU lagged behind with (88±3.1)% of cell viability. The cytotoxicity of the leached out products/extracts from PNC, MNC and HBPU were found to be (6±0.78), (10±0.93) and (5±0.67)%, respectively. The enhanced cytocompatibility of PNC compared to HBPU is due

to the presence of nano/macro structures along with the biocompatible r-protein. PNC guided the cells behavior positively by providing a physiological three dimensional supporting matrix with interconnected porous architecture. Moreover, r-protein also acts as a serum supplement¹⁰ that augmented cell viability, adherence and proliferation on PNC scaffold. Moreover, the non-fatal effect of leached out/degraded products of PNC extracts vouched the important role of r-protein to modulate the bio-interfacial attributes of MWCNT and PNC. However, to ascertain the exact scenario within the complex interplay of different cell types and enzymes, the *in vivo* study on Wistar rats was conducted.

6.3.8 *In vitro* proliferation and differentiation study of MG63 cells

The osteoblast proliferation on the control scaffold reached to peak value ($95\pm 2.30\%$) at 5th day of test, while on PNC scaffold osteoblast reached that proliferation rate ($95\pm 3.57\%$) at 7th day. However, significant decline in the cell proliferation by ($30\pm 2.8\%$) was observed on control sample at 11th day. On the other hand cell proliferation on PNC, was quite steady with 80% proliferation rate (**Figure 6.3c**). The results were in accordance with our previous result (as discussed in section 4.3.8 of Chapter 4), as MNC scaffold also sustained the osteoblasts proliferation up to a longer period of time compared to the control one. However from the 1st day of test, PNC showed better cells proliferation ($70\pm 3.1\%$), whereas MNC showed only 40-45% of cells proliferation. Thus, the contribution of r-protein modified MWCNT in bone cells proliferation rate can be confirmed as it assisted better cellular adherence and stimulated the bioactivity of PNC. It is also pertinent to mention that the cell proliferation on the non-porous PNC scaffold after 11th day was $\sim(50\pm 2.0)\%$. This fact suggests that not only the porosity but the compositional and structural benefits of PNC scaffold over the control and MNC aid better growth of cells. SEM images (**Figure 6.4**) also witnessed better cellular adhesion, proliferation and differentiation on PNC scaffold compared to HBPU and MNC scaffolds. The cells formed a mat like network on the surface of the scaffold and well spread over the entire surface. This may be due to the presence of large surface area, high surface functionalities and bioactive nanotubes of PNC. The osteoblast cluster can be observed (**Figure 6.4**) that promoted formation of matrix and active cells on PNC scaffold. The star shaped cells with osteocyte like appearance with extensive microfilaments (containing cytoplasmic processes) extension²⁶ were seen in more number on PNC scaffold along with the osteoblasts. These microstructures served to transport

nutrient and gases from blood capillaries. On MNC and HBPU scaffolds, osteoblasts (polyglonal microstructure) with extended filopodia were more in number with irregular cells spreading and dead cells (HBPU). This depicted that augmented proliferation and differentiation of osteoblast on PNC scaffold.

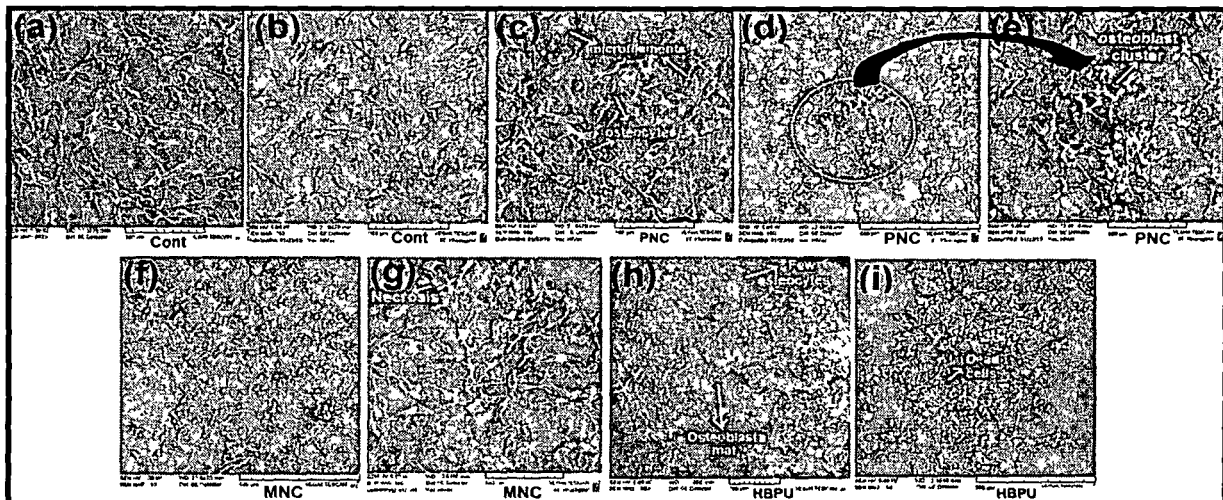


Figure 6.4: Representing the proliferation and differentiation of MG63 cells on the control (a and b), PNC (c-e), MNC (f and g) and HBPU (h and i)

Moreover, *in vitro* ALP enzyme activity (an early osteogenic marker) also elaborated that osteoblast differentiation potency of PNC was better than MNC, HBPU and the control. The initial ALP activity on PNC and the control was comparable. In each system, the threshold enzyme activity was reached at 9th day of cell seeding, where PNC scaffold showed the maximum activity (**Figure 6.3c**). Initially on 3rd day, the activity of ALP showed by MG63 cells on HBPU scaffold is quite low compared to the control and PNC scaffold ($p < 0.0001$). Notably, on PNC scaffold there was constant increase in enzyme activity till 9th day of test (130 ± 5.1 mU/mg protein), whereas there was no increase in ALP activity in control after 6th day. The enzyme activity on HBPU scaffold also increased up to 9th day (20 ± 2.0 mU/mg). In MNC, the initial activity was very low compared to the control and PNC. However on 9th day, the enzyme activity suddenly jumped to two fold (70 ± 3.82 mU/mg), though this was significantly less compared to the activity shown on PNC scaffold ($p < 0.0001$). The gradual increase in ALP activity was due to the initial acclimatization of MG63 cells with the scaffolds to adhere and

proliferate. This was followed by differentiation of the cells on the suitable supported matrix. This depicts the role of mMWCNT in enhancing the bioactivity of HBPU to a great extent. On modification with r-protein, not only the toxicity of MWCNT was reduced, but fascinatingly it improved the osteoconductivity and bone differentiation ability of the scaffold. These findings illustrated that method of functionalization as well as nature of modifying material plays a governing role at bio-interface. The significantly enhanced adhesion, proliferation and differentiation of MG63 cells on PNC scaffold, thus endorsed r-protein and mMWCNT as bioactive materials.

6.3.9 In vitro biodegradation study

The *in vitro* biodegradation in terms of weight loss was evaluated. Almost (5±0.41)% degradation was observed for PNC scaffold in first month of test. Then, the weight loss was accelerated to (8±0.35)% in the second months. At the end of three month, the weight loss percentage reached the escalated value of more than (16±0.74)%. Moreover, compared to the degradation rate of HBPU and MNC (as provided in section 4.3.12 and **Figure 4.9d** of Chapter 4), structural attributes of PNC supported more surface and bulk degradation of PNC ($p < 0.001$).

6.3.10 In vivo bone healing potency of nanocomposite

The excellent *in vitro* results encouraged to carry on the *in vivo* study with PNC scaffold. To further improve the biological performance, the sticky scaffold of PNC was prepared in sterilized DMEM nutrient medium. Therefore, the scaffold was expected to absorb some of the essential components from nutrient media to perform well at the fractured site. **Figure 6.5** showed the pictorial representation of the creation of the tibial critical sized defect model and the implantation procedure. One of the advantageous aspects of this process is that use of screw and fixative plates to set the PNC was avoided.²⁷ Thus, the surgical procedure became easier and the surgery time was minimized.

6.3.11 Radiographic analysis

The critical sized defect in tibia and the subsequent bone healing at the defect site was analyzed by radiographical study at regular interval. X-ray photographs on the first day of experiment showed that the defect was created successfully (**Figure 6.6**). At 15th day, bone regeneration was

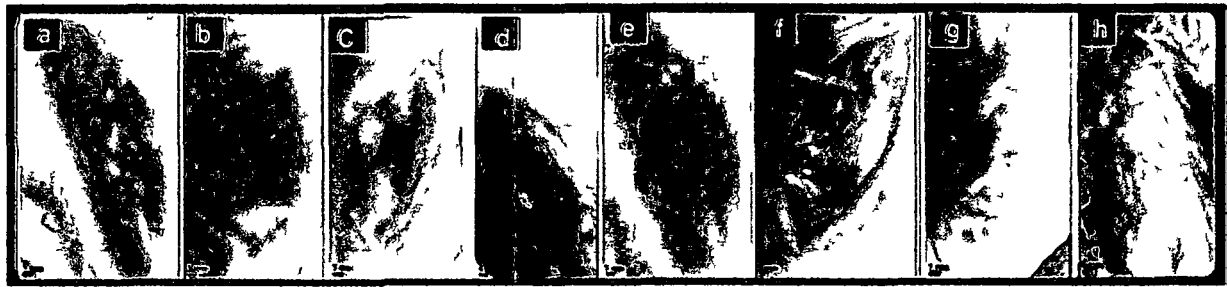


Figure 6.5: The pictorial representation of the operative procedure: creation of tibial shaft defect (a-c), implantation of the sticky PNC at the fractured site (d and e) and stitching of inner and outer layers (f-h); scale bare=5 mm

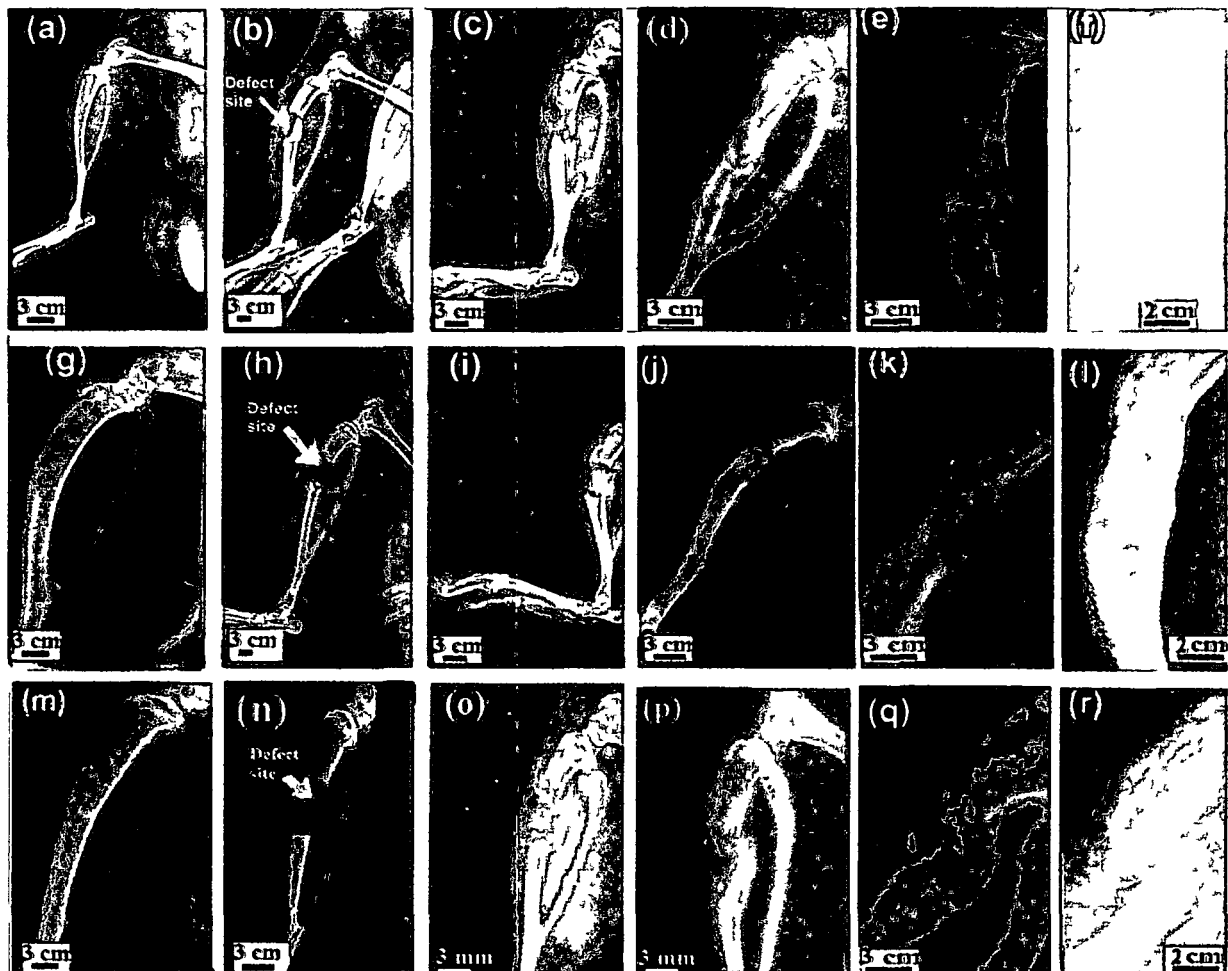


Figure 6.6: Representing the radiography of the fractured site of ST (a-f), BT (g-l) and UT (m-r) groups before fracture and at 1st, 15th, 22nd, 60th and 90th days of experiment

noted on three groups of animals (ST, BT and UT groups). The regeneration was very slow in UT group due to the lack of any postoperative treatment ($p < 0.0001$). On 22nd day, ST group showed bone regeneration in a non-uniform manner, where the growth of bone was noticed from the upper fracture ends of epiphysis towards the lower end. In contrast, bone regeneration in BT-group was uniform and the growth progressed towards the both fractured ends. The normal locomotion of the treated rats was resumed within 30th day of experiment. The complete bridging of bone at the defect site was perceived at 40th day. However, area with radio-transparency can still be observed at few regions at the defect site of the treated groups. But, the bone alignment was better and smooth in BT group than in ST group. Even after 40th day, randomly organized callus, with non-aligned bridging was noted at left region of the tibial shaft in UT group. Whereas, bone regeneration was almost ~90-93% in treated groups, as measured by dividing the area of bone neoformation by total area of defect⁷ using software-ImageJ analyzer (National Institutes of Health, Maryland, USA). The 60th day of post-implantation photograph clearly verified the radiopacity of the defect region and ongoing remodeling phases in treated groups. The tibial lining at that region was observed to be thickened compared to normal rats. However on 90th day, the thickening was much reduced. BT group showed well organized healing site compared to ST group ($p < 0.05$).

Radiographical analysis thus provided the direct visualization of the bone healing process in the experimental animals. The function of PNC in healing of bone is thus demonstrated. PNC with immobilized DMEM nutrients acted as an ECM that supported the infiltration and adherence of the osteoprogenitor cells (mainly from the peritoneal tissue) and growth factor as well as deposition of calcium ion for effective bone neoformation. Furthermore, as demonstrated that PNC stimulated enhanced proliferation and differentiation of the bone cell, which clearly accelerated the *in vivo* bone healing process at the defect area as well. However, remodeling phase to regain the original shape was in the verge of completion. The regeneration phase in UT group was still on progress even after 90th day of analysis.

6.3.12 Analysis of biochemical and hematological parameters

To evaluate the long term *in vivo* consequence of PNC, the biochemical analyses viz. kidney, liver and lipid profiles was studied in experimental and the control group. The results of biochemical analyses at regular intervals are given in **Table 6.2**. The indicators of kidney

function (Creatinine (cre); Uric acid and Urea) showed that in all the cases, the values were within the reference range. Likewise, the proper functioning of liver was attested from the safety ranges of the indicators like serum glutamic-pyruvic transaminase (SGPT), serum glutamic oxaloacetic transaminase (SGOT) and ALP (Table 6.2) in the serum of recipient rats post-implantation. The lipid profile also suggested the harmless effect of PNC scaffold and its leached out/degraded products. However, compared to the control and non-treated rats, the ALP level was higher in PNC treated rats ($p < 0.001$). This result was in accordance with the *in vitro* results. Though, elevated ALP is an indicator of liver damage, but during bone healing process the scenario is different. The osteoblastic activity including new bone formation, calcification and secretion of bone matrix results in the increased concentration of this enzyme.²⁸ ALP content marked the occurrence of bone formation. On PNC treated rats (ST and BT groups), ALP level was high till (45-50)th day. Thereafter, the level declined within the reference range. In case of control rats the level of ALP remained constant. However in UT group, the level was high, but due to slow rate of healing the increment was not significant ($p > 0.05$).

The non-toxic and non-immunogenic responses of host on exposure to PNC were again illustrated from hematological parameters of the rats (Table 6.3). The level of lymphocytes in the treated animal (with implanted foreign material) was determined in peripheral blood of host to ensure the biocompatibility and non-immunogenic nature of an implantable material. A reduction in the lymphocytes level indicates the toxicity of the material, while significant increase of lymphocytes depicts immunogenic conduct. From the results, it was found that compared to the control rats, there was an increase in the level of neutrophils and monocytes (Table 6.3) after implantation due to the surgical wound, though it did not surpass the reference limit. The periodic observation thus suggested the safety aspect of this material as no outburst of inflammatory response on BT and ST groups throughout the experimental period was observed (Table 6.3). In UT group, neutrophils level remained elevated upto 60th day ($p < 0.05$) that may be due to the slow healing process and acute inflammatory response. The number of platelet increased after surgery due to subsequent wound healing process. However up to 90th day of the test, no detrimental effect of PNC on the hematological parameters of the treated rats was observed. Though sudden increment in the lymphocytes count was encountered due to the leaching of components or degraded fragments. But, their fast normalization emphasized that they may get engulfed by the immune cells or degraded further by the cellular mechanism into

harmless products.²⁹ Moreover, from 1st to 90th days, the implantation site was carefully observed for any post implantation syndrome viz. fever, cardinal sign, abnormal feeding habit and rejection of the implant. The absence of these signs accords for its non-toxic and non-immunogenic behavior.

Table 6.2: Biochemical profiles of Wistar rats upon exposure to the studied materials

Biochemical parameter	ALP	Glucose	Urea	UA	Chol	Cre	SGPT	SGOT	
Control	145±4.1	98±2.1	65±1.1	0.6	34±0.7	1.0	50±1.0	106±2.1	
7 th d a y	ST-group	207±5.0	85±3.0	56±2.3	1.1	31±1.2	0.7	56±1.5	113±2.0
	BT-group	233±4.8	83±3.5	61±1.0	1.2	27±1.0	0.9	55±0.4	121±3.0
	UT-group	174±3.6	87±3.0	69±1.1	1.8	36±0.2	1.1	53±0.4	124±1.8
	M-group	256±4.0	91±2.0	65±1.4	0.9	34±0.5	1.0	81±2.3	130±3.6
	MM-group	141±3.2	86±2.4	61±2.3	1.0	36±0.9	1.1	61±2.0	100±2.5
	P-group	119±3.5	80±1.8	53±1.5	1.0	37±0.2	0.9	69±1.9	119±4.1
30 th d a y	ST-group	361±4.6	81±2.4	55±1.0	1.0	34±1.2	0.5	59±0.5	97±4.5
	BT-group	390±3.0	84±1.7	64±1.2	0.9	31±0.4	0.8	57±1.0	103±2.0
	UT-group	292±5.1	88±3.2	61±1.1	0.7	42±1.0	0.9	69±2.5	117±1.9
	M-group	278±4.3	93±3.0	63±0.6	3.1	48±2.0	1.1	81±1.9	111±3.5
	MM-group	149±4.2	87±2.9	62±1.0	1.7	42±0.5	1.0	74±1.4	103±2.5
	P-group	123±3.8	79±3.1	53±2.0	1.0	38±2.2	0.9	65±0.8	120±3.0
90 th d a y	ST-group	156±4.6	83±1.2	55±1.4	1.1	33±1.0	0.8	54±1.0	100±2.7
	BT-group	149±3.1	80±1.0	63±0.5	0.9	30±0.5	1.0	50±1.5	104±1.9
	UT-group	230±4.0	85±2.1	62±1.0	0.7	36±1.1	1.0	55±1.0	113±2.0
	M-group	271±5.2	90±3.1	64±1.2	3.0	48±1.3	1.2	79±0.6	117±3.2
	MM-group	143±2.9	95±2.5	60±2.2	1.7	40±1.9	1.0	65±0.3	103±4.2
	P-group	125±3.0	83±2.1	54±2.0	1.0	38±0.4	0.8	64±0.5	119±2.1

*ALP =Alkaline phosphatase; UA=Uric acid; Chol=Cholesterol; Cre=Cretinine; SGPT= Serum glutamic pyruvic transaminase; SGOT=Serum glutamic oxaloacetic transaminase

6.3.13 Bio-toxicity study of protein, MWCNT and protein functionalized MWCNT

The *in vivo* biocompatibility of r-protein and MWCNT with and without functionalization was investigated after intra-peritoneal injection in rats. It was observed that the leukocytes count was higher in M group compared to MM and P groups (Table 6.3). Initially up to 10th day, no significant difference was observed between the groups, but gradually the difference became

Table 6.3: Hematological parameters of Wistar rat upon exposure to the studied materials

Cell type		WBC	LYM	MON	NEU	RBC	HcT	RDW	Hb
Normal range		3.0-12 m/mm ³	65-85%	0.0- 5.0%	9.0- 34.0	7-10 M/mm ³	30- 39 %	8-12	11-18 g/dl
7 th d a y	ST group	4.9±0.2	25.2±3.4	12±0.9	63±2.5	9.77±1.5	30.8±2.0	11.0±0.3	14.9±1.0
	BT group	9.9±1.0	32.5±2.7	15±1.0	52±1.7	7.75±2.0	31.2±1.44	12±0.46	11.8±0.3
	UT group	5.4±0.3	32±2.0	14±1.1	54±0.9	10±2.7	36.1±1.41	13±0.72	15.5±0.5
	M group	10.5±0.9	42.6±1.1	14±0.4	44±0.7	7.96±1.1	31.5±0.5	10.8±1.8	11.6±1.9
	MM group	10.9±1.1	37.4±0.8	15±0.7	48±1.0	8.3±2.04	36.5±1.1	11.0±1.5	11.4±0.4
	P group	7.8±0.41	64.0±3.4	5.1±0.7	36±2.7	8.2±3.1	33.1±2.23	13.2±1.8	12.1±0.5
30 th d a y	ST group	4.0±0.32	60.0±4.2	6.4±1.1	34±3.1	9.74±0.8	30.7±0.56	11.2±0.3	14.9±0.5
	BT group	5.97±0.7	63.7±2.8	4.9±0.8	31±2.0	7.75±1.3	31.0±0.5	11.4±1.3	11.9±0.9
	UT group	5.5±0.73	43.0±1.6	11±0.5	45±1.1	10.4±1.4	36.0±1.78	12.7±2.7	15.3±1.2
	M group	12.3±1.4	32.1±1.2	10±0.5	58±0.7	7.32±0.5	31.3±0.91	10.8±1.0	11.0±0.2
	MM group	7.8±1.1	47.8±2.5	7.4±0.2	45±2.3	8.2±1.23	35.9±2.9	10.9±1.0	11.3±0.4
	P group	5.53±0.6	65.7±2.6	4.4±0.8	30±1.8	8.24±1.2	33.3±4.1	13.4±0.5	12.0±1.6
60 th d a y	ST group	6.23±0.9	31.5±1.7	9.2±1.0	59±0.7	9.76±0.8	30.3±0.49	11.0±2.4	15.0±2.0
	BT group	7.1±0.4	40.0±2.3	6.3±0.3	54±2.0	7.74±1.4	36.3±3.2	11.5±1.9	12.3±1.1
	UT group	5.7±0.6	43.3±1.6	12±0.5	45±1.1	9.9±1.1	31.1±1.01	12.4±1.5	15.0±1.6
	M group	12.7±1.3	34±1.43	10±0.32	56±1.12	7.06±0.7	36.0±2.15	11.2±0.7	11.0±0.8
	MM group	6.93±0.8	50.9±1.9	7.0±0.5	42±1.4	8.2±0.45	33.1±2.0	10.7±0.3	11.4±0.5
	P group	5.54±1.2	65.9±3.0	5.0±1.3	29±2.7	8.3±0.81	33.2±1.78	12.4±1.8	12.2±1.0
90 th d a y	ST group	4.87±0.5	66.9±2.1	3.8±1.0	29±1.1	9.81±1.9	30.4±0.7	11.0±1.0	15.1±2.8
	BT group	5.8±0.54	69.0±2.4	4.3±0.7	27±1.3	7.98±0.4	36.2±2.41	11.4±0.5	12.2±0.4
	UT group	5.32±0.9	57.2±3.6	6.4±1.7	36±1.1	10±0.83	30.8±1.12	12.1±2.7	15.1±2.1
	M group	13.3±1.9	35±2.3	8.0±1.4	56±0.9	7.3±1.01	29.1±0.5	10.4±0.6	10.7±1.6
	MM-group	7.01±1.4	55.8±3.1	7.8±2.5	36±0.6	8.2±1.5	32.0±0.52	10.6±1.0	11.1±0.2
	P-group	5.04±0.5	66.0±2.9	5.1±0.7	28±2.2	8.9±1.5	33 ±1.93	12.3±1.1	12.3±0.7

*WBC=White blood cell; LYM= lymphocyte; MON= Monocyte; NEU=Neutrophile; RBC= Red blood cells; HcT= Hematocrit; RDW= Red blood cell distribution width; Hb= Hemoglobin and Pct=Plateletcrit

relevant ($p < 0.0001$). The neutrophils count was very high around 57.8% and monocytes count was 10.1% in M group. In MM group, the neutrophils count gradually decreased to reference range after 90 days of test, but in M group the value remained almost constant throughout the experiment. This showed significant immunogenic nature of pristine MWCNT ($p < 0.0001$), in contrast to the functionalized one. Sakamoto et al. also reported the long lasting inflammation with fibrous thickening and granuloma formation upon administration of MWCNT via interperitoneal route.³⁰ Further, P group showed no immunogenic response against the injected r-protein. This also clearly depicted the favorable role played by anchored r-protein on the surface of mMWCNT to down regulate the immunogenic response in MM group.

The serum biochemical study further demonstrated the role of surface modulation of MWCNT on host. The excess level of ALP (256.6 ± 6.3) U/L in M group was observed compared to (141 ± 3.8) U/L and (108 ± 4.0) U/L in MM and P group, respectively after 7th day of administration. This clearly indicated the adverse effect of MWCNT on liver. The changes of shape of liver and creation of roughness on its wall on post interperitoneal administration of MWCNT were reported in literature.³¹ Simultaneously, SGOT and SGPT level along with the glucose level also increased in M-group ($p < 0.05$) compared to the other two groups. The results of the serum biochemistry are presented in **Table 6.2**. P-group displayed comparable result with the control group ($p > 0.05$), whereas in MM group, the level of the vital determinants was within the reference range.

The cytokine level viz IL-6 and TNF- α was also measured in the serum of the treated and control groups. The results are presented in **Figure 6.7a**. It was observed that these cytokine levels increased two folds in M group ($p < 0.001$), though the level was low in MM group. In P group, the cytokines levels were comparable with the control rats. Therefore, it could be established that MWCNT induced systematic inflammatory responses in rats which persist even up to 90th day of test, whereas mMWCNT escaped from eliciting such responses due to the adhered biocompatible r-protein on its surface.

The overall enhanced biocompatibility may be due to the reduction in surface reactivity and thus riddance from the undesired aggregation of biomolecules on the surface of mMWCNT and their disruption. Secondly, anchored r-protein might have prevented MWCNT accumulation on narrow passages as it has conferred solubility to MWCNT. Thirdly, the

immobilization of r-protein may further aid in recognition and hence degradation of nanotubes by the phagocytes.^{29, 32}

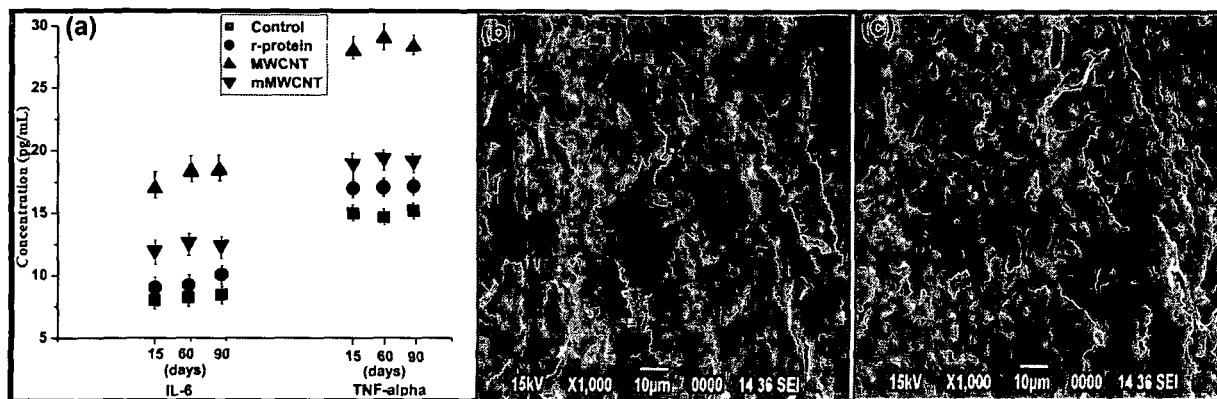


Figure 6.7: Cytokine expression (a) on M, P and MM groups after administration of MWCNT, r-protein and mMWCNT, respectively as well as SEM images showing cross section view of tibia shaft of normal (b) and BT group (c) after 90 days of post implantation

6.3.14 *In vivo* fate of the implanted nanocomposite in the tibial defect rat model

The implanted scaffold was not found at the healed tibia and the surrounding region after 90 days of implantation in the sacrificed rats. The absence of any trace of PNC scaffold suggested that during healing process, the scaffold got degraded and eventually making space available for the native cells/tissue to proliferate and differentiate. The finding was further confirmed by analysis of SEM images (Figure 6.7b). The SEM images also depicted the absence of the supported matrix at the treated site. However, the minute PNC debris could not be recognized through these images. Interestingly no inflammatory response or post implantation syndrome was observed during the experimental period up to 12 weeks. Furthermore, the degraded products were also non-toxic and non-immunogenic as supported by biochemical analyses of liver, kidney, heart and lipid profiles study. Thus, the *in vivo* results synchronized with the *in vitro* findings of degradation and toxicity studies. It could be speculated that the hydrolysable linkages of PU matrix started to degrade upon interaction with the body fluids and internal enzymes. Moreover, the fragments or leached out products may get engulfed by the phagocytes and digested through normal cellular mechanism. It was also reported that the neutrophilic peroxides are capable to degrade the nanotubes, once they are engulfed by them.²⁹ Thus, it is relevant to depict the non-

toxic nature of PNC scaffold and mMWCNT. The biodegradability together with non-toxic nature of the degraded products ascertained PNC potentiality in the domain of bone healing endoprosthesis or TE scaffold. The presence of long alkyl chain and ester bond owing to the presence on MG, degradable PCL moiety, the amide linkages of r-protein and ester/ether/secondary linkages in HBPU with HB morphology facilitated the effective biodegradation process of PNC. Thus, the biodegradable scaffold eliminated the need of repetitive surgery, as it degraded within the host body during the healing process itself.

6.3.15 Histopathological study at the fracture site

The representative histological photographs of the bone tissues of treated and non treated groups are shown in **Figure 6.8**. Bone were harvested and histologically examined on 90th post-operative day. It was observed that the structural integrity of the bone in the treated animal group was recuperated, however in the non-treated animal group the outer lining was not completely repaired. BT group showed a compact bone tissue with properly arranged lamellar bone, however in some places woven/hyaline cartilage were also present (**Figure 6.8b**). Whereas, in ST group mature lamellar bone with abundant coarsen woven bone or hyaline cartilage was observed. In UT group, histopathological sections showed the initial phase of bone regeneration as extensive coarsen woven bone or hyaline cartilage with lesser density of mature bones was observed. These histopathological findings also corroborated with the X-ray examination of the experimental animals, as the untreated animal showed the less bone density and imperfect healing of the fracture. On the other hand, PNC scaffold implanted animal groups (ST and BT groups) showed higher calcium density with significantly improved bone structure.

These suggested efficient and faster replacement of cartilaginous tissue by trabecular bone in the treated groups due to the positive guidance by the bioactive PNC scaffold. The rapid bone neoformation in BT group results in the successful repairing of defect region by around 90-93% bone formation within very short span. The possible reason for such observation is the sealing of defect region with PNC that inhibited the penetration of soft tissue and served as a bioactive matrix to promote endogenous adhesion and proliferation of the bone cells.⁷ Interestingly, compared to clinically approved (by Food and Drug Administration)⁷ *Ricinus communis* oil based PU/calcium carbonate, which showed 79% bone formation after 120th day of postoperation, this PNC scaffold showed significantly improved results. Most importantly, no

inflammatory or foreign-body-giant cell was observed through histopathological evaluation. This is in accordance with the non-toxicological and non-immunogenical studies stated above. Moreover, the absence of any fibrous capsules enclosed PNC both in BT and ST groups suggested its excellent osteointegration ability and its biodegradability into non-harmful by-products. These kinds of synthetic biomaterials are reported to accelerate the bone healing process by osteoconduction and osteoinduction.³³ PNC scaffold not only guided the cellular healing process, but also helped in the differentiation of bone cells as evident from *in vitro* studies. These parameters work towards making PNC scaffold as one of the promising biomaterial for bone healing.

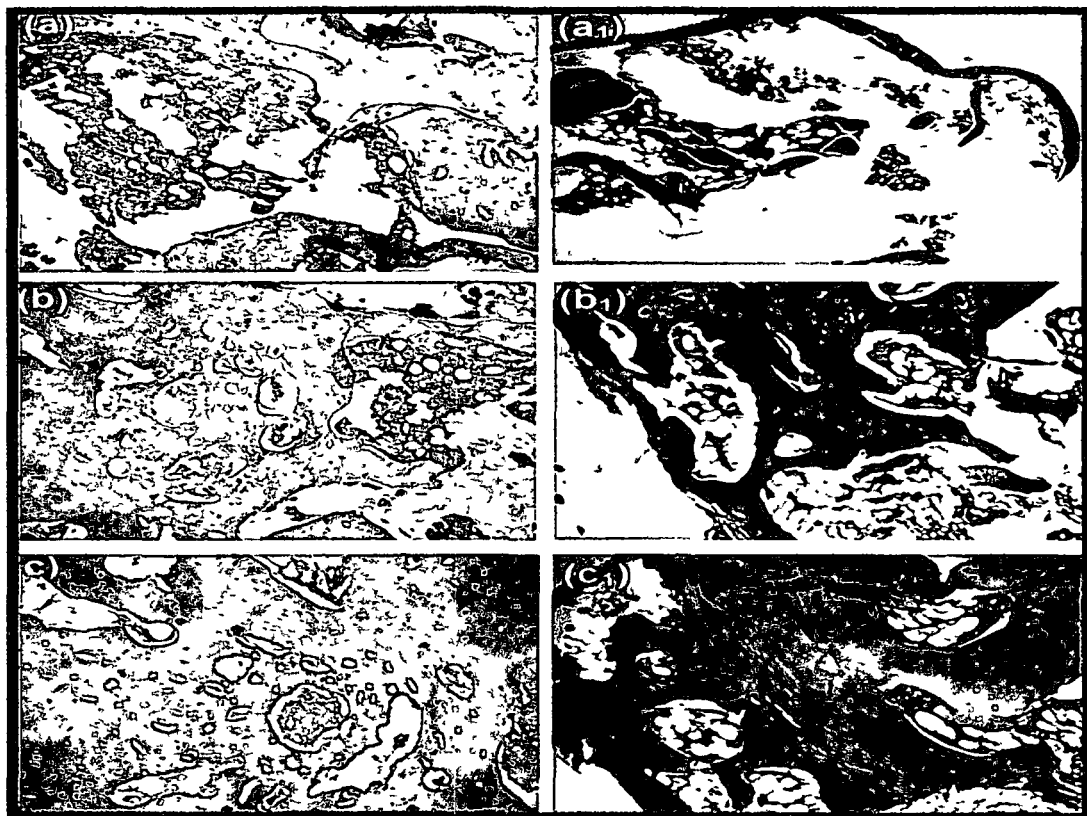


Figure 6.8: Microscopic view of the respective tibial sections of UT (a and a₁), ST (b and b₁) and BT (c and c₁) groups stained with hematoxylin and eosin stain (a, b and c) as well as Masson's trichrome stain (a₁, b₁ and c₁) after 90th day of experiment

6.4 Conclusion

The unison of structural attributes of r-protein (extracted from industrial waste) and cavitation energy of sonication effectively functionalized mMWCNT. The exquisiteness of mMWCNT and *Helianthus annuus* oil derived HBPU-NC was explored as an advanced bone healing endoprosthesis. This NC promoted the endogenous regeneration of the bone in tibial defect model within a very short time span of 5-8 weeks. The host did not elicit any immune response towards PNC and the vital organs showed normal functions. Biodegradability of the scaffold within the host with safe degraded by-products flaunted its utility for effective bone repairment in osteolytic bone destruction or accidental fracture. The study depicted the suppression of toxic effect of MWCNT on functionalization with r-protein and thus enrolled the usefulness of biomacromolecules to offer biocompatibility to the scaffold for long term utility. Thus, biophysiological attributes of PNC supports that all the design criteria of such applications can be efficiently fulfilled. However, at this stage, it is quite sketchy to utilize such materials to patients without clinical investigation.

Reference

1. Guaraldi, G., et al. *Aids*, **15** (1), 137--138, 2001.
2. Coleman, R.E. *Cancer Treat Rev* **27** (3), 165--176, 2001.
3. Grimer, R.J., et al. *J Bone Joint Surg Br* **81** (3), 488--494, 1999.
4. Miller, K., et al. *Angew Chem Int Ed* **48** (16), 2949--2954, 2009.
5. Kalfas, I.H. *Neurosurg Focus* **10** (4), 1--8, 2001.
6. Saffar, K.P.A. JamilPour, N. & Rouhi, G. *Carbon Nanotubes in Bone Tissue Engineering*, In Biomedical Engineering, C.A.B. deMello, ed., InTech, Europe, 2009.
7. Pereira-Junior, O.C.M.M., et al. *J. Biomater Appl.* **21** (3), 283--297, 2007.
8. Tonelli, F.M.P., et al. *Int J Nanomed.* **7**, 4511--4529, 2012.
9. Cui, D. Biomolecules Functionalized Carbon Nanotubes and their Applications, in *Medicinal Chemistry and Pharmacological Potential of Fullerenes and Carbon Nanotubes*, F Cataldo & T.D. Ros, eds., Springer, New York, 2008, 181--221.
10. Farges-Haddani, B., et al. *Process Biochem.* **41** (11), 2291--2304, 2006.
11. Zhu, J., & Marchant, R.E. *Expert Rev Med Devices* **8** (5), 607--626, 2011.

12. Purkayastha, M.D., et al. *J. Agric. Food Chem.* **61** (45), 10746--10756, 2013.
13. Firme III, C.P., & Bandaru, P.R. *Nanomedicine* **6** (2), 245--256, 2010.
14. Gisselalt, K., et al. *Biomacromolecules* **3** (5), 951--958, 2002.
15. Roach, P., et al. *J. Mater. Sci. Mater. Med.* **18** (7), 1263--1277, 2007.
16. Purkayastha, M.D., & Mahanta, C.L. *J. Food Sci. Technol.* DOI 10.1007/s13197-014-1299-5, 2014.
17. Temenoff, J.S. & Mikos, A.G. *Biomaterials: The Interaction of Biology and Material Science*; Prentice Hall, USA, 2008.
18. Rolls, G. *An Introduction to Decalcification*, Leica Biosystems, Wetzlar, Germany, 2012.
19. Dumeé, L., et al. *Nanomaterials* **3** (1), 70--85, 2013.
20. Yang, W., et al. *Nanotechnology*, **18** (41), 412001--412013, 2007.
21. Li, M., et al. *J. Biol. Chem.* **277** (40), 37888--37895, 2002.
22. Barth, A. *Biochim. Biophys. Acta, Bioenerg.* **1767** (9), 1073--1101, 2007.
23. Schmid, F.X. *Biological Macromolecules: UV-visible Spectrophotometry*; eLS, Macmillan Publishers Ltd, London, 2001.
24. Meng, J., et al. *Plos One* **7** (7), e38995, 2012.
25. Shvedova, A.A., et al. *Pharmacol. Ther.* **121** (2), 192--204, 2009.
26. Nakamura, H. *J. Hard Tissue Biol.* **16** (1), 15--22, 2007.
27. Ebrahimi, A.S., et al. *Iran Red Crescent Med. J.* **14** (2), 96--103, 2012.
28. Roudsari, J.M., & Mahjoub, S. *Caspian J. Intern. Med.* **3** (3), 478--483, 2012.
29. Kagan, V.E., et al. *Nat. Nanotechnol.* **5** (5), 354--359, 2010.
30. Sakamoto, Y., et al. *Toxicol. Sci.* **34** (1), 65--76, 2009.
31. Patlolla, A., et al. *J. Appl. Toxicol.* **31** (1), 75--83, 2011.
32. Jain, S., et al. *J. Nanomed. Nanotechol.* **3** (5), 3--5, 2012.
33. Carlo, D., et al. *Ciencia Rural* **33** (6), 1081--1088, 2003.

Chapter 7

Conclusion and future scopes

Highlights

This chapter provides the concluding remarks of the present investigation. This chapter also highlights the major findings of this work and precisely elaborates the interesting observations, and future scopes.

7.1. Summary and concluding remarks

The present investigation endeavors to address the objectives of the thesis in a comprehensive and conclusive manner. In brief, this investigation presented the successful synthesis of *Helianthus annuus* oil based HBPU and their nanocomposites as prospective biomaterials. The thesis is compiled into seven chapters. The first chapter is the general introduction with a brief review on polymeric biomaterials emphasizing polyurethanes, especially HBPU and their NC. The materials, methods of preparation, characterization and properties of such biomaterials are also discussed. The potential applications of biodegradable polyurethane NC based biomaterials are demonstrated here. This chapter speculates that biodegradable and biocompatible vegetable oil based HBPU and its NC could be employed as a biomaterial for different biomedical applications. Finally, the objective and plans of the thesis are also presented in this chapter.

Biodegradable polyurethane is extensively used as a thin film material as TE scaffold, catheter, blood bag, disposable syringe, etc. In this context, second chapter focuses on the synthesis of *Helianthus annuus* oil based HBPU for its feasibility in biomedical applications. This chapter is divided into two subchapters. The first subchapter deals with the synthesis, characterization and properties evaluation of HBPU. The performance of HBPU was compared with its linear analog. The results demonstrated the superiority of HB architecture over the linear one and forwarded HBPU as a suitable biodegradable thin film material. In this avenue, the second subchapter scrutinizes the effect of the content of multifunctional component in tailoring the mechanical, thermal, chemical and bio-interfacial attributes of HBPU. The performance of HBPU was also compared with a similar architectural PU without using *Helianthus annuus* oil. The best results were obtained for bio-based HBPU with 5 wt.% of pentaerythritol (branch generating unit) among the other studied compositions. The bio-based HBPU showed immense potential to be used as a scaffold material in the domain of TE with good biocompatibility, biodegradability with cell adherence and proliferation ability. The best HBPU was thus selected as the matrix for the incorporation of nanomaterials for further studies.

Polymer NC are the advanced materials in biomedical domain as they can combat the limitations associated with the pristine polymers. In this context, third chapter deals with the preparation of a thermo-magnetic responsive shape memory HBPU/Fe₃O₄ nanocomposite (FNC) as an implantable biomaterial. Fe₃O₄ was utilized due to its biocompatibility, superparamagnetic like behavior and antibacterial activity. The chapter depicts good interfacial interactions between

HBPU and well dispersed Fe_3O_4 . The incorporation of Fe_3O_4 in HBPU improved the thermo-mechanical properties as well as shape-memory behavior of the pristine HBPU. Interestingly, HBPU acquired antibacterial activity and magnetic properties upon incorporation of Fe_3O_4 nanoparticles. FNC and its degraded products were found to be cyto- and hemo-compatible. In addition, the *in vivo* biocompatibility and non-immunological behavior of FNC with bacterial resistive surface make it a strong contender as a smart implantable biomaterial.

Polymer NC based on MWCNT are also extensively researched biomaterials, especially in tissue engineering. In this avenue, fourth chapter demonstrates the significance of MWCNT incorporated HBPU as a scaffold for bone tissue engineering. It also describes the formation of stable NC based on covalently functionalized MWCNT and HBPU (MNC). MNC showed dramatic improvement in mechanical properties compared to the pristine HBPU. Most importantly, this chapter reveals that MNC with interconnected pores size showed better proliferation and adherence of osteoblast (MG63) cells compared to HBPU. The cytokines detection and cytocompatibility assay approved the non-toxic behavior of MNC. Moreover, the hematological, histological and immunological indices of toxicity suggested the safety potential of MNC and its degraded products within the tested animal.

Spurred by the outstanding performance of the above mentioned NC, fifth chapter endeavors to utilize the concomitant effect of MWCNT and Fe_3O_4 on the performance of HBPU NC. The nanohybrid was prepared by a non-covalent approach employing *in situ* generation of Fe_3O_4 nanoparticles in the presence of MWCNT. This chapter delves to explore the potency of HBPU/nanohybrid NC (NNC) as a wound healing material with drug releasing aptitude. The dressing patch of NNC showed excellent *in vivo* wound healing potency in albino mice with enhanced wound closure rate. This chapter also provides a comparative study in terms of drug (gentamicin sulfate) loading efficacy, antibacterial activity, mechanical performance, fluid handling capacity and moisture vapor permeability for NNC, HBPU, FNC and MNC. The results showed NNC has the best performance. This NC also showed good hemocompatibility, non-immunogenicity, controlled drug release capability and wound healing efficiency.

Moreover, prompted by the good results of covalently functionalized MWCNT and HBPU based bone tissue scaffold, sixth chapter scrutinizes the effect of the non-covalently functionalized MWCNT. This chapter deals with the fabrication of a bioactive scaffold by exploring the grandeur of rapeseed protein functionalized MWCNT and HBPU based NC (PNC).

PNC showed enhanced osteoblast differentiation with better cellular adhesion, spreading and proliferation compared to the control and MNC. PNC scaffold illustrated rapid bone neoformation on a critical sized tibial fracture gap with 90-93% filling up of the defect area within 60 days. Moreover, good mechanical performance of PNC like high load bearing ability together with flexibility and biodegradability promote it as one of the alternatives for clinical challenges as a bone endoprosthesis.

The present chapter is the summary and conclusion of this investigation. It precisely elaborates the interesting observations and the future scopes of this present work. The major findings of this work are provided underneath:

- ❖ The significant role of *helianthus annuus* oil based polyurethane for biomedical application is appraised. The oil based polyurethane leads to enhance cellular adherence, biocompatibility and biodegradability compared to non-vegetable oil based one.
- ❖ The investigation revealed the concomitant benefits of multidimensional hyperbranched geometry and vegetable oil based HBPU in biomedical domain, especially in tissue engineering application. It also reveals the role of multifunctional moiety and degree of branching in tailoring the physico-mechanical and biological attributes of hyperbranched polymer.
- ❖ Fe₃O₄ based NC showed promising potential to be used in innovative applications as thermally and magnetically controlled shape memory biomaterial (like stent, clot remover, catheter, etc.) that may surmount the limitations associated with conventionally used medical devices and surgical procedures.
- ❖ This investigation also demonstrated that inclusion of covalently carboxyl functionalized MWCNT dramatically improved the toughness, osteoconductivity, cell adherences and proliferation ability of MWCNT based NC compared to HBPU. Thus, this NC could be forwarded as a bone tissue scaffold. However, before actual application, the *in vivo* assessment of bone/cartilage tissue growth on this scaffold must be tested.
- ❖ Fe₃O₄-MWCNT nanohybrid based NC depicted its immense role as an antibacterial and biocompatible wound healing material with accelerated wound closure rate and controlled drug release profile. This nanohybrid based NC possess structural and compositional benefits over HBPU as well as MWCNT and Fe₃O₄ based NC in terms of fluid handling capability, moisture vapor transmission rate, antibacterial activity and drug loading ability.

- ❖ One of the significant findings of this investigation is the rapid *in vivo* bone healing potency of the protein functionalized MWCNT based NC scaffold in tibial defect model within a very short time span of 5-8 weeks. The anchorage of rapeseed protein molecules on MWCNT showed an improvement in osteoconductivity and cell differentiation ability of this NC. Noticeably, rapeseed protein modified MWCNT based NC showed better cellular adhesion, proliferation and differentiation of MG63 cells compared to carboxyl functionalized MWCNT based NC. Thus, this NC can be forwarded as a promising bone endoprosthesis.
- ❖ The investigation also depicted the suppression of toxic effect of MWCNT on functionalization. Adhered rapeseed protein on MWCNT noticeably downregulated the immunogenic nature of MWCNT and protected the vital organs from any damage. Thus, this finding enrolled the usefulness of biomacromolecules to offer biocompatibility to nanomaterials for long term utility.

In brief, the study achieved to modulate the physico-mechanical and bio-interfacial attributes of polymeric NC based biomaterial by compositional and architectural variation of polymer, types of nanomaterial, functionalization approaches and surface properties of materials. The amalgamation of macro- as well as nano- structural elements is found to be beneficial for *in vivo* applications.

This investigation illustrated that the *Helianthus annuus* oil based HBPU NC can be forwarded as potential multifunctional biomaterials. Moreover, these NC are best suited scaffold materials for tissue engineering application. However, clinical investigation is needed before leaping into any final conclusion.

7.2 Future scopes

This investigation sparks a light on the immense potential of hyperbranched architectural and *Helianthus annuus* oil based PU and its NC as biomaterials. Even though, it is a thorough and comprehensive study, but many other aspects related to this work can be further delved into. It provides a wider scope for future investigation and few of these are mentioned below.

- ❖ Scrutinization of the potentiality of other vegetable oils and branch generating moieties on the performance of hyperbranched polyurethane and their nanocomposites at bio-interface.
- ❖ Incorporation of other nanomaterials like graphene oxide, carbon dot, hydroxyapatite nanoparticles, chitosan nanoparticles on HBPU and investigation of their biological aspects.
- ❖ Synthesis of injectable and tough vegetable oil based hyperbranched polyurethane and their NC as a scaffold for tissue engineering.
- ❖ Detail investigation on the leached out nanomaterials as well as the degraded polymeric products during the service period and monitoring their ultimate fate within the host.
- ❖ Examinations of genotoxicity, carcinogenicity and mutagenic effects of the studied HBPU and its NC for their practical applications.
- ❖ Clinical investigation on human subjects to evaluate the safety potential.

List of publications

In journal

1. Das, B., Chattopadhyay, P., Mandal, M., Voit B., & Karak, N. Bio-based biodegradable and biocompatible hyperbranched polyurethane: A scaffold for tissue engineering *Macromol. Biosci.* **13** (1), 126--139, 2012.
2. Das, B., Konwar, U., Mandal M., & Karak, N. Sunflower oil based biodegradable hyperbranched polyurethane as a thin film material, *Ind. Crops Prod.* **44**, 396--404, 2013.
3. Das, B., Chattopadhyay, P., Mishra, D., Maiti, T.K., Maji, S., Narayan, R., & Karak, N. Nanocomposites of bio-based hyperbranched polyurethane/functionalized MWCNT as non-immunogenic, osteoconductive, biodegradable and biocompatible scaffolds in bone tissue engineering, *J. Mater. Chem. B* **1** (33), 4115--4126, 2013.
4. Das, B., Mandal, M., Upadhyay, A., Chattopadhyay, P. & Karak, N. Bio-based hyperbranched polyurethane/Fe₃O₄ nanocomposites: smart antibacterial biomaterials for biomedical devices and implants *Biomed. Mater.* **8** (3), 035003--035015, 2013.
5. Das, B., Chattopadhyay, P., Upadhyay, A., Gupta, K., Mandal M., & Karak, N. Biophysico-chemical interfacial attributes of Fe₃O₄ decorated MWCNT nano hybrid/bio-based hyperbranched polyurethane nanocomposite: An antibacterial wound healing material with controlled drug release potential, *New J. Chem.* DOI: 10.1039/C4NJ00732H, 2014.
6. Das, B., Chattopadhyay, P., Maji, S., Upadhyay, A., Purkayastha, M.D., Mohanta, C.L., Maity T.K., & Karak, N. Rapeseed protein functionalized MWCNT/ *Helianthus annuus* derived hyperbranched polyurethane nanocomposite as a promising biodegradable, bioactive and non-toxic scaffold for rapid tibial-bone healing. (revision submitted)

In conference/workshop/seminar

1. Das B., & Karak, N. Nanocomposites of sunflower oil based hyperbranched polyurethane/protein modified MWCNT as a biodegradable bone scaffold, in Advanced Polymeric Material (APM' 2014), International conference, CIPET. Bhubaneswar, India.
2. Das, B., Chattopadhyay, P., & Karak, N. Fe₃O₄ decorated MWCNT/hyperbranched polyurethane nanocomposite: Antibacterial biomaterial, in 7th Conference of Medical Anthropology' 2013, DRL, Assam, India.

3. Das, B., Chattopadhyay P., & Karak, N. Vegetable oil based mMWCNT/polyurethane nanocomposites for bone tissue engineering applications, in TEZCON' 2012, DRL, Assam, India.
4. Das, B., Konwar U., & Karak, N. Sunflower oil modified hyperbranched polyurethane/magnetic nanoparticles nanocomposites for biomedical applications, in National conference on chemistry, chemical technology and society (NCCCTS' 2011), Tezpur University, Assam, India.